

STRUCTURAL FEATURES OF A CRETACEOUS COAL OF ALGAL AFFINITIES

By Peter H. Given, Zifambi Mudamburi and Lawrence J. Shadle

College of Earth and Mineral Sciences
408 Walker Building
The Pennsylvania State University
University Park, Pennsylvania 16802

This coal from the King Cannel seam in southwest Utah attracted attention some years ago because of its high hydrogen content (>7%), high volatile matter yield (65%) and excellent performance in liquefaction (1). The principal macerals in it have been provisionally identified as bituminite (55%), vitrinite (20%), alginite and liptodetrinite (2). Bituminite has been thought to be derived from disrupted algal or bacterial cells (3). Infrared spectra (2) and ^{13}C CP-MAS nmr (4) show that the samples are highly aliphatic ($f_a=0.38$), but less so than such purely algal coals as torbanite ($f_a=0.19$) (5). Very little is known of the chemistry of bituminite or liptodetrinite, and so the coal has been extensively studied by various methods. We wish to report here some of the results, as they bear on the structures present in a particularly interesting, if somewhat unusual, coal.

The original sample collected (in 1967) was designated PSOC 155 and represented, it was discovered later, only part of one lithotype in a seam in which four can be readily distinguished. In 1978 fresh samples, including all four lithotypes, were collected. Of these the middle two (PSOC 1109 and 1110) are the ones of interest here, having cannelloid-boghead character, and 1109 is the lithotype corresponding closely to PSOC 155. The lines of investigation pursued were: GC/MS analysis of solvent extracts and the hexane-soluble part of liquefaction products; oxidation of coals and asphaltenes from liquefaction with trifluoroperoxyacetic acid and dilute nitric acid; FTIR and ^1H nmr spectra of asphaltenes. Only a selection of the results will be presented here.

EXPERIMENTAL

A selection of analytical data for the coals is shown in Table 1. FTIR spectra indicate that the samples had been slightly weathered in the seam, PSOC 1110 somewhat more than the others (2).

Liquefaction was performed in tubing bomb reactors with tetralin and hydrogen as previously described (6,7) (10 MPa pressure at 400°C for 1 h). After removal of the ethyl acetate extraction solvent, the liquefaction products were mixed with a large excess of hexane and left to stand for 24 h before being filtered. Hexane, naphthalene and excess tetralin were removed as completely as possible by distillation, the latter two substances *in vacuo*. The hexane-solubles were separated into five fractions by column chromatography on alumina (hexane, toluene, chloroform and methanol used as eluants).

Oxidation with trifluoroperoxyacetic acid was carried out by the procedure described by Deno et al. (8), and also by a modified procedure. The principal feature of the latter is that the reaction is carried out in the presence of chloroform. The boiling of this serves as a heat sink and to regulate the temperature at 62°. Also, products extracted by it from the acidic aqueous phase are to some extent protected from further oxidation.

Product analyses were performed in a Finnigan Model 4000 GC/MS/data system, using a Microflexil DB-5 capillary column, with 95% methyl-5% phenyl silicone bonded to the wall. An ionization potential of 70 e.v. was used, and a range of 50 to 700 a.m.u. was scanned every two seconds during a chromatogram.

RESULTS AND DISCUSSION

Of particular interest in the results is the diverse evidence, from several sources, of the importance of long aliphatic chains both in the extractable mobile phase and in the macromolecular network. Also of interest is the evidence of the presence of some aromatic structures.

The FTIR spectra of the coals show intense well-resolved bands near 2920 and 2850 cm^{-1} , characteristic of methylene chains (2). The hexane-soluble part of both the pyridine and benzene/ethanol extracts represents 5-6% of the coal. Regenerated single ion chromatograms ($m/z = 74, 98, 60$ and 58) showed that the extracts consisted chiefly of a mixture of the methyl esters of series of long-chain mono- and dicarboxylic acids, with some free alkanolic acids and long-chain methyl alkyl ketones (see examples of chromatograms in Figure 1). These oxygenated compounds were not found in the liquefaction products, but a nearly equivalent quantity of alkanes was found. The alkanes consisted chiefly of straight chain hydrocarbons, but pristane, phytane and minor amounts of cyclic hydrocarbons were present as well. There is a difficulty in assuming that the alkanes were generated from the oxygenates during liquefaction: the homologous series of the latter extended up to about C₂₃, whereas alkanes up to C₃₂ were found. However, the oxygenates are considerably less volatile than the hydrocarbons, and it is quite likely that the higher homologs simply failed to get through the capillary column with the elution times used.

Extensive use was made of regenerated single ion chromatograms in the analysis of the fractions of hexane-soluble oil from liquefaction of the samples. These are specially useful when homologous series are present, as they proved to be here. Thus all alkyl benzenes give the tropylium ion (C_7H_7^+) as a major mass spectral peak, and alkylnaphthalenes give a corresponding peak of m/z 141 and/or 142 (9). Thus homologous series of alkylnaphthalenes (m/z 142), alkylfurans (m/z 82) and alkylphenols (m/z 108) were major constituents of fractions 2,3 and 5 from the column chromatography. An example of a single ion chromatogram is shown in Figure 2. It was generally true that the peaks are so uniformly spaced in the single ion chromatograms that we infer that mono-substituted long-chain alkyl derivatives are present rather than poly-substituted short chain. In confirmation of this, there were in the alkylnaphthalene and alkylfuran chromatograms closely spaced doublets for each carbon number, corresponding to the 1- and 2-isomers. We have inferred that these homologous series were physically trapped in the coal as part of the mobile phase (they were not found in the solvent extracts), rather than being part of the macromolecular network.

Estimating as well as possible from integrations of peak areas in total ion current chromatograms it was concluded that the alkanes and the linear alkyl chains (with the aromatic nuclei subtracted) together account for 15-16% of dmf coal in each of the 3 samples studied. Not included in these estimates are the alkyl chains in the substituted cyclohexenones and hydroxy-pyridines and quinolines present, since the evidence is not clear that the alkyl groups are long, linear, chains.

The ratio of hexane-soluble oils to asphaltenes for these coals was 2.0-2.4, whereas the mean ratio for 6 other coals of more normal vitrinite content was 0.94. The mean hydrogen content of the asphaltenes from the same 6 coals was 6.3%, while it was 7.5% for the 3 canneloid-boghead samples. ¹H nmr showed that only about 20% of the hydrogen atoms are attached to aromatic nuclei, and about the same fraction of aliphatic H is on carbon atoms in the benzylic position. That is, about 60% of

the H atoms are in aliphatic carbon atoms not adjacent to an aromatic ring. The aromaticity calculated by assuming the average composition of the aliphatic structures to be CH_2 is about 0.55. The aliphatic C-H stretching bands at 2920 and 2850 in the FTIR spectra of the asphaltenes are particularly intense and sharp (Figure 2). The frequencies are characteristic of long hydrocarbon chains, and this is confirmed by the presence of a weak skeletal vibration at 720 cm^{-1} . There is a small but distinct aromatic C-H vibration at 3030 cm^{-1} , and a distinct 1600 cm^{-1} band. There is also a small carbonyl band at 1705 cm^{-1} .

In what follows all of the information about the oxidation of the coal samples is provided by A. Daniel Jones (10), to whom we are indebted. Data on asphaltenes were generated in this laboratory, using the same techniques.

The principal products from the oxidation of the coals with dilute nitric acid were a mixture of long-chain fatty acids ($\text{C}_9\text{-C}_{23}$, maximum at $\text{C}_{13}\text{-C}_{18}$) and long-chain dicarboxylic acids ($\text{C}_4\text{-C}_{20}$, maximum at C_7) the latter being much more abundant than the former (see Table 2). Products from oxidation of the asphaltenes showed similar distributions (see Figure 3) but the mono-carboxylic acids were relatively more important.

The yields of acids from oxidation of the coals are equivalent to the presence of 20% by weight of long alkyl chains (determined with the aid of m. xylene as internal standard). It was noted above that the alkanes and the alkyl chains attached to aromatic nuclei in the hexane-soluble liquefaction products account for 15-16% of the coal. The oxidation products indicate that 17.7% of the asphaltenes consists of long alkyl chains, which corresponds to 3.7% of the coal. Thus the liquefaction products *in toto* contain alkyl chains equivalent to 19-20% of the coal, in remarkably good agreement with the estimate for the coal itself. However, the oxidation yields predominantly di-carboxylic acids, which presumably are derived from α,ω -diarylalkanes; but no evidence of these has been sought yet in the hexane-soluble liquefaction products or the asphaltenes.

When the procedure described by Deno et al. (8) was used for oxidation of the coals with trifluoroperoxyacetic acid, the major products were aliphatic dicarboxylic acids in the range C_3 to C_8 , malonic dominating. The second most abundant class of product was alkyl butyrolactones, in which the alkyl group has 0-6 carbon atoms. The asphaltenes gave similar distributions, but the relative abundance of the lactones was somewhat less, and succinic acid predominated over malonic acid, as it does with the asphaltenes from other coals (11). Also, acids derived from aromatic and hydroaromatic structures (benzene and oxirane polycarboxylic acids) are somewhat more abundant in the asphaltene oxidation products.

Use of the modified procedure for trifluoroperoxyacetic acid oxidation gave results very appreciably different from those provided by the original procedure. Butyrolactones became much less important. The lower dicarboxylic acids ($\text{C}_3\text{-C}_8$) became less abundant relative to the higher dicarboxylics ($\text{C}_9\text{-C}_{22}$; see Table 3), and the highest concentration was now found for succinic rather than malonic acid. The distribution of longer chain dicarboxylic acids is rather flat compared with that of the monocarboxylics (see Figure 4). The asphaltenes gave similar distributions (see Figure 4), but the ratios of the total concentrations of mono- and di-acids were quite different (see Table 2).

The benzene-insoluble residue from the liquefaction of PSOC 1109 also gave abundant long-chain acids on oxidation; the distribution of mono-acids was quite similar to that in the coal and its asphaltene, but the distribution of di-acids was different.

Estimation of the fraction of the coal corresponding to the long-chain material

in the TFPA oxidation products gave a value of only 6%. The work-up procedure for isolation of products from the two oxidation reactions is identical, so evidently in the Deno oxidation secondary reactions shorten the chain and/or destroy some of the primary products to a greater extent than in the nitric acid oxidation. The butyrolactones presumably result from the oxidation of long chains. Their abundance is less with the modified procedure but is not zero.

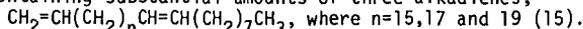
The hydrogen contents of alginite macerals is 10-11%; and the aromaticity of a sample was found to be 0.18 (5). Other alginites show little evidence of aromatic character in their IR spectra; pyrolysis at 375° for 24 h yields much straight chain aliphatic material but also some aromatic hydrocarbons, thought to be generated during the pyrolysis (12). Curie-point pyrolysis of some alginite-rich coals (at 610° for 12.5 sec.) gave a series of n. alkanes and alk-1-enes in the range C₈ to C₃₅, but significant amounts of polycyclic aromatic hydrocarbons were generated during the pyrolysis (13,14). The aromaticity of the coals studied here is higher (0.38), but additional aromatic structures could be generated during liquefaction. Polycyclic aromatic hydrocarbons (biphenyls, 3-, 4- and 5-fused ring compounds) were detected in the hexane-soluble part of the liquefaction products, as well as the long-chain alkyl aromatics discussed above (yet the hexane-soluble part of the solvent extracts was almost totally aliphatic).

The 25-30% vitrinite in these samples might have an aromaticity around 0.65-0.7. The value for the liptodetrinite, if, as is likely, this is related to sporinite, would be a little lower. Presumably the alginite and bituminite are largely aliphatic, though probably we need to assume some aromaticity to achieve a mean value of 0.38 for the whole coal.

The asphaltene from PSOC 1110 showed somewhat fewer benzylic protons in the ¹H nmr, and oxidation afforded less malonic and succinic acids, suggesting that dihydroaromatic structures are less abundant, perhaps because of weathering of the coal. Also, the (H/C)_{ar} ratio inferred from the nmr data was somewhat less than for the other lithotypes, indicating a higher degree of condensation to fused ring systems.

The analysis of the products from the modified trifluoroperoxyacetic acid oxidation of PSOC 1109 is shown in Table 3, classified by structural type. Acids having linear aliphatic structures account for 44% of the total products. Compounds deriving from aromatic or aromatic/hydroaromatic structures account for some 37% of the products. This is not a fair comparison, since some of the aliphatic diacids derive from hydroaromatic structures, and the other acids with aromatic associations will include in the structures what were aliphatic carbon atoms. Nevertheless, comparisons of the data with results for other coals are consistent with the suggestion of low aromaticity and the structural importance of long aliphatic chains in the Utah coal. Indeed, as we have seen, long aliphatic chains are prominent in the solvent extracts, hexane-soluble liquefaction oils, asphaltenes and insoluble residues from the liquefaction of this coal. Such chains are clearly important in the macromolecular network as well as in the mobile phase of relatively small molecules.

The alginite in these samples, as in most other coals that contain the maceral, is derived from the colonial green alga, *Botryococcus braunii* (2,3). This alga is peculiar in containing substantial amounts of three alkadienes,



The organism has many habitats. It is commonly found in coastal lagoons along the south coast of Australia. When these dry out, as they sometimes do, the lagoon bed is left covered with a sheet of rubber-like substance, thought to have been formed by the oxygen-catalyzed polymerization of the alkadienes (16). This polymer, not necessarily formed only in dried-out lagoons, is considered to be the precursor of alginite macerals, though this view does not explain how the colonial morphology is preserved, or why visible fluorescence should be excited by illumination with the 365 nm line of the mercury arc.

If bituminite is indeed derived from disrupted algal cells, then the colonial morphology is not preserved, but it still seems a reasonable possibility that a major part of the Utah cannelloid-boghead coal is derived from metamorphism of the rubber-like polymer associated with *B. brownii*. An open water pond is envisaged as a probable environment of deposition, rather small amounts of woody material being washed in from wooded areas around the margin (2).

ACKNOWLEDGEMENTS

This work was supported by contract No. DE-AC22-81-PC-40784 from U.S Dept. of Energy.

REFERENCES

- Given, P.H., Cronauer, D.C., Spackman, W., Lovell, H.L., Davis, A. and Biswas, B. Fuel, 1975, 54, 40-49.
- Given, P.H., Davis, A., Kuehn, D., Painter, P.C. and Spackman, W., submitted to Int. J. Coal Geol., Feb. 1984.
- Teichmüller, M., Stach's Textbook of Coal Petrology, 1982, Third Ed., eds. E. Stach, G.H. Taylor, M.-Th. Mackowsky, D. Chandra, M. Teichmüller and R. Teichmüller, Gebrüder Borntraeger, Berlin, 219-294.
- Wilson, M.A., Pugmire, R.J., Karas, J.V., Alemany, L.B., Woolfender, W.R., Grant, D.M., and Given, P.H., Anal. Chem., in the press, 1984.
- Pugmire, R.D., Zilm, K.W., Grant, D.M., Larter, S.R., Allen, J., Senftle, J.T., Davis, A. and Spackman, W., in New Approaches in Coal Chemistry, eds. B. D. Blaustein, B.C. Bockrath and S. Friedman, Amer. Chem. Soc. Symp. Series 169, 1981, 23-42.
- Szladow, A.J. and Given, P.H., Ind. Eng. Chem., Proc. Des. Div., 1981, 20, 27-33.
- Yarab, R.F., Given, P.H., Davis, A. and Spackman, W., Fuel, 1980, 59, 81-92.
- Deno, N.C., Jones, A.D., Koch, C.C., Minard, R.D., Potter, T., Sherrard, R.S., Stroh, J.G. and Yevak, R.J., Fuel, 1982, 61, 490-492.
- McLafferty, F.S., Interpretation of Mass Spectra, University Science Books, Mill Valley, Calif., 3rd Edn., 1980.
- Jones, A.D., Ph.D. Thesis, The Pennsylvania State University, The Chemical Structures of Coals as Determined by Selective Oxidative Degradations, 1984.
- Shadle, L.J. and Given, P.H., Fuel, 1982, 61, 972-979.
- Allan, J., Bjørøy, M. and Douglas, A.G., Advances in Organic Geochemistry, 1979, eds. A.G. Douglas and J.R. Maxwell, Pergamon, Oxford, 599-618. (1981)
- Philp, R.P. and Saxby, J.D., Advances in Organic Geochemistry, 1979, eds. A.G. Douglas and J.R. Maxwell, Pergamon, Oxford, 639-652. (1981)
- Meuzelaar, H.L.C., McClennen, W.H., Tomlinson, J.H. and Pope, D.L., Proc. Int. Conf. on Coal Science, Düsseldorf, 1981, 816-821.
- Cane, R.F., and Albion, P.R., Geochim. and Cosmochim. Acta., 1973, 37, 1543-9.
- Cane, R.F., Oil Shale, eds. T.F. Yen and G.V. Chilingarian, Elsevier, 27-60.

Table 1. Some Analytical Data for One of the Coals Used, PSOC 155
[abstracted from full data in Given et al. (2)]

% by vol., vitrinite	24	%dmmf C	74.5
alginate	7	H	7.4
liptodetrinite	12	S (org)	1.0
bituminite	52	O (diff)	15.0
inertinites	2	VM	~70

MM, 25.3% of dry coal

Table 2. Yields of Long-Chain Acids from Oxidation of PSOC-1109

	<u>Coal</u>	<u>Asphaltene</u>
HNO ₃ Oxidation:		
diacids, C ₄ -C ₂₀	66.0	48.5
monoacids, C ₉ -C ₂₃	<u>11.1</u>	<u>26.5</u>
Total	77.1	75.0
Deno Oxidation:		
diacids, C ₇ -C ₂₅	26.7	10.3
monoacids, C ₉ -C ₂₅	<u>16.7</u>	<u>12.4</u>
Total	43.4	22.7

Table 3. Yields of Product Classes from TFPA Oxidation of Asphaltene (PSOC 1109)
(Modified procedure)

<u>Class of Acids</u>	<u>% of GC area</u>	<u>Breakdown of alkane dioic acids</u>	<u>% of G-C area</u>
alkane dioics, C ₃ -C ₇	14.5		
alkane dioics, C ₈ -C ₂₂	12.0	malonic	1.7
alkane monoic, C ₉ -C ₂₆	10.5	succinic	3.6
alkyl lactones, C ₄ -C ₁₀	3.0	glutaric	4.7
alkane trioic	4.0	adipic	2.3
cyclohexene dioic	0.2	pimelic	<u>2.2</u>
aryl alkanolic	3.2		14.5%
alkene dioic	1.9		
oxirane polycarboxylic	7.7		
benzene polycarboxylic	23.1		
phenol polycarboxylic	<u>3.2</u>		
Total	84.3%		

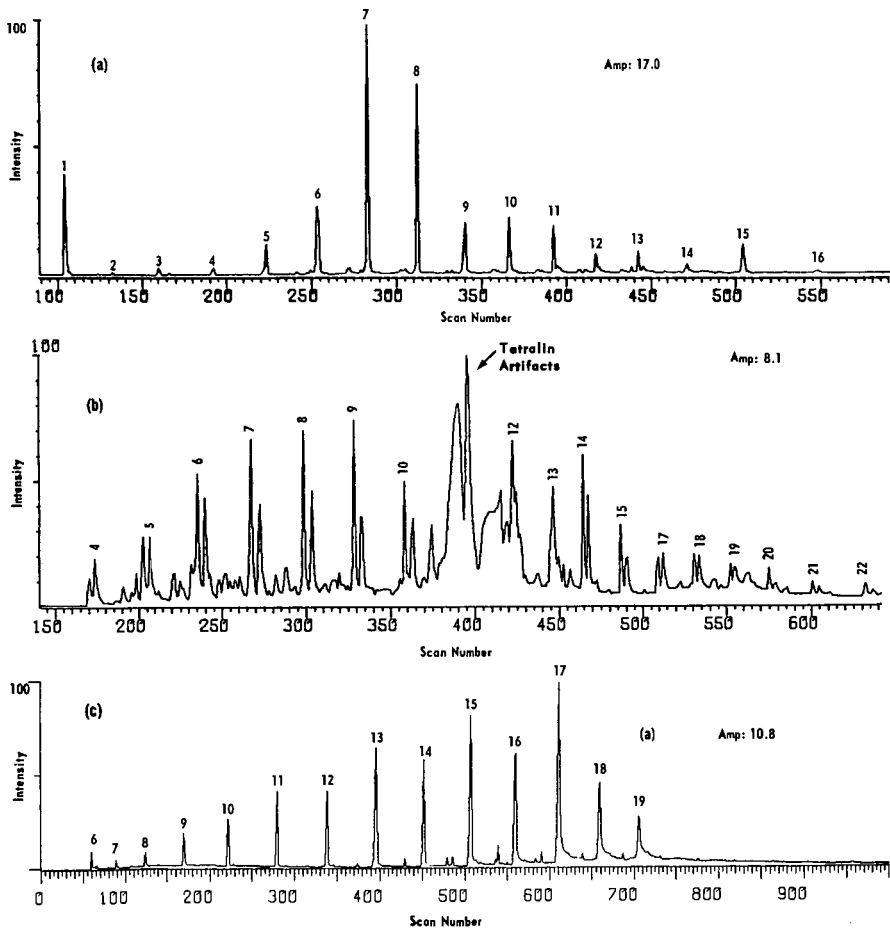


Figure 1. SINGLE ION CHROMATOGRAMS FOR HEXANE-SOLUBLE FRACTIONS FROM KING CANNEL COAL
 (a) pyridine extract, $m/z = 60$ (fatty acids), (b) liquefaction product fraction 2, $m/z = 142$ (alkyl naphthalenes), (c). liquefaction product fraction 5, $m/z = 108$ (alkyl phenols)

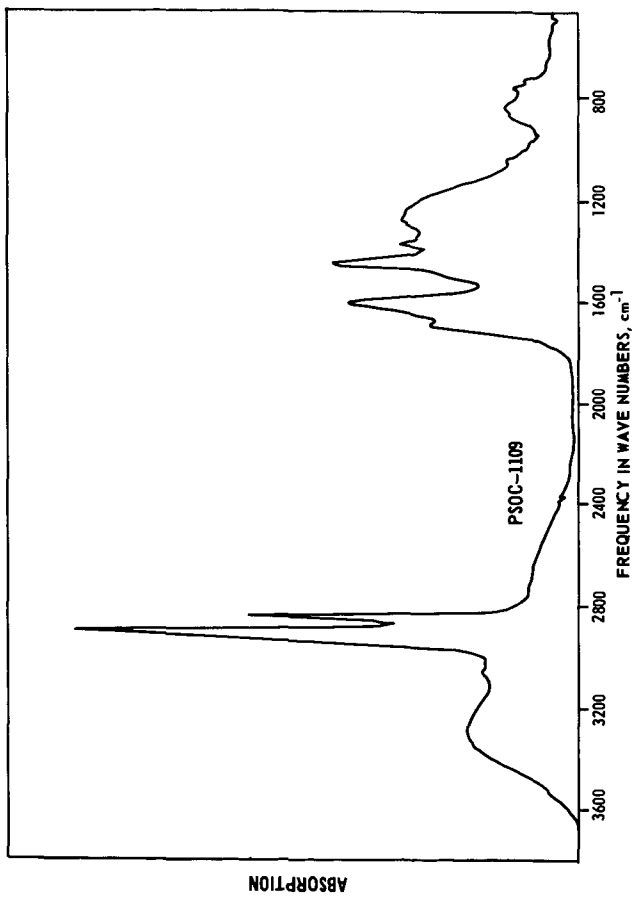


Figure 2. FTIR SPECTRUM OF ASPHALTENE FROM KING CANNEL COAL

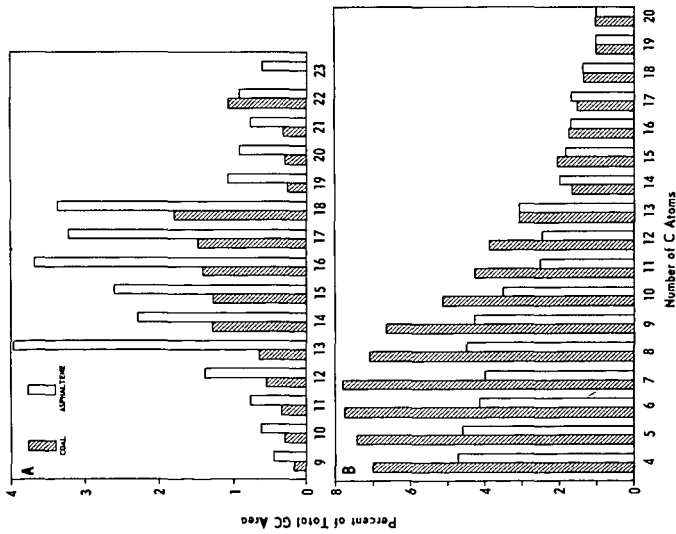


Figure 3. LONG-CHAIN ACIDIC PRODUCTS FROM NITRIC ACID OXIDATION OF PSOC-1109 A. Monocarboxylic Acids B. Dicarboxylic Acids

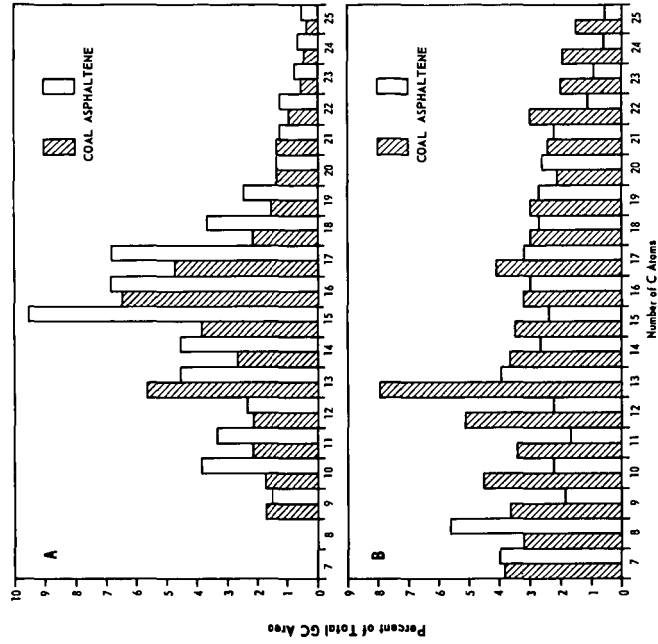


Figure 4. DENO OXIDATION PRODUCTS OF PSOC-1109 USING PROCEDURE II A. Monocarboxylic Acids B. Dicarboxylic Acids

NEW INSIGHTS INTO THE STRUCTURE OF COAL AND COAL MACERALS. R. J. Pugmire, A. Soderquist, A. L. Beeler, and D. M. Grant, Departments of Fuels Engineering and Chemistry, University of Utah, Salt Lake City, Utah 84112:

The use of dipolar dephasing techniques has been demonstrated as a very useful probe into the details of the carbon skeletal structure of whole coals and coal maceral groups. The data thus obtained indicates that T_2 values observed in coals and coal macerals are comparable to those observed in model organic compounds with similar types of structural units. Hence, relative amounts of protonated and nonprotonated carbons can be obtained from detailed dipolar dephasing studies. These data also reveal the presence of a highly mobile phase in the aliphatic region of the spectra of low rank coals. A comparison of the skeletal structural units in low rank coals, liptinite, vitrinite, and inertinite maceral groups and variations within maceral groups separated by density gradient centrifugation techniques will be given.

MACROMOLECULAR STRUCTURE AND COALIFICATION. J. W. Larsen, Dept. of Chemistry,
Lehigh University, Bethlehem, PA 18015

After having been proposed and ignored several times, the macromolecular gel structure of coals is gaining acceptance. It provides a useful and enlightening framework within which to discuss the coalification process. Indeed, if early results are general, major revisions in coalification models will be necessary. Between ca 78% C and 86% C, the cross-link densities of coals generally decrease. Over this range, coalification is probably a depolymerization. This notion is supported by the molecular weight distributions of pyridine extracts. Above 88% C, a rapid polymerization takes place as coalification increases. It is possible that the depolymerization results in part from a loss of ether linkages during coalification. It is tempting to associate the increase in cross-link density above 88% C with bonds formed as a result of dehydrogenation. Natural deoxygenation and dehydrogenation have very different consequences for coal structure.

SOME STRUCTURAL CHARACTERISTICS OF AUSTRALIAN COALS. R. B. Johns, T. V. Verheyen,
Chemistry School, University of Melbourne, Australia.

Victorian brown coal occurs in five lithotypes. Pyrolysis-MS groups them into two sets, the resinous content distinguishing the darker from the lighter lithotypes. Chemically they vary between seams (the oldest being the most aliphatic), but the same chemical trends are shown within each lithotype profile. Even though seams differ and aromaticities by solid state ^{13}C nmr can differ, IR spectral subtraction routines between lithotypes confirm the correlation between loss of carbonyl absorption and loss of aliphatic absorption. Humic acids fractionated from an aliphatic south Australian lignite qualitatively are similar in aliphatic components, but the most soluble humic acid in the profile is also the most aliphatic and is dominated by long chain structures. These aliphatic residues are bonded into this humic acid fraction. The light, in contrast to the dark lithotypes, show more degraded lignin phenolic components, consistent with gelification in chemical terms, but at variance with petrographic assessments. The aromatic residues are chemically involved in upgrading reactions of brown coals to technologically valuable low-moisture-content fuels. The chemistry of the lithotype and seam dependence of the upgrading procedures will be discussed.

ACTION OF PEROXY ACIDS ON COALS. Norman C. Deno, Chemistry Dept., Pennsylvania State University, University Park, PA 16802.

Peroxyacetic acid reacts with vitrinite coals to open some of the phenolic rings to hexadienedioic acids without loss of carbon. The product is soluble in methanol and largely soluble in water. There is no evidence for any other action from yields and spectra, and the view is supported by model studies on poly-p-vinylphenol.

The action of trifluoroperoxyacetic acid is more extensive. The diene diacids are degraded so that the final products are largely the aliphatic components attached to carboxylic or maleic acid groups. Isolated methylenes do not survive. The major products are oxiranetri and tetracarboxylic acids derived from phenolic acids and polyaromatic phenols, benzenetetracarboxylic acids from dihydroanthracene moieties, malonic acid of uncertain origin, acetic acid from arylmethyl, and methanol from arylmethoxy. Minor amounts of pyridine polyacids indicate acridine precursors. Significant amounts of products are not volatile and so their methyl esters and their nature has not been determined.

USE OF AQUEOUS CATALYTIC PROCESSING FOR WATER-GAS SHIFT CONVERSION

Douglas C. Elliott and L. John Sealock, Jr.

Pacific Northwest Laboratory*
P.O. Box 999
Richland, WA 99352

INTRODUCTION

The water-gas shift reaction involves the reaction of carbon monoxide and steam to produce hydrogen and carbon dioxide and derived its name from its industrial use to increase the hydrogen content of water gas produced from the reaction of steam with hot coke or coal. Current interest in this reaction lies in the tailoring of the hydrogen to carbon monoxide ratio of gas streams employed for chemical synthesis. For example, product gas from a typical coal gasification unit may have an H_2 to CO ratio of approximately 1 to 1 while the synthesis gas composition required for methanol production would have a ratio of 2 to 1 and the ratio for methane synthesis is 3 to 1.

The study of catalysts for this reaction has focused primarily on heterogeneous catalysts (1). Specifically, iron oxide-chromium oxide catalysts have been used at high temperature (350 to 450°C) and newer low temperature (200-260°C) copper-zinc oxide catalysts have been developed for secondary treatment of gas product streams. The low-temperature catalysts are particularly susceptible to poisoning by chlorine or sulfur as well as deactivation due to sintering. More recent studies of homogeneous catalysts for the water-gas shift reaction have dealt primarily with organometallics (2,3).

The use of a high-pressure water system for the water-gas shift reaction was first proposed by Casale (4) although he was unaware of the potential of basic catalyst solutions. The pressurized water system finds its advantage in a kinetic effect due to pressure as well as a shift in product composition due to the large excess of water driving the reaction to completion. The work of Yoneda et al. (5) during World War II established the concept of using an aqueous solution of metal carbonate as a catalyst for the water-gas shift reaction. This work included a comparative study of a large number of transition metals; however, potassium was the only alkali metal tested. The application of this mechanism in a process scheme was recently examined (6).

PROCESS DESCRIPTION

The water-gas shift concept being developed at Pacific Northwest Laboratory is a continuous process in which raw product gas is contacted with an aqueous catalyst system in the temperature range of 250 to 350°C and at pressures from 500 to 2500 psig. The catalyst of choice is sodium carbonate at a concentration of 6% in water, but any material which can generate hydroxide ions at the process conditions will effectively catalyze the reaction (7). Previous batch scale research conducted under sponsorship of the Gas Research Institute (8) has demonstrated the chemistry of the concept and has substantiated that the reaction rates of the experiments varied depending upon catalyst concentration, temperature and pressure. Based on these rates it is apparent that useful water-gas shift conversion can be obtained with the aqueous system and that the required gas contacting time is in the range of minutes depending on the extent of shift reaction required. These batch studies proved that a simple system of circulating the reactant gas

*Operated by Battelle Memorial Institute.

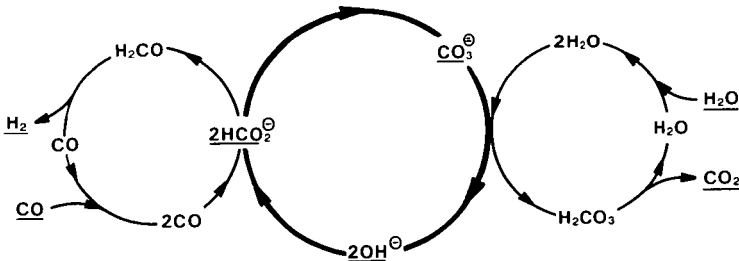
through an aqueous pool of catalyst sealed in a high pressure autoclave can be used to study the reaction chemistry of the concept.

Current research being funded by the U.S. Department of Energy Morgantown Energy Technology Center is designed to demonstrate the concept of continuous use of an aqueous catalyst system for conducting the water-gas shift reaction and to prove the initial engineering of continuous processing. Work in progress is designed to:

- establish optimum operating conditions;
- determine pressure effects and limitations;
- establish catalyst lifetimes;
- obtain kinetic information;
- determine H₂S removal efficiencies;
- establish tar and oil removal/conversion efficiencies;
- determine catalyst regeneration/recycle requirements and catalyst costs;
- establish effect of gas residence times and concentration on conversion efficiencies;
- determine the improvement to current technology; and
- establish cost savings/benefits.

MECHANISM OF CONVERSION

The chemistry of aqueous alkali catalyzed water-gas shift conversion can be described as a cyclical scheme as depicted below.



The ionization of the carbonate catalyst generates hydroxide ions which react in the presence of carbon monoxide at the processing conditions to produce formate ions. Two formate ions can then rearrange to formaldehyde and carbonate to complete the cycle. The rapid decomposition of the formaldehyde results in the production of hydrogen. We have described the elucidation of this cycle previously (9).

PROCESS ADVANTAGES

Operation of the water-gas shift reaction in the pressurized aqueous system has several processing advantages. These advantages are related to the chemical equilibrium of the system, the range of catalysts which can be used, and improvements specific to the incorporation of this type of water-gas shift process into a pressurized, coal (or other carbonaceous material) gasification system.

- Equilibrium Considerations

Thermodynamic studies have shown that the water-gas shift reaction is limited by equilibrium considerations at high temperature and that the conversion of CO to

CO₂ is not complete. This equilibrium condition is the major impetus for the development of a low-temperature water-gas shift catalyst. The current commercial water-gas shift processing technology utilizes a two-step system wherein the bulk of the reaction occurs at high temperature. The temperature is lower in the second catalyst bed to obtain a more favorable equilibrium gas composition at the exit from the water-gas shift system. The aqueous alkali catalyst system maintains this low temperature advantage because it exhibits substantial activity at temperatures as low as 250°C. The effect of temperature on catalytic conversion of carbon monoxide by the water-gas shift reaction using 0.32M sodium carbonate aqueous catalyst is depicted in Figure 1. The data shows the measurable activity begins in the range of 200 to 250°C while very high activity is attained at temperatures of 350°C and above. In addition, the use of the pressurized water system gives added driving force to the water-gas shift reaction. The large excess of water tends to push the reaction to completion in the presence of the alkali catalyst.

Range of Catalyst Choice

Current water-gas shift processing requires a high temperature catalyst, usually a combination of cobalt and molybdenum oxides or iron and chromium oxides on an alumina support, and/or a low temperature copper-zinc oxide catalyst formulation. The latter are sensitive to deactivation by sulfur-containing compounds. All are orders of magnitude more expensive than the water solution of alkali carbonate used in our system. The recent development of homogeneous organometallic catalysts also holds potential for lower temperature operation with undetermined sensitivity to gas contaminants.

The mechanism presented in this paper for our water-gas shift system shows that a wide range of potential catalysts exist which could serve as catalyst in the pressurized aqueous system. Essentially, any compound which can generate hydroxide, formate or carbonate at the reaction conditions will exhibit catalytic activity. Results of our experiments have demonstrated that even ammonia gas or ammonium hydroxide or carbonate can act as a catalyst in the pressurized aqueous system (10).

Table 1 presents some of the many chemicals which have been tested for water-gas shift catalyst activity in the one-liter batch system. Group 1 consists of high to medium activity metal carbonates while Group 2 is a listing of very low activity carbonate catalysts (mostly alkaline earths). Group 3 is a list of some of the most active catalysts (on a equimolar basis) tested. Group 4 consists of medium activity catalysts while Group 5 consists of low activity catalysts. In this ranking of high, medium, and low activity, sodium carbonate at 0.32M is used

Table 1. Aqueous Catalysts for the Water-Gas Shift Reaction

High to Medium Group 1	Very Low Group 2	High Group 3	Medium Group 4	Low Group 5
Carbonates of: nickel cadmium potassium sodium silver lithium cesium copper	Carbonates of: barium zinc magnesium strontium calcium	Na ₃ citrate Na ₂ oxalate NaH oxalate K ₂ tartrate KNa tartrate K ₂ oxalate K quadroxalate	Na acetate NaH carbonate KH tartrate KH carbonate NaH ₂ citrate Na formate Na hydroxide Na ketomalonate	sodium salts of: glyoxalate phenolate pyruvate malonate propionate maleate benzoate

as the dividing point between high and medium activity while sodium carbonate at 0.16M concentration serves as the dividing point between medium and low activity. Very low activity is equivalent to sodium carbonate at $\leq 0.03M$ concentration. Figure 2 shows the effect of sodium carbonate concentration on catalytic conversion of carbon monoxide by the water-gas shift reaction at 300°C.

The aqueous catalyst system as used in a gas-liquid contacting scheme has no potential for catalyst surface contamination or pore plugging. Deactivation of the catalyst through chemical combination can be used to an advantage as a gas scrubbing system as discussed in the next section.

- Relationship to Coal Gasification Technology

In addition to its primary function of adjusting the H_2 to CO ratio in gas streams, the successful development of a shift conversion process based on the use of an aqueous catalyst system could have a significant impact on a number of gas processing streams associated with commercial coal gasification. Associated processes that are expected to be affected or eliminated due to use of the concept include gas quenching (gas liquor separation/gas cooling), raw gas treating, sulfur removal, conventional shift conversion, and steam generation.

It is envisioned that the raw gas from the coal gasifier can be fed directly in whole or in part to the shift conversion system. The system is expected to quench the gas as well as treat the raw gas. Laboratory data has demonstrated that the aqueous catalyst system will cause tars to be gasified in the system and that the system will remove H_2S from the gas stream. Use of the catalytic system should significantly reduce costs of raw gas treating and favorably impact acid gas removal costs. The total extent of H_2S removal has not been established as yet, but is expected to be significant and an important consideration of the process concept.

The use of a cheap material (Na_2CO_3) in approximately a six percent solution will be economically favorable over conventional supported shift catalysts; it is also expected to be less susceptible to deactivating forces. Steam requirements are expected to be significantly lower for the advanced system since the sensible heat of the raw gas leaving the gasifiers should supply the required heat for the process. In addition, ammonia is stripped by the system and ammonium compounds have also been shown to be excellent shift catalysts in the system. In addition, ammonia is generated as a by-product of many coal gasification processes and is therefore potentially a source of an excellent, available, cheap catalyst.

It is impossible at this point in process development to quantify the economic advantage of the advanced shift conversion system. However, it is obvious from the previous discussion that the process concept has potential to significantly impact commercial coal gasification technology. Key impacts resulting from the use of this system are envisioned to be:

- establishment of an improved water-gas shift conversion system;
- reduced gas cooling and gas liquor separation costs;
- increased carbon utilization by further gasification of tars;
- reduced cost of by-product recovery by removal of ammonia and phenols from the gas stream;
- reduced acid gas treatment cost by significant H_2S removal; and
- reduced steam generation cost due to utilization of the sensible heat of the raw gas.

CONTINUOUS EXPERIMENTAL SYSTEM

In order to advance the concept of aqueous water-gas shift conversion a bench-scale continuous reactor system was developed. The system which is shown in Figure 3 is assembled around a one-liter, high-pressure autoclave. An air driven gas compressor is used to circulate the reactant gas through a rotameter for gas flow measurement and into the reactor. The product gas exits the reactor through the primary condenser. A back-pressure regulator is employed to drop the product gas pressure to near atmospheric. The product gas then flows through a secondary condenser, gas volume meter, and gas chromatograph sampling loop. The cooling water temperatures and flows are monitored to provide data for an energy balance around the reactor system. The careful monitoring of gas flows and composition, as well as the catalytic solution composition, provide the needed input for mass balance calculations.

Inside the reactor, the gas enters near the bottom of the catalyst pool from the end of a dip tube. The gas bubbles up through the catalyst pool and enters the stirrer shaft at an opening near the top of the reactor cavity. At this point, the gas can proceed through the hollow stirrer shaft to the bottom of the catalyst pool and is discharged by the turbine impeller into the catalyst solution (the turbine actually generates the pressure differential which draws the gas through the hollow stirrer shaft to shaft bottom outlet). Alternately, the gas can proceed out of the reactor after entering the stirrer shaft by proceeding upward through the primary condenser which cools the gas stream and returns the vaporized water which has been condensed to the catalyst pool. The turbine impeller has a dual importance in the reactor system as it provides the required mixing of gas and liquid phases, and serves to "pump" the gas down into the liquid bath to increase the gas/liquid contacting. This type of reactor system has been recently demonstrated as an effective gas/liquid contactor (11).

Gas flow is monitored as both inlet and outlet gas volume. The gas composition is determined on both the inlet and outlet streams. The flow control is provided by regulating valves which vary the air flow to the air-driven compressor. A pressure regulator controls the feed gas pressure on the suction side of the compressor. In addition, regulating needle valves are used to vary the flow after it exits the compressor. The pressure in the reactor is limited by the back-pressure regulator.

The one-liter continuous reactor system was put in operation in June 1984. Results of initial shakedown and kinetic tests will be presented.

CONCLUSION

A new catalytic gas processing system is being used to perform the water-gas shift reaction with a pressurized aqueous catalyst solution at low temperature. The chemistry of the system has been documented using batch reactor tests and continuous gas processing is now being studied in a bench scale apparatus. The new process has numerous advantages over conventional shift technology which make it intrinsically compatible with advanced gasification systems which operate pressurized reactors.

ACKNOWLEDGMENTS

The continuous gas processing studies are being funded by the U.S. Department of Energy through the Morgantown Energy Technology Center. The authors wish to thank Dr. Hsiao-Ya L. Lai and Dr. Madhav R. Ghate of the Advanced Gasification Section at the Morgantown Energy Technology Center for their support of the research.

REFERENCES

- 1) Hawker, P. N. Hydrocarbon Processing (1982) 61,4, 183-187.
- 2) Ungermann, C. et al. J. Amer. Chem. Soc. (1979) 101, 5922-5929.
- 3) King, A. D., Jr; King, R. B.; Yang, D. C. J. Amer. Chem. Soc. (1980) 102, 1028-1032; King, A. D., Jr.; King, R. B.; Yang, D. C. J. Amer. Chem. Soc. (1981) 103, 2699-2704.
- 4) Casale, L., U.S. Patent 1,843,540, 1932.
- 5) Yoneda, K.; Kondo, S.; Abe, R. J. Chem. Soc. Jpn. (1941) 44, 385-391; Yoneda, K.; Honda, Y.; Momiyana, N.; Abe, R. J. Chem. Soc. Jpn. (1943) 46, 554; Yoneda, K.; Kondo, S.; Abe, R. J. Chem. Soc. Jpn. (1943) 46, 667; Yoneda, K.; Kondo, S.; Abe, R. J. Chem. Soc. Jpn. (1944) 47, 5-10.
- 6) Zieke, C. W.; Rosenhoover, W. A.; Gorin, E. Prepr., Div. Fuel Chem., Amer. Chem. Soc. (1976) 21, 7, 163-186.
- 7) Elliott, D. C. and Sealock, L. J., Jr. Ind. Eng. Chem. Prod. Res. Dev. (1983) 22, 426.
- 8) Sealock, L. J., Jr.; Elliott, D. C.; and Hallen, R. T. "Kinetics and Catalysis of Producing Synthetic Gases from Biomass," Final Report GRI-82/0038, NTIS PB83-188664, December 1982, 81pp.
- 9) Elliott, D. C.; Hallen, R. T.; Sealock, L. J., Jr. Ind. Eng. Chem. Prod. Res. Dev. (1983) 22,431.
- 10) Elliott, D. C.; Sealock, L. J., Jr.; Hallen, R. T. "Ammonia-Based Catalyst for Water-Gas Shift Reaction" patent application #510,908, July 5, 1983.
- 11) Gollakota, S. V. and Guin, J. A. Ind. Eng. Chem. Process Des. Dev. (1984) 23, 52-59.

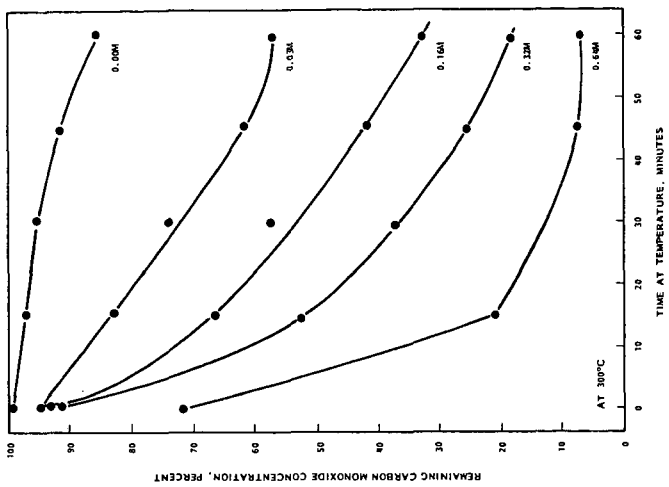


Figure 2. Sodium carbonate concentration effect on catalytic conversion of carbon monoxide by the water-gas shift reaction.

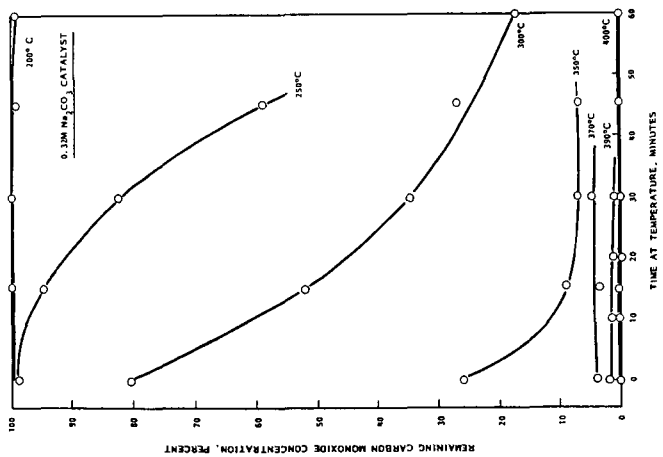


Figure 1. Temperature effect on catalytic conversion of carbon monoxide by the water-gas shift reaction.

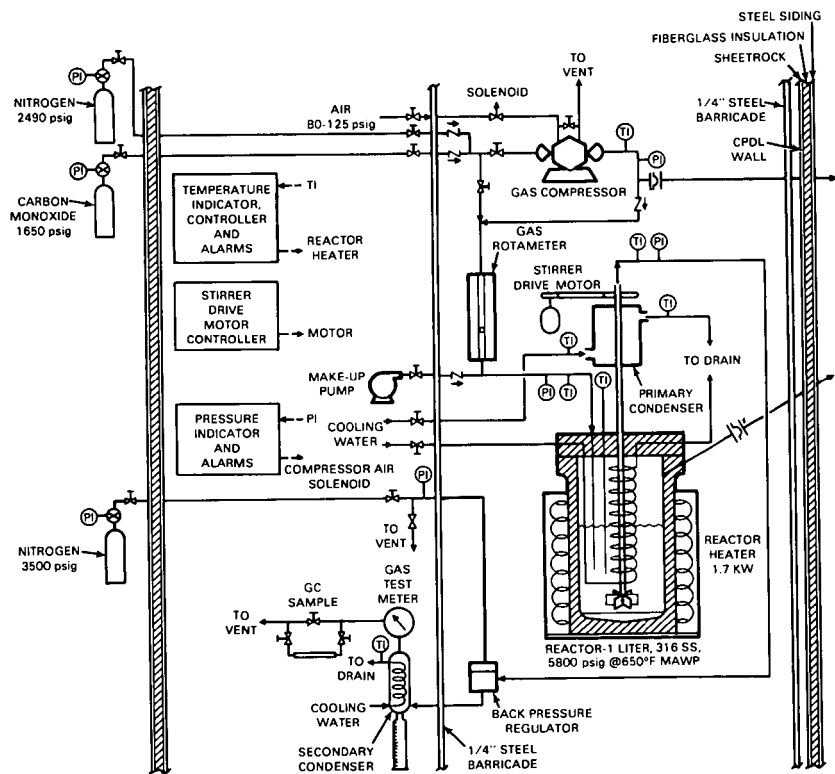


Figure 3. Continuous water-gas shift conversion reactor system.

FLUID CRACKING CATALYST WITH CARBON SELECTIVITY

M. L. Occelli* and D. C. Kowalczyk
Gulf Research & Development Company
P. O. Drawer 2038
Pittsburgh, PA 15230

ABSTRACT

A fluid cracking catalyst was formed by spray drying a silica sol slurry containing an acid-leached kaolin mineral (with a $\text{SiO}_2/\text{Al}_2\text{O}_3$ ratio of 2.6) and calcined rare earth exchanged zeolite Y (CREY). Microactivity testing (MAT) data show the catalyst (with ~22% CREY) can give 66 vol% conversion in the presence of 5000 ppm Ni-Equivalents. Carbon generation (4.3%) seems to be independent of metals concentration over the range investigated. In the presence of 1.0% vanadium, the catalyst is as active as when metal-loaded with 5000 ppm Ni-Equivalents. With 2% vanadium, there is a drastic decrease in activity. Commercial catalysts have similar activity and gasoline selectivity but generate considerably more hydrogen and carbon, especially at high metals loading.

INTRODUCTION

Oil shortages have, at the present, disappeared, but refiners are nonetheless under economic pressure to process cheaper, metals-contaminated crudes. In fact, because of nationwide conservation efforts, gasoline consumption in the U.S. has and is projected to steadily decline in the 80's. Therefore, refiners without the capability of converting less costly, heavier oils into transportation liquids will suffer competitively in this shrinking energy market (4-6). Several units have already reported using heavy crudes in their FCC operations (7-9).

Catalyst requirements to process Ni- and V-contaminated feedstocks have been described elsewhere; (9-11) a recent discussion has been given by Magee (6). Vanadium is known to destroy catalyst activity, and its effects can be mitigated by tin addition (12). Nickel, while not causing zeolite destruction, generates large amounts of gases and coke, placing severe demands on gas compressors' capability. Antimony organics have been shown to reduce by 50% gas formation due to metal contaminants, especially nickel (13-15). Cracking catalysts capable of forming inactive metal silicates or even aluminosilicates on their surface could crack heavy oils to useful products and minimize coke, hydrogen, and light gas generation.

Examples of silica-bound zeolite containing FCC have been described by Elliot (16), Ostermaier and Elliot (17), Flaherty et al. (18), and Seese et al. (19). It is the purpose of this paper to report a silica-rich cracking catalyst resistant to deactivation by metals contaminants like nickel and vanadium.

*To whom all correspondence should be addressed.

EXPERIMENTAL

Catalyst Preparation

A silica sol was prepared by simultaneously mixing diluted sodium silicate, alum, and sulphuric acid in a manner to keep the slurry pH between 2.8 and 3.2. The sol was then vigorously homogenized and aged for three hours at room temperature. Calcined and acid-washed kaolin ($\text{SiO}_2/\text{Al}_2\text{O}_3=2.6$) was then added to form a slurry containing 639 g SiO_2 , 231.6 g Al_2O_3 , and 126 g clay. Calcined rare earth exchanged zeolite Y (CREY from Davison) was then added to obtain the desired cracking activity. The catalyst zeolite level (% CREY) is defined as $\text{CREY}/(\text{SiO}_2 + \text{Al}_2\text{O}_3 + \text{CLAY} + \text{CREY}) \cdot 100$.

The fluidized cracking catalyst was obtained by spray drying the slurry at ~15-20% solids. The microspheres were slurried in a 5 l 2% NH_4OH solution to remove sodium ions. After a final washing with a large excess of deionized water and drying at 400°C for 10 h, the catalysts were submitted for evaluation. The microspheres with ~22% CREY had 250 m^2/g BET surface area, 0.23 cc/g pore volume, and an average pore radius of 18.6 Å; their bulk density was 0.66 g/cc .

Catalyst Testing

Catalytic evaluation was performed using a microactivity test similar to the one described by Ciappetta and Henderson (1). The weight hourly space velocity was 15 with 80 sec catalyst contact time at $T = 480^\circ\text{C}$. The charge stock was a Kuwait gas oil having a 260°-426°C boiling range (see Table 1); a catalyst-to-oil ratio of 2.5 was used. Prior to testing, catalysts were steam-aged for 10 h at 730°C with a ~50-50% N_2 -steam mixture. (Ni-V) naphthenates were used to metal-load fresh catalysts according to a procedure described elsewhere (2). Ni-equivalents is defined as the sum $(\text{Ni} + 1/5 \text{ V})$ expressed in parts per million (ppm). Percent conversion is defined as: $(V_f - V_p) 100/V_f$ where V_f is the volume of the fresh feed (FF) and V_p is the volume of product boiling above 204°C.

RESULTS AND DISCUSSION

As expected (3), cracking activity of this silica-rich catalyst increases with zeolite content (Figure 1). In the 15-22% CREY range, conversion changed from 74 to 81.6%. Gasoline make remained at ~53%; this and the increase in hydrogen and carbon generation indicates the occurrence of overcracking, Figures 2, 3, and 4.

Metals (Ni + 1/5 V) effects on catalyst activity are given in Figures 5-8. Losses in gasoline yields follow the decrease in catalyst activity with metal loadings (Figures 5 and 6) since both effects are due to losses in catalyst crystallinity. The silica-rich catalyst (with 15 or 22% CREY) deactivates in a manner similar to that of a commercial catalyst having comparable initial activity (Figure 5). The catalyst (with ~22% CREY) appears to be more selective with respect to hydrogen generation (Figure 7), and its carbon make (~4.3%) is independent of metals loading up to 5000 Ni-Equivalents. In contrast, the commercial catalyst carbon generation monotonically increases with metals level (Figure 8). Both catalysts have similar resistance to vanadium poisoning. In the presence of 1.0% V conversion was ~60% (down from ~82% for the fresh catalysts); with 2% V, cracking activity was reduced to ~30%. The silica-rich matrix of the catalyst did not prevent zeolite destruction by the vanadium. CREY has a strong diffraction peak at $2\theta=23.8^\circ$. With 1% V, the original peak intensity was reduced by ~50%; with 2% V, evidence of crystallinity disappeared.

Results in Table 2 show the silica-rich catalyst's hydrothermal stability (50/50% nitrogen-steam for 10 h at 730°C) and carbon selectivity. Even after steaming at 815°C for 5 h with 95% steam the catalyst was able to retain 90% of the cracking activity measured after aging with 50% steam. Steaming, however, affects the stability of vanadium-contaminated catalysts. In fact, after aging with 95% steam (10 h at 730°C) microspheres with 0.5% V retained ~70% of their initial activity; with 0.75% V, they became inactive. X-ray diffractograms showing crystallinity losses due to vanadium loadings are given in Figure 9.

Without metals, the steam-aged catalyst had 177.8 m²/g BET surface area, 0.19 cc/g nitrogen pore volume, and an average pore radius of 21.2 Å. In Figure 10 its carbon selectivity is represented as the weight of carbon by-product per volume percentage of conversion. This value is plotted as a function of conversion to show that for conversion levels in the 65 to 80% range, the silica-rich catalyst generates lower coke yields than the commercial cracking catalysts tested.

The use of acid-leached calcined kaolin has little effect on a fresh catalyst (with ~15% CREY) activity, but it may increase gasoline yields, see Table 3. The catalyst exhibits improved resistance to metals deactivation when it contains an acid-leached calcined kaolin mineral (with SiO₂/Al₂O₃ = 2.6) instead of untreated kaolin. The acid treatment removes aluminum and establishes octahedral vacancies in the mineral lattice. These "holes" could host metals like Ni and V and negate their deleterious effects on cracking activity and product selectivities. The catalyst's low carbon generation has probably been enhanced by its silica-rich matrix's ability to form inert nickel silicates. Nickel passivation, due to silicates formation, has been previously postulated by Meisenheimer (20) for amorphous (silica-alumina) cracking catalysts.

REFERENCES

1. F. Ciapetta and D. Henderson, *Oil and Gas Journal*, 65, 88 (1967).
2. B. R. Mitchell, *Ind. Eng. Chem. Prod. Res. Dev.*, 19, 209 (1980).
3. J. S. Magee and J. J. Blazek, "Zeolite Chemistry and Catalysis," ACS Monograph #171, J. A. Rabo, Ed., 615 (1976).
4. C. P. Reeg, NPRA Annual Meeting, AS82-3, 1 (1982).
5. C. P. Carter, *Hydro. Proc.*, 96 (1981).
6. J. S. Magee, "Adv. in Cat. Chem., II Symposium," Salt Lake City, Utah (1982).
7. J. R. Murphy and A. K. Logwinuk, NPRA Annual Meeting, AMS1-29, 11 (1981).
8. R. E. Ritter et al., NPRA Annual Meeting, AM81-44, 1-4 (1981).
9. R. E. Ritter et al., *Oil and Gas Journal*, 103 (1981).
10. R. N. Cimbalò et al., *Oil and Gas Journal*, 112 (1972).
11. J. G. Sikonia et al., *Oil and Gas Journal*, 141 (1981).
12. A. English and D. C. Kowalczyk, *Oil and Gas Journal* (1984), to be submitted.
13. J. R. Murphy in "Sym. Prod., Character., Process of Heavy Oils, etc.," University of Utah, 5 (1981).

14. J. W. Gall et al., NPRA Annual Meeting, AM82-50, 5 (1982).
15. D. L. McKay and B. J. Bertus, "Symp. on Advances in Petr. Proc.," Div. of Petr. Chemistry Preprints 24, 2, 645 (1979).
16. C. H. Elliot, Jr., U.S. Patent No. 3,867,308 (1975).
17. J. J. Ostermaier and C. H. Elliot, Jr., U.S. Patent No. 3,957,689 (1976).
18. T. V. Flaherty, Jr., et al., U.S. Patent No. 4,126,579 (1978).
19. M. A. Seese et al., U.S. Patent No. 4,226,743 (1980).
20. R. G. Meisenheimer, J. Cat., 1, 356 (1962).

WPC#4082

Table 1. Kuwait gas oil inspections.

Gravity, API	23.5
Viscosity, 130°F	94.7
Viscosity, 150°F	70.5
Viscosity, 210°F	50.8
Pour Point, °F	+80
Nitrogen, wt%	0.074
Sulfur, wt%	2.76
Carbon, Res., wt%	0.23
Bromine No.	5.71
Aniline Point, °F	176.5
Nickel, ppm	<0.1
Vanadium, ppm	<0.1
Distillation, at 760 mm	
End Point, °C	426
5 Pct. Cond.	263
Approx. Hydrocarbon Type Analysis: vol%	
Carbon as Aromatics	23.1
Carbon as Naphthenes	10.5
Carbon as Paraffins	66.3

Table 2. Hydrothermal stability data of a SiO₂-rich cracking catalyst containing ~22% CREY. Steaming was performed with a 50-50% steam-nitrogen mixtures at 1 atm for 10 h.

	<u>Steaming Temperature (°C)</u>		
	<u>730</u>	<u>760</u>	<u>790</u>
Conversion (V%ff)	81.26	80.06	76.03
Gasoline (V%ff)	52.83	54.92	52.45
Hydrogen (wt%ff)	0.03	0.02	0.02
Carbon (wt%ff)	3.99	3.56	3.20

Table 3. Effects of an acid-leached kaolin mineral on the metals resistance of a FCC containing ~15% CREY. Test conditions: T = 480°C, Kuwait G0; aging with 50% steam for 10 h at 730°C.

Kaolin (SiO ₂ /Al ₂ O ₃)	2.6	2.6	2.0	2.0
Metals (Ni-Equiv.)	0	3000	0.0	3000
Conversion (V%ff)	72.2	62.9	72.9	51.0
Gasoline (V%ff)	52.1	42.5	50.2	32.9
Hydrogen (wt%ff)	0.05	0.50	0.03	0.44
Carbon (wt%ff)	2.78	2.94	2.46	3.04

Figure 1 Cracking Activity

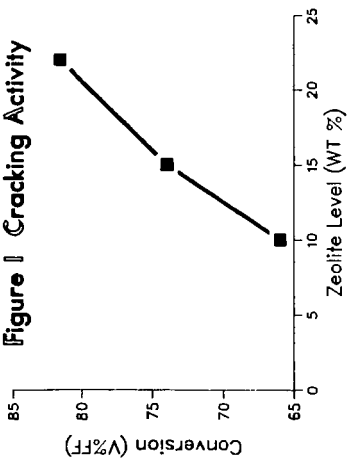


Figure 3 Hydrogen Yields

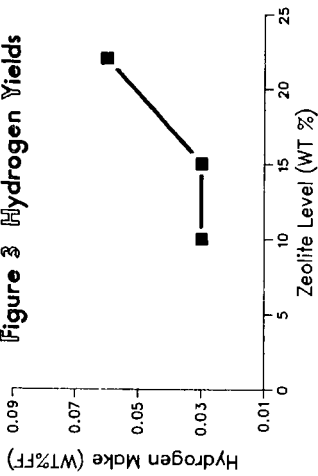


Figure 2 Gasoline Yields

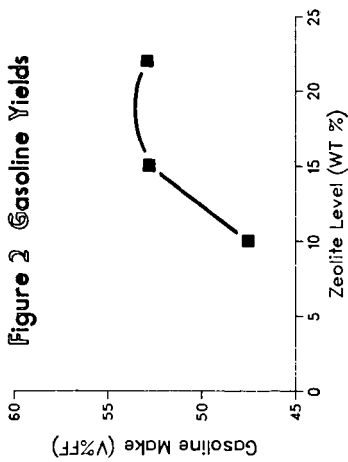


Figure 4 Carbon Yields

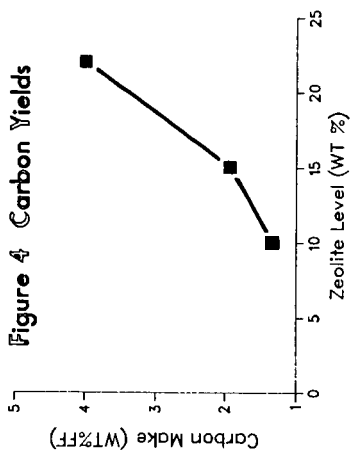


Figure 5 Metal (Ni + V) Effects on Catalyst Activity

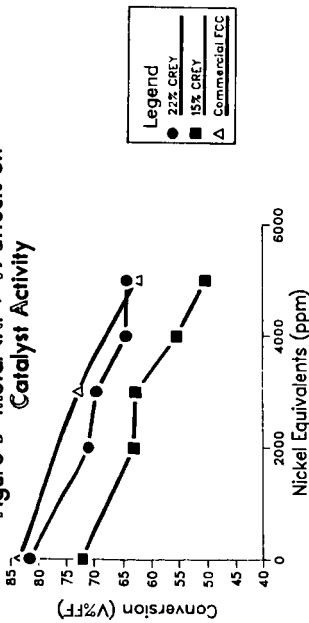


Figure 7 Metal (Ni + V) Effects on Hydrogen Make

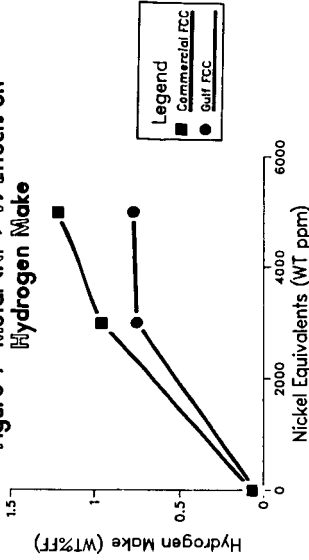


Figure 6 Metal (Ni + V) Effects on Gasoline Generation

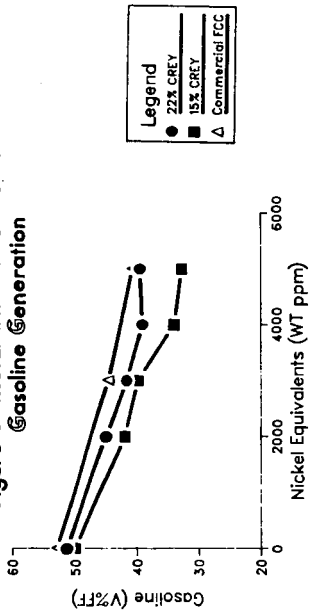


Figure 8 Metal (Ni + V) Effects on Carbon Make

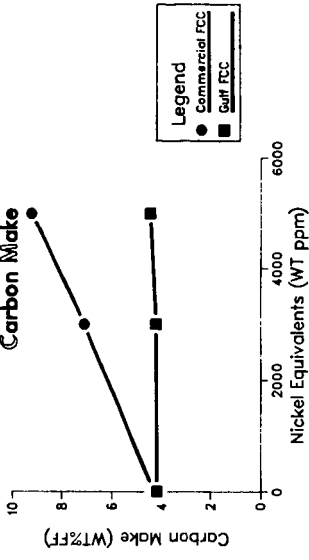


FIGURE 9:

X-RAY DIFFRACTOGRAMS SHOWING VANADIUM EFFECTS ON CRYSTALLINITY. CATALYSTS WERE STEAMED FOR 10h AT 730°C, WITH 95% STEAM AT 1atm.

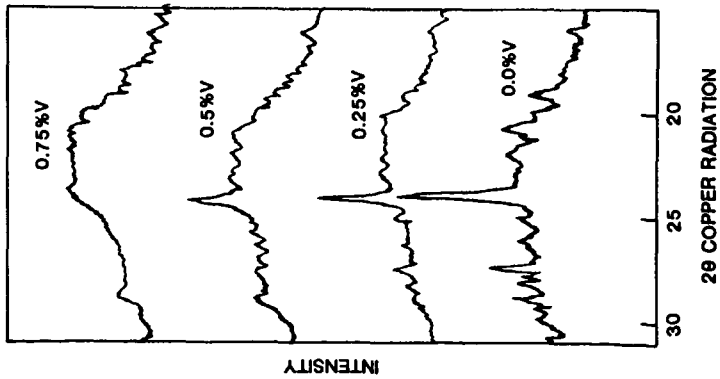
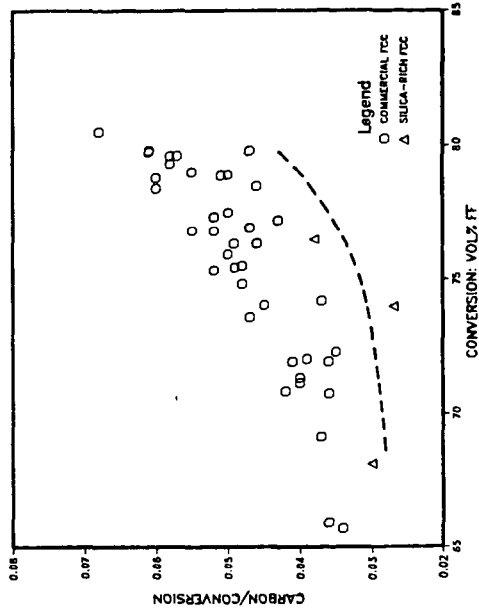


FIGURE 10
GULF SILICA-RICH FCC CATALYST
MAT CARBON SELECTIVITY



HYDROCRACKING WITH PILLARED CLAYS

Mario L. Occelli* and Raymond J. Rennard
Gulf Research & Development Company
P.O. Drawer 2038
Pittsburgh, PA 15230

ABSTRACT

Pillared bentonites have been prepared by ion-exchanging the clay charge compensating cations with zirconyl-aluminum halohydroxy complexes $(ZrOCl_2 \cdot Al_8(OH)_{20})^{+4}$, hydroxyaluminum oligomers $[Al_{13}O_4(OH)_{24}(H_2O)_{12}]^{+7}$ and colloidal silica. These interlayered clays have 250-320 m^2/g BET surface area, 0.15-0.22 cc/g pore volume, and pore height between 6 and 9 Å; thermal stability (in air, 10 h) is limited to 550°C. After a mild thermal pretreatment at 400°C in air, their cracking activity for gas oil conversion was related to the clay cations in the following manner: $Ca \ll (Si, Al) < (Zr, Al) < Al$.

Pillared clays were evaluated for use both as a cracking component and a hydrogenation component (Ni and Mo) support for the hydrocracking of an Agha Jari vacuum gas oil (VGO) in a combined hydrodenitrogenation-hydrocracking (HDN-HC) upgrading reactor. When used as the hydrocracking component with an Al_2O_3 hydrogenation support, catalyst activity was: Ca-bentonite < (Al,Zr)-bentonite < ACH-bentonite < HY zeolite. When used as the hydrogenation component support with 30 wt% HY zeolite as the cracking component, the activity order was Al_2O_3 < (Al,Zr)-Bentonite < (Si-Al)-Bentonite < ACH-bentonite. Pillared bentonites based hydrotreating catalysts showed superior selectivity to middle distillates.

INTRODUCTION

Bentonites pillared with oxoaluminum cations are characterized by an open, two-dimensional pore structure which behaves like a strong Lewis acid and allows sorption and transport of branched aromatics and normal paraffins.⁽¹⁻³⁾ Mesitylene diffusion in a pillared Na-bentonite is twice as fast as in Na-Y zeolite⁽⁴⁾ and is characterized by an apparent energy of activation (6.4 kcal/mole) similar to that observed for the transport of 1,3,5-triisopropylcyclohexane in NaY. C_5 - C_{10} normal paraffin equilibrium loadings resemble those observed in Mobils' ZSM-5; diffusion coefficients are, in general, significantly greater than those measured in zeolites.⁽³⁾ Therefore, pillared clays could find utility as catalysts for converting high molecular weight hydrocarbons like those found in heavy oils.^(5,6)

After mild steam deactivation, pillared clays exhibit cracking activity for gas oils conversion comparable to that of commercial cracking catalysts containing 15 to 25% zeolite, but they generate two to three times as much coke in the 60-80% conversion range.^(5,7) Coking experiments have shown that catalytic coke may not be the main cause of catalyst deactivation during gas oil conversion. Coking

* To whom all correspondence should be addressed.

has been attributed primarily to hydrocarbon occlusion and thermal degradation within the pillared clay microspace.⁽⁸⁾

The following paper reports the effects of using pillared clays as cracking components or as a metals support component in composite hydrogenation-hydrocracking vacuum gas oil catalysts.

EXPERIMENTAL

Pillared Clays Preparation

Pillared clays were prepared with a bentonite sample obtained from the American Colloid Company; its chemical composition is shown in Table 1. The aluminum chloro-hydroxide (ACH) solution containing the $(Al_{13}O_4(OH)_{24}(HO)_{12})^{+7}$ cation and the solution containing the $(Al_8(OH)_{20}ZrO)^{+6}$ complex (RETZEL-36G) were obtained from the Reheis Chemical Company. Colloidal silica, with a SiO_2/Al_2O_3 ratio of 16, was provided by NALCO Chemicals. These solutions were added to a 20-L slurry containing 100 g of bentonite. After stirring the slurry for 1-2 h at 65°C the clay was filtered and then reslurried in 5 L of distilled water (at 65°C) to remove excess reactants. After a second filtration and wash, the clay was dried at 120°C, crushed, and sized to <100 mesh and then used for hydrotreating catalysts preparation. X-ray diffractograms of these pillared clays are shown in Figure 1; their composition is given in Table 1.

Catalyst Forming

Two forming methods were employed. When the clay was used as the cracking component, a Harshaw Al-4100P alumina hydrate powder was calcined at 400°C and then loaded with 4% Ni-14% Mo via a one-step, co-impregnation with nickel nitrate-ammonium paramolybdate solution. The oven-dried impregnated alumina was then mix-mulled with the clay, peptized with 1% nitric acid, and extruded. The extrudates were oven-dried overnight at 120°C and then calcined at 450°C for 18 h. The composition of the finished catalysts were by weight, 70% (4 Ni-14 Mo/ Al_2O_3) + 30% clay.

When clays were used as metals support, the pillared bentonite was calcined at 400°C and then loaded with 4 Ni-14% Mo by weight using the same one-step procedure described above. The oven-dried, metals-loaded clay was then mix-mulled with ammonium Y zeolite, peptized with 1% nitric acid, and extruded. The extrudates were heat-treated as before; their composition (in wt%) were 70% (4 Ni-14 Mo/clay) + 30% HY. The ammonium Y zeolite was prepared by NH_4^+ -exchanging Linde NaY until the residual sodium level was less than 0.5%.

Catalyst Testing

Pillared bentonite cracking activity was evaluated by a microactivity test similar to the one described by Ciapetta and Anderson.⁽⁹⁾ Test conditions as well as chargestock inspections are described elsewhere.⁽⁷⁾ Before testing, catalysts were heated (in dry air) at 400°C for 10 h. Percent conversion is defined as: $(V_f - V_p) / 100 V_f$ where V_f is the volume of the fresh feed (FF) and V_p is the volume of product boiling above 204°C.

HDN-HC runs were conducted in an externally heated 1.43 cm ID by 122 cm stainless steel, down flow, trickle bed reactor. A 0.48 cm OD concentric thermowell running the length of the reactor was used to monitor temperatures in the reactor zones. For all runs a 75 mL catalyst bed was employed. The top 35 mL of catalyst was a commercially available Nalco NM-504 hydrotreating catalyst. The bottom 35 mL of the bed was loaded with the experimental composite hydrocracking catalyst to be evaluated. No product separation was carried out between catalyst beds. Both catalysts were sized to 16x40 mesh and presulfided in situ at 204°C and 35 psig for 6 h with 56 L/h of a 92% hydrogen-8% hydrogen sulfide gas blend.

An Agha Jari VGO containing 1500 ppm organic nitrogen and 1.2% sulfur was the feed for all runs. The reaction conditions in Table 2 were chosen to allow the hydrotreating catalyst to reduce the feed organic nitrogen and sulfur levels to <50 ppm and <0.2%, respectively; reactor configuration is shown in Figure 2. Hydrocracking test runs were 34 h in duration, with a 2-h off-stream period and five, 3 h on-stream periods at each temperature. Analyses were performed on products collected from the last on-stream period.

RESULTS AND DISCUSSION

Exchange reactions of Ca-bentonite with polynuclear cations generate molecular sieve-like materials stable to 500-600°C with 250-320 m²/g surface area and 0.15-0.22 cc/g pore volume (Tables 1 and 3). This microspace is attributed to the pillaring induced by stable oxide clusters formed by dehydroxylating the inter-layering cations. As in HY zeolites, pillared clays exhibit a narrow distribution of pore sizes with more than 85% of this area in pores with radius less than 10 Å, Table 3. At cracking conditions (400°C) in vacuo acidity in clays pillared with aluminum oxide clusters is mostly of the Lewis type; a Lewis/Bronsted (L/B) acid sites ratio of four has been found.⁽⁶⁾ In HY, a L/B ratio of 0.6 has been estimated from literature data.⁽⁶⁾ In powder form (100 x 325 mesh granules) pillared bentonites have (after aging in air at 400°C/10 h) cracking activity for gas oil conversion similar to that of HY (Table 4). The ranking is as follows:

Ca-Bentonite << (Si,Al)Bentonite < (Zr,Al)Bentonite < ACH-Bentonite < HY

However, the HY zeolite retains useful cracking activity even after a hydrothermal (10 h at 730°C with 95% steam at 1 atm) aging period, whereas pillared clays do not.

To isolate the two catalysts contribution to the overall HDN-HC activity, blank runs were performed with the composite catalyst bed replaced with 37.5 mL of inert, fired quartz chips. Results in Table 5 show the ability of the commercial hydrotreating catalyst (Nalco NM-504) for sulfur and nitrogen removal. The decrease of the 360°C⁺ fraction with temperature indicate its activity for hydrocarbon cracking; therefore, conversion over the combined HDN-HC catalyst at each temperature is expressed as,

$$CON = 100 \times (TGO^B - TGO^R) / TGO^B,$$

where TGO^B and TGO^R are the 360°C⁺ content of the blank and run product, respectively.

Three clays (Ca-bentonite, ACH-bentonite, and (Al,Zr) bentonite) were tested, along with HY, as cracking components in composite catalysts containing 70% alumina loaded with 14% Mo and 4% Ni. Results in Table 6 show that bentonite pillared with Al_2O_3 -clusters (ACH-bentonite) is the most active clay for VGO cracking; at 400°C it is significantly less active than the HY-containing catalyst. While the relative ranking of the catalysts in terms of activity is the same as that observed in cracking gas oils, the hydrocracking activity differences between pillared clays and HY zeolite are much more pronounced. At 415°C this difference is even more evident (see Table 6). In fact, while the activity of the zeolite-containing catalyst increases to 98.3% (up from 48.2% at 400°C), the activity of the ACH-bentonite containing catalyst remained unchanged at 31-32%. Rapid deactivation due to hydrocarbons occlusion and coking, is believed responsible for the pillared clays apparent low hydrocracking activity (see Table 6).

ACH-bentonite (Si,Al)-Bentonite and (Al,Zr)-Bentonite were used as metal (14% Mo + 4% Ni) support in composite catalysts promoted with 30% HY for hydrocracking activity. A similar catalyst containing metal-loaded alumina (and 30% HY) was used as reference material. Results in Table 7 indicate the greater activity of the pillared clays containing catalysts and their selectivity with respect to light furnace oil (LFO) generation. The rapid deactivation previously observed was not evident in these runs. Metal loading the pillared clays may have reduced their acidity and minimized coke formation. (Al,Zr) pillared bentonite has greater cracking activity than (Si,Al) bentonite (Table 4). The higher hydrocracking activity of the (Si,Al) bentonite composite catalyst with respect to the one containing (Zr,Al) Bentonite (see Table 7) is due to the different surface area of these pillared clays (Table 3). As expected, the ACH-bentonite containing catalyst was most active. At 400°C conversion was 70% and generated a liquid containing 37.7% LFO. The selectivity of these clays for LFO production during VGO hydrocracking can be attributed to the pillared clay microporous structure, which appears to control the cleavage of high molecular weight hydrocarbons and retards further cracking to lighter fractions.

CONCLUSION

Because of rapid deactivation due to excessive coke formation, pillared clays are ineffective when used as the cracking component in composite hydrocracking catalysts. When used as metals supports in composite catalysts containing zeolites, the pillared clays show excellent hydrocracking activity and selectivity to light furnace oil. This is probably due to the moderation of their acidity resulting from the addition of hydrogenation metals like Mo and Ni and to the open microstructure resulting from pillaring.

REFERENCES

1. D. E. W. Vaughan and R. J. Lussier, "Preparation of Molecular Sieves Based on Pillared Interlayered Clays (PILC)," Proc. 5th Inter. Conf. Zeolites," L. V. Rees, Ed., Heyden, London 1980, 94.
2. M. L. Occelli, and R. M. Tindwa, "Physicochemical Properties of Montmorillonite Interlayered with Cationic Oxyaluminum Pillars," Clays and Clay Minerals 1983, 31, 1, 22.

3. M. L. Occelli, V. Parulekar, and J. W. Hightower, Proc. 8th Inter. Congress Catalysis, Berlin (1984), in press.
4. M. L. Occelli, R. A. Innes, F. S. S. Hwu, and J. W. Hightower, "Catalytic Activity of Sodium-Montmorillonite Interlayered with Aluminum Oxide Clusters," J. Applied Catalysis 1984, Submitted.
5. D. E. W. Vaughan, R. J. Lussier, and J. S. Magee (1970), U.S. Patent No. 4, 175,090.
6. D. E. W. Vaughan, R. J. Lussier, and J. S. Magee (1981), U.S. Patent No. 4, 248,739.
7. M. L. Occelli, I&EC Prod. Res. Dev. Journal 1983, 22, 4 (1983), p. 553.
8. M. L. Occelli and J. E. Lester, I&EC Prod. Res. Dev. Journal (1984), Submitted.
9. F. G. Ciapetta and D. Anderson, Oil and Gas J., 65 (1967), 88.

FIGURE 1:

X-RAY DIFFRACTOGRAMS OF (a) BENTONITE BEFORE AND AFTER PILLARING WITH (b) Al (c) Al AND Zr (d) Al AND Si OXIDE CLUSTERS. CLAYS WERE HEATED FOR 10H AT 300°C IN AIR

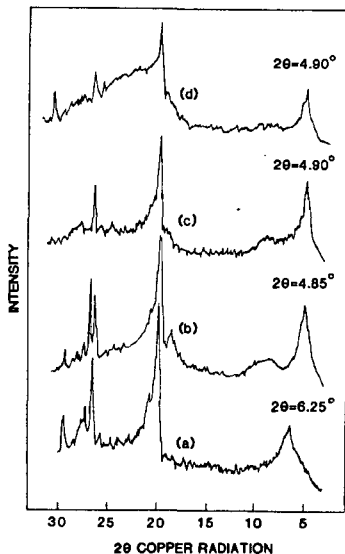


Figure 2

HDN-HC REACTOR CONFIGURATION

o
T C = 380-415
LHSV = 1.0
PSIG = 2000
H₂, scf/bbl = 6000
2
FEED = AGHA JARI VGD
S, wt% = 1.75
N, ppm = 1500
o
API = 23.1

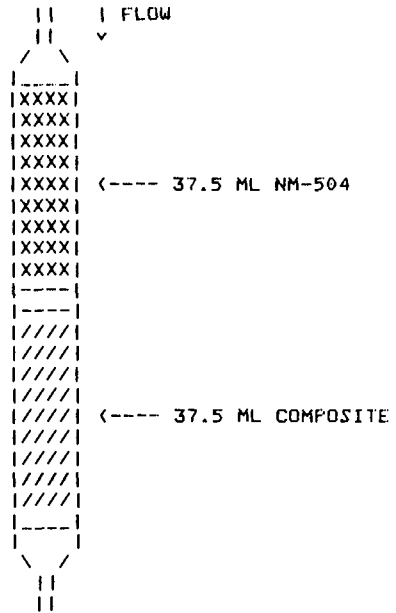


Table 1. Bentonite composition before and after pillaring (Galbraith Laboratories Data).

	Oxides Composition (Wt%)			
	Calcium Bentonite	ACH- Bentonite	(Zr-Al) Bentonite	(Si-Al) Bentonite
SiO ₂	62.9	55.9	55.3	78.1
Al ₂ O ₃	20.0	31.6	25.8	13.9
Na ₂ O	0.53	0.67	0.50	0.35
K ₂ O	2.32	0.37	0.35	0.20
MgO	2.16	1.55	1.58	0.90
CaO	2.58	0.43	0.24	0.48
Fe ₂ O ₃	4.38	3.59	3.60	1.8
ZrO ₂	--	-	6.1	--

Table 2. Hydrotreating-hydrocracking run conditions.

Feedstock	Agha Jari V60
Gravity, °API	23.1
Sulfur, wt%	1.75
Nitrogen, ppm	1500
Temperature, °C	390-415
Pressure, kpa (psig)	13,891 (2000)
Catalyst Volume, mL	37.5 Hydrotreating 37.5 Hydrocracking
Catalyst Bed Length, cm	52.8
LHVS, h ⁻¹	1.0
Feed Volume, mL/h	75
Hydrogen/Oil, m ³ /m ³ (scf/bbl)	1069 (6000)

Table 3. Pillared clays surface properties after heating in dry air at 400°C/10 h and sizing to 100x325 mesh granules.

	<u>ACH-</u> <u>Bentonite</u>	<u>(Zr,Al)</u> <u>Bentonite</u>	<u>(Si,Al)</u> <u>Bentonite</u>	<u>Calcium</u> <u>Bentonite</u>	<u>HY</u> <u>Linde</u>
BET Surface Area (m ² /g)	255.0	254.0	303.5	46.6	508
Pore volume (cc/g)	0.16	0.17	0.21	0.08	0.32
Pore Volume Distribution					
Area % in Pores with Radius					
< 10 Å	88.0	90.0	87.8	25.2	94.9
10 < R < 20 Å	9.4	7.1	8.6	36.1	2.3
20 < R < 100 Å	2.4	2.4	3.2	29.1	1.4
> 100 Å	0.2	0.5	0.4	9.6	1.4

Table 4. Cracking activity for gas oil conversion before and after pillaring. Clays were heated at 400°C/10 h in dry air and sized to 100 x 325 mesh before testing.

	<u>Calcium</u> <u>Bentonite</u>	<u>ACH-</u> <u>Bentonite</u>	<u>(Zr,Al)</u> <u>Bentonite</u>	<u>(Si,Al)</u> <u>Bentonite</u>
Conversion (V% ff)	28.4	82.1	73.8	67.9
Gasoline (V% ff)	16.7	59.8	55.6	51.5
Furnace Oil (V% ff)	30.3	13.6	19.0	22.3
Slurry Oil (V% ff)	41.6	4.2	7.2	9.8
Hydrogen (wt% ff)	0.75	0.24	0.21	0.28
Carbon (wt% ff)	7.8	12.2	9.6	7.48

Table 5. HDN-HC blank runs.

<u>Component</u>	<u>T°C</u>	<u>% NAP</u>	<u>% KER</u>	<u>% LFO</u>	<u>% TGO</u>	<u>°API</u>	<u>% CON</u>	<u>% S</u>	<u>ppm N</u>
Quartz	380	0.9	3.5	15.6	83.4	28.3	0	0.0	50
Quartz	390	1.6	3.9	16.9	81.5	32.3	0	0.0	30
Quartz	400	3.3	7.8	24.1	72.6	31.2	0	0.0	<20
Quartz	415	6.6	13.5	32.2	61.2	33.3	0	0.0	<10

Table 6. HDC-HC with pillared clays as cracking component.

<u>Cracking Component</u>	<u>Reactor</u>		<u>Liquid Composition*</u>				
	<u>T°C</u>	<u>% NAP</u>	<u>% KER</u>	<u>% LFO</u>	<u>% TGO</u>	<u>°API</u>	<u>% CON</u>
HY Zeolite	400	28.0	29.5	34.4	37.6	41.3	48.2
	415	80.0	34.1	18.1	1.0	54.1	98.3
ACH-Bentonite	400	11.6	21.9	39.0	49.5	36.5	31.8
	415	14.2	26.8	43.9	41.9	37.9	31.5
(Al,Zr) Bentonite	400	9.2	14.9	31.2	59.7	34.6	17.8
	415	11.8	19.0	36.6	51.7	36.2	15.5
Ca-Bentonite	400	6.6	14.3	32.7	60.6	34.4	16.5
	415	11.6	21.7	41.4	47.0	36.6	23.2

NAP = Naptha (OP-154°C)

LFO = Light Furnace Oil (190-360°C)

KER = Kerosene (190-271°C)

TGO = Total Gas Oil (360°C+)

Table 7. HDN-HC with clays as hydrogenation component support at 400°C.

Support	Reactor T°C	Liquid Composition*					
		% NAP	% KER	% LFO	% TGO	°API	% CON
Alumina	390	13.1	17.5	28.4	58.6	35.4	28.1
	400	28.0	29.5	34.4	37.6	41.3	48.2
(Al,Zr) Bentonite	390	14.6	25.2	34.6	50.8	36.0	37.7
	400	27.2	32.0	36.4	36.4	40.5	49.9
(Si-Al) Bentonite	390	21.4	26.9	36.7	41.9	39.5	48.6
	400	34.5	30.5	35.8	39.6	42.9	59.2
ACH-Bentonite	390	20.3	34.6	43.4	36.3	40.5	55.5
	400	40.6	35.7	37.7	21.7	45.0	70.1

(a) NAP = Naphtha (OP-154°C); (b) KER = Kerosene (190-271°C); (c) LFO = Light Furnace Oil (190-360°C); (d) TGO = Total Gas Oil (360°C+).

Table 8. HDN-HC with clays as hydrogenation component support at 390°C.

Component	T°C	% NAP	% KER	% LFO	% TGO	°API	% CON
Alumina	390	13.1	17.5	28.4	58.6	35.4	28.1
ACH-Bentonite	390	20.3	34.6	43.4	36.3	40.5	55.5
Si-Bentonite	390	21.4	26.9	36.7	41.9	39.5	48.6
Al,Zr-Bentonite	390	14.6	25.2	34.6	50.8	36.5	37.7

(a) NAP = Naphtha (OP-154°C); (b) KER = Kerosene (190-271°C); (c) LFO = Light Furnace Oil (190-360°C); (d) TGO = Total Gas Oil (360°C+).

CATALYTIC HYDROPROCESSING OF ACIDIC FRACTIONS
OF COAL LIQUID HEAVY DISTILLATE

by

D. W. Grandy and L. Petrakis

Gulf Research & Development Company
P.O. Drawer 2038
Pittsburgh, PA 15230

and

Cheng-lie Li and Bruce C. Gates

Department of Chemical Engineering
University of Delaware
Newark, DE 19711

Individual compound and molecular class kinetics were determined for the catalytic hydrodeoxygenation of coal liquid acid fractions. The coal liquid acidic fractions were prepared from a coal liquid heavy distillate, derived from Powhatan #5 coal, by ion exchange chromatography(1). A commercial sulfided Ni-Mo/ γ -Al₂O₃ catalyst was used to hydrotreat the coal liquid acids which were fed through a microreactor as a 0.25 wt% solution in cyclohexane. The coal acid feeds and hydrotreated products were separated by capillary column gas chromatography and detected by either standard FID techniques or by mass spectrometry. Upon hydrotreating, the product chromatograms (Figure 1) show a large increase in the number of compounds relative to the feed (Figure 2) and a shift to lower boiling range. This change in the chromatogram, and the change in carbon number distribution in the product molecules demonstrates that cracking as well as hydrogenation is taking place. Since many of the feed and product compounds could only be identified by their empirical formula, the results of the catalytic hydrotreating of the acidic fractions can be described in terms of carbon number classes and classes which denote the degree of saturation of the compounds. The carbon number data show evidence of cracking, while the Z numbers, which indicate the degree of saturation, show that compounds of the biphenyl class decrease in relative concentration with increased inverse space velocity; and compounds of the tetralin, indane, and cyclohexylbenzene class show an increase in relative concentration with increased inverse space velocity. Tables I and II list the compound classes identified in the feed and hydrodeoxygenated product of the very

weak and weak acids, respectively. The formation of most of the product molecules can be rationalized using the pure compound hydroprocessing data on cyclohexyl phenol; phenyl phenol(2) and naphthol(3). The examination of the feed and products in terms of the lumps illustrates several points: 1. The feeds contain a relatively small number of major components which, upon hydrotreating, are reduced in concentration, forming many more product molecules. 2. In addition to the removal of the oxygen functionality typically occurring as in the hydroxyl group, there was significant ring hydrogenation. 3. There is evidence of cracking, both from the formation of compounds having fewer carbons than the feed compound and from shifts in carbon number distributions among the compounds existing in the feeds; this cracking is inferred to involve principally the methyl substituents bonded to rings(4).

The hydrodeoxygenation kinetics of tetrahydronaphthol, methyl-tetrahydronaphthol, phenylphenol, methylphenylphenol, dimethylindanol, and cyclohexylphenol are shown in Figure 3 in a plot of fraction of species unconverted vs. inverse weight hourly space velocity. Methyl substitution tends to increase the rate of disappearance of the parent compound, probably by providing an additional pathway for the change in molecular structure. Neither this observation, nor the order of reactivity in disappearance implies hydrodeoxygenation reactivity(5). Methyl groups may hinder heteroatom removal, in some cases, if they prevent easy access to the catalyst by steric hindrance.

1. L. Petrakis, R. G. Ruberto, and D. C. Young, Ind. Eng. Chem. Process Des. Dev. 22, 292 (1983).
2. S. Krishnamurthy, S. Panvelker, and Y. T. Shah, AIChE J. 27, 994 (1981).
3. C. L. Li, Z. R. Xu, Z. A. Cao, and B. C. Gates, Submitted for publication.
4. J. F. Patzer II, R. J. Ferrauto, A. A. Montagna, Ind. Eng. Chem. Process Des. Dev. 18, 625 (1979).
5. C. L. Li, S. S. Katti, B. C. Gates, and L. Petrakis, J. Cat. 85, 256 (1984).

Table I

Number of Compounds by Type in the Very Weak Acid
Feed and Hydrotreated Product

<u>Compound Type</u>	<u>Feed</u>	<u>Product^a</u>
Benzene	9	13
1-Ring Phenols	2	NF ^b
2-Ring Phenols	4	NF
Carbonyl Compounds ^c C-	8	NF
Ethers ^d , R-O-R	6	6
Nitrogen Compounds	6	1
3-Ring Aromatics	1	2
Cyclic Alkanes, Alkenes	NF	7
2-Ring Aromatics	NF	5
Fused Cycloalkyl Aromatics ^e	NF	15
Cycloalkyl Aromatics	NF	4

^a Obtained at a space velocity of 0.4 g of fraction/
(g of catalyst·h).

^b Not found.

^c Furanone is considered to be a carbonyl compound.

^d Ethers include methoxy, phenoxy, and furan.

^e Fused cycloalkyl aromatics include tetralin and indanes.

Table II

Number of Compounds by Type in the Weak Acid Feed
and Hydrotreated Product

<u>Compound Type</u>	<u>Feed</u>	<u>Product^a</u>
Benzenes	4	3
2-Ring Phenols	8	3
Carbonyl Compounds	1	NF ^b
Ethers	2	3
Nitrogen Compounds	2	NF
Cyclo- and Dicycloalkanes, Alkenes	NF	9
Fused Cycloalkylaromatics	NF	14
2-Ring Aromatics or ???	NF	5
3-Ring Aromatics	NF	3
Cycloalkylbenzenes	NF	3

^a Obtained at a space velocity of 0.78 g of fraction/
(g of catalyst·h).

^b Not found.

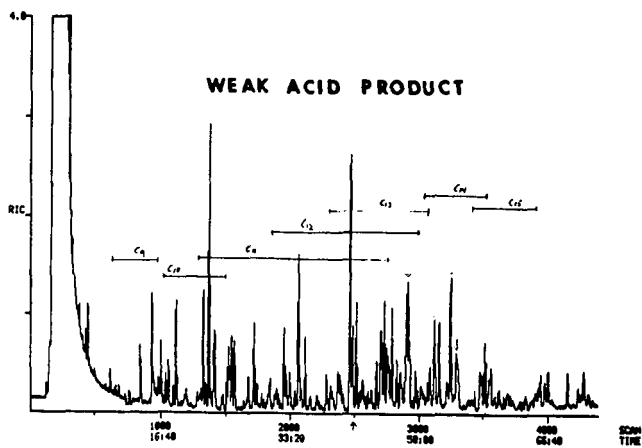


Figure 1

Weak Acid Product Ion Chromatogram

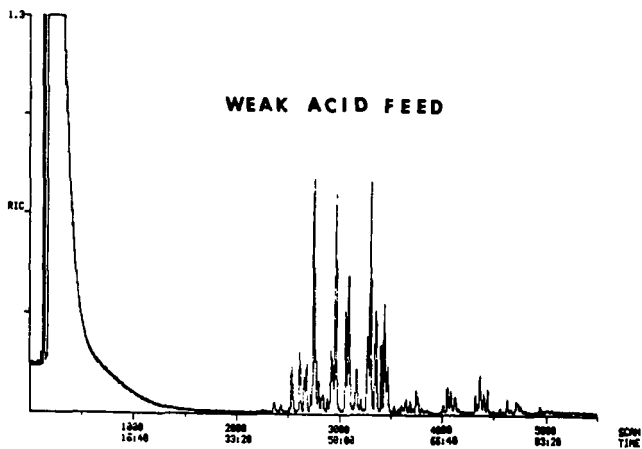


Figure 2

Weak Acid Feed Ion Chromatogram

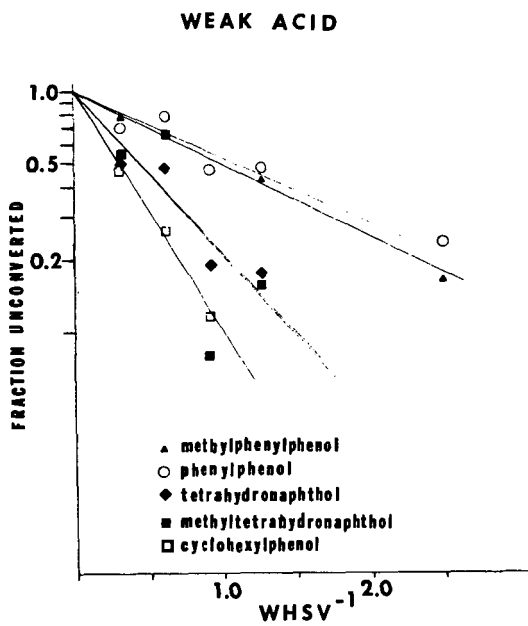


Figure 3

Fraction Unconverted vs. Inverse Space Velocity
Compounds in the Weak Acid

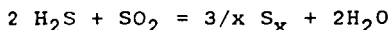
The Kinetics of the Reaction of Hydrogen Sulfide and Sulfur Dioxide in Organic Solvents

Dan W. Neumann and Scott Lynn

Department of Chemical Engineering
University of California
Berkeley, Ca. 94720

I. Introduction

Hydrogen sulfide is an undesirable component found in many industrial process streams. Traditionally its removal and recovery have been accomplished in an absorber-stripper operation, followed by the Claus process in which the H_2S is reacted over alumina catalyst with SO_2 obtained by burning a portion of the inlet stream. The gas-phase reaction to produce sulfur is



This reaction is equilibrium-limited to 95 to 97% conversion in 2 to 4 stages because the temperature must be kept above the dewpoint of sulfur. Additional processing must be provided to reduce the concentration of sulfurous compounds in the effluent to environmentally acceptable levels.

When the reaction between H_2S and SO_2 is carried out in organic liquids at temperatures below $150^{\circ}C$ it is irreversible and goes essentially to completion. In many organic solvents, such as triethylene glycol, dimethyl ether (Triglyme) and diethylene glycol, methyl ether (DGM), the reaction is impractically slow and, at room temperature, the sulfur formed is too finely divided to be readily separated. Urban (3) found that the presence of *N,N*-dimethyl aniline (DMA) increased the crystal size of the precipitated sulfur. Furthermore, DMA accelerates the reaction to the extent that 99+% removal of H_2S is possible with careful selection of the solvent mixture.

The present work was undertaken to study the reaction between H_2S and SO_2 in mixtures of DMA/Triglyme and DMA/DGM. Experiments performed by monitoring the temperature rise of this exothermic reaction in an adiabatic calorimeter show the effects of various solvent compositions on the kinetics of the reaction. Solvent selection criteria for an appropriate process scheme can then be set. This reaction system is suitable for application to a process currently being studied in this laboratory for the removal of hydrogen sulfide from industrial gas streams.

II. Experimental Methods

All rate measurements were made in a 50-ml Erlenmeyer flask that contained a magnetic stir bar and was sealed by a septum cap (see Figure 1). Insulation was provided by a styrofoam block with a hole drilled out for the reactor. Reaction progress was monitored by recording the temperature rise in the form of a millivolt potential produced by a bare, type J thermocouple connected to a chart recorder. A measured quantity of a solution of one reactant was first placed in the reaction vessel. The reaction was initiated when a measured quantity of a solution of

the second reactant at the same temperature was injected quickly into the stirred vessel by syringe.

III. Methods of Analysis

A. Acid-Base Experiments

Reactions between NaOH and HCl were carried out in the calorimeter to determine the rate of mixing, the thermal mass of the apparatus, and the rate of heat loss from the system. The experimental method was that used in the H₂S-SO₂ reactions and the quantities of reactants used gave similar temperature rises. Since the acid-base reaction is practically instantaneous, the time necessary for completion is the mixing time.

A heat balance applied to the apparatus and solution allows calculation of the thermal mass of the reactor. Furthermore, by measuring the decrease in temperature with time after the initial rise, the rate of heat loss from the system can be determined.

A chart recorder trace of thermocouple potential (i.e., temperature) versus time for an acid-base reaction is shown in Fig. 2. The estimated heat leakage from the reaction vessel and styrofoam block corresponds to a rate of temperature loss that is less than 0.002 °C/sec. Thus, there was a loss of about 0.02 °C over the course of a typical H₂S - SO₂ run. Since in the majority of experiments the temperature rise is 5 °C or less, this amounts to an uncertainty of about 0.4% in the maximum temperature.

The average value of t_{mix} is approximately 0.7 sec for the solution volumes of acid and base and stirrer speeds used in these experiments. Presumably, in cases where the reaction between H₂S and SO₂ takes longer than this period, the reaction is then occurring in a homogeneous solution.

From the known heat of reaction for $H^+ + OH^- (= -13.4$ kcal/mole of H₂O formed) and the heat capacity of the aqueous solutions (approximated as water, $C_p = 1$ Cal/g °C), the thermal mass of the apparatus was determined to be 0.6 cal/°C. Since in these experiments the thermal mass of the solution for a typical run was 12-15 cal/°C., the contribution of the apparatus to the total heat capacity of the system was small.

B. Kinetics

If the reaction between H₂S and SO₂ is first order in both reactants, then the differential rate equation for the disappearance of SO₂ or H₂S is

$$-dC_A/dt = -1/2 dC_B/dt = k_2 C_A C_B \quad 1)$$

By stoichiometry

$$C_B = C_B^0 - 2(C_A^0 - C_A) \quad 2)$$

in which the superscript 0 refers to time = 0. Substituting Eq. 2 into Eq. 1 and rearranging yields the following rate expression:

$$k_2 dt = dC_A / (C_A * (2C_A - 2C_A^0 + C_B^0)) \quad 3)$$

Integration of Eq. 3 and simplification gives

$$k_2 t = (1/(2C_A^0 - C_B^0)) \ln ((C_B^0/C_A^0) * (C_A/C_B)) \quad 4)$$

If a reaction is first order with respect to both A and B then a plot of the integrated rate expression on the right-hand side of Eq. 4 versus time should lie on a straight line with a slope of k_2 . Note that when the initial concentrations of H_2S and SO_2 are stoichiometrically equivalent, Eq. 4 reduces to the more familiar second-order relationship

$$k_2 t = 1/C_A^2 - 1/C_A^{02} \quad 5)$$

Equation 4 is in the form of concentration and time whereas the quantities measured experimentally are temperature and time. If the temperature rise for the exothermic reaction between H_2S and SO_2 is assumed to be proportional to the extent of reaction (i.e. ΔT is a measure of reaction progress) and if the maximum temperature corresponds to complete reaction (fraction conversion = 1.0) with any uncertainty arising from thermal losses, then for any time $t < t_{max}$ the concentration of the limiting component is related to the temperature rise by the expression

$$C = C^0 * (1 - \Delta T/\Delta T_m) \quad 6)$$

From this concentration and the known stoichiometry, the concentration of the other reactant can be calculated. In order to keep the uncertainty arising from thermal losses to a minimum, only temperature rises less than 90% of the maximum value are used for determining reaction-rate constants.

In the preceding analysis perfect mixing has been assumed. Since these experiments require the injection of one of the reactant solutions into the other, a finite period, whose length depends on the sample volumes, solvent viscosity, and stirrer speed, is needed to completely mix the components. Before mixing is complete, local inhomogeneities exist in which one of the reactants is in large excess. The other reactant is rapidly depleted, effectively reducing the reaction rate in these regions to zero. Overall, the experimentally measured rate is lowered and the kinetics of the reaction under such conditions is of uncertain significance. Once the solutions are thoroughly mixed, the rate becomes that for the homogeneous reaction. The rate constant can be determined from plots of the integrated rate expression (Eq. 4) versus time by considering only the portion of the plot for which the time is greater than the mixing time.

C. Heat of Reaction

The heat of reaction for each of the experiments is calculated from the measured temperature rise and the thermal properties of the system. An enthalpy balance yields

$$\Delta H_{rxn} = ((mC_p)_s + (mC_p)_{app}\Delta T)/1000 n_L \quad 7)$$

The heat capacity of the organic solution, which was assumed to include all solvents and products, was estimated by a group contribution method applied to the bulk solvent used in a given run. Calculations for Triglyme and DGM using Missenard's group contribution method (2) give a value of $C_p \sim 0.5 \text{ cal/g-}^\circ\text{C}$.

IV. Results and Discussion

A. Results for the Reaction of H_2S and SO_2 in Triglyme/DMA/ H_2O

Kinetic data were analyzed using equation Eq. 4. Plots of the concentration expression on the right side of Eq. 4 versus time yield a straight line (in the region $t > t_{mix}$) with a slope of value k_2 when the reaction follows second-order kinetics. Data pairs of potential/time obtained from the chart-recorder traces were converted into concentration/time pairs and plotted in the integrated rate form.

A sample plot for the reaction of H_2S and SO_2 in a DMA/Triglyme mixture is shown in Fig. 3. Values of k_2 were obtained from similar plots by drawing the best straight line through the data. The curvature at times less than 1 sec. results from the finite time required for injecting the SO_2 sample and mixing the solution. In nearly all of the runs the time intercept, as found by extrapolating the line drawn through the integrated rate data back to the time axis, is about 0.5 to 0.8 seconds. These values, which approximate the mixing time in the HCl - NaOH experiments, show little variation from run to run and thereby indicate a high degree of reproducibility in the experimental conditions and technique. Furthermore, since this result agrees with the mixing time obtained in the acid-base experiments, data points at longer times presumably represent the progress of the reaction in a well-mixed solution.

Most of the experiments presented here were performed with nearly stoichiometric equivalents of H_2S and SO_2 . Additional experiments were carried out with the ratio of H_2S to SO_2 varying from about 2:1 to 1:2. In all cases the second-order rate expression provided the best straight line fit to the data in spite of a four-fold change in SO_2 concentration. Attempts to analyze the data using a rate expression which is second order in H_2S and first order in SO_2 yielded non-linear integrated rate plots.

The results for the reaction in Triglyme with DMA and water present are summarized in Fig. 4, where the second-order rate constant is plotted as a function of wt% DMA for various H_2O concentrations. With pure Triglyme as the sole solvent, plots of the integrated rate expression versus time are non-linear, increasing in slope as time progresses. Tangents to these curves correspond to k_2 values of 0.5 lit/mole-s or lower. The curvature, which reflects an increase of the rate constant with time, may be due to an autocatalytic effect of water formed during the reaction or possibly to a change in the reaction mechanism. Note that while a mixture of water/Triglyme speeds the reaction, it is unclear whether the same reaction pathway is followed since some of the integrated rate plots are non-linear. Perhaps other products such as sulfoxy acids, which frequently form in aqueous media, are being created in these cases.

When DMA is added to Triglyme, the integrated rate plots become linear, i.e. there is a first - order dependence on both H_2S and SO_2 . Furthermore, there is a substantial increase in the rate when DMA is added to the Triglyme. Addition of only 2 wt% DMA more than doubles the reaction rate over that observed for Triglyme alone. Increasing the DMA concentration increases the rate constant, k_2 , which asymptotically approaches a value of 8 lit/mole-s.

The presence of water in DMA/Triglyme greatly accelerates the rate as evidenced in Fig.4. Addition of 4 to 5 wt% H₂O doubles the observed rate constant. Also, the value of k_2 for the mixed solvents exceeds the sum of those for the reaction carried out with only one of the catalysts (DMA or H₂O) present. This suggests a synergism between the effects of the water and DMA.

B. Results for the Reaction in DMA/DGM/Water

The kinetic behavior of the reaction in DGM alone is similar to that observed for Triglyme. DGM has little or no catalytic effect, and plots of the integrated rate expression exhibit an increase in rate with time. However, values for k_2 are considerably higher when a given wt% DMA is added to DGM than are those found in the Triglyme runs. The rate constants for the reaction of H₂S and SO₂ in DMA/DGM mixtures are shown in Fig. 5. The DGM also seems to have a catalytic effect on the reaction; increasing the DMA percentage toward pure DMA causes a noticeable decrease in rate as opposed to the monotonic increase observed in Triglyme mixtures. The maximum value of k_2 , which is approximately 20 lit/mole-s, is more than twice as large as that obtained in the Triglyme/DMA cases with no water present.

The addition of water to DMA/DGM mixtures has little or no effect on the rate, as is reflected in the data presented in Table 1. At 10 wt% DMA the rate constant has attained its maximum value and the addition of water does not increase the rate.

A few runs with 2.5 wt% DMA in DGM, performed at 7 to 10 °C, yielded an average k_2 of 4.5 lit/mole-s (see Table 2). On the basis of these data and those in Fig. 5, the estimated activation energy is 7.4 kcal/mole, which corresponds to a doubling of the rate every 20 °C.

C. Results for the Reaction in DMA/Triglyme/Methanol

A reasonable hypothesis to explain the fact that both H₂O and DGM accelerate the reaction between H₂S and SO₂ in the presence of DMA is that the hydroxyl group is exerting a positive catalytic effect. In order to further substantiate this idea, a few experiments were performed in which methanol was added to DMA/Triglyme. The data are summarized in Table 3. The presence of the indicated methanol concentration increased the rate constant by a factor of 6 over that for the same concentration of DMA alone in Triglyme. As in the DMA/Triglyme/Water runs, adding methanol to the mixture enhances the observed reaction rate. Also, the rate constant for this mixture, which contains an eight-to-one mole ratio of methanol to DMA, is about the same as the value of k_2 for the same molar ratio of DGM to DMA. Thus, for cases in which the same ratio of hydroxyl groups to DMA is used, similar effects on the reaction kinetics might be expected.

D. Heat of Reaction

The heat of reaction between H₂S and SO₂, taken as the average for a large number of data points, is 28 to 29 kcal/mole of SO₂ reacted. This value seems to apply equally well to all mixtures of the solvents used in these experiments. Evidently, effects such as heats of solution are small or similar in magnitude for the range of cases considered.

E. Summary

From these experimental results it is readily apparent that the presence of DMA greatly accelerates the reaction of H_2S and SO_2 in organic solvents. The nitrogen of the amine, which is noted for its ability to form complexes with sulfur dioxide (1), presumably provides a favorable site at which the reaction can occur. This effect seems to be dependent on the concentration of the catalytic agent rather than its ratio to either of the reacting components, since the mole ratio of DMA to SO_2 exceeds one at less than 1 wt% DMA in most of the experiments. This suggests that the enhancement is related to the accessibility of sites rather than the actual number present. In the DMA/Triglyme experiments the rate constant increases with increasing DMA, implying that the Triglyme has little or no catalytic effect and actually reduces the rate by diluting the concentration of useful reaction sites.

For the reaction in DGM an additional factor is found to be important. The DGM appears to work with DMA in accelerating the reaction, producing a maximum rate when intermediate concentrations of both solvents are present. This enhancement seems to be related to a catalytic effect of the OH group of the DGM that is synergistic with DMA. Further evidence of the OH effect can be seen in the results for the reaction in DMA/Triglyme with water present; indeed this effect may be expected for alcohols in general since the experiments performed with DMA/ Triglyme/Methanol yielded similar results. Determination of whether the hydroxyl provides an alternate reaction site or speeds an intermediate or parallel step or causes some other enhancement will require further investigation. It is clear however, that mixtures of DMA with glycol mono ethers are good solvents for the catalysis of the reaction between H_2S and SO_2 to form sulfur.

Acknowledgement

This work was supported by the Morgantown Energy Technology Center, Assistant Secretary for Fossil Energy, Office of Coal Utilization, Advanced Research and Technology Development, Division of Surface Coal Gasification, through the US Department of Energy under Contract No. DE-AC03-76SF00098.

References

1. Hill, Arthur E., and Thomas B. Fitzgerald, "The Compounds of Sulfur Dioxide with Various Amines," J. of Am. Chem. Soc., 57, 250 (1935).
2. Reid, Robert C. , John M. Prausnitz, and Thomas K. Sherwood, "The Properties of Gases and Liquids", McGraw-Hill, NY, (1977).
3. Urban, Peter, "Production of Sulfur," U.S. Patent #2,987,379 (June 1961).

Notation

- C_A, C_B = Concentration of SO_2 and H_2S at time t (mole/lit)
 C_A^0, C_B^0 = Concentration of SO_2 and H_2S at time 0 (mole/lit)
 ΔH_{rxn} = Heat of reaction (kcal/mole)
 k_2 = Second-Order Rate Constant (lit/mole-s)
 $(mC_p)_s$ = Thermal mass of solution (cal/°C)
 $(mC_p)_{app}$ = Thermal mass of apparatus (cal/°C)
 n_L = Moles of limiting reactant
 t = time (sec)
 $\Delta T, \Delta T_m$ = Temp. change and maximum temp. change (°C)

Table 1
Rate Constants for the Reaction of H_2S and SO_2 in
DMA/DGM with Water Added

Wt% H_2O	Wt% DMA	k_2 (lit/mole-s)
0.5	9.8	20.4
0.5	9.8	21.6
1.4	9.7	22.8
1.6	9.7	22.1
2.4	9.6	21.3
2.6	9.6	23.5

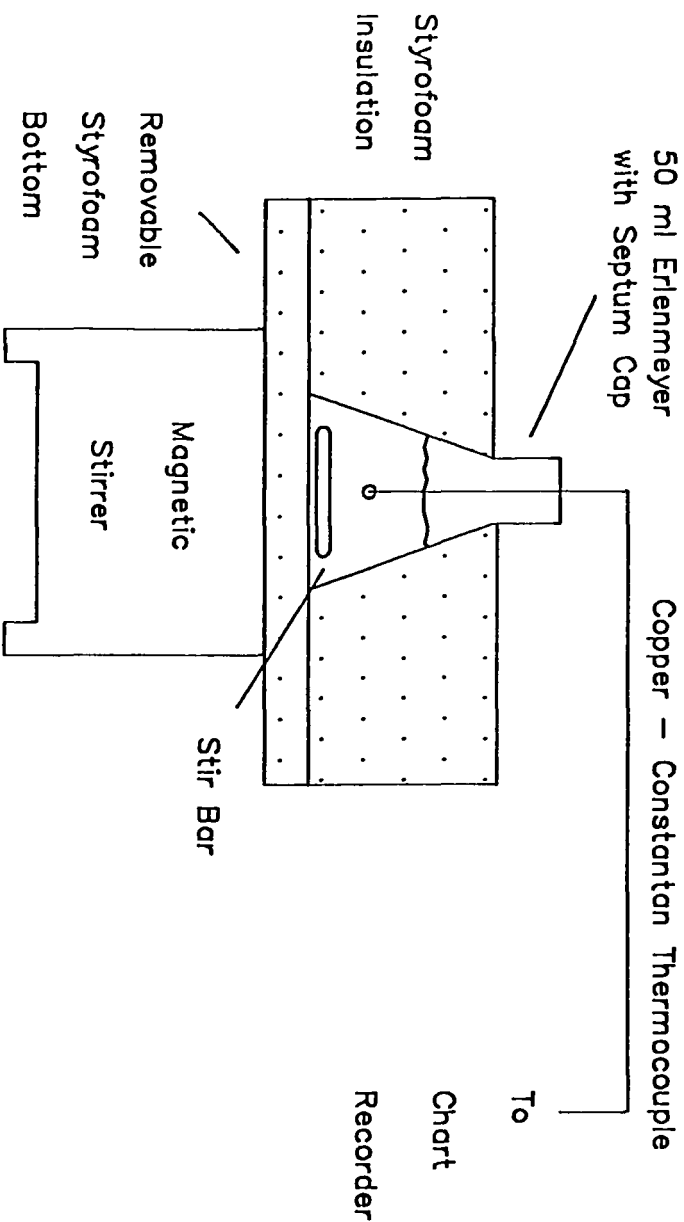
Table 2
Rate Constants for the Reaction Between H_2S and SO_2 in
2.5 Wt% DMA in DGM at 7-10 °C

RUN	k_2 (lit/mole-s)
1	2.5
2	4.3
3	5.0
4	4.3

Table 3
Rate Constants for the Reaction of H_2S and SO_2 in
DMA/Triglyme/Methanol Mixtures

RUN	Wt% DMA	WT% Methanol	k_2 (lit/mole-s)
1	10.1	45.1	23.5
2	10.1	45.2	24.0
3	10.1	45.1	22.8

Figure 1
Experimental Apparatus



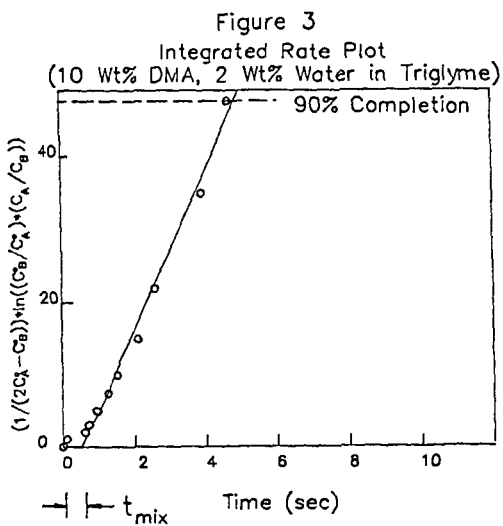
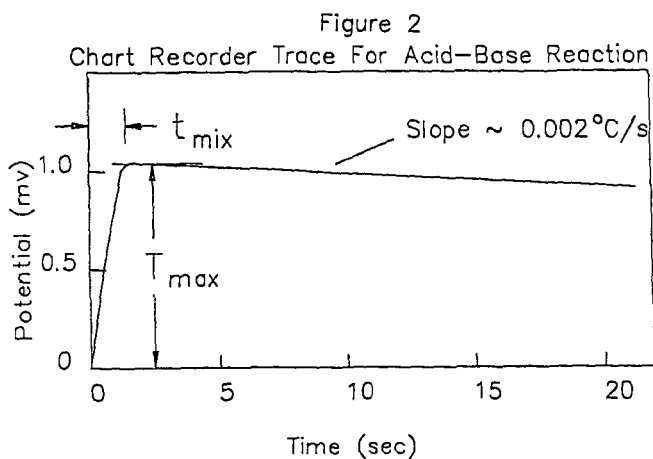


Figure 4

Variation of Second-Order Rate Constant
with DMA and Water Content for the Reaction
of Hydrogen Sulfide and Sulfur Dioxide in Triglyme

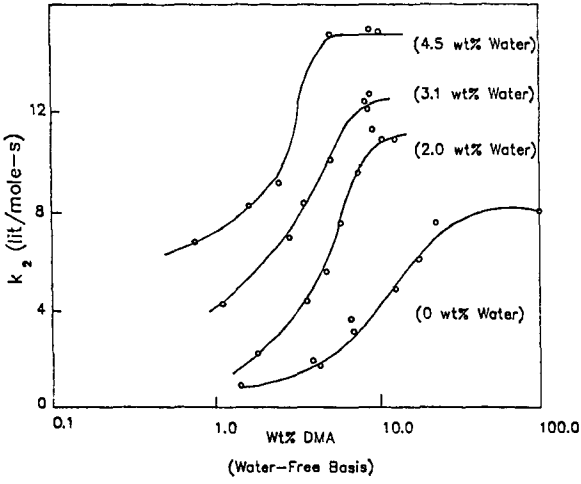
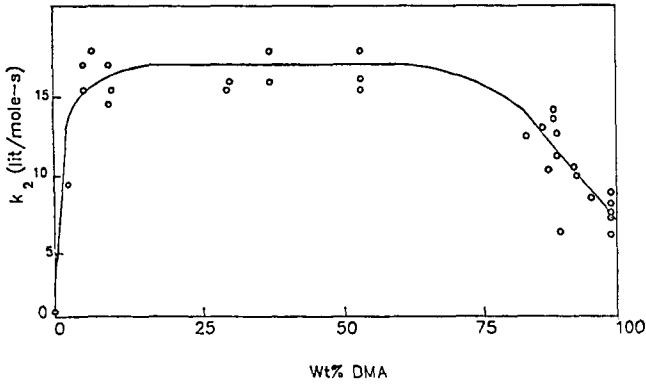


Figure 5

Variation of Second-Order Rate Constant with Wt% DMA
For DMA in DGM at 17-23°C (No Water)



PRODUCTION OF HYDROGEN FROM LOW HEATING VALUE FUEL GASES BY THE BEACON PROCESS

J. Blumenthal, T. Fitzgerald, A. Grossman, E. Koutsoukos, B. Pote

TRW, One Space Park, Redondo Beach, California 90278

M. Gbate

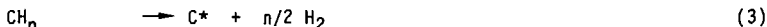
Department of Energy, METC, P.O.. Box 880, Collins Ferry Road

Morgantown, West Virginia 26505

Background

BEACON is an acronym for Btu Extraction And CONcentration. The process is based on the catalytic deposition of a highly reactive carbon (C*) from low heating value gases (LBG = low Btu gas). As illustrated in Figure 1 the BEACON process involves circulating a very easily fluidizable, solid carbonaceous material containing a catalyst between two fluid bed reactors.

In one reactor the solid material contacts the low heating value fuel gas feedstock resulting in the rapid deposition of very reactive carbonaceous material by reactions of the type:



Thus, in this reactor the incoming carbonaceous material and catalyst are enriched in carbon content through the deposition process and the low heating value fuel gas is depleted in energy content by an amount which is nearly equal to the heating value of the deposited carbon. The fuel gas is brought into the fluid bed carbon deposition reactor at near ambient temperature and the depleted fuel gas exits the reactor at 450°C to 550°C. Thus, most of the exothermic heat associated with carbon deposition is taken up in the depleted fuel gas as sensible heat in the nitrogen diluent, available for steam or power generation.

The carbon rich, solid, carbonaceous material and associated catalyst produced in the deposition reactor is separated from depleted fuel gas and circulated to a second reactor where the material is contacted with steam. In this reactor the steam-carbon reaction is very rapid at temperatures as low as 550°C or some 300°C below the temperature at which coals or chars will react effectively with steam. Depending on operating conditions (pressure, temperature and steam utilization) and catalyst type, either of the following overall reactions may predominate:



or



Heat must be supplied for the steam-carbon reactions described above. However, since the reaction temperature is modest (550-650°C) this heat can readily be supplied (indirectly) from the hot, depleted, and fully combusted fuel gas. Thus, a part of the residual energy content of the depleted fuel gas is used to drive the

steam-carbon reactions. This endothermic heat of reaction, of course, adds to the final total heating value of product methane or hydrogen at near 100% efficiency. That is to say, the higher heating value of the product methane or hydrogen rich gas exceeds the heating value of the reactant carbon by an amount equal to the endothermic heat of reaction.

To complete the solids circulation loop, carbon lean solids from the steaming reactor are returned to the carbon deposition reactor for carbon enrichment. For example, the carbon lean solids may contain 50-60% carbon and the carbon rich solids may contain 80-90% carbon.

In the BEACON technology there are three key areas of technical advantage:

1. A novel chemistry which results in very fast reactions at moderate temperature.
2. An ability through modifications of operating conditions and catalysts to produce either methane or hydrogen as a primary product.
3. An intermediate carbonaceous material and associated catalyst which has excellent fluid mechanical properties.

In both the carbon deposition and steaming reactions, utilizing the catalysts developed, near equilibrium compositions are obtained with gas-solid contact times that are well within commercially practical ranges. Carbon deposition is rapid above 400°C and the steam-carbon reaction becomes effective above 550°C.

The fluid mechanical properties of unsupported carbonaceous material are very different from other solid powders. Of great importance is the fact that this material fluidizes very well at commercially reasonable gas velocities.

Experimental Approach and Theoretical Comparisons

The objective of the work described in this paper was to demonstrate the viability of a catalyst system which is selective for hydrogen production in the reaction of deposited carbon with steam. In this case we want to suppress the formation of methane as completely as possible in the steaming reaction. In assessing our results we will compare the experimental measurements with two types of equilibrium calculations. The first type of thermochemical calculation allows methane and all other possible species to be present in the equilibrium product mixture. The second calculation excludes all hydrocarbon species (principally CH₄) from the calculation and gives a pseudo-equilibrium distribution of product species under conditions where methane is not allowed to form.

The experimental system shown in Figure 2 and described previously (Ref. 1) was used in the investigation. The system is a two reactor apparatus based on a variable differential pressure transfer line concept for the transfer of solids between BEACON carbon deposition and carbon gasification reactors. The "huff-puff" transfer system does not require gas/solids separation prior to transfer, and therefore it is simpler than a lock-hopper type system for fluidized bed operations. Adaptation of the "huff-puff" concept in BEACON processing was considered possible because of the unique properties of the solids-gas mixtures which give rise to stable fluid beds.

In this tandem concept the two reactors are connected with a fluid bed transfer line located below the top of the beds. Transfer is accomplished by establishing a small differential pressure between the two reactors and opening the transfer line valve. Solids are transferred back and forth by changing the sign of the differential pressure. About 10% of the bed is transferred each time. The

two reactors can be operated at different operating conditions, except pressure, as needed to optimize deposition or gasification; pressure, however, must be nearly equal in the reactors. Two additional requirements are that the relative size of the two reactors be such that the quantities of carbon deposited and gasified per unit time are equal and that both reactors operate under fluidized bed conditions. Ranges of allowable operating conditions were as follows:

<u>Parameter</u>	<u>Deposition Reactor</u>	<u>Steaming Reactor</u>
Temperature	400-600°C	500-750°C
Pressure	1-10 Atm	1-10 Atm
Gas Velocity	5-45 cm/sec	5-56 cm/sec
Feed Gas Composition:		
o Nitrogen	10-85%	0-50%
o Hydrogen	5-30%	0
o Carbon Monoxide	10-50%	0
o Carbon Dioxide	0-10%	0
o Steam	0	50-100%

The system shown in Figure 2 consists of the following sections: gas feed system, steam boiler, carbon deposition reactor, steam gasification reactor, product gas cleanup train, reactor pressure control and product gas metering system, solids transfer system, and data acquisition system. The deposition reactor has a 6-inch inside diameter and the gasifier a 3-inch inside diameter (the difference in reactor size was dictated by the difference in deposition and gasification rates at the desired operating ranges). Both reactors are constructed from 316 stainless steel parts and are surface aluminized by the Alon Process to prevent catalyst contamination from the reactor walls (especially through carburization of the deposition reactor walls).

Carbon deposition and steaming took place simultaneously and at equal rates. Typical rates were approximately 400 grams carbon deposited or steamed per hour; thus, the net solids transfer from the deposition reactor to the gasifier was about 400 grams per hour. Nominally, transfers were conducted about once an hour; approximately 700 grams were transferred from the carburizer to the gasifier and about 300 grams in the opposite direction. These quantities represented about 10% of the total solids in the system so that the disturbance of steady state was minor (the transfer was noticeable for one gas chromatogram of the product gas of the gasifier but had no effect on the product gas of the carburizer). Solids were transferred from the bottom of the reaction zone of one reactor to the top of the reaction zone of the other reactor; occasionally, the direction was reversed. The two-directional transfer operation took about three minutes, including the time (about one minute) required for system equilibration between the single transfers.

A single batch of catalyst solids (No. 11) which had shown outstanding activity and selectivity (methane suppression) in previous, small atmospheric pressure laboratory tests was subjected to approximately 375 hours of processing (simultaneous carbon deposition and steaming in separate reactors). Processing time consisted of 265 hours of steady state operation and about 110 hours of transient operation (mostly start-up and shutdown). Steady state processing time consisted of about 200 hours of operation at 4.4 atmospheres (50 psig), 50 hours at 6.1 atmospheres (75 psig), and 15 hours at 7.8 atmospheres (100 psig) reactor pressure.

The nominal conditions during the multi-cycle testing of Catalyst No. 11 solids were 620°C and six centimeters per second linear superficial velocity for steam gasification and 400°C and 15 centimeters per second velocity for carbon deposition at the above three pressures. The feed to the gasifier was 100% steam, but in the reaction zone it was diluted by approximately 20% v/v nitrogen gas used to maintain the DP legs and solids transfer lines free of solids (purge gas). The nominal deposition reactor feed gas composition was 10% v/v CO, 5% v/v H₂, with the balance being nitrogen gas.

Results

Figure 3 summarizes the catalyst performance data generated during the 375 hours of simultaneous operation (265 hours of steady state processing). The top portion of Figure 3 summarizes the performance of the carbon deposition operation expressed in terms of "fuel" (CO and H₂) utilization. Carbon monoxide utilization was near equilibrium and constant. Hydrogen utilization was high and also constant throughout the 265 hours of steady state processing. The middle and bottom graph of Figure 3 summarize the data pertaining to the performance of the steam gasification operation. Over the range of pressures investigated, nominally 80% methane suppression was obtained at equilibrium steam utilization for the duration of the 265 hours of steady state operation. Neither the deposition nor the gasification data revealed any trend of catalyst deterioration.

The stability of Catalyst No. 11 performance is also evident from the data presented in Tables 1 and 2, where a set of product gas composition data (dry and nitrogen free) is presented for every 50 hours of steady state operation. Table 1 summarizes steaming data which are compared to compositions predicted by thermodynamics for equilibrium operation at 650°C, 4.4 and 6.1 atmospheres (50 and 75 psig). The comparison of experimental data to equilibrium composition reveals that after 50 hours of processing time some CO (and steam) have shifted to CO₂ and H₂. It is expected that this shift occurs in the transition and expansion zone of the reactor. This conclusion is consistent with on-line DP monitoring which indicated an increase in the mass of solids contained in the expansion zone during the latter part of testing. Table 2 presents data for the carbon deposition operation. Product gas composition stability is excellent, CO conversion is high and approaches equilibrium values, but hydrogen conversion is significantly lower than equilibrium predicted values.

Including laboratory data, four pressures were investigated during the course of performance testing of Catalyst No. 11. Figure 4 illustrates the effect of reactor pressure on steam utilization and methane concentration in the product gas during steam gasification of Catalyst No. 11 solids at 620°C. The experimental data are compared to thermodynamically predicted values for the same conditions (solid lines on Figure 4). Methane suppression was nominally 80% or greater at all pressures investigated. The experimental values of the steam utilization fall in between the thermodynamically predicted values represented by the solid lines for normal and zero methane equilibria. This was expected since methane suppression was not complete.

Acknowledgment

This work was performed by TRW under Department of Energy Cooperative Agreement DE-FC21-80MC14400.

Reference

1. Blumenthal, J. L., et al, "Tandem Reactor Testing of the BEACON System," 11th Energy Technology Conference, March 20, 1984, Washington, D.C.

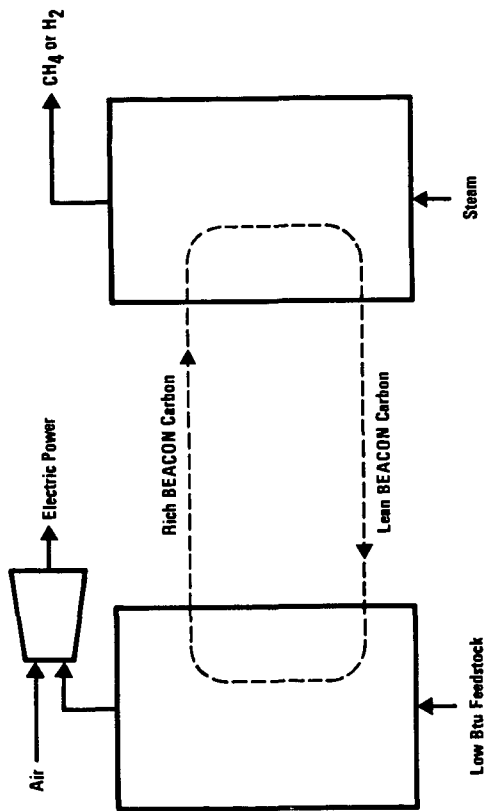


FIGURE 1. BEACON PROCESS CONFIGURATION

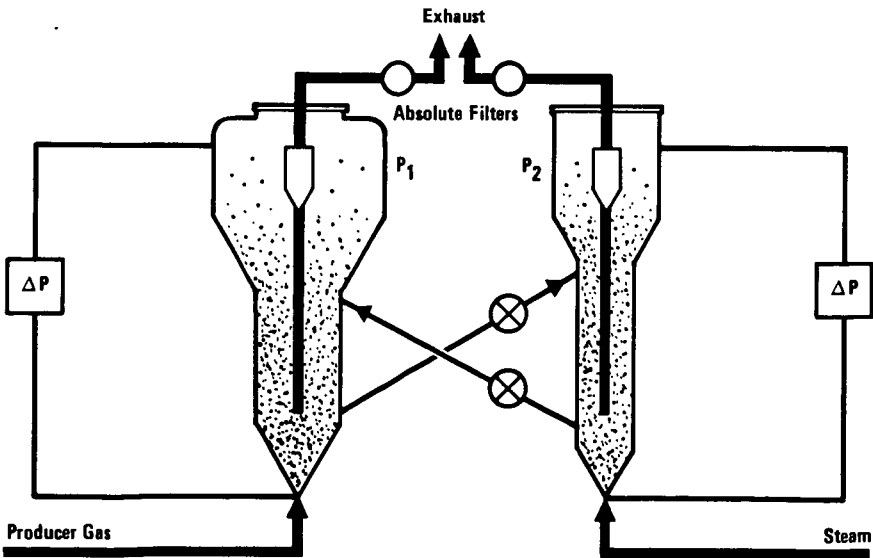
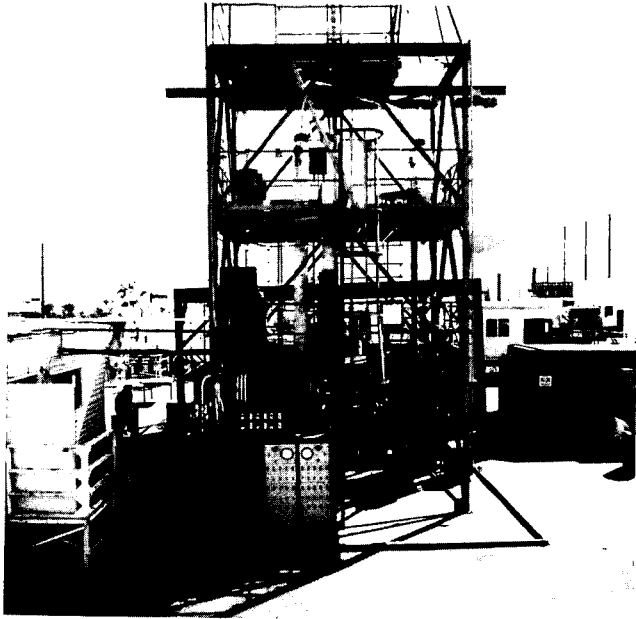
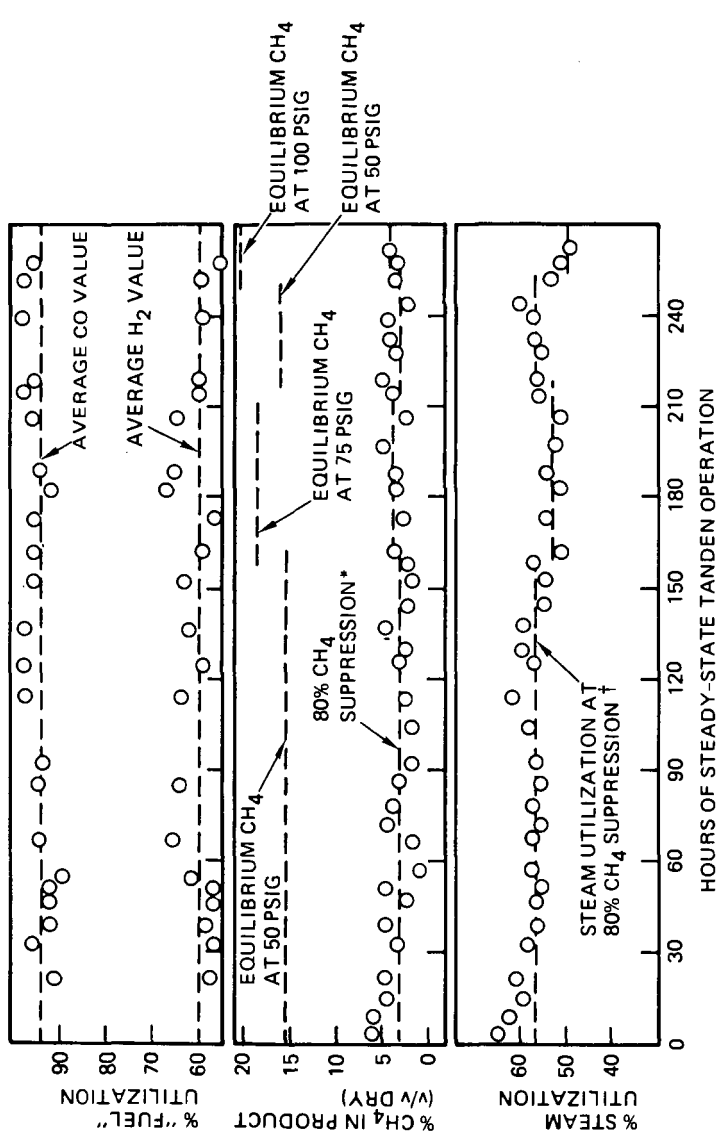


FIGURE 2. EXPERIMENTAL APPARATUS



*EQUILIBRIUM CH₄ AT 50/75/100 PSIG IS 15.8/18.3/20.2 PERCENT. AT 80% SUPPRESSION, METHANE IS 3.2/3.7/4.0 PERCENT RESPECTIVELY.
 †EQUILIBRIUM STEAM UTILIZATION AT : 50/75/100 PSIG IS 64.7/63.0/61.8 PERCENT AT NORMAL METHANE (METHANE IS ALLOWED TO FORM) AND 54.2/50.5/47.7 PERCENT AT 100% CH₄ SUPPRESSION (METHANE IS NOT PERMITTED TO FORM). BY INTERPOLATION, AT 80% CH₄ SUPPRESSION, STEAM UTILIZATION SHOULD BE 56.3/33.0/50.5 PERCENT, RESPECTIVELY.

FIGURE 3. STABILITY TESTING OF CATALYST NO. 11 IN TANDEM REACTORS (400°C/620°C, 50/75/100 PSIG)

TABLE 1. STABILITY OF PRODUCT GAS COMPOSITION IN TANDEM REACTORS (STEAM GASIFICATION OF CATALYST NO. 11 SOLIDS AT 620°C, 50 PSIG AND 75 PSIG)

Species	Thermodynamically Predicted Composition				Product Composition, 5 v/v Versus Hours of Operation					
	50 Psig		75 Psig		50 Hrs*	100 Hrs*	150 Hrs*	200 Hrs**	250 Hrs*	
	Normal	Zero Methane	Normal	Zero Methane						
CH ₄	15.8	0	18.3	0	4	3	2	3	2	
H ₂	41.2	62.5	38.4	62.9	57	61	60	63	62	
CO	13.0	12.3	11.5	11.0	12	9	7	6	7	
CO ₂	30.0	25.2	31.8	26.1	27	27	31	28	29	
% Steam Utilization	64.7	54.2	63.0	50.5	55	60	54	54	58	
% Methane Suppression	0	100	0	100	75	81	87	84	87	

● Typical Feed Composition: 80% v/v Steam, 20% v/v N₂ (Nitrogen was used to purge DP probes)

* 50 psig data

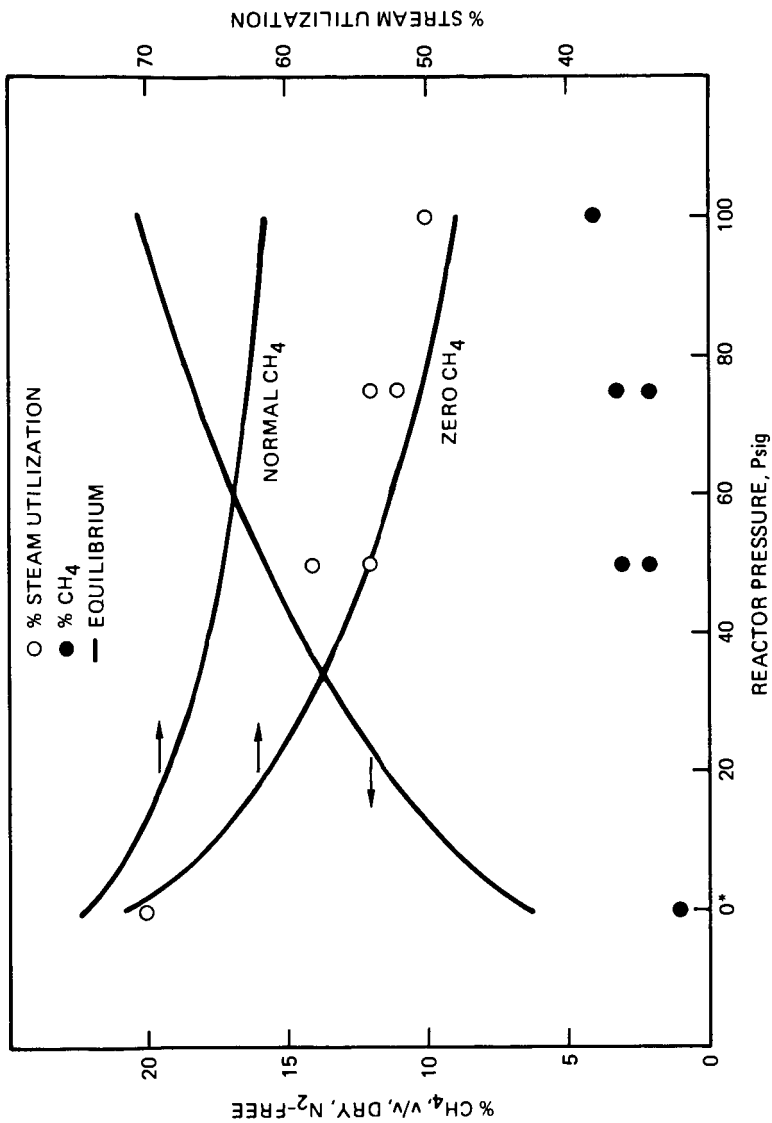
** 75 psig data

TABLE 2. STABILITY OF PRODUCT GAS COMPOSITION IN TANDEM REACTORS (CARBON DEPOSITION ON CATALYST NO. 11 SOLIDS AT 400°C, 50 PSIG AND 75 PSIG)

Specie	Thermodynamically Predicted Composition			Hours of Operation (Test Data)					
	50 Psig	50 Psig	75 Psig	50 Hrs*	100 Hrs*	150 Hrs*	200 Hrs**	250 Hrs*	
A. Feed Gas Composition, % v/v (Balance Nitrogen)									
CO	9	13	13	9	13	11	13	11	
H ₂	4	6	6	4	6	5	6	4	
B. Product Gas Composition, % v/v (Nitrogen Free)									
CH ₄	8.5	10.0	10.6	2	4	4	6	4	
H ₂	16.1	14.5	12.9	28	25	26	29	25	
CO	1.6	1.4	1.2	12	4	6	4	5	
CO ₂	73.8	74.1	75.3	58	67	64	61	66	
C. Fuel Utilization									
% CO	99.2	99.4	99.5	92	97	96	97	97	
% H ₂	82.6	85.3	87.3	56	63	61	59	58	

* 50 psig data

** 75 psig data



*AMBIENT PRESSURE DATA GENERATED AT 100% STEAM FEED. EQUILIBRIUM CURVES AND PRESSURIZED DATA ARE FOR A 80% v/v STEAM, 20% v/v N₂ REACTOR FEED.

FIGURE 4. EFFECT OF PRESSURE ON PERFORMANCE OF CATALYST NO. 11 IN HYDROGEN PRODUCTION FROM BEACON CARBON (620 °C)

THE EFFECT OF CATALYSTS ON COAL GASIFICATION

Reuel Shinnar
C.A. Feng
Alan I. Avidan

Department of Chemical Engineering
The City College of the
City University of New York
New York, New York 10031

INTRODUCTION

There have been a number of studies dealing with the impact of various catalysts in coal gasification (1,2,3,4,5) and one catalytic process for SNG (6) has been operated successfully in a large pilot plant. This paper analyzes the potential value of catalysts in coal gasification. The paper will first discuss what is the proper operating range for a gasifier by reviewing the thermodynamic and kinetic constraints of coal gasifiers, then analyze the question as to what type of catalyst is really required. Both syngas processes and SNG production will be discussed.

There are a few separate areas in which catalysts would be valuable in coal gasification.

1) SNG Production. In SNG production it has already been shown (8) that there would be a significant process advantage for a catalyst that could operate at 1000-1100°F. The global equilibrium at these temperatures contains mainly CH₄ and CO₂. The reaction heat requirements are low and can be supplied by superheated steam, which simplifies the process considerably. Steam conversion is low, but this disadvantage is overcome by the other advantages of such a simple process. The lowest operating temperature that has been achieved with good conversion of carbon and steam is 1300°F. Operating at 1300°F requires a very high concentration of potassium hydroxide or potassium carbonate in the coal. As recovery is difficult, the high concentration of potassium increases catalyst losses and reduces the economic incentive. At a temperature of 1300°F significant amounts of CO and H₂ are formed. The process developed by Exxon separates these gases from the methane and recycles them to the reactor. This requires a catalyst with a high methanation activity. We will show that a catalyst operating at 1400-1500°F could also be acceptable but the process would have to be modified. By proper modification this process should be competitive with the process proposed by Exxon and could utilize cheaper catalysts, or lower catalyst concentrations.

2) Syngas Generation. In syngas generation the thermodynamic optimum (8) is at conditions where coal gasification is fast. However, for many coals it is difficult to operate at these conditions. The only gasifier that has achieved operation close to the thermodynamic optimum is the British Gas Corporation slagging-type gasifier or BGC slagger. However, the BGC slagger is not suitable for all coals. In fluid bed gasifiers, one has to operate at lower temperatures to prevent agglomeration or ash melting. Under such conditions high conversion of the char is difficult as the gasification reaction is very slow at temperatures below 1700°F if char conversion is to exceed 70% (9).

The Winkler gasifier as well as present second generation fluid bed gasifiers for syngas all operate in a partial oxidation regime which reduces their thermal efficiency and increases the amount of oxygen required. A proper catalyst operating at 1500-1600°F could allow high

carbon and steam conversion and could potentially solve the inherent operating problems faced by all fluid bed gasifiers.

3) Gas Cleanup. The third area in which catalysts could significantly contribute to improved coal gasification processes is in the area of gas cleanup. There is a strong advantage in devolatilizing the coal prior to feeding it to the gasifier. However, this leads to the formation of tars and phenols which require expensive gas cleanup, and prevent efficient heat recovery from the product gas. If those products could be cracked at high temperatures, preferably in the devolatilization zone itself to methane and char, this would simplify the process scheme.

4) Improved Devolatilization. In a two-stage process, the results obtained in the devolatilization zone are very important. The amount of coal devolatilized in this stage as well as the product distribution strongly depends on the devolatilization conditions. A proper catalyst could change both the product yield and product distribution in the devolatilization zone.

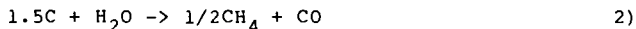
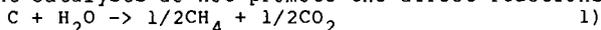
Aside from the development of the Exxon process, most work on the effect of catalysts has concentrated on item two: acceleration of the gasification reaction. Almost no measurements are available as to whether these catalysts also accelerate the methane formation reaction, nor is there any reported study of the effect of catalysts on items 3 and 4 listed above.

Let us now shortly discuss each item separately.

1) Use of Catalysts in SNG Production

The thermodynamic and kinetic constraints of SNG processes are discussed in detail in (ref. 10), and we will here only summarize them.

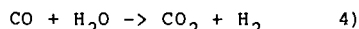
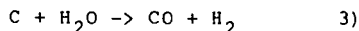
Present catalysts do not promote the direct reactions



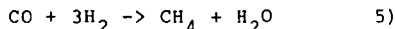
In present gasifiers and catalysts, methane is formed in several ways:

- 1) devolatilization of coal
- 2) reaction between CO and H₂O or CO and H₂
- 3) hydrogasification of coal

The CO, H₂ and CO₂ are formed by the reaction



Methanation of CO (or CO₂)² with hydrogen by the reaction



requires (10) that the CH₄ concentration is lower than:

$$[CH_4] < \frac{[H_2]^3 [CO]}{[H_2O]} K_P \quad 6)$$

where K_P is the equilibrium constant of reaction 5.

This only occurs when the CH₄ concentration is less than required by global equilibrium.

In the gasification zone the maximum amount of methane that can be generated by gasification is therefore limited by global equilibrium over char (10). There is one exception. At high temperatures the amount of methane generated by devolatilization is larger than is consistent with global equilibrium. This excess methane will react

with steam in the reverse reaction (10). However, if this reaction is slow, the methane concentration at the gasifier outlet will be above the global equilibrium.

If SNG is the desired product, then there is an advantage to increasing the direct methane yield in the gasifier. We define here direct methane yield for an SNG process as

$$\text{Direct methane yield} = \frac{\text{CH}_4}{\text{CH}_4 + \frac{1}{4}(\text{CO} + \text{H}_2)}$$

where $[\text{CH}_4]$, $[\text{CO}]$ and $[\text{H}_2]$ are the molar fractions of these compounds in the gasifier outlet. Increasing this ratio has two advantages for SNG production.

- 1) It reduces the cleanup cost of the product gas.
- 2) It reduces the heat requirements in the gasification zone (or the recycle requirements in the Exxon process). This is only correct if the methane formation occurs in the gasification zone. If the CO formed in a high temperature zone reacts to methane in a low temperature zone, this does not reduce the heat requirements.

The direct yield can be increased by proper utilization of the methane formed in the devolatilization zone (10). This requires a countercurrent scheme such as the one given in Fig. 1, model 2. This scheme can be approximated in a fluid bed by using a two-stage gasifier such as in model 3. Both countercurrent schemes have the further advantage that the coal is preheated with gasifier effluents. The difference in the thermodynamic constraints between model 2 and 3 is small. We will therefore use model 3 for presenting our results.

The maximum direct methane yield will, therefore, depend also on gasifier design. In a countercurrent or moving bed or two-stage gasifier, the methane from devolatilization has no impact on the global equilibrium. In a one-stage gasifier this methane is generated in the gasification zone and affects the equilibrium.

There are no accurate estimates as to how much methane is formed by devolatilization. This strongly depends on coal, operating conditions, temperature and of partial pressure of steam and hydrogen. The best estimates we have are from the BGC slagger and the Dry Ash Lurgi, though in both cases the flow is countercurrent and part of the methane could be formed by methanation in the cool zone just below the devolatilization zone.

Our estimates of the methane formed by devolatilization are taken from ref. 11. There is one more factor that affects direct methane yield. Without a catalyst methanation is slow. Some catalysts promote gasification (reaction 3), but do not promote methanation. We can therefore look at a limiting case in which no methanation occurs in the gasifier.

In Fig. 2 the direct methane yield ratio is plotted for several types of gasifiers operating at global equilibrium with Eastern coal. We choose Eastern coal as our main example since the main need for a catalyst is in the gasification of Eastern caking coals. We give direct methane yield ratio for two pressures (400 and 1000 psia) and for two gasifier models. One, (curve B), is a single stage mixed gasifier. For it we present two limiting cases. In the first we assume global equilibrium in the gasification zone. In the second (curve D) we assume that no methanation occurs in the gasifier, only devolatilization. If the methane yield at global equilibrium is higher than that formed by devolatilization, we assume it to be equal to that formed by devolatilization. If it is lower, we assume that it is equal to global equilibrium. This assumption makes sense at high temperature

since the methane steam reaction is fast without a catalyst.

We also give the results for a two-stage countercurrent gasifier (model III). Here, we also give two cases. One (curve A) in which the methane formation in the gasification zone is at global equilibrium. The other (curve C) where no methane formation occurs in the gasification zone.

Fig. 2 is based on an oxygen steam gasifier operating at equilibrium. Oxygen and steam are fed to the gasifier at 1000°F. We note that at low temperatures (below 1700°F) there is very little difference between curve C and D. At still lower temperatures the difference between A and B disappears. The main advantage of prior devolatilization is at higher temperatures. At 1500°F the advantage in terms of direct methane yield is significant only for the case where we have a catalyst that promotes methanation in the gasification zone.

We note in Fig. 2 that while increased pressure (Fig. 2b) increases the direct methane yield, the trends are similar in both cases. The main impact of increased pressure is to shift the curves towards higher temperatures.

In Fig. 3 we give the oxygen and steam requirements for SNG production as a function of temperature for a two-stage countercurrent and a one-mixed-stage gasifier. The oxygen and steam requirement are given in the form of the performance parameter proposed in ref. (7) and (8).

$$E_{CH_4} = \frac{H_2O + 4O_2}{CO + H_2 + 4CH_4}$$

which is proportional to the energy requirements to generate the feed for 0.25 mole CH₄. (The 0.25 CH₄ was chosen to make the parameter comparable to the performance parameter used for syngas and fuel gas, see later).

This parameter is an approximate performance parameter which gives different weight to the oxygen and steam requirements in the feed. This weighting factor is based on energy requirement of the feed and correlates quite well with total cost of the feed preparation. Oxygen use also involves another penalty. If its use is more than required by the stoichiometry (8,13), it reduces the cold gas efficiency. To evaluate this we need a complete heat balance of the gasifier. However, simplified performance criteria such as given here, give a reasonable picture of the impact of process parameters on cost and thermal efficiency.

In Fig. 3 we also give actual results for different gasifiers for Eastern coal. None of these is really commercial, but the data in either for a semi-commercial operation (Dry Ash Lurgi, BGC slagger, Texaco), or a large pilot plant (Shell, Westinghouse). We also give the performance of the Exxon process in an equivalent form. The Exxon gasifier does not use oxygen. It reduces the heat of reaction required by cryogenically separating the CO and H₂ from the methane and recycling them to the gasifier. The remaining small heat of reaction is supplied by superheating the recycle stream to 1500°F by burning part of the product gas. We try to present this gasifier here in an equivalent form by using an equivalent amount of oxygen. This is obtained by computing the energy used by the cryogenic separation process per mole net methane produced and converting it to oxygen by computing the number of moles of oxygen that could be produced by the same energy. This is reasonable as the cost of an oxygen plant and of the cryogenic separator are quite similar if based on the same energy consumption.

We note that a process operating with oxygen at 1500°F close to

equilibrium would have an advantage in terms of energy expanded over the Exxon process as proposed.

Figs. 2, 3 and 4 give us a good picture of the potential value of a catalyst that operates at low temperatures. At high temperatures such as in a slagger, it would not affect steam and oxygen consumption. But at low temperatures such as 1400°-1500°F its effect would be very beneficial. However, in this case it is essential that the catalyst promotes the methanation reaction.

A two-stage scheme based on such a catalyst at 1500°F would be competitive in terms of efficiency with the Exxon gasifier operating at 1300°F. Its overall thermal efficiency would be slightly better or equal and investment cost would be lower especially if the higher temperature leads to faster reactions and lower residence times.

At 1400°-1500°F there is very little chance of ash agglomeration. The main problem would be the agglomeration of caking coals. Pretreatment with a catalyst seems to prevent this phenomenon. Another way out is use of a high velocity mixing zone into which the fresh coal is introduced.

Introduction of fresh oxygen can also cause a locally excessive temperature that would lead to agglomeration. One way of minimizing this is to introduce the oxygen together with the steam and some recycle gas (or coal fines). This would raise steam temperature in the feed. By proper design of the steam nozzles and the mixing zone, this heat would be easier to dissipate than the heat generated by direct combustion of oxygen inside the gasifier.

There is therefore a strong incentive to look for cheap catalysts operating at 1400°F to 1500°F provided they not only accelerate the gasification reaction but also the methanation reaction. If they promote gasification only, we really deal with a case identical to fuel or syngas production which will be discussed in the next section.

One might even consider using a combination of two catalysts as it is not clear that a cheap efficient gasification catalyst operating at 1500°F will also promote methanation. Iron is a good methanation catalyst but loses its activity in the presence of sulphur. Sulphur resistant methanation catalysts are known but are expensive.

Regrettably, most studies in catalysis in coal gasification only report the gasification rate and do not measure the effect of the catalyst on methanation.

If such a catalyst would operate at 1100-1200°F, then one would be able to get a very simple process of supplying the process heat with superheated steam in a one-stage fluid bed. At 1400-1500°F the most promising candidate would be a two-stage fluid bed, the upper stage operating around 1200°F and the lower stage at 1400-1500°F. Heat could be supplied either by direct oxygen introduction or by superheating the steam to high temperatures with oxygen and raw product gas.

2) Syngas and Fuel Production

Syngas production is similar to fuel gas production, with one important difference. In fuel gas production the percentage of methane in the gas is irrelevant. In syngas production there is a premium for methane free syngas.

For some syngas processes such as methanol and Fischer Tropsch, the presence of methane up to a certain amount (10% of syngas) has only a low penalty in the syngas conversion process. On the other hand, there is a severe penalty to operate a gasifier such that the methane formed by devolatilization is destroyed. The difference in cost for syngas from a BGC slagger as compared to a Shell or Texaco gasifier is such that the incremental methane formed in the slagger is very cheap, both in terms of incremental investment and coal use.

We therefore would like to have a gasifier such as the slagger.

Fig. 5 compares the oxygen and steam requirements (reported as $H_2O + 4O_2$) for a unit of syngas. It is just a replot of Fig. 3 as we deal here with the same constraints. We give here methane a reduced value (half of final product), and therefore use as a criterion

$$E_S = \frac{H_2O + 4O_2}{CO + H_2 + 2CH_4}$$

For fuel gas the denominator would change to $CO + 0.85H_2 + 2.83CH_4$ (see ref. 8). But here we are interested in syngas. The overall conclusions for fuel gas would be very similar.

Looking at this ratio for the various cases in Fig. 5, we note again the advantage of a two-stage countercurrent unit. We also note that the optimum is clearly at a high temperature especially if we want to minimize methane at the same thermal efficiency. A catalyst would not change that. All a catalyst would do is to allow operation at lower temperature close to the equilibrium line.

That means we would have to pay a price for operating at lower temperature. This is justified if we need a gasifier for coals not suited for the slagger, or want to handle fines. It may also lead to simpler, more robust gasifiers.

Another goal would be a gasifier for a smaller plant in which simplicity has a high value. The tars found in the slagger make the total system quite complex and less suitable for smaller sized plants.

Here a gasifier operating close to equilibrium at temperatures around 1500-1800°F could have significant advantages. We want the temperature to be as high as possible, close to the limit dictated by agglomeration. However, gasification at these temperatures is slow. This is especially true at high carbon conversion. Gasification rate seems to drop severely as conversion exceeds 70% (9). One way to achieve high conversion is to operate with excess oxygen. Partial combustion of char to CO is fast. One then has to remove the excess heat. One can either operate at very high temperatures in a single stage gasifier (Shell, Koppers Totzek and Texaco) or use excess steam or recycle gas as a coolant (Winkler, Westinghouse). This reduces the thermal efficiency, as can be noted from Figs. 4 and 5.

All present fluid bed gasifiers operate in the partial combustion regime, using large excesses of oxygen and steam as compared to equilibrium requirement. We define this regime of the oxygen-to-converted coal ratio (8). If this exceeds the ratio required to convert all carbon to CO we call the gasifier a partial combustor.

Ref. (8) shows that the critical ratio of O_2 to carbon that distinguishes gasification from partial combustion can be defined for a coal of composition CH_aO_b as

$$R_{crit} = \frac{1 - b}{2}$$

The values of R for an equilibrium gasifier without methane formation in the gasification zone was given in Fig. 4. Values of the Westinghouse pilot plant, as well as other gasifiers, are given in the same plot. We note that while all equilibrium gasifiers have a value of R less than $R_{critical}$ only the countercurrent gasifiers achieve such low value and in that sense they are at present the only true gasifiers. Cheap catalysts could allow fluid beds to operate in the same regime and thereby increase their efficiency.

Here, the only catalyst property that counts is promotion of reaction (3) at high coal conversion and temperatures of about 1600°F. Several cheap catalysts tested seem to have the property and merit further investigation.

3) Devolatilization

One potential area of catalysis that has been completely neglected is the direct reaction of coal with H_2 and steam. When coal devolatilizes primary pyrolysis products are formed (1,12,13,14), which then either decompose into char and gases or react with steam or hydrogen. Sometimes this is called active char, but we really deal with a reaction of pyrolysis intermediates with steam (or hydrogen). This reaction can be promoted by high temperatures and high steam or hydrogen pressure. This involves other penalties. An attractive alternative would be a cheap catalyst that promotes the reaction of pyrolysis products with steam. To be really attractive this catalyst should preferably also promote the decomposition of tars and phenols and should operate at moderate pressures (400 psi) and low temperatures (less than $1400^\circ F$).

Shinnar et al. (10) discuss thermodynamic reasons why direct reaction of coal with steam is not likely. It is much more likely to involve an irreversible intermediate step, which would lead to the overall reaction

coal + steam (or hydrogen) \rightarrow products + char

The amount of char could be quite small (less than 40%). Study of such reaction in the presence of catalysts at reasonable temperatures and pressures could be of significant value. Another item is the decomposition of tars and phenols found directly in the devolatilization stage, at reasonably low temperatures ($1100-1200^\circ F$). Here there are a range of catalysts that could have this effect. The problem is that such catalysts must be effective in reasonably small amounts. Otherwise, the ash removal problem becomes more difficult.

4) Gas cleanup

Devolatilization of coal leads, in addition, to methane, CO and H_2 , also to tars and phenols. In a two-stage fluid bed it would be desirable to decompose them in the devolatilization zone, which should be possible and could be one of the main advantages of fluid bed gasifiers. However, in a slagger this is impossible and it would be very desirable if we had a catalyst which could decompose these tars and oxygenate with low excess of steam, which is probably very hard to achieve. However, the gas in a Dry Ash Lurgi used for Western coals contains almost 50% excess steam. A catalyst that decomposes all phenols and tars would make gas cleanup and waste water removal simpler and cheaper for such a gasifier and could have significant value if Dry Ash Lurgi gasifiers ever become more widely used.

Summary and Conclusion

Several key areas have been identified in which proper, cheap disposable catalysts could have significant impact on coal gasification processes.

For SNG production it would be desirable to find a cheaper throwaway catalyst operating at low temperatures, preferably below $1200^\circ F$. As such a catalyst is not in sight, one could also achieve significant advantages with a catalyst operating at $1400-1500^\circ F$ provided the catalyst (or mixture of catalysts) promotes both gasification and methanation of CO. A gasifier design that could utilize such a catalyst in an optimal way is described.

A catalyst that would promote direct formation of methane (without CO and H_2 as intermediate) would be desirable at high temperatures but no such catalyst is in sight.

For syngas production the advantages are smaller and we require a catalyst that promotes gasification without promoting methanation. Such a catalyst could overcome the inherent disadvantages of fluid beds and allow development of efficient fluid bed gasifiers.

Another area discussed is catalysts that would promote better yields in the devolatilization section by promoting the reactions of

pyrolysis products with steam at low temperatures and pressures, to prevent their polymerization.

Also of potential importance is the catalytic decomposition of tars and oxygenated compounds in the offgases of a Lurgi Dry Ash gasifier.

References

- 1) Walker, P.L. et al. Kinetics of Coal Pyrolysis and Gasification, DOE Report DE-83012279 (1983).
- 2) Cabrera, A.L., Heinemann, H., Somooryai, G.A. "Methane Production from Catalyzed Reaction of Graphite and Water Vapor at Low Temperatures (500-600 K)", LBL-12812, 1981.
- 3) McKee, D.W. "The Catalyzed Gasification Reactions of Carbon," Chemistry and Physics of Carbon, (Ed. P.L. Walker, Jr. and P.A. Thrower), Marcel Dekker Inc., New York), 16, 1(1981).
- 4) McCoy, L.R. et al., "Investigation of Coal Gasification Catalysis Reaction Mechanism," Quarterly Report, Sept. 1981, Rockwell Science Center, DOE Contract DE-AC21-80MC14592.
- 5) Kosky, P.G. et al. Coal Gasification Catalysis Mechanism, DOE Report DE-82013824 (1982).
- 6) Exxon Research & Engineering Co. "Exxon Catalytic Coal Gasification Process", FE-2369-24, 1978.
- 7) Shinnar, R., Kuo, J.C.W. "Gasifier Study for Mobil Coal to Gasoline Processes", FE-2766-13, 1978.
- 8) Shinnar, R. Thermodynamic and Process Constraints in Coal Gasification and their Economic Impact. Paper given at METC Symposium on Coal Gasification, Morgantown, November 1983.
- 9) Johnson, J.L. Adv. Chem. Ser. 1974, No. 131, 145.
- 10) Shinnar, R., Fortuna, G. and Shapira, D. IEC Process Design and Development 21, 728(1982).
- 11) Yoon, H., Wei, J., Denn, M.M. "Modelling and Analysis of Moving Bed Coal Gasifiers", Final Report, EPRI AF-590, 1977.
- 12) Zaharadnik, R.L., Grace, R.J. Adv. Chem. Ser. 1974, No. 131, 127.
- 13) Gavalas, G.R. Coal Pyrolysis, Elsevier, New York 1982.
- 14) Solomon, P.R. and Colbet, M.B., 17th International Symposium on Combustion, The Combustion Institute, Pittsburgh 1979.

SCHEMATIC REPRESENTATION OF GASIFIERS

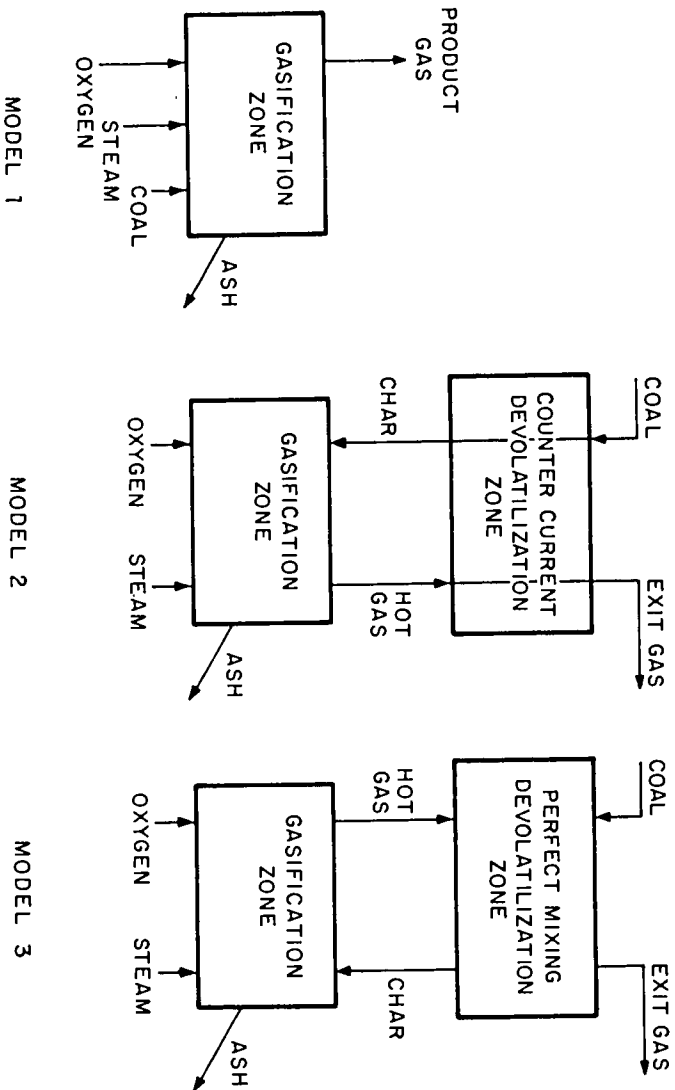


Fig. 1. Schematic Representation of Gasifier Models.

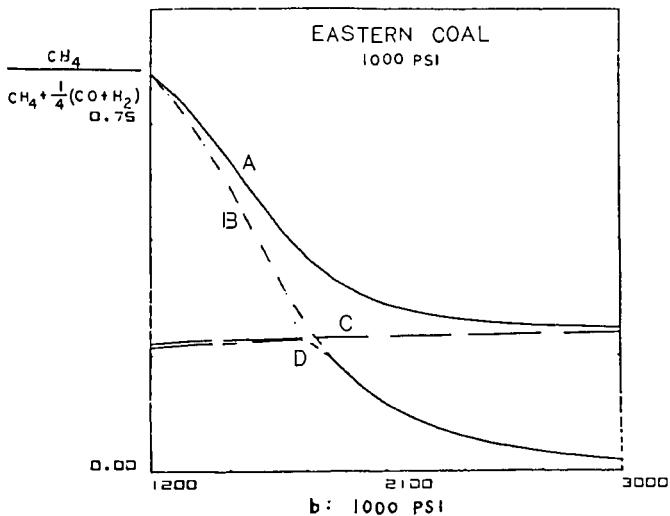
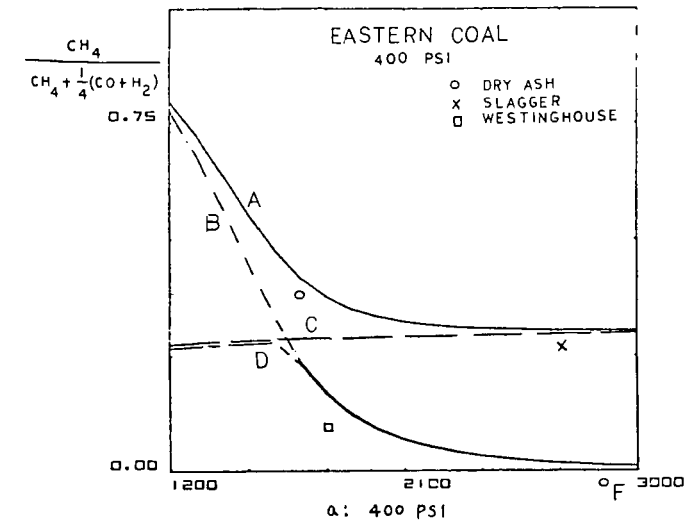


Fig. 2. Direct Methane Yield in a Steam Oxygen-Blown Coal Gasifier at Global Equilibrium. Effect of pressure, temperature, gasifier design and promotion of the methanation reaction.

- A) Two-stage countercurrent gasifier (model III, Fig. 1): Devolatilization in low temperature stage (1000°F). Global equilibrium over char in high temperature stage. (Temperature shown is temperature of high temperature stage).
- B) One-stage mixed gasifier, global equilibrium.
- C) Similar to A, but no methane formation in gasifier stage.
- D) One-stage mixed gasifier, with devolatilization (see text).

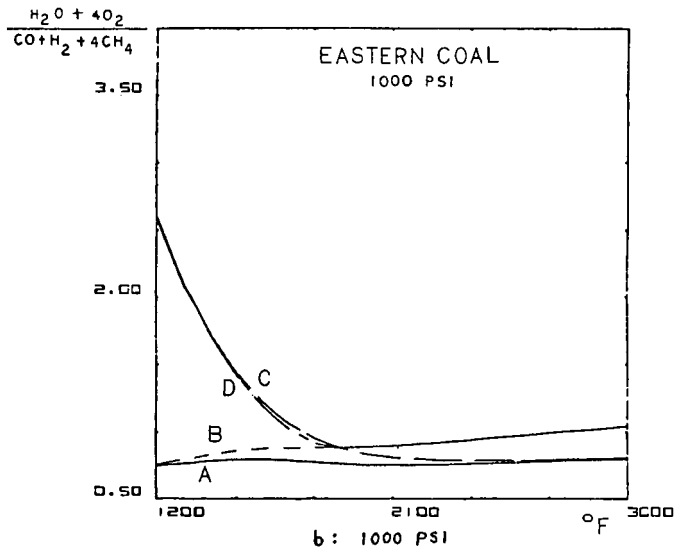
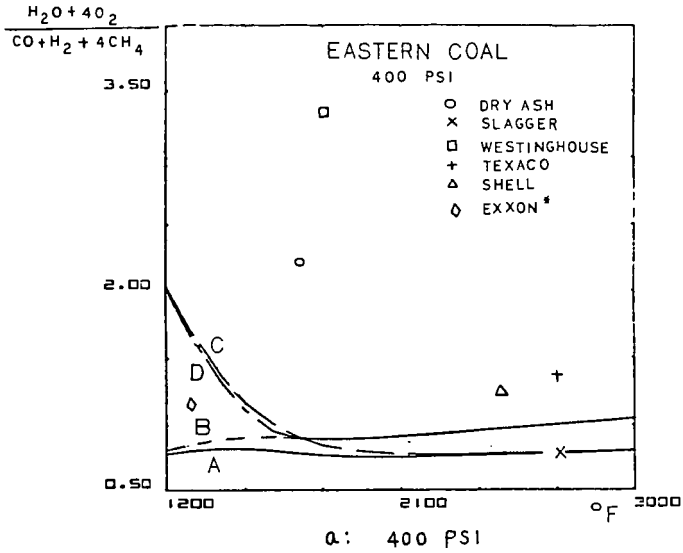
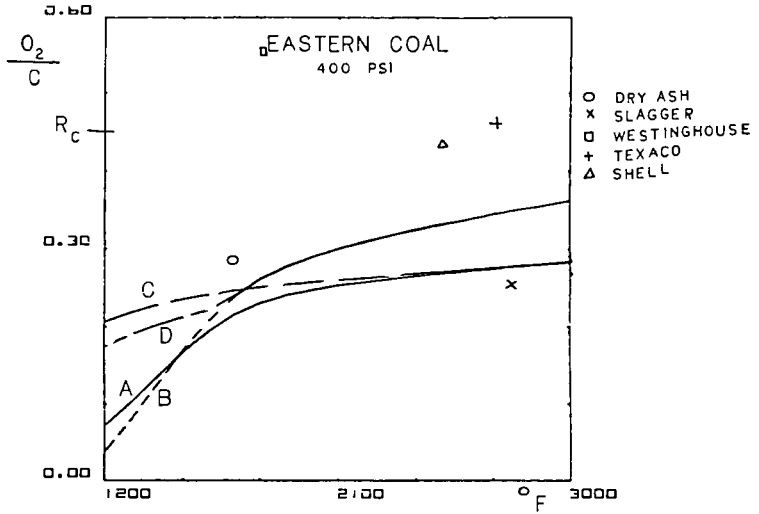
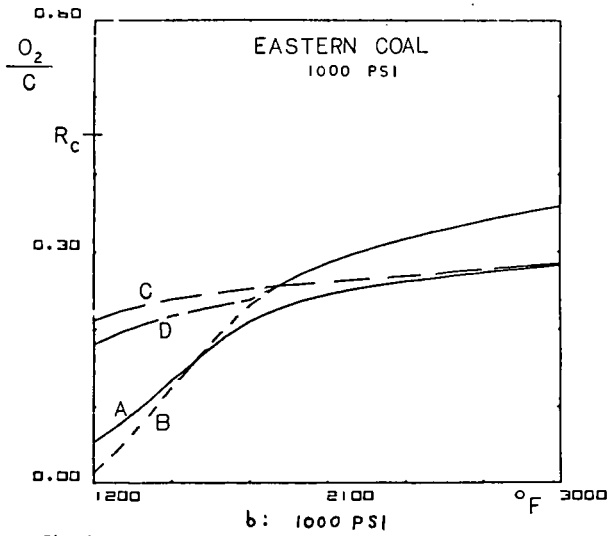


Fig. 3. Oxygen and steam requirements for gasifiers in Figure 1.
For explanation of curves see Figure 2.
*For Exxon gasifier see text for explanation.



a: 400 PSI



b: 1000 PSI

Fig. 4. Oxygen to carbon ratio for gasifiers in Figure 3.

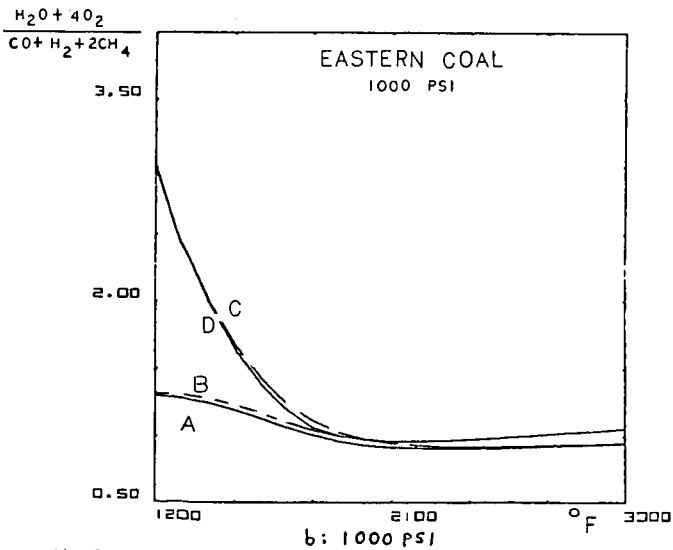
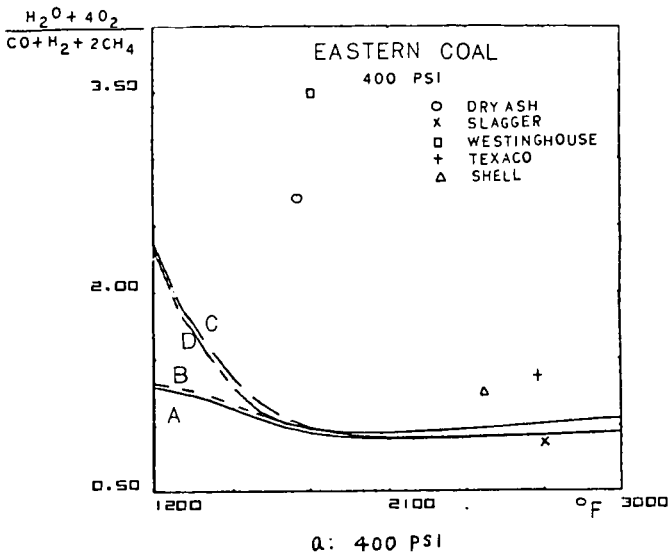


Fig. 5. Oxygen and steam requirements for syngas production (results of Fig. 3 replotted).

DETERMINATION OF THE INTRINSIC ACTIVITY AND EFFECTIVE
DIFFUSIVITY OF AGED COAL LIQUEFACTION CATALYSTS*

H. P. Stephens and F. V. Stohl

Sandia National Laboratories, Albuquerque, NM 87185

INTRODUCTION

Although severe, rapid catalyst deactivation remains a major economic impediment to the production of liquid fuels from coal by direct processing, there have been few quantitative investigations of aged catalyst intrinsic activity and effective diffusivity. This study reports a method for determining these important properties under experimental conditions that accurately model actual conditions for the processing of coal-derived liquids. The power of the technique has been demonstrated by determination of the intrinsic hydrogenation activity and effective diffusivity of catalysts obtained from the Wilsonville, Alabama coal liquefaction test facility. In addition, modeling of the experimental results has conclusively identified the modes of catalyst deactivation.

The values of intrinsic catalyst activity and effective diffusivity reported here are based on kinetic measurements of the catalytic hydrogenation of pyrene. Pyrene was chosen as a chemical probe of these properties because it appears to play a key role (1,2) as a hydrogen transfer agent in coal liquefaction: hydropyrenes are good hydrogen donors; they have low vapor pressures at liquefaction temperatures; and significant amounts are found in liquefaction solvents (3).

From determination of the pyrene hydrogenation rate constants for pairs of experiments, one with powdered catalyst and the other with whole extrudates, the fraction deactivated and the Thiele modulus, which relates the intrinsic rate constant to the extrudate effective diffusivity, were determined. Experiments with fresh, aged and regenerated catalysts have allowed the contribution of deactivation due to metallic contaminants to be separated from that due to carbonaceous material, and thus has allowed the mode of deactivation for each contaminant to be determined.

THEORY OF DIFFUSION AND REACTION OF PYRENE IN CATALYSTS

Pyrene Hydrogenation Kinetics

Although pyrene (Py) is catalytically hydrogenated to several products, under the conditions used in this study the major product is 4,5-dihydroxyrene (H_2Py). Previous work (4,5) has shown that the hydrogenation of pyrene (reaction [1]) can be precisely described by pseudo first order reversible kinetics (equation [2]):



* This work supported by the U. S. Dept. of Energy at Sandia National Laboratories under contract DE-AC04-76DP00789.

$$\ln \frac{X_e}{X_e - X_t} = kt \quad [2]$$

where k is the sum of the forward (k_1) and reverse (k_{-1}) rate constants, and X_t and X_e are the extents of reaction of pyrene to dihydropyrene at time t and equilibrium. X_t is calculated directly from the experimental product distribution:

$$X_t = \frac{[H_2PY]_t}{[PY]_t + [H_2PY]_t} \quad [3]$$

X_e is calculated from the experimentally observed hydrogen pressure p and the pressure equilibrium constant K_p :

$$X_e = \frac{[H_2PY]_e}{[PY]_e + [H_2PY]_e} = \frac{pK_p}{1 + pK_p} \quad [4]$$

where:

$$K_p = \frac{1}{p} \frac{[H_2PY]_e}{[PY]_e} \quad [5]$$

Catalyst Activity and Effective Diffusivity

Fresh Catalysts. For fresh catalyst extrudates, the fraction of the surface area used for chemical reaction is given by the effectiveness factor ϵ , defined as the ratio of the actual reaction rate for the extrudate to the intrinsic reaction rate (i.e., without diffusion resistance). The effectiveness factor may be determined from the intrinsic rate constant (k_i) for experiments with finely powdered catalyst and the apparent rate constant (k_a) for experiments with whole catalyst extrudates

$$\epsilon = \frac{k_a}{k_i} \quad [6]$$

Upon solving the differential equation for simultaneous diffusion and reaction in a catalyst particle (6), it is found that the effectiveness factor is a function of the Thiele modulus, h :

$$\epsilon = \frac{\tanh(h)}{h} \quad [7]$$

The Thiele modulus for catalyst pellets of all shapes may be closely approximated (7) by the following equation:

$$h = \frac{V_p}{S_x} \sqrt{\frac{\rho k_w}{D_e}} \quad [8]$$

where V_p and S_x are the volume and external surface area of the catalyst pellet, ρ is the pellet density, k_w is the intrinsic rate constant on a catalyst weight (w) basis [equal to $(k_1 + k_{-1})/w$ for reversible reactions (6)] and D_e is the effective diffusivity (diffusion coefficient within the catalyst pellet). Because the Thiele modulus can be determined from equation [7] using the effectiveness factor given by equation [6], the effective diffusivity can be readily calculated by rearrangement of equation [8]:

$$D_e = \left(\frac{V_p}{S_x} \right)^2 \left(\frac{1}{h} \right)^2 \rho k_w \quad [9]$$

Aged and Regenerated Catalysts. The relationship of the fraction F of aged pellet activity remaining to the Thiele modulus h and fraction poisoned α is given by the following equations for the limiting cases of uniform and pore mouth poisoning (8):

Uniform poisoning -

$$F = \left[\frac{\tanh(h \sqrt{1 - \alpha})}{\tanh(h)} \right] \sqrt{1 - \alpha} \quad [10]$$

Pore mouth poisoning -

$$F = \left[\frac{\tanh[(1 - \alpha)h]}{\tanh(h)} \right] \left[\frac{1}{1 + \alpha h \tanh[(1 - \alpha)h]} \right] \quad [11]$$

These equations were derived assuming deactivation results only from poisoning. However, coal liquefaction catalysts may deactivate as a result of the combined effects of uniform and pore mouth poisoning, and pore size reduction. We therefore modified equation [11] to include all of these modes of deactivation. The resulting equation models the fraction of pellet activity remaining for an aged catalyst which may have a completely deactivated shell due to pore mouth poisoning, a partially deactivated core due to uniform poisoning and an effective diffusivity which is less than that of the fresh catalyst:

$$F = \left[\frac{\tanh[(1 - \alpha_s)h]}{\tanh(h_f)} \right] \left[\frac{1}{1 + \alpha_s h \tanh[(1 - \alpha_s)h]} \right] \sqrt{\frac{\rho k_c D_e}{\rho_f k_f D_{ef}}} \quad [12]$$

where h_f , ρ_f , k_f and D_{ef} are the Thiele modulus, pellet density, rate constant and effective diffusivity for the fresh catalyst; h , ρ and D_e are the corresponding parameters for the aged catalyst; α_s is the fraction deactivated by shell progressive pore mouth poisoning; and k_c is the rate constant of the partially deactivated catalyst core given by:

$$k_c = (1 - \alpha_c) k_f \quad [13]$$

where α_c is the fraction of the core that is deactivated. Use of equation [12] to calculate effective diffusivities for aged and regenerated catalysts is discussed in the Results Section.

EXPERIMENTAL

Catalysts

Extrudates (0.8 mm diameter by 4 mm long) of Shell 324M, a 12.4% Mo, 2.8% Ni on alumina catalyst used in second-stage processing (9) of liquids derived from Illinois No. 6 (Burning Star) coal were obtained from the Wilsonville, Alabama coal liquefaction test facility. Fresh catalyst samples, used for baseline activity comparisons, were activated by presulfiding for 6 hours at 400°C and atmospheric pressure using a mixture of 10 mole % H₂S in H₂. Aged catalysts consisted of samples periodically withdrawn from the hydroprocessing reactor during run 242. In addition, samples were obtained from runs 242, 243 and 244, following process catalyst presulfiding with dimethyldisulfide in an oil vehicle, but prior to coal-derived liquid processing. Upon receipt, the aged catalysts, which were shipped in toluene, were Soxhlet extracted with tetrahydrofuran (THF) to remove as much of the soluble hydrocarbons as possible, then dried under vacuum at 100°C to remove traces of THF.

To investigate the effect of deactivation by contaminant metals, carbonaceous material was removed from the aged catalysts by slowly heating the extrudates to 500°C in air over a period of several hours and leaving them at this temperature overnight. These regenerated samples were then resulfided by the same method used for presulfiding the fresh catalyst in the laboratory. The baseline catalyst for experiments with these regenerated samples was a fresh catalyst sample which was treated by the same method as the regenerated samples.

All of the aged catalysts were characterized by a number of techniques including quantitative analysis for metals and carbon, BET surface area and desorption pore volume. In addition, the catalyst sample with the greatest age (527 lb SRC/lb catalyst) was subjected to electron microprobe analysis for metals distribution within the catalyst extrudate.

Pyrene Hydrogenation

The techniques used for the catalytic pyrene hydrogenation reactions and subsequent product analyses have been reported in detail elsewhere (4) and are only briefly described here. Batch reactions were performed (at a temperature of 300°C and nominal hydrogen pressure of 525 psia) in stainless steel microreactors loaded with 100 mg of pyrene, 1 g of hexadecane solvent and 15-19 mg of catalyst. The reactors, which could be rapidly heated to reaction temperature and quenched to ambient temperature at the completion of an experiment, were agitated during the heating period.

Several initial experiments were performed to determine the pressure equilibrium constant for hydrogenation of pyrene to 4,5-dihydropyrene at 300°C and to verify that pseudo first order reversible kinetics accu-

rately modeled the rate of reaction. Following these, hydrogenation experiments for all the fresh, aged and regenerated catalysts were performed in pairs, one experiment with catalyst ground to pass through a 200 mesh sieve (particle diameter 75 μm) to eliminate intraparticle diffusion and the other with whole catalyst extrudates (usually 4-5 per reactor). A nominal weight of 15.4 mg was used for the fresh catalyst. The weights of the aged and regenerated catalysts were increased in proportion to their density to compensate for the weight of contaminants.

Reaction times, which ranged from 10 to 120 minutes, were adjusted according to the activity of the catalysts. Following the completion of an experiment, the products were quantitatively removed from the reactor for analysis by gas-liquid chromatography. In order to determine the ratio of extrudate volume to external surface area, each catalyst extrudate was carefully recovered for measurement of the diameter and length.

RESULTS

Catalyst Characterization

Table I lists the results of characterization of the fresh and aged catalysts. As can be seen from Table I, carbon contents increased rapidly during process presulfiding and initial coal-liquids processing, then remained approximately constant after an age of 88 lbs SRC/lb catalyst. However, the amount of contaminant metals, Fe and Ti, continued to increase throughout the run. Catalyst surface areas and pore volumes varied inversely with the carbon contents. Both exhibit a rapid decline during the initial phase of processing followed by nearly constant values after an age of 88 lb SRC/lb catalyst. These trends in amounts of contaminants and physical properties are similar to those found by other investigators of hydroprocessing catalysts (10,11).

Figure 1 shows distribution of the iron and titanium contaminants, determined by electron microprobe analysis, across a circular cross-section of the 527 lb SRC/lb catalyst extrudate (sample 97001). These metals are deposited in an annular shell of the extrudate, a behavior typical of shell progressive pore mouth poisoning.

Figure 2 illustrates the pore volume distribution for fresh Shell 324M and the aged and regenerated 527 lb SRC/lb catalyst sample. As can be seen, the aged catalyst appears to suffer a large loss of pore volume (and related surface area) in the 70 to 140 A diameter pore region. Previous investigators (12,13) have hypothesized that this loss of pore volume and surface area, which is obviously due to the gain in carbon content, is responsible for loss in catalyst activity due to pore blockage with carbonaceous deposits. However, much of the carbonaceous material may simply be trapped reactant and product which is mobile at reaction temperature and does not contribute to pore blockage. Comparison of the curves for the fresh and regenerated catalyst shows that nearly all of the pore volume of the aged catalyst is restored upon removal of the carbonaceous material by regeneration.

Rate Constants

Results of the initial experiments with ground, freshly presulfided catalyst were used to calculate the pressure equilibrium constant, $1.4 \times 10^{-3} \text{ psia}^{-1}$, (equation [5]) for reaction [1] at 300°C. Figure 3, a plot of $\ln(X_e/(X_e - X_t))$ vs time for these experiments, demonstrates that the reaction rate follows pseudo first order kinetics. The slope of the linear fit of the data is $k_1 + k_{-1}$ or k of equation [2]. Because $\ln(X_e/(X_e - X_t))$ varies linearly with time and has an intercept of zero, the rate constant may be calculated from the results of a single experiment:

$$k = \ln (x_e / (x_e - x_t)) / t \quad [14]$$

Catalyst Activity and Effective Diffusivity

Fresh Catalyst. The Thiele moduli of the fresh catalysts were calculated from the experimental effectiveness factors ϵ (ratio of rate constant for the extrudate catalyst to that of the ground, equation [6]) by determining the value of h which satisfied equation [7]. The effective diffusivities were calculated using equation [9] where the ratio of the volume to external surface area is calculated from the average extrudate diameter d and length l :

$$\frac{V_p}{S_x} = \frac{ld^2/4}{d^2/2 + ld} \quad [15]$$

Regenerated Catalysts. The fraction of catalyst shell poisoned, α_s was given by the ratio of the rate constant for ground regenerated catalyst k_r to that of the ground fresh catalyst k_f :

$$\alpha_s = 1 - k_r/k_f \quad [16]$$

while the fraction F of extrudate activity remaining is the ratio of regenerated extrudate rate constant k_{re} to that of the fresh, k_{fe} :

$$F = k_{re}/k_{fe} \quad [17]$$

Because electron microprobe analysis showed that the contaminant metals were deposited in an annular shell of aged extrudates, it was assumed that the cores of the regenerated catalysts were contaminant free and had activities equal to that of the fresh catalyst. The behavior of F vs α_s for regenerated catalyst, discussed in the next section, supports this assumption. Effective diffusivities for the regenerated catalysts were determined by finding the value D_e which satisfied equation [12]. Note that because $\alpha_c = 0$ for regenerated catalysts, the value of the k_c in equations [12] and [13] is equal to k_f .

Aged Catalyst. Calculation of the effective diffusivities for the aged catalysts is similar to that for the regenerated catalyst. Equation [12] is again used; however, the rate constant for the partially deactivated core k_c must be determined from rate constant for the ground aged catalyst experiment k_{wa} and α_s for the corresponding regenerated catalyst

$$k_c = k_{wa} / (1 - \alpha_s) \quad [18]$$

The fraction of the core which is deactivated α_c is:

$$\alpha_c = 1 - k_c/k_f \quad [19]$$

and the total fraction deactivated α_T is:

$$\alpha_T = 1 - (k_{wa}/k_f) = \alpha_s + \alpha_c - \alpha_s \alpha_c \quad [20]$$

Table II lists the rate constants for the ground catalyst and extrudate experiments and Table III gives the fraction poisoned (α_s for the regenerated catalysts and α_s , α_c and α_T for the aged catalysts), the fraction F of extrudate activity (compared to fresh extrudate) remaining, the Thiele modulus h, and the effective diffusivity D_e .

DISCUSSION

The results given in Tables II and III can be used to describe the trends in catalyst activity and diffusivity with age and to identify the modes of catalyst deactivation.

Catalyst Activity. Intrinsic catalyst activity, i.e., the activity without diffusion limitations, is given by the rate constants for ground catalyst experiments (Table II). Loss of intrinsic activity is best characterized by the α parameters (Table III). For the regenerated catalysts, the total fraction deactivated, α_T , is equal to that due to the metallic contaminants, α_s . However, the total fraction deactivated for the aged catalysts is related to the fraction deactivated by carbonaceous deposits α_c and that by metals α_s as given by equation [20]. As can be seen by the values of α_c in Table III, carbonaceous contaminants contribute to a loss of intrinsic catalyst activity of up to 80% during process presulfiding (sample 94074) before processing of coal even begins. However, nearly all of this activity can be recovered by laboratory regeneration methods. After processing of coal begins, metallic contaminants add to the loss in activity and these losses cannot be recovered by regeneration.

Effective Diffusivity. Both the aged and regenerated samples show the same trend in the decrease in effective diffusivities (Table III) with catalyst age. After an initial decrease of 50% from a value of 6×10^{-6} cm²/sec/cm³ for fresh catalysts to 3×10^{-6} for catalyst ages greater than 42 lb SRC/lb catalyst, the diffusivity remains relatively constant. Thus, compared to a decrease in intrinsic activity (Table II) of a factor of 30 over the course of the run, a decrease in effective diffusivity of a factor of two appears to have a smaller impact on extrudate activity.

Modes of Deactivation. For the limiting modes of uniform or pore mouth deactivation, equation [12] reduces to equation [10] or [11], respectively. The limiting modes of deactivation may be identified (8) by plotting the fraction of initial extrudate activity remaining after deactivation (F in Table III adjusted by the ratio $\sqrt{\rho_D e / \rho_f D_{ef}}$) vs the fraction of catalyst deactivated (α_T in Table III). Uniform deactivation behavior, due to the deactivation of catalytic sites homogeneously throughout the extrudate is described by equation [10] which depicts a decrease in activity approximately proportional to $\sqrt{1 - \alpha_T}$. Pore mouth deactivation behavior, which results in an annular shell of deactivation, is described by equation [11] and shows a much different behavior. For pore mouth deactivation, the loss in extrudate activity as a function of fraction deactivated is much greater than that of homogeneous poisoning for the same degree of deactivation.

Because the regenerated catalysts contain only the metallic contaminants, a plot of F vs α_s identifies the mode of deactivation by metals. However, the aged catalysts contain both metallic and carbonaceous contaminants. The plot of F vs α_T for the aged catalysts may identify the dominant mode of deactivation by the deactivating materials.

Figure 4 shows a plot of $F/\sqrt{\rho D_e/\rho_f D_{ef}}$ vs α_T for the regenerated (circles) and aged catalysts (squares). The points for the regenerated samples were accurately fit with the limiting progressive shell pore mouth deactivation model, equation [11], using the average of the Thiele moduli, 5.7, for the samples with significant metals contamination. In contrast, the points for the aged samples were accurately fit with the limiting uniform deactivation model, equation [10], using the average sample Thiele modulus of 2.1. Thus, the catalysts were deactivated by two different modes--progressive shell pore mouth deactivation by metallic contaminants and uniform deactivation by carbonaceous materials. Although the pore mouth mode of deactivation by metals is permanent and limits the amount of extrudate reactivity which can be recovered upon regeneration, the dominant mode of deactivation, which occurs rapidly, is a uniform deactivation by carbonaceous material.

REFERENCES

1. F. J. Derbyshire and D. D. Whitehurst, *Fuel* 60, 655 (1981).
2. F. J. Derbyshire, P. Varghese and D. D. Whitehurst, *Fuel* 61, 859 (1982).
3. B. R. Rogers, R. L. Jolly and R. M. Whan, "ITSL Solvent Quality Studies," Proceedings of the Dept. of Energy Integrated Two-Stage Liquefaction Meeting, Albuquerque, NM, October 1982.
4. H. P. Stephens and R. N. Chapman, "The Kinetics of Catalytic Hydrogenation of Pyrene--Implications for Direct Coal Liquefaction Processing," ACS Fuel Division Preprints, 28, No. 5, 161 (1983).
5. H. P. Stephens in "Coal Liquefaction Process Research Quarterly Report for July 1 - September 30, 1983, Sandia National Laboratories, SAND83-2426, p. 15, January 1984.
6. C. G. Hill, Jr., "An Introduction to Chemical Engineering Kinetics and Reactor Design," John Wiley, NY (1977).
7. R. Aris, *Chem. Eng. Sci.*, 6, 262 (1957).
8. A. Wheeler, *Catalysis* 2 (105), edited by P. H. Emmett, Reinhold, NY (1955).
9. A. K. Rao, R. S. Pillai, J. M. Lee and T. W. Johnson, "Recent Advances in Two-Stage Coal Liquefaction at Wilsonville," Proceedings of the 8th Annual EPRI Contractors Conference on Coal Liquefaction, EPRI AP-3366-SR, February 1984.
10. G. J. Stiegel, R. E. Tischer and D. L. Cillo, "Catalyst Testing for Two-Stage Liquefaction," Proceedings of the 8th Annual EPRI Contractors Conference on Coal Liquefaction, EPRI AP-3366-SR, February 1984.
11. R. Galiasso, R. Blanco, C. Gonzales and N. Quinteros, *Fuel* 62, 817 (1983).
12. M. J. Chiou and J. H. Olson, *ACS Symp. Ser.* 23, 1421 (1978).
13. B. D. Prasher, G. A. Gabriel and Y. H. Ma, *Ind. Eng. Chem. Process Des. Dev.* 17, 266 (1978).

Table I. Elemental Analysis, Surface Areas and Pore Volumes for the Fresh and Aged Catalysts

Sample	Age (lb feed/lb catalyst)	Active Metals (Wt %)		Major Contaminants (Wt %)			Surface Area (m ² /g)	Pore Volume (cc/g)
		Mo	Ni	C	Fe	Ti		
Fresh	--	12.4	2.8	0.11	.02	.07	158	0.49
15923	Process Presulfided	NA	NA	2.33	NA	NA	142	0.41
97888	Process Presulfided	NA	NA	4.40	NA	NA	137	0.38
94074	Process Presulfided	10.3	2.3	6.1	.04	.14	135	0.35
94495	43	10.3	2.3	8.2	.14	.14	125	0.32
94811	88	10.0	2.2	9.3	.22	.21	113	0.29
94966	133	10.1	2.4	9.6	.28	.30	108	0.28
96460	381	9.5	2.5	9.2	.67	.46	102	0.27
97001	527	9.7	2.4	9.4	.72	.56	100	0.27

Table II. Weight Basis Rate Constants for Ground Catalyst and Extrudate Experiments

Sample	Age (lb/lb)	Aged Catalyst Rate Constants (sec ⁻¹ g ⁻¹ x10 ²)		Regenerated Catalyst Rate constants (sec ⁻¹ g ⁻¹ x10 ²)	
		Ground	Extrudate	Ground	Extrudate
Fresh	--	15.9	4.1	17.6	4.7
15923	Process Presulfided	8.9	3.3	17.6	5.0
97888	Process Presulfided	3.4	1.5	17.2	4.3
94074	Process Presulfided	2.3	0.99	16.8	3.8
94495	43	1.6	0.39	13.6	1.3
94811	88	1.2	0.59	12.1	1.7
94966	133	0.88	0.37	11.8	0.98
96460	381	0.49	0.32	7.2	0.85
97001	527	0.49	0.26	5.2	0.45

Table III. Fractions Poisoned, α , Fraction Extrudate Reactivity Remaining, F, Thiele Modulus, h, and Effective Diffusivities, De, for Fresh, Aged, and Regenerated Catalysts.

Sample	Aged Catalysts						Regenerated Catalysts			
	α_T	α_S	α_C	F	h	Dex10 ⁶	α_S	F	h	Dex10 ⁶ *
Fresh	--	--	--	1.0	3.8	5.6	--	1.0	3.7	6.2
15923	.44	.003	.44	.81	2.5	6.7	.003	1.06	3.5	6.3
97888	.77	.02	.77	.39	2.1	4.2	.02	.92	3.8	6.0
94074	.84	.04	.84	.26	2.1	2.9	.04	.80	4.2	5.4
94495	.89	.22	.85	.11	3.1	1.3	.22	.28	5.9	2.6
94811	.92	.30	.88	.16	1.6	3.7	.30	.35	4.6	4.5
94966	.93	.30	.91	.11	1.9	2.0	.30	.22	6.2	2.3
96460	.96	.57	.92	.09	1.3	4.2	.57	.19	5.0	3.4
97001	.96	.68	.88	.08	1.8	2.9	.68	.10	6.9	2.1

*De has units of cm²/sec/cm³.

FIGURE 1. Distribution of Fe and Ti across a circular cross-section of extrudate sample 97001, aged 527 lbs SRC/lb catalyst.

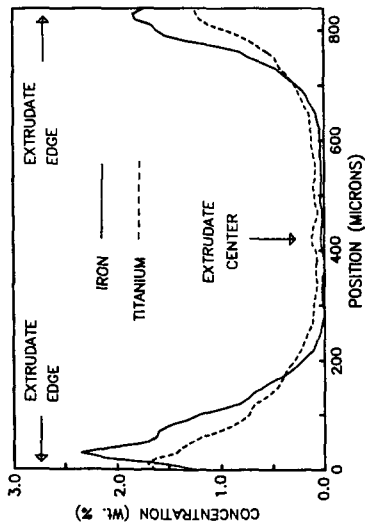


FIGURE 2. Pore volume distribution for fresh catalyst, aged, and regenerated sample 97001.

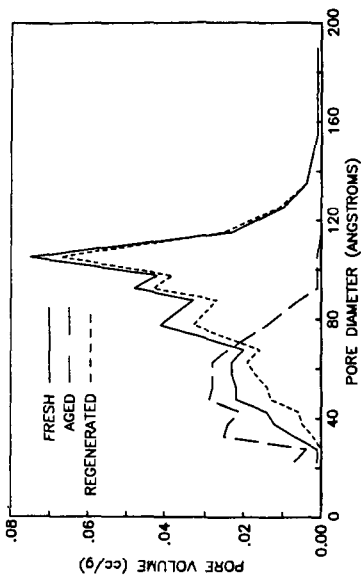


FIGURE 3. Plot of pseudo first order reversible reaction kinetics for hydrogenation of pyrene to 4,5-dihydropyrene.

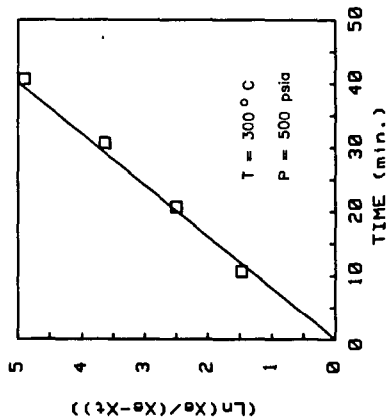
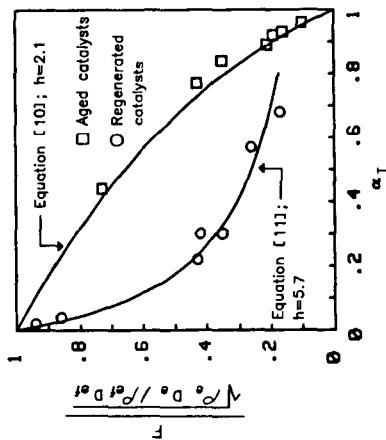


FIGURE 4. Plot of fraction extrudate activity remaining vs total fraction deactivated for aged and regenerated extrudates.



A CATALYTIC REACTION MODEL FOR FILAMENTOUS CARBON GASIFICATION

J. A. Starkovich, Wei-Yue Lim, H. Peng

Chemical Processes Department, TRW Energy Development Group,
Redondo Beach, California 90278

1. Introduction

Filamentous coke deposition is a major fouling problem for catalysts used in synthesis gas methanation, the water-gas shift reaction and hydrocarbon steam reforming. Significant effort has been spent in studying carbon deposition rate, deposit morphology and structure, and process conditions for minimization of deposition rate. A collection of papers from a special symposium and an excellent review article which survey this work have recently appeared. (1,2) Much less study, however, has been devoted to modeling the inverse reaction or the gasification/removal of filamentous carbon deposits. Information and fundamental understanding of the kinetics of the inverse reaction are needed for improved design of catalyst regeneration schemes used in commercial catalytic fuel gas processing. Better understanding of the inverse reaction may also assist identification of improved deposit prevention methods.

The present research was undertaken to develop a model for correlating conversion rate with the extent of conversion for the gasification of filamentous carbon. In our studies of the gasification reactions of filamentous carbon, we find that traditional fluid-solid reaction models such as the "shrinking core", "shrinking sphere" and progressive conversion, are not adequate for describing conversion kinetics. We suspect from our work and the results of others (3,4,5) that certain filamentous carbon gasification reactions proceed via a catalytic mechanism involving an embedded catalyst particle. We have developed a new model for this type of reaction which we have termed the "axially shrinking filament" model. The conceptual basis and formulation for this new model are presented in this paper. Refinement and experimental verification/application of this new model are in progress. An illustrative example of the model's ability for describing the conversion kinetics of the filamentous carbon-hydrogen reaction is presented from this work.

2. Axially Shrinking Filament Model

Essential features of the axially shrinking filament (ASF) model are illustrated in Figure 1. As depicted, the solid grain consists of a consumable filament-shaped particle attached to a small catalyst nodule. For a grain situated in a fluid reactant medium, the catalyst nodule serves as the site of reaction between fluid reactant and the filament particle. In reaction, fluid reactant is adsorbed by the catalyst nodule and combines with filament material in the vicinity of the nodule. The initially formed reaction product is subsequently desorbed and lost to the bulk fluid phase. Continuing reaction and loss of filament material results in axial shrinkage of the grain without change in filament cross-section. The rate of the topochemical reaction is constant throughout conversion of an individual filament and is proportional to the interfacial area between the nodule and filament. Different diameter filaments thus exhibit the same linear shrinkage rate, v , under a given set of reaction conditions. The shrinkage observed for each filament in a collection of reacting grains is given by vt , where t

is the reaction time. The shrinkage rate may be a function of temperature, reactant, nodule composition and orientation, and possibly other physiochemical conditions of the reaction. Interphase heat and mass transport resistances, if significant, are assumed to be constant during reaction.

A global conversion expression may be developed for this reaction model by considering the particle collection to have a time-dependent filament length distribution. Change in filament length distribution due to reaction is related to conversion extent or in the present case, the amount of carbon gasified. A general expression for relating fractional conversion, α , to the filament length distribution is given by Equation (1). The terms l and $p_0\{l\}$ are the filament length and the fraction of the initial ($t=0$) population having length l . $p_0\{l\}$ is the probability density function or the length distribution function for the particle collection and may be considered a continuous function of l for large number filament populations.

$$\alpha = 1 - \frac{\int_{vt}^{\infty} p_0\{l\} dl - vt \int_{vt}^{\infty} p_0\{l\} dl}{\int_0^{\infty} p_0\{l\} dl} \quad (1)$$

While the derivation of this expression is being presented elsewhere, the intuitive correctness of the expression may be appreciated by pointing out the essence of the integral terms. The entire ratio on the right-hand side of Equation (1) is the mass fraction of carbon remaining at time t . The denominator integral simply represents the average filament length for the particle collection before any reaction ($t=0$). The numerator is the difference between the average length of that portion of the initial filament population with a length equal to or greater than vt and the total shrinkage length suffered by this population segment up to time t . It is important to note that Equation (1) is a general conversion expression independent of filament geometry and is valid for any continuous probability density function. In order for the equation to be useful in practice, the distribution function must be known a priori from independent measurement or ascertained from a gasification experiment. Application of Equation (1) for describing the gasification of filamentous carbon is shown below.

3. Experimental

Filamentous carbons used in these studies were prepared by carbon monoxide disproportionation over cobaltosic oxide. Cobaltosic oxide is an active CO disproportionation catalyst and produces filamentous carbon as the principal deposit form at temperatures below approximately 873°K. In the preparation, heated carburizing gas mixture is flowed over a sample of thinly-dispersed, fine oxide powder. Deposition is carried out until the deposit solid contains approximately 90-95 wt. percent carbon. A CO-H₂ mixture (85:15 mole ratio) is used for the carburizing gas and the deposition temperature is maintained at 723°K. These conditions lead to the production of filaments with diameters in the range of 50-200 nm and large apparent length-to-diameter ratios when examined by scanning and transmission electron microscopy.

Reaction of a filamentous carbon sample with hydrogen was conducted

using a differential, micro-packed bed reactor system. In a typical gasification experiment, hydrogen of a constant flowrate is passed through a loosely-packed 1 gram sample of filamentous carbon and the flowrate and composition of exit gas measured as a function of time. Hydrogen and methane content of the exit gas is measured by an automatic sampling gas chromatograph. Exit flowrate is measured and recorded by a custom-designed volumetric displacement type flowmeter. The precision and accuracy of all measurements permitted carbon mass balances for test reactions of 96-102% to be routinely obtained. All reactions were conducted at near atmospheric pressure over the temperature range from 798 to 1073°K. Commercially pure bottled hydrogen and deuterium were used in all reactions. Further description of the reactor system and experimental procedures is being reported elsewhere.

4. Results and Discussion

Representative gasification curves for filamentous carbon are shown in Figure 2. For the temperature range investigated, all reactions displayed a similarly shaped conversion curve. During the initial 60-70% carbon gasification, the global rate for all reactions was virtually constant, exhibiting a zero-order dependence on carbon. Beyond approximately 70% conversion, reaction rate declined rapidly with further conversion. The zero-order rate dependence is consistent with a catalytic or topochemical reaction involving axial attack of long length filaments. The reaction span marked by an unsteady rate probably has zero-order rate dependence also, but this is masked by a diminishing percentage of reacting filaments. The zero-order dependence observation agrees with observations made in other studies (4,5) involving carbons produced from hydrocarbons and employing different deposition catalysts. The activation energy determined for the gasification reaction below 873°K is approximately 178 KJ/mole. Between approximately 873 and 1023°K an apparent maximum in reaction rate was observed. This maximum, however, was an experimental artifact due to the attainment of equilibrium and the onset of hydrogen feedrate control of the reaction.

The ability of the ASF model to quantitatively fit experimental data is illustrated in Figure 3. This correlation was made using the Gaussian normal probability function (6) for the filament length distribution term in Equation (1) and using non-linear least squares regression analysis to determine the model parameters. The integral expression used for regression is given in Equation (2). The terms \bar{l}_0 and σ^2 used in this equation refer to the filament length distribution parameters, mean length, and variance for the initially unreacted sample. Selection of the Gaussian function to represent the filament length distribution is a reasonable choice in the absence of any foreknowledge about the length distribution. It is intermediate between a monodisperse and uniform length distribution in its effect on the predicted shape of the gasification curve. Additionally, it requires only two parameters, a mean and variance, to fully describe the distribution.

$$\alpha = 1 - \frac{\int_0^{\infty} l \exp \left\{ -\frac{1}{2} \left(\frac{l - \bar{l}_0}{\sigma} \right)^2 \right\} dl - vt \int_0^{\infty} \exp \left\{ -\frac{1}{2} \left(\frac{l - \bar{l}_0}{\sigma} \right)^2 \right\} dl}{\int_0^{\infty} l \exp \left\{ -\frac{1}{2} \left(\frac{l - \bar{l}_0}{\sigma} \right)^2 \right\} dl} \quad (2)$$

As indicated by Figure 2 the model appears adequately capable of describing the conversion kinetics of filamentous carbon. Appropriateness of the ASF model was further evaluated in a special series of tests. In this series, samples of carbon produced from a single deposition experiment were reacted at different temperatures and model parameters determined for each reaction. If the model is an appropriate one, only the filament shrinkage rate, v , should be observed to vary with temperature; the filament length distribution parameters should be constant within sampling and experimental error. That this is indeed the case may be seen from the results presented in Table 1. While v increases by nearly a factor of five in going from a reaction temperature of 798 to 848°K, \bar{l}_0 and σ remain relatively constant. Increasing the reaction temperature to 1073°K, where there is a definite change in Arrhenius activation energy, and also switching to deuterium reactant yield the same distribution parameter values. This is further evidence of the appropriateness of the model. The ASF model is a macro-physical description of the reaction and is not based on any particular, molecular rate-controlling mechanism.

Table 1. Regression fitted model parameters for various temperature reactions.

Gasification Temperature, °K	Model Parameter		
	v^a	\bar{l}_0^b	σ
798	.39	84	16
823	1.00	84	15
848	1.91	82	22
1073	0.80	83	20
1073	0.81 ^c	82 ^c	26 ^c
	Average	83	20

a Filament shrinkage rate relative to 823°K value.

b Filament distribution average length and standard deviation expressed in dimensionless length units.

c Results for deuterium - carbon gasification reaction.

5. Summary and Conclusions

A general reaction model has been proposed for describing the gasification of filamentous carbons. The model, termed the "axially shrinking filament" model, successfully correlates gasification data obtained for the hydrogen-filamentous carbon reaction where the carbon is produced from CO disproportionation over a cobalt catalyst. The model may be applicable for other filamentous carbon gasification reactions and should be useful in the design of coked catalyst regeneration schemes.

REFERENCES

1. Albright, L. F., Baker, R. T. K. eds Coke Formation on Metal Surfaces, American Chemical Society Symposium Series 202, ACS, Wash, D.C., 1982.
2. Baker, R. T. K., Harris, P. S., The Formation of Filamentous Carbon, in Chemistry and Physics of Carbon, Vol. 14, P. L. Walker, P. A. Throer eds., 83-165, 1978.
3. Figueiredo, J. L., Trimm, D. L., J. Catal. (1975), 40, 154.
4. Nishiyama, Y., Tamai, Y., Carbon (1976), 14, 13.
5. Figueiredo, J. L., Carbon (1981), 19, 146.
6. Abramowitz, M., Stegun, I. A., eds, Handbook of Mathematical Functions, Dover Publications, N.Y., 1965.

FIGURE 1. AXIALLY SHRINKING FILAMENT MODEL.

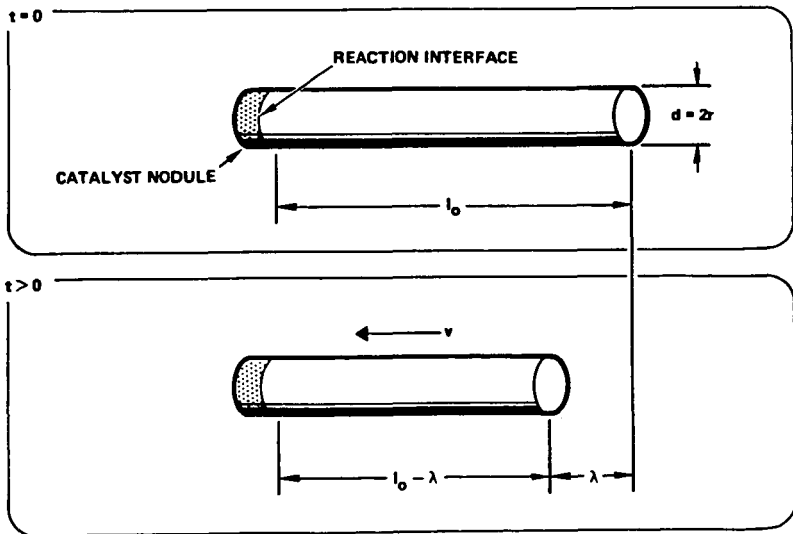


FIGURE 2. REPRESENTATIVE CONVERSION-TIME CURVES FOR FILAMENTOUS CARBON GASIFICATION.

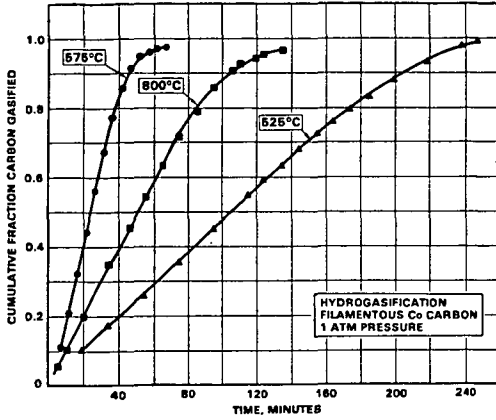
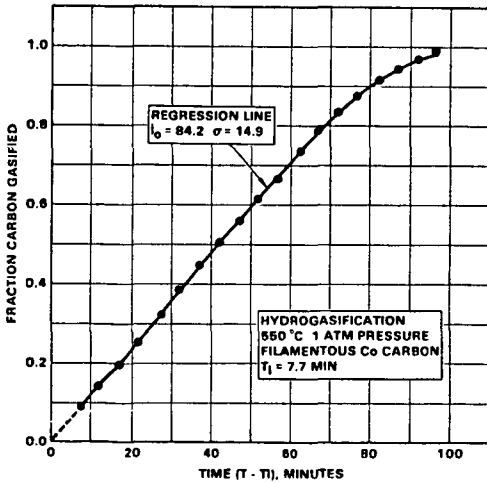


FIGURE 3. MODEL CORRELATED REACTION DATA FOR FILAMENTOUS CARBON GASIFICATION.



Metal Particle Characterization of Zeolite-Based Syngas Conversion Catalysts

V.U.S. Rao, R.T. Obermyer,* A. Shamsi, R.K. Wicker,**
R.J. Gormley and R.R. Schehl

U.S. Department of Energy
Pittsburgh Energy Technology Center
P.O. Box 10940, Pittsburgh, PA 15236,

*Department of Physics, Pennsylvania State University
McKeesport, PA 15132, and

**Washington and Jefferson College, Washington, PA 15301

INTRODUCTION

The conversion of $\text{CO} + \text{H}_2$ in one step to a mixture of hydrocarbon species that are the constituents of high octane gasoline appears possible with catalysts composed of ZSM-5 and a group VIII metal (1-5). The group VIII metal acts as a Fischer-Tropsch (F-T) catalyst and converts synthesis gas to a mixture of olefins, paraffins, and oxygenates. The ZSM-5 component of the catalyst converts some of the F-T intermediates and products to aromatics and branched-hydrocarbon species.

The present study attempts to characterize the metal crystallite size and the degree of reduction of cobalt-ZSM-5 catalysts using chemisorption and magnetization measurements. The catalysts prepared by the solution-impregnation method were examined. It was realized that the method could result in partial ion exchange of the acidic protons in ZSM-5 with cobalt ions (5-7). The ion-exchanged cobalt (Co^{2+}) is catalytically inactive in synthesis gas conversion (6,7), since it cannot be reduced to metallic cobalt under usual reduction treatment, namely, flowing hydrogen at 350°C. The present study attempts to demonstrate how chemisorption and magnetization measurements on Co/ZSM-5 catalysts with different Co concentrations can enable one to estimate the weight percent Co that has been ion-exchanged into ZSM-5.

It has been reported (8,9) that $(\text{Fe}^{2+}, \text{NH}_4^+)Y$ can react with an anionic, metal-containing coordination compound that is water-soluble, such as $(\text{NH}_4)_3[\text{Fe}(\text{CN})_6]$, to yield an insoluble compound, $\text{Fe}_3[\text{Fe}(\text{CN})_6]_2$, distributed throughout the zeolite while the zeolite itself returns to the ammonium form. The insoluble complex can later be reduced in hydrogen to finely dispersed metal in the zeolite (9). The present work attempts to examine whether the above method could be used to convert ion-exchanged Co^{2+} in ZSM-5 to a reducible and catalytically active form. Since it was of interest to examine the catalytic activities of both the metal component and the zeolite component, before and after the reaction with the coordination compound, separate experiments were performed with syngas and ethylene as the reactants. Syngas conversion is primarily catalyzed by the metal component; and ethylene conversion, by the zeolite component in the catalyst.

EXPERIMENTAL

(a) Preparation of Catalysts

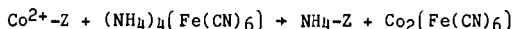
The ZSM-5, with $\text{SiO}_2/\text{Al}_2\text{O}_3 \sim 30$, was synthesized using the procedure given in the patent literature by Argauer and Landolt (10), with minor modifications. The procedure yields ZSM-5 having crystallites approximately one micron in size. The zeolite was calcined in air at 538°C to decompose the tetrapropylammonium (TPA^+)

cation. It was converted to the ammonium form by three successive exchanges using NH_4Cl solution.

To prepare the metal-loaded catalysts, the solution-impregnated method was used. Aqueous cobalt (II) nitrate solution was added to $\text{NH}_4\text{-ZSM-5}$ until incipient wetness was reached. The atmosphere surrounding the mixture was evacuated after the solution was added. The mixture was dried with stirring at 100°C . Three samples with 2.7, 5.9, and 9.0 wt% $\text{Co/NH}_4\text{-ZSM-5}$ were prepared by this method.

In order to prepare a sample of $\text{Co/NH}_4\text{-ZSM-5}$ in which the cobalt could be expected to be almost entirely in the ion-exchanged form, the following procedure was used. Ten grams of $\text{NH}_4\text{-ZSM-5}$ was added to 120 mL of 9.5 wt% $\text{Co(NO)}_3\cdot 6\text{H}_2\text{O}$ solution in water at 90°C . The mixture was stirred for one hour and filtered. The procedure was repeated two more times, and the zeolite sample was thoroughly washed with water until no nitrate was present. The sample had 0.9 wt% Co , presumably in the ion-exchanged form (IE), and will be designated 0.9 wt% $\text{Co/NH}_4\text{-ZSM-5}$ (IE).

"Back-exchange" (BE), i.e., removal of the ion-exchanged Co^{2+} from the zeolite, was attempted on the basis of the following reaction (8):



The $\text{Co}_2(\text{Fe}(\text{CN})_6)$, an insoluble compound, would be distributed throughout the zeolite. Subsequent reduction in hydrogen at 400°C should result in a zeolite containing cobalt and iron, while the zeolite itself is converted to the H-form.

To carry out the back-exchange, 15 g of 0.9 wt% $\text{Co/NH}_4\text{-ZSM-5}$ (IE) was stirred in 150 mL of 3.3 wt% $(\text{NH}_4)_4\text{Fe}(\text{CN})_6\cdot\text{H}_2\text{O}$ solution in water for 4 hours at room temperature. The mixture was filtered. The back-exchanged zeolite sample was analyzed and found to contain 0.9 wt% Co and 0.2 wt% Fe , and will be designated 0.9 wt% Co , 0.2 wt% $\text{Fe/NH}_4\text{-ZSM-5}$ (BE).

A part of each of the five samples was pelleted into 3-mm-diameter tablets for catalytic activity tests. The pellets were calcined in air at 450°C for one hour to convert the $\text{NH}_4\text{-ZSM-5}$ to the H-form. Parallel studies using infrared spectroscopy showed deammoniation was nearly complete under these conditions (7).

(b) Magnetization Measurements

Samples for magnetic analysis were placed in 4-mm-outside-diameter glass tubes and reduced in flowing hydrogen at 350°C for 16 hours. The tubes were then sealed under vacuum.

The magnetic measurements were performed using a vibrating sample magnetometer in applied fields up to 15 kOe. The saturation magnetization was obtained by plotting σ versus $1/H$ and extrapolating to zero (infinite fields). The values obtained were compared with the known saturation magnetization of bulk metallic cobalt, and the degree of reduction was obtained. The percent reduction is reported in Table I.

(c) Chemisorption Measurements

Hydrogen adsorption measurements were performed using a conventional glass volumetric adsorption apparatus. One gram of catalyst sample was used. The sample was heated to 200°C ($4^\circ\text{C}/\text{min}$) under flowing He (60 mL/min) and kept at that temperature for 1 hour. The sample chamber was evacuated and cooled to 50°C . Hydrogen (60 mL/min) was introduced and the temperature was raised to 350°C ($4^\circ\text{C}/\text{min}$). The sample was reduced at 350°C for 16 hours. The sample chamber was evacuated to 10^{-5} torr and cooled to the adsorption temperature.

The H₂ adsorption measurements were conducted at 100°C. The adsorption isotherms are shown in Figure 1.

(d) Metal Particle Size Calculations

The values of hydrogen uptake were extrapolated to zero hydrogen pressure from the linear portion of the isotherm (Figure 1), as outlined by other workers for nickel catalysts (11,12).

The metal dispersions $D = \text{Co}_s / \text{Co}_t$, where Co_s is the number of surface cobalt atoms and Co_t is the total number of cobalt atoms, were calculated using the adsorption stoichiometry of $\text{H}/\text{Co}_s = 1$. Average crystallite diameters (Table I) were calculated from $\%D$ for spherical hcp metal crystallites (6) of uniform diameter using the following relation (13):

$$d(\text{nm}) = 73.81/\%D$$

(e) Catalytic Conversion Tests

The equipment used was a downflow, fixed bed reactor of 1-cm inner diameter. The mass of the catalyst sample was 1.35 g. The sample was reduced in hydrogen at 350°C. The conversion of syngas ($\text{H}_2/\text{CO} = 1$) at 280°C, 12 bar, and a flow of 0.659 g/g cat. hr was examined for a 24-hour period.

The products of the reaction were CO_2 , H_2O and hydrocarbons, and were analyzed using gas chromatography. The C_5+ product was analyzed using simulated distillation. It was also separated into aromatics, olefins and saturates using the FIA method.

Ethylene conversion studies were also conducted in a reactor similar to that mentioned above. After treatment with hydrogen at 350°C, the reaction mixture consisting of 30 vol% C_2H_4 and 70 vol% H_2 , was introduced at 1 atm and a flow rate of 0.983 g/g cat. hr. The temperature of the reactor was maintained at 320°C. The products were analyzed as described above.

RESULTS AND DISCUSSION

The results of magnetization and chemisorption studies are shown in Table I, Figure 1, and Figure 2. For the three catalysts containing 9.0, 5.9, and 2.7 wt% Co, approximately 2.2 wt% of the catalyst is the amount of cobalt that has not been reduced to metallic cobalt in flowing hydrogen at 350°C (see Table I). The hydrogen uptake and the degree of reduction exhibit similar trends when plotted against the cobalt loading (Figure 2), and each curve intercepts the horizontal axis at nearly 2.2 wt%.

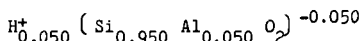
The amount of hydrogen chemisorbed can be expected to be approximately proportional to the metal surface area. The absence of metallic cobalt in a sample would result in zero chemisorption of hydrogen. It is thus understandable that both the hydrogen uptake and the degree of reduction obtained from the magnetization study become vanishingly small at the same concentration (2.2 wt%) of cobalt in the catalyst.

The results from $\text{H}_2 + \text{CO}$ conversion experiments are shown in Figure 2 and Table II. The variation of the rate of conversion with cobalt loading also follows the same trend as the chemisorption and degree of reduction. Of the liquid hydrocarbon products obtained with these catalysts, nearly 95% is in the gasoline boiling range, as revealed by simulated distillation. The C_5+ product consists of aromatics, branched olefins, and branched paraffins, which are constituents of high octane gasoline.

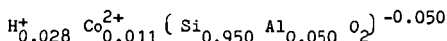
The conversion of H_2+CO by 0.9 wt% Co/ZSM-5 (IE) is zero, consistent with the observation that the degree of reduction is zero after exposure to hydrogen at 350°C (Table I and Figure 2). This provides additional support that the cobalt in this sample is in an ion-exchanged form that cannot be reduced to the catalytically active metallic cobalt. When the sample is back-exchanged to yield 0.9 wt% Co, 0.2 wt% Fe/ZSM-5 (BE), the $CO+H_2$ conversion is 17.3%, and the degree of reduction is 48%. The existence of a ferromagnetic moment indicates that Co (and possibly Fe) is in the metallic state in the back-exchanged sample.

The conversion of ethylene over H-ZSM-5 and the metal-zeolite samples (ion-exchanged and back-exchanged) was used as a method for comparison of their catalytic acid function. The results are shown in Table III for the first six hours on stream. The cobalt-exchanged sample exhibits C_2H_4 conversion of 78.7%, while the H-ZSM-5 (parent sample) exhibits a conversion of 86.1%. The cobalt-exchanged sample also yields a lower fraction of aromatics (37%) in comparison to H-ZSM-5, which yields 53% aromatics in the liquid hydrocarbon product. It is thus indicated that the acid function of the zeolite is weakened by the presence of cobalt in ion-exchanged form. Back-exchange of the cobalt results in a catalyst that brings about an improved ethylene conversion (89.8%) and larger aromatic fraction (42%).

The above results obtained from physical measurements (chemisorption and magnetization) and catalytic activity tests indicate how metal speciation in cobalt/ZSM-5 can be characterized. The parent sample of H-ZSM-5 with $SiO_2/Al_2O_3=38$ can be represented by



The ion-exchanged sample 0.9 wt% Co/ZSM-5 (IE) can be represented by



It can be noticed that 44% of the H^+ sites have been exchanged with cobalt, resulting in weakened acidity. In the back-exchanged sample, at least 48% of Co^{2+} has been replaced by NH_4^+ , while the cobalt is converted to the insoluble compound $Co_2Fe(CN)_6$. Calcination at 450°C, followed by reduction in H_2 at 350°C, results in the conversion of the zeolite to the H^+ -form and the formation of metallic cobalt. The resulting sample exhibits catalytic activity for synthesis gas conversion.

CONCLUDING REMARKS

This study demonstrated that magnetic and chemisorptive techniques can be used to characterize metal speciation in catalysts such as Co/ZSM-5. In particular, the amounts of ion-exchanged cobalt and cobalt external to the zeolite can be estimated. These measurements enable one to interpret the catalytic activity and selectivity of the catalyst.

In our attempts to introduce cobalt in cationic form in ZSM-5 a temperature of 90°C has been used for the exchange with aqueous cobalt nitrate solution. It appears that 0.9 wt% Co can be introduced into ZSM-5 of $SiO_2/Al_2O_3=38$ under these circumstances. Analyses of the Co/ZSM-5 samples that were prepared by impregnation at room temperature with cobalt nitrate solution showed that approximately 2.2 wt% Co was in a form not reducible to metallic cobalt (Table I). In earlier work (6,7), the Co/ZSM-5 samples were subsequently washed with water to yield samples that contained 1.4-1.7 wt% Co. Hence it is possible that exchange at temperatures lower than 90°C would yield samples containing more than 0.9 wt% Co in ion-exchanged form (14).

This study has shown that $\text{Co}^{2+}/\text{ZSM-5}$ can be back-exchanged and reduced to yield metallic cobalt supported on H-ZSM-5. Chemisorption measurements are currently being carried out to determine the degree of dispersion of such samples. The back-exchanged samples are catalytically active in synthesis gas conversion. The method of back-exchange should be generally applicable for preparing metal-zeolite catalysts where it is desirable to free the zeolite of metal cations in order to restore the acidity to its original strength, and to have the metal on the exterior of the zeolite crystallites in a highly dispersed, catalytically active form.

ACKNOWLEDGMENTS

The authors would like to thank Bernard D. Blaustein, John M. Stencel, and Kee H. Rhee for helpful discussions.

REFERENCES

1. C.D. Chang, W.H. Lang, and A.J. Silvestri, *J. Catal.* 56, 268 (1979).
2. P.D. Caesar, J.A. Brennan, W.E. Garwood, and J. Ciric, *J. Catal.* 56, 274 (1979).
3. V.U.S. Rao and R.J. Gormley, *Hydrocarbon Process.*, 59(11), 139 (1980).
4. T.J. Huang and W.O. Haag, *ACS Symposium Series* 152, 308 (1981).
5. V.U.S. Rao, *Physica Scripta* T4, 71 (1983).
6. J.M. Stencel, V.U.S. Rao, J.R. Diehl, K.H. Rhee, A.G. Dhere, and R.J. DeAngelis, *J. Catal.* 84, 109 (1983).
7. V.U.S. Rao, R.J. Gormley, R.R. Schehl, K.H. Rhee, R.D.H. Chi, and G. Pantages, in "Catalytic Conversions of Synthesis Gas and Alcohols to Chemicals," Ed. R.G. Herman, Plenum (1984), p. 151.
8. J. Scherzer and D. Fort, *J. Catal.* 71, 111 (1981).
9. J. Scherzer, *J. Catal.* 80, 465 (1983).
10. R.J. Argauer and G.R. Landolt, U.S. Patent 3,702,886 (1972), Example 24.
11. M.A. Vannice and R.L. Garten, *J. Catal.* 56, 236 (1979).
12. C.H. Bartholomew and R.B. Pannell, *J. Catal.* 65, 390 (1980).
13. R.C. Reuel and C.H. Bartholomew, *J. Catal.* 85, 63 (1984).
14. P. Chu and F.G. Dwyer, *ACS Symp. Series* 218, 59 (1983).

TABLE I
Results from Magnetization and Chemisorption on Co/ZSM-5

Metal Loading (wt%)	% Reduction in H_2 at 350°C (from magnetization)	Wt% Co Unreduced	H_2 Uptake at 100°C ($\mu \text{ mol g}^{-1}$)	d(nm)
9.0	78	2.0	35.4	12.4
5.9	64	2.1	22.5	10.4
2.7	10	2.5	2.4	8.5
0.9 (IE)	0	0.9		
0.9 (BE) +0.2 Fe	48	0.4		

TABLE II

Conversion and Product Distribution From Co/ZSM-5 Catalysts
During the Initial 24-Hour Period
IE: ion-exchanged; BE: back-exchanged

H₂/CO = 1; P = 21 bar; Temperature = 280°C; Feed Rate = 0.659 g/g cat. hr

Co in Catalyst (wt%)	9.0	5.9	2.7	0.9 (IE)	0.9 (BE) +0.2 Fe
CO Conversion (%)	56.5	54.6	21.0	0.0	13.7
H ₂ Conversion (%)	85.8	80.8	34.3	0.0	20.9
CO+H ₂ Conversion (%)	70.7	67.3	27.4	0.0	17.3
<u>Product Composition (wt%)</u>					
CO ₂	18.6	13.2	8.1		13.9
H ₂ O	46.1	50.9	56.6		55.9
CH _n	35.2	35.8	35.3		30.2
<u>Composition of CH_n (wt%)</u>					
CH ₄	24.4	24.0	33.6		42.4
C ₂ H ₄	0.0	0.4	0.0		0.0
C ₂ H ₆	2.7	2.3	5.2		3.1
C ₃ H ₆	0.8	0.6	0.0		0.0
C ₃ H ₈	2.7	2.7	7.7		18.4
C ₄ H ₈	0.8	1.4	0.9		0.0
C ₄ H ₁₀	5.4	6.6	18.7		24.2
C ₅ +	63.0	61.9	33.8		11.8
<u>Liquid Product Composition (vol%)</u>					
Aromatics	19.5	23.0			
Olefins	32.5	30.5			
Saturates	48.0	46.5			

TABLE III

Conversion of 30 vol% C₂H₄ + 70 vol% H₂ Mixture
over H-ZSM-5 and Co/ZSM-5 (SiO₂/Al₂O₃=38).

Feed Rate = 0.983 g/g cat. hr; Temperature = 320°C

Catalyst	H-ZSM-5	0.9% Co/H-ZSM-5 (ion-exchanged)	0.9% Co, 0.2% Fe/H-ZSM-5 (back-exchanged)
Period (hours)	0-6	0-6	0-6
C ₂ H ₄ Conversion (%)	86.1	78.7	89.8
H ₂ Conversion (%)	9.2	8.5	13.4
<u>Product Composition (wt%)</u>			
CH ₄	0.0	0.0	0.0
C ₂ H ₆	14.5	13.3	27.0
C ₃ H ₆	7.6	12.6	6.1
C ₃ H ₈	5.5	2.5	4.3
C ₄ H ₈	11.6	14.0	9.7
n-C ₄ H ₁₀	5.8	6.3	5.7
i-C ₄ H ₁₀	7.6	5.4	5.7
C ₅ +	47.3	45.8	41.1
<u>Liquid Product Composition</u>			
Aromatics	53	37	42
Olefins	31	50	43
Saturates	16	13	15

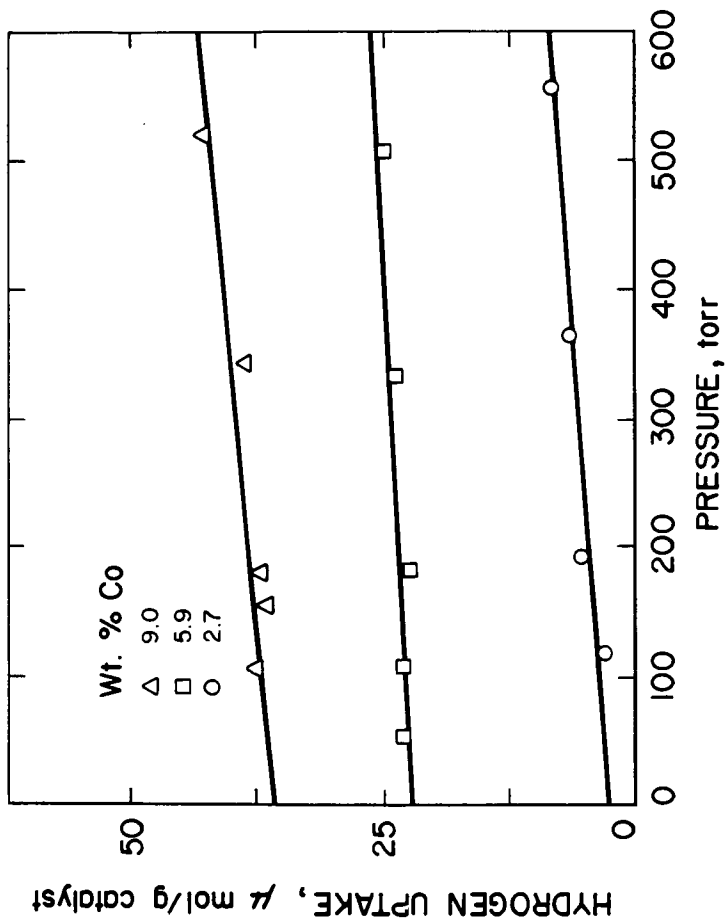


Figure 1. Hydrogen adsorption Isotherms at 100°C on Co/ZSM-5 catalysts.

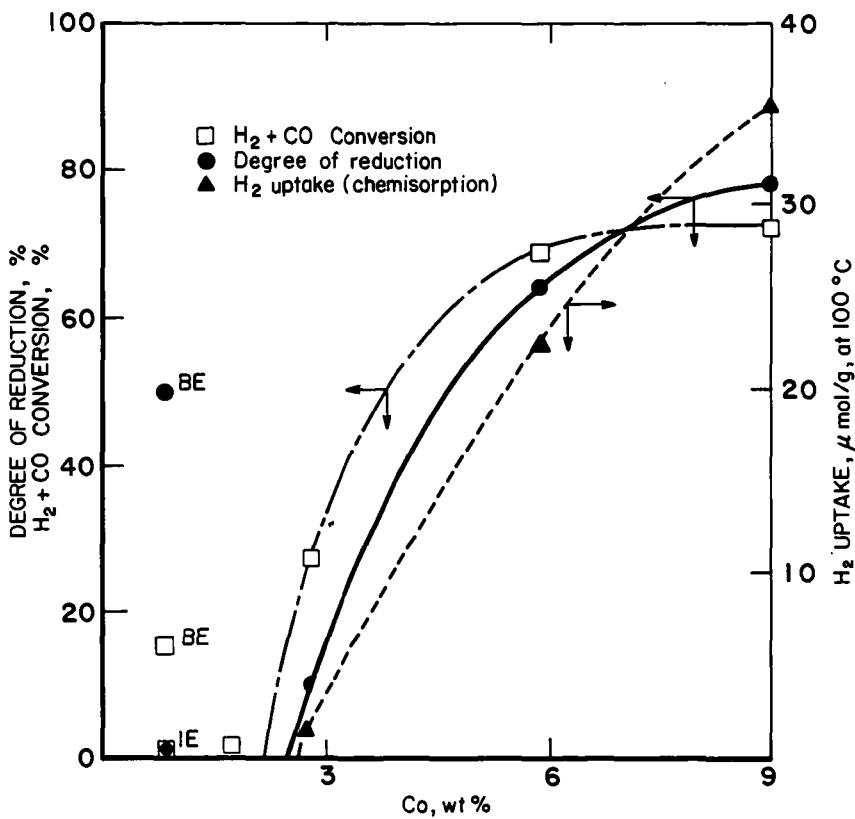


Figure 2. Degree of reduction, chemisorption and H₂ + CO conversion on Co/ZSM-5. IE: ion-exchanged, BE: back-exchanged.

BSI/3382

A CURRENT VIEW OF THE MECHANISM FOR THE CATALYTIC GASIFICATION OF COAL CHAR

Bernard J. Wood and Kenneth M. Sancier

Materials Research Laboratory, SRI International
333 Ravenswood Avenue, Menlo Park, CA 94025

INTRODUCTION

The addition of modest quantities of certain inorganic salts to coal substantially promotes its reactivity with steam or carbon dioxide. Because of the cost of the added salt and the addition of process steps for admixture and recovery, technoeconomic analysis predicts that this catalytic coal gasification process can be of practical value only in cases where the maximum process temperatures are limited by outside constraints.[1] One such case is the production of methane, where high equilibrium yield is favored by lower temperatures.[2] Current predictions, based on natural gas demand and reserves, suggest that methane from coal will not be needed in the next 25-50 years. Consequently, industrial interest in the catalytic gasification of coal, once high, has waned, and full-scale development of the process has been given lower priority.

Another potentially attractive application of the catalytic gasification process is the utilization conversion, storage, and transport of heat produced by a gas-cooled nuclear reactor where the attainable coolant temperature has an upper limit of about 950°C.[3] Implementation of this technology is being considered[4], but large-scale application lies some distance in the future.

However, the low probability of near term applications has not hampered scientific interest in the process. In the last few years, many investigators have studied the process, using a wide variety of approaches and tools. Since 1980 more than 100 papers have been published on the subject of the mechanism of catalytic gasification of char or carbon.[5] This investigative activity has given us sufficient insight into the process to suggest a detailed mechanism that defines the nature and role of the catalyst during gasification.

CHARACTERISTICS OF CATALYST ACTION

Effective coal/char gasification catalysts are ionic salts with oxygen-bearing anions (or anions that are converted to oxygen-containing species under gasification conditions). The cations of the salt react

with the carbonaceous material to form a chemically and thermochemically distinct active species that mediates the gasification process. The anions of the salt may modify the pathway of formation of the active species, but for all effective salts this species is certainly formed at sub gasification temperatures.

There is broad agreement among recent investigators that the catalyst supplies oxygen to the carbon. Many investigators favor involvement of a redox cycle in which the catalyst is reduced by the carbon and oxidized by the gaseous reactant, but few speculate on a detailed mechanism. Nevertheless, there are a number of details of the gasification reaction system for which evidence is particularly strong:

- The working catalyst forms a liquid film that wets the carbon surface;
- The molten catalyst is a metal-rich (oxygen deficient) compound, probably an oxide, over which the metal vapor pressure has a characteristic equilibrium value;
- Chemical attack by the catalyst and during gasification occurs at the carbon atoms on edges of aromatic arrays;
- The reduction step occurs by donation by the carbon of an electron to the catalyst phase, neutralizing the cationic charge;
- A metal-oxygen-carbon complex analogous to a phenolate salt is a reaction intermediate;
- The intermediate is a precursor of gaseous CO production by a decarbonylation step that is likely rate governing.

A PROPOSED MECHANISM

Based on these considerations, we have devised a detailed mechanism of catalyst action. Dispersion of the catalyst is a critical initial step that occurs at subgasification temperatures when the catalyst becomes a liquid film that wets the carbon and spreads over its exposed surface. Evidence for such a process comes from microscopic studies[6-8], measurements of surface area changes,[9,10] and the observed increase in electrical conductance upon heating of carbon-catalyst admixtures,[10] indicative of the formation of a phase with high charge carrier mobility. More quantitative information about the nature of alkali metal carbonates admixed with carbon is obtained from Knudsen cell mass spectrometry.[11] At about 900 K, both carbon-K₂CO₃ and carbon-Cs₂CO₃ admixtures in a Knudsen cell gradually lose oxygen, as evidenced by a progressive diminution in the equilibrium partial pressures of CO and CO₂. At the same time the pressure of the alkali metal increases, indicating an increase in thermodynamic activity possibly produced by a change in metal/oxygen stoichiometry. Opposite changes occur when steam

or CO_2 is admitted to the Knudsen cell. These observations suggest that the liquid film in contact with the carbon is a non-stoichiometric oxide that contains an excess of the metal as atoms in a dissolved state. During gasification, the composition of the film is determined by a dynamic balance between a reducing process at the carbon-catalyst interface and an oxidizing process at the surface in contact with the gaseous reactant. The composition and characteristics of some Cs-rich oxides have been characterized as crystalline solids at room temperature.[12] At high temperatures they melt into liquid phases (for which free energies of formation have been evaluated) comprised of a higher oxide containing excess Cs.[13] Using the equilibrium partial pressures of Cs and CO measured over a Cs_2CO_3 -carbon sample in the Knudsen cell, together with the published thermochemical data[13], we estimated the composition of the liquid phase to be Cs_4O . [11] A similar analysis of the K_2CO_3 -carbon system was not possible because of the lack of thermochemical data at low oxygen partial pressures. By analogy, however, all alkali-metal-oxygen systems would be expected to behave in a parallel fashion. Further, very recent evidence of the conversion of K_2CO_3 to a nonstoichiometric oxide in the presence of carbon is provided by studies with isotope-labelled catalysts.[14]

The existence of an oxide with an excess of the alkali-metal component requires an equivalent number of oxygen vacancies. Thus, the affinity of this phase for reaction with an oxidizing gas will be proportional to the alkali metal activity. Oxygen ions produced by this reaction between the catalyst phase and an oxidizing gas are transported to the carbon/catalyst interface by diffusion, a process that is fast at gasification temperatures. One principal product of steam gasification, H_2 , would be formed at the catalyst/steam interface.

The reaction steps occurring at the carbon/catalyst interface require some explanation because the carbon structure is comprised to some degree of planar aromatic arrays, and aromatic hydrocarbons are known to be quite unreactive toward oxide and hydroxide ions. Transmission electron microscopy[7,8] has confirmed that the catalyst interacts with carbon atoms located at the edges of the planar arrays, but the mechanism of the attachment remains obscure. We suggest that the initial reaction step is a simple electron transfer from the aromatic material to the alkali metal ion of the catalyst. Recently reported[15] measurements made in an electrochemical cell with a molten Na_2CO_3 electrolyte provide strong evidence for such an electron transfer step. In this work, the addition of graphite to the electrolyte (in the absence of air) rapidly shifted the rest potential of the cell from -0.511 to -1.348 V, indicative of the formation of an easily oxidized species, such as sodium metal, due to reduction of the sodium ions in the carbonate by the solid carbon. This process produces directly an excess of metal atoms in the catalyst and leaves the carbon array with a net positive charge, termed a radical cation. Such a species would be highly reactive toward the negatively charged oxygen ions in the catalyst. It is highly probably that reaction of the radical cation and the O^- leads to formation of a phenolate ion, the presence of which in

the carbon array has been confirmed.[16] Indeed, phenolate ion structures would be stabilized by alkali metal ions in the molten catalyst film. The existence of some type of K-O-C structure has been suggested also on the basis of infrared spectra of partially gasified K_2CO_3 -char admixtures.[17,18]

The rate of formation of CO during char gasification has been correlated with the concentration of phenolate groups.[19] This observation, in conjunction with the observed stability and steady state population of these groups at gasification temperatures,[20] suggests that decomposition of the phenolate groups is the rate-governing step in the catalytic gasification process. Decomposition may occur through conversion of the phenol functionality to the ketone followed by thermolytic decarbonylation.[10] This part of the gasification reaction pathway remains speculative, although such decarbonylation reactions have been observed to occur at high temperatures.[21]

CONCLUSION

Inorganic salts composed of alkali metal cations and oxygen-bearing anions are effective catalysts for the steam or CO_2 gasification of coal char. Under gasification conditions the catalyst is converted to a nonstoichiometric oxide that is highly dispersed over the char surface as a liquid film. This catalyst film mediates the transfer of oxygen from the oxidizing gas to the char surface by way of a redox cycle. At the catalyst/char interface, electron donation by the char reduces the cation to a neutral metal atom dissolved in the catalyst, leaving a positively-charged radical cation on the char surface. The radical cation reacts readily with oxygen ions from the catalyst forming a phenolate functionality that is stabilized by the metal ions in the catalyst phase. The oxygen ions lost from the catalyst are replenished at the gas/catalyst interface by oxidation of the dissolved metal atoms by the oxidizing gas. The reactive intermediates are transported between gaseous oxidant and char by diffusion through the catalyst phase. CO is formed by decarbonylation of the phenolate species, a process that governs the rate of the gasification reaction.

ACKNOWLEDGEMENT

Our studies of the mechanism of catalytic gasification of char were supported by the U.S. Department of Energy, Morgantown Energy Technology Center under Contract No. DE-AC21-80MC14593.

REFERENCES

- [1] H. Juntgen, Fuel, 62 (2), 234 (1983).
- [2] N. C. Nahas, Fuel, 62 (2), 239 (1983).
- [3] H. Kubiak, H. J. Schroter, A. Sulimma, and K. H. van Heek, Fuel, 62 (2), 242(1983).

- [4] D. A. O'Sullivan, Chem. & Eng. News 62(10), 20-21 (1984).
- [5] B. J. Wood and K. M. Sancier, Catal. Rev. Sci. Eng., in press (1984).
- [6] H. Marsh and I. Mochida, Fuel, 60 (3), 231 (1981).
- [7] D. J. Coates, J. W. Evans, A. L. Cabrera, G. A., Somorjai, and H. Heinemann, J. Catalysis, 80, 215 (1983).
- [8] C. A. Mims, R. T. K. Baker, J. J. Chludzinski, and J. K. Pabst, Preprints Am. Chem. Soc. Fuel Chem. Div., 28 (1), 71 (1983).
- [9] K. Otto, L. Bartosiewicz, and M. Shelef, Fuel, 58 (8), 565 (1979).
- [10] B. J. Wood, R. H. Fleming, and H. Wise, Fuel, in press (1984).
- [11] B. J. Wood, R. D. Brittain and K. H. Lau, Carbon, in press, (1984).
- [12] A. Simon, Structure and Bonding (Berlin), 36, 81 (1979).
- [13] C. F. Knights and B. A. Phillips, J. Nuclear Mat., 84, 196 (1979).
- [14] J. M. Saber, J. L. Falconer, and L. F. Brown, private communication
- [15] G. B. Dunks, Proceedings International Conference on Coal Science, Pittsburgh (1983), p. 457.
- [16] C. A. Mims, K. D. Rose, M. T. Melchior, and J. K. Pabst, J. Am. Chem. Soc. 104, 6886 (1982).
- [17] I. L. C. Freriks, H. M. H. van Wechem, J. C. M. Stuiver, and R. Bouwman, Fuel 60, 463 (1981).
- [18] S. J. Yuh and E. E. Wolf, Fuel 62, 252 (1983).
- [19] C. A. Mims and J. K. Pabst, Am. Chem. Soc. Fuel Chem. Div. Preprints 25(3), 258 (1980).
- [20] C. A. Mims and J. K. Pabst, Fuel, 62 (2), 176 (1983).
- [21] G. Schaden, Proc. 3rd. International Symp. Analyt. Pyrolysis, C.E.R. Jones and C. A. Cramers, editors, Elsevier, New York, 1977, p. 289.

CARBONACEOUS AEROSOL FROM RESIDENTIAL WOOD COMBUSTION

J.A. Rau and J.J. Huntzicker

Department of Chemical, Biological, and Environmental Sciences
Oregon Graduate Center, 19600 N.W. Walker Road, Beaverton, Oregon 97006

Because of rising conventional energy prices wood has made a resurgence as a residential heating fuel. As a result residential wood smoke aerosols are becoming a major component of fine ambient aerosols in many areas. However, the quantification of the impact of residential wood smoke on the ambient aerosol concentration has been difficult because these aerosols are variable in composition and size and have no unique elemental tracers.

The purpose of this study has been to examine the size distribution and composition of residential wood smoke aerosols which have been sampled from cooled, diluted smoke plumes. Particles sampled in this manner should be more representative of wood smoke aerosols as they exist in the atmosphere than those sampled with EPA Method 5. Sampling was usually done about 1.5 m from the stack on days when the breeze was sufficient to move the plume in a mostly horizontal direction. Carbon dioxide measurements in the flue gas and in the sampled air indicated that the dilution factor was from 50 to 100. Air sampled from the plume was taken into a mixing chamber which was a 2 m long, 20 cm diameter aluminum pipe. Six samplers were located in the far end of the pipe. Each sampler consisted of a section of 5 cm diameter pipe which contained an impactor at its upstream end and a filter holder at its downstream end. Bypass air flow was maintained in the pipe to provide isokinetic sampling conditions. Single stage impactors with cut points at 2.5, 1.2, 0.6, 0.3, and 0.1 μm were used. One sampler which contained no impactor was used to sample the total aerosol concentration. Samples were collected on 37 mm diameter quartz filters for organic and elemental carbon analysis by thermo-optical carbon analysis (1,2). Samples were also collected on Teflon filters for analysis by x-ray fluorescence.

The composition and size distribution of wood smoke aerosols are a function of the burning conditions, fuel type, and stove type. In order to examine the range of variation of wood smoke characteristics, a series of tests which bracketed the typical burn conditions in residential applications was used. These consisted of burning hot (with the damper full open) and burning cool (with the damper closed). Testing was done with a conventional box type air-tight stove installed in a residence. The flue pipe was 20 cm in diameter and rose vertically from the top of the stove for a distance of 3.5 m. Enough air leaked into the stove with the damper closed to maintain combustion. This is a typical burn condition for residential heating. Fuel loads were usually three to four pieces of well-aged Douglas fir (quarter sections out of a 25 cm diameter log) that were about 0.5 m long. With this size fuel load (about one-quarter of the stove capacity) a reasonably intense fire could be maintained when the damper was fully open. By opening or closing the damper, operating conditions could be changed from hot operation to cool operation or vice versa. A test was started by adding the fuel load to a bed of coals. Sampling was started 10-15 minutes after fuel addition so as to be representative of average continuous burning where wood is added periodically to maintain a constant heat output. The length of the sampling period was chosen to obtain appropriate samples for analysis, usually 10-20 minutes.

In all cases the particles emitted during hot burning were significantly different from those emitted during cool burning. Qualitatively the mass loading in the sampled air was from three to six times greater for cool burn plumes than it was for hot burn plumes. However, the heat output of the stove was much less during a cool burn than it was for a hot burn. During hot burning the plume was almost invisible. The color of the collected aerosol was black and up to 60% of its carbon content was in the form of elemental carbon. The aerosol mass was primarily in

particles below 0.6 μm in diameter. Table 1 lists several aerosol mass distributions during hot burn conditions.

For cool burn tests the plume was always very visible and similar to plumes typically associated with residential wood burning. The color of the collected aerosol ranged from light yellow to dark tan. Table 2 shows some typical aerosol mass distributions as a function of size for cool burn tests.

In both hot and cool burns $70 \pm 10\%$ of the aerosol mass was carbon. In hot burns, as noted previously, elemental carbon predominated, but in cool burn conditions most of the carbon was organic. Size distributions of organic, elemental, and total (i.e., organic plus elemental carbon) are given in Table 3 for both hot and cool burn conditions. These results indicate that the mass distribution of carbon in cool burns is shifted to larger particle sizes relative to the hot burn cases.

In summary these results show that residential wood stove smoke particles are broadly distributed in the fine aerosol mode and that their composition can vary widely as a function of burn temperature. Studies on both source and ambient aerosols are continuing.

Acknowledgment. This research was sponsored in part by U.S. Environmental Protection Agency Grant R810091. The paper has not been subjected to EPA's peer review and therefore does not necessarily reflect the views of EPA.

References.

1. J.J. Huntzicker, R.L. Johnson, J.J. Shah, and R.A. Cary. "Analysis of Organic and Elemental Carbon in Ambient Aerosols by a Thermo-Optical Method." In Particulate Carbon Atmospheric Life Cycle, G.T. Wolff and R.L. Klimisch (editors), Plenum Press, New York, 1982, pp. 79-88.
2. R.L. Johnson, J.J. Shah, R.A. Cary, and J.J. Huntzicker. "An Automated Thermo-Optical Method for the Analysis of Carbonaceous Aerosol." In Atmospheric Aerosol: Source/Air Quality Relationships, E.S. Macias and P.K. Hopke (editors), American Chemical Society Symposium Series No. 167, American Chemical Society, Washington, D.C., 1981, pp. 223-233.

TABLE 1

Percent of aerosol mass in given size ranges for hot stove burns.

Stove Temperature (°C)	<0.3 μm	0.3-0.6	0.6-1.2	>1.2
650	39	41	20	0
550	56	30	9	5
550	40	18	21	21
430	56	28	0	15

TABLE 2

Percent of aerosol mass in given size ranges for cool stove burns.

Stove Temperature (°C)	<0.3 μm	0.3-0.6	0.6-1.2	>1.2
260	53	5	36	7
230	46	7	15	32
220	35	0	60	5
200	36	2	32	30

TABLE 3

Percent of organic, elemental, and total carbon in given aerosol size ranges.

Size Range	Organic Carbon	Elemental Carbon	Total Carbon
HOT BURN			
<0.3 μm	37	43	39
0.3-1.2	39	49	42
>1.2	24	8	19
COOL BURN			
<0.3 μm	18	22	19
0.3-1.2	49	37	47
>1.2	33	41	34

AIR POLLUTANT EMISSIONS, CONCENTRATIONS, AND EXPOSURES FROM
BIOMASS COMBUSTION: THE CIGARETTE ANALOGY

Kirk R. Smith

Resource Systems Institute
East-West Center
1777 East-West Road
Honolulu, Hawaii 96848

In recent years, scientific interest in biomass as a fuel has been rekindled, and along with it, concerns over potential environmental effects. This has come about in several ways:

- o In those areas of industrial countries where space heating is important, the use of wood has experienced rapid repopularization. Indeed, in the United States, since the first oil crisis the use of wood for fuel has grown much faster than any other energy source, 7 percent per year since 1973 (1).
- o In many developing countries traditional biomass fuels, which include wood, crop residues, and animal dung, still supply energy needs. Since the energy crisis, international concern has grown about the dual problems of finding more energy for economic development and at the same time preventing the rapid deforestation that has come to accompany too much reliance on local biomass fuels. Efforts to solve these problems have focused on increasing supply through such innovations as fast-growing tree plantations and improving the efficiency of use through such devices as improved stoves. This problem is recognized to be significant since more than half the world's population relies on these traditional biomass fuels for nearly all their energy needs, a situation that has not changed since the discovery of fire.
- o In both developed and developing countries, there is at least one other reason for increased interest in biomass fuels. Partly through reapplication of processes developed and left by the wayside in the past and partly through application of sophisticated new understandings of biomass processing, there are now a range of technologies being examined that basically act to convert simple biomass feedstock into high-quality solid, gaseous, and liquid fuels. These are the fuels that will be needed to hasten economic development in poor countries and to fulfil the biomass portion of the renewable-energy promise in all countries.

With the revitalization of biomass fuels, the citizens of developed countries are discovering what their ancestors knew well and their neighbors in developing countries still experience--in small-scale combustion conditions biomass fuels have significant emission factors for several important air pollutants. As shown in Table 1, the emission factors for three of the five priority pollutants, particulates, hydrocarbons, and carbon monoxide, compare unfavorably with those of coal combustion when the burn rate is in the range of a few kilograms per hour (2-25 kW). At industrial scale (a few hundred kilograms per hour) biomass emission factors do not usually appear so much worse than coal, a conclusion tempered by the significant affect on emissions of the particular combustion conditions and quality of the fuels.

In the last few years, an increased amount of effort has gone into studying the emission characteristics of biomass-fueled (mainly by wood) heating stoves of the types commonly in use in developed countries (2). This is becoming more of a concern as outdoor smoke* levels rise in communities relying on such appliances. In some states of the United States, for example, emissions from wood stoves have exceeded

*Here I will use the term "smoke" to refer to the entire mixture of emissions from biomass combustion: all gases and aerosols.

those from industry for critical pollutants (3). Woodsmoke studies have characterized a large number of organic compounds in the "hydrocarbon" portion of the emissions. Indeed, several hundred have been identified, many of which are polycyclic aromatic hydrocarbons (PAH) that have been shown to be mutagenic or carcinogenic (4).

Although the problem of smokey village kitchens has long been noted by observers in rural areas of developing countries, it has been only recently that systematic indoor measurements have been undertaken (5). The human exposures to several important pollutants that can be estimated as a result of these concentrations are orders of magnitude higher than typical urban exposures.

Unfortunately, just as there have been few and only relatively recent quantitative studies of the concentrations, there are very few quantitative epidemiological studies about the health effects of biomass smoke, although there exists much anecdotal information by medical observers and others. Until this lack is remedied, it is necessary to rely on extrapolations from studies of other situations.

The most obvious extrapolation is from urban epidemiological studies of air pollution. Unfortunately, however, there are severe limitations with respect to extrapolating these studies to biomass smoke. Although many of the same pollutants have been studied, the mix is so different as to make comparisons suspect. Urban particulates, for example, are usually associated with sulfur oxides because of the composition of their principal source--fossil fuels. Consequently, the major official reviews of the health effects of particulates are unable to separate the effects of the two pollutants (6). In air polluted by biomass smoke, however, particulates are usually associated with carbon monoxide and hydrocarbon vapors and droplets. There are further important differences between typical fossil-fuel smoke and biomass smoke in the size distribution and chemical nature of the aerosols, percentage of elemental carbon, content of trace metals, and so on.

There is, however, a form of biomass smoke that has been studied extensively, to an extent rivaling urban air pollution. This is entirely appropriate because this form of biomass smoke is the cause of more human air pollution exposure and greater human ill-health than all other causes of air pollution combined. It is, of course, tobacco smoke.

If an analogy could be drawn between exposures to tobacco smoke and exposures to the smoke from biomass fuels, then investigators of the impact of the latter would have access to a vast health effects literature available for the former. It is the purpose of this paper to begin an exploration of the viability of this analogy.

To effect this comparison, I have chosen to examine four pollutants found in significant amounts in biomass smoke of all kinds: respirable particulates (RSP), carbon monoxide (CO), formaldehyde (HCHO), and particulate benzo(a)pyrene (BaP). Each of these has been the subject of considerable attention in its own right as a health-damaging pollutant. They each also represent an important member of one of the four principal classes of pollutants found in biomass smoke: particulates, gases, hydrocarbons, and PAH. To test this analogy in a quantitative manner, I will separately examine for cigarettes and woodfuel the relative emission factors, air concentrations, and nominal human doses of these four pollutants.

Emission Factors

Researchers of cigarette emissions have had to develop a standard smoking procedure such that different brands can be compared on as much of an equivalent basis as possible. The procedure used in most studies today is to smoke each cigarette in 10 puffs at one-minute intervals with a puff volume of 35 ml and a puff duration of 2 sec. The smoke coming through the mouthpiece of the cigarette that

would normally be respired by the smoker is called the mainstream smoke. The smoke released from all points of the cigarette between puffs is called sidestream smoke. Specialized machines have been developed to "smoke" cigarettes in this fashion and to measure the particulate and gaseous emissions (7).

At present there is no standard procedure for measuring emissions from small cooking or heating stoves although such procedures are under development (3, 8). In order to make quantitative comparisons between cigarette smoke and the smoke from biomass-fueled appliances it will be necessary to choose emission factors from those available in the literature. Since the emissions from enclosed metal heating stoves vary dramatically with stove operating conditions, it would seem appropriate to confine this initial set of comparisons to what seems to be the less variable open combustion conditions typical in fireplaces and simple cooking stoves. Excluding cigarette burning, open combustion of this sort is, after all, the most common combustion situation in the world regardless of fuel type.

Although over 3000 different compounds have been identified in cigarette smoke, a few dozen are singled out as most important. A few of these are shown in Table 2 and include the four being considered in this paper. Note that the tobacco smoke literature calls "tar" what the air pollution literature calls "total suspended particulates (TSP)." The emission factors in the table refer to mainstream smoke and a separate column lists the relative amounts of emissions from sidestream smoke. These emission factors vary by brand, by type of filter, and way of smoking. They also vary by time in that cigarettes in the United States, at least, have lower average emission factors today than they did in past years, and the relative toxicity of the emissions on a mass basis seems to be going down as well (9).

Since the amount of biomass actually burned in a typical cigarette is about one gram, the emission factors in Table 2 that are listed in mg are equivalent to g/kg. The first column of Table 3 compares the emission factors of mainstream and sidestream cigarette smoke with those representative of woodsmoke from small-scale combustion. Note that, except for TSP, the emission factors for wood are similar to or higher than those for tobacco. Note also, that the difference between sidestream and mainstream tobacco smoke is large for many species, indicating HCHO and a number of the gas-phase nitrosamine compounds. For TSP (tar), CO, and BaP, on the other hand, the ratio is much smaller.

Another factor of interest with particulates is their size range. In this respect, as well, cigarette smoke and woodsmoke are similar. Each has a mass median diameter of less than 0.4 μ m, indicating that essentially all the particulate matter penetrates into the deep lungs upon respiration (10). In air pollution terminology, essentially all TSP is RSP.

Concentrations

There are two distinct types of cigarette smokers--active and passive (or voluntary and involuntary). The active smoker experiences high concentrations of pollutants because the mainstream smoke is mixed with the relatively small amount of air in a breath, the tidal volume. In the standard cigarette smoking sequence there is one "puff" per minute for ten minutes. Since the sales-weighted cigarette in the United States in 1980 released 14 mg of "tar" per cigarette in the mainstream smoke and the tidal volume of air for an adult woman in light activity is about 940 ml (11), the particulate concentration would be about 1500 mg/m³. This is some two or three orders of magnitude higher than the measured average TSP concentrations in air breathed by women cooks in rural field studies in Asia (5).

BaP concentrations in mainstream cigarette smoke, on the other hand, are quite similar to those in village homes, as are HCHO concentrations. CO levels are intermediate. The second column of Table 3 lists the relative concentrations experienced by a village cook and a smoker for these four pollutants.

A passive smoker will experience concentrations that are determined and can be accurately estimated by the number and location of cigarettes being smoked nearby, the room volume, ventilation rate, and mixing conditions. (12). In a well-mixed conference room (200 m³; 2ACH; 40 people half of whom are smokers, each of whom smokes 2 cigarettes per hour), indoor concentrations of the four principal pollutants can be calculated from the sidestream emission factors in the first column of Table 3 and the result is shown in the second column. By this estimate, the passive smoker would experience concentrations of three of the pollutants much lower than the active smoker and consistently lower than the village cook. Note also, that because of the large ratio of sidestream to mainstream emission factors for HCHO (Table 2), the passive smoker can actually experience concentrations of HCHO comparatively similar to those experienced by the smoker. It is important to remember, however, that the smoker "puffs" only once a minute (~ 5 percent of breaths) while the passive smoker and village cook experience these concentrations in every breath during the exposure period. The relative doses, therefore, are not the same as the relative concentrations.

There is a further refinement possible in these concentration estimates. Since the mainstream smoke is not entirely deposited or absorbed by the respiratory system of the smoker, there is an addition to the surrounding indoor air concentrations resulting from the exhaled air of the smokers. (13) Furthermore, of course, the active smokers in the room with passive smokers will experience at least as high "passive" concentrations in the 95 percent of breaths that are not "puffs" on the cigarette.

Nominal Doses

To understand the relative health effects of pollutants it is always best to measure dose, the actual amount of material absorbed or deposited in the body. There is variability, however, in the way air contaminants are deposited or absorbed by different people at different times. The breathing rate, whether mouth or nose breathing is occurring, and the condition of the respiratory system all affect deposition, for example. In cigarette smokers, there are the additional variables of smoking behavior. If the smoker inhales the smoke and smokes the butt down to almost nothing, the dose per cigarette is going to be much larger than that of a normal smoker.

In addition, although woodsmoke and tobacco smoke have many similarities, there are also differences. The temperature of cigarette smoke, for example, would normally be higher. There may be some sort of saturation effect at the generally higher concentrations experienced by the active smoker leading to lower deposition rates per gram of material inhaled. On the other hand, the hot dense smoke from smoking may inhibit or damage natural lung clearance and other defense mechanisms to the extent that deposition efficiency is higher with such exposures. It may be, however, that the 95 percent of breaths that are low exposure for the active smoker allow the lung defense mechanisms to operate more efficiently than they can when every breath contains significant concentrations.

Not knowing the deposition or absorption rates with accuracy means that it is not possible to calculate exact doses. For the purposes here, it is sufficient to address what has been called "nominal dose" (12), here being defined as the amount of material actually breathed in by the smoker or cook. I will assume linearity in response to exposures and correct for breathing rates and particle sizes. The reference woman in (13) breathes 18.2 m³ of air during 16 hours of light activity and 2.3 m³ during sleep per day and about 95 percent of the particles are respirable (10). Consequently, the comparative daily exposures of the four major pollutants for a two-pack-per-day smoker and a village cook are as shown in the last column of Table 3. The village cook receives nominal doses of BaP and HCHO that are higher than those received by the smoker by factors of 12 and 2.8 respectively. The smoker, on the other hand, receives nominal doses of CO and TSP that are greater by factors of 4 and 24.

Using the same assumptions as those used to calculate concentrations in Table 3, and assuming a 4-hour meeting in the conference room, the passive smoker would receive daily nominal doses lower than either the active smoker or the village cook. This assumes, of course, that this person is exposed to no other conditions of poor air quality during the day. Note that the exposure to HCHO is much closer to that of the active smoker than are the relative exposures of the other species. This is because of the large emissions of HCHO in sidestream as compared to mainstream cigarette smoke. Indeed, the HCHO exposure rate per hour during the conference meeting for the passive smoker is nearly three times that of the mainstream exposure rate received by the smoker in smoking two cigarettes per hour. This means that the total HCHO nominal dose of the active smoker at such a meeting is mostly due to her role as passive rather than active smoker.

In Table 3, the Upland Sleeper is someone who lives in a highland area such as those in Nepal, Peru, Kenya, and Papua New Guinea. She is presumed to spend 14 hours a day in the house during which she sleeps for 8. If one assumes that the average exposure during this period is about 50 percent of that received by the cook near the fire, the upland sleeper would receive a total daily nominal dose of each pollutant roughly 40 percent greater than the cook.

Of course, active smokers also receive passive exposures if they attend conference meetings with smokers present and village cooks in upland areas also must sleep. To a first approximation, the total daily nominal dose for women in these situations would be the total of the active and passive smokers' nominal doses and the total of the cooking and sleeping nominal doses respectively. Further corrections could be made to account for any ambient exposures received by these groups.

Conclusion

Of the four pollutants examined here it seems that nominal doses to two of them are roughly similar for cigarette smokers and village cooks--HCHO and CO. For RSP, active smokers receive more than a factor of 10 larger nominal doses. On the other hand, village cooks receive more than a factor of ten greater nominal doses to BaP. In all cases, village cooks receive higher nominal doses than passive smokers. On the basis of these comparisons, therefore, it might be expected that the health impacts among village cooks would lie somewhere below those for active smokers and well above those for passive smokers. It should be mentioned, however, that many other pollutants are not addressed here. Nicotine, in particular, would seem to be something nearly absent in woodsmoke and yet an important health-damaging pollutant in tobacco smoke. Nevertheless, even a rough index such as the one here is suggestive. There has long been evidence that smokers harm themselves (9, 14) and there is a rapidly growing consensus that passive smokers' health is also affected (15). The index could also be expanded to characterize the particulate fraction by chemical (16) or bioassay (17) techniques or a combination (18).

The data in Table 3 can also be used for other comparisons. Consider the relative emissions of a coal-fueled electric power plant and a cigarette. In 1981, the average U.S. resident was responsible for the burning of about 3.5 kg of tobacco and 290 kg of coal, 82 percent of which was used in power plants (19). In a study at Brookhaven National Lab, it was determined that a typical coal power plant delivers about 0.1 mg-person-year/m³ of exposure for every ton of particulate emissions (20). Assuming that all the coal power plants emit particulates at the legal limit implies that the coal-derived electricity needs of the average U.S. citizen cause about 0.003 mg-person-year/m³ of exposure. Using the data and assumptions in Table 3, it can be shown that typical wood needs for cooking in a developing country (about 400 kg/capita-year) would produce about 0.15 mg-person-year/m³ or 40 times the exposure caused by six times more fuel in the U.S. power plants. Even more strikingly, it can be estimated that compared to the coal

used per capita the tobacco needs of the average U.S. citizen causes about four orders of magnitude more exposure simply to the passive smokers nearby and not even counting the much larger exposures to the smokers themselves.

The lesson should be clear. When the objective is to protect human health, it can be quite misleading to concentrate solely on emission factors and total emissions. Distributed combustion sources, such as cook stoves and, in the extreme, cigarettes, can be responsible for much larger human exposures per unit fuel. This fact has important implications for the design of alternative energy systems. (21)

References

- (1) U.S. Department of Energy. Estimates of U.S. Wood Energy Consumption from 1949 to 1981. DOE/E/A-0341, Washington, D.C., 1982.
- (2) Cooper, J.A., and Malek, D. Residential Solid Fuels: Environmental Impacts and Solutions; proceedings of a conference held in Portland, Oregon, June 1-4, 1981. Oregon Graduate Center, Beaverton, OR, 1982.
- (3) Hough, M.L., and Kowalczyk, J.F. J. Air Pollut. Contr. Assoc. 1983. 33(11):1121-1125.
- (4) Hubble, B.R., Stetler, J.R., Gebert, E., Harkness, J.B.L., and Flotard, R.D. Experimental measurements of emissions from residential wood burning stoves. In (2), pp. 79-138.
- (5) Smith, K.R., Aggarwal, A.L., Dave, R.M. Atmos. Environ. 1983. 17(11):2343-2362.
- (6) World Health Organization. Sulfur Oxides and Suspended Particulate Matter. WHO Environmental Health Criteria 8, Geneva, 1979. U.S. Environmental Protection Agency. Air quality criteria for particulate matter and sulfur oxides (5 volumes). USEPA, Research Triangle Park, NC, (1981 draft & 1982 draft final).
- (7) Wynder, E.L., and Hoffmann, D. Tobacco and Tobacco Smoke Studies in Experimental Carcinogenesis. Academic Press, New York, 1967.
- (8) Butcher, S., Rao, U., Smith, K.R., Osborn, J., Azuma, P., and Fields, H. Emission factors and efficiencies for small-scale open biomass combustion: Toward standard measurement techniques. To be presented at the American Chemical Society Annual Meeting, Philadelphia, August, 1984.
- (9) U.S. Surgeon General. The Health Consequences of Smoking--The Changing Cigarette, A report of the Surgeon General. Washington, D.C., 1981.
- (10) Dasch, J.M. Environ. Sci. Technol. 1982. 16:635-645. Hinds, W.C. AIHAJ 1978. 39(1):48-54. Smith, K.R., Apte, M., Menon, P., and Shrestha, M. Carbon monoxide and particulates from cooking stoves: Results from a simulated village kitchen. To be presented at the Third Annual Conference on Indoor Air Quality and Climate, Stockholm, August, 1984.
- (11) International Commission on Radiological Protection. Report of the Task Group on Reference Man. ICRP No. 23, Pergamon Press, Oxford.

- (12) Repace, J.L., and Lowrey, A.H. Science 1980. 208:464-472. Hoegg, U.R. Environ. Hlth. Persp. 1972. 2:117-128. Repace J.L., and Lowrey, A.H. Modeling exposure to nonsmokers to ambient tobacco smoke. Presented at the 76th Annual Meeting of the Air Pollution Control Association, June 19-24, 1983, Atlanta, Georgia. Bridge, D.P., and Corn, M. J. Environ. Res. 1972. 5(2):192-209.
- (13) Blanchard, J.D., and Willeke, K. AIHAJ 1983. 44(11):846-856.
- (14) U.S. Surgeon General. The Health Consequences of Smoking--Cancer: A Report of the Surgeon General. Pub. No. DHHS(PHS) 82-50179, Office on Smoking and Health, Rockville, MD, 1982.
- (15) Weiss, S.T., Tager, I.B., Schenker, M., and Speizer, F.E. Am. Rev. Respir. Dis. 1983. 128(5):933-942. Kauffmann, F., Tessier, J., and Oriol, P. Am. J. Epidemiol. 1983. 117(3):269-280. Ekwo, E.E., Weinberger, M.M., Lachenbruch, P.A., and Huntley, W.H. Chest 1983. 84(6):662-668. Ware, J.H., Dockery, D.W., Spiro, III, A., Speizer, F.E., and Ferris, Jr., B.G. Am. Rev. Respir. Dis. 1984. 129:366-374. Spengler, J.D., and Soczek, M.L. ASHRAE Trans. 1984. 90(Pt. 1). Lefcoe, N.M., Ashley, M.J., Pederson, L.L., and Keays, J.J. Chest 1983. 84(1):90-95. Weiss, S.T., Tager, I.B., and Speizer, F.E. Chest 1983. 84(6):651-652. Shephard, R.J. The Risks of Passive Smoking. Oxford University Press, New York, 1982.
- (16) Hoffmann, D., Rathkamp, G., Brunemann K.D., and Wynder, E.L. Science of the Total Environment 1973. 2:157-171.
- (17) Beck, B.O. Prediction of the pulmonary toxicity of respirable combustion products from residential wood and coal stoves. In Proceedings of the Residential Wood & Coal Combustion Specialty Conference held in Louisville, Kentucky, March 1-2, 1982. SP-45, Air Pollution Control Association, Pittsburgh, PA, 1982.
- (18) Ramdahl, T., Alheim, I., Rustad, S., and Olsen, T. Chemosphere 1982. 11(6):601-611.
- (19) U.S. Bureau of the Census. U.S. Statistical Abstract 1983. Bureau of the Census, Dept. of Commerce, Washington, D.C., 1983.
- (20) Rowe, M.D. Human Exposure to Particulate Emissions From Power Plants. BNL 51305, Brookhaven National Laboratory, Long Island, NY, 1981.
- (21) Smith, K.R. Village cooks: The bright and dark sides of small is beautiful. Presented at the Association of Women in Development Conference on Women in Development: A Decade of Experience, Washington, D.C., October 1983.
- (22) Martin, W., Morris, C.A., and Koenigshofer, D.R. Environmental impacts of wood combustion. Integrated Energy Systems, Inc., Chapel Hill, NC, 1981.
- (23) Dary, O., Pineda, O., and Belizan, J.M. Bull. Environ. Contam. Toxicol. 1981. 26:24-30.
- (24) Cleary, G.J., and Blackburn, C.R.B. Arch. Environ. Hlth. 1968. 17:785-794.

Table 1. Comparison of Air Pollutant Emission from Energy-Equivalent Fuels
(in kilograms)

Fuel (Efficiency)	Fuel Equivalent to One Million Megajoules Delivered	Particulates	Sulfur Oxides	Nitrogen Oxides	Hydro- carbons	Carbon Monoxide
Industrial						
Wood (70 %)	80 metric tons	480	56	360	360	400
Coal (80 %)	43 metric tons	2,080	810	1,180	6	45
Residual oil (80 %)	33,000 liters	94	1,310	240	4	20
Distillate oil (90 %)	31,400 liters	8	1,120	83	4	19
Natural gas (90 %)	28,200 cubic meters	7	neg.	99	2	8
Residential						
Wood (40 %)	144 metric tons	2,170	86	110	1,450	18,790
Coal (50 %)	69 metric tons	520	1,200	270	430	2,380
Distillate oil (85 %)	32,900 liters	11	1,170	71	4	20
Natural gas (85 %)	30,000 cubic meters	7	neg.	38	4	10

Source: 22.

NOTE: These are typical but not average figures. Actual efficiencies and emissions depend on fuel quality and combustion conditions. Residential heating stoves under US conditions.

Table 2: Major toxic and carcinogenic species in cigarette smoke; ratio of sidestream smoke (SS) to mainstream smoke (MS)

A. Gas phase	Amount/cigarette		SS/MS
Carbon dioxide	45	mg	8.1
Carbon monoxide	13.25	mg	2.5
Nitrogen oxides (NO _x)	308	µg	5.25
Ammonia	70	µg	58.50
Hydrogen cyanide	415	µg	.27
Hydrazine	32	µg	3
Formaldehyde	55	µg	51
Acetone	520	µg	2.85
Acrolein	75	µg	12
Acetronitrile	110	µg	10
Pyridine	32	µg	10
3-Vinylpyridine	23	µg	28
N-Nitrosodimethylamine	92	ng	420
N-Nitrosoethylmethylamine	20.5	ng	17
N-Nitrosodiethylamine	14.05	ng	14.5
B. Particulate phase	Amount/cigarette		SS/MS
Total particulate phase (tar)	14	mg	1.6
Nicotine	1.18	mg	2.95
Toluene	108	µg	5.6
Phenol	85	µg	2.6
Catechol	160	µg	0.7
Naphthalene	2.8	µg	16
2-Methylnaphthalene	1.0	µg	29
Phenanthrene	41	ng	2.1
Benz(a)anthracene	40	ng	2.7
Pyrene	52.5	ng	2.75
Benzo(a)pyrene	24	ng	3.05
Quinoline	1.7	µg	11
Methylquinoline	6.7	µg	11
Harmene	2.1	µg	1.7
Norharmene	5.65	µg	2.85
Aniline	650	ng	30
o-Toluidine	32	ng	19
2-Naphthylamine	15.65	ng	39
4-Aminobiphenyl	3.5	ng	31
N-Nitrosornicotine	1.95	µg	3
N-Nitrosoanatabine	2.38	µg	4

Source: 14.

Table 3: Summary of Emission Factors, Concentration, and Nominal Doses of Tobacco and Woodsmoke

	Active Smoker	Passive Smoker	Village Cook	Upland Sleeper
Emission Factors (per kg of biomass)				
CO	17 g	43 g	40 g	40 g
TSP	14 g	24 g	2.0 g	2.0 g
BaP	0.03 mg	0.1 mg	1.0 mg	1.0 mg
HCHO	0.03 g	1.5 g	0.4 g	0.4 g
Concentration (per cubic meter of air)				
CO	1800 mg	5.2 mg	50 mg	25 mg
TSP	1500 mg	3.1 mg	7 mg	3.5 mg
BaP	3100 ng	13 ng	4000 ng	2000 ng
HCHO	3.1 mg	0.15 mg	1.0 mg	1.0 mg
Nominal Dose (per day)				
CO	680 mg	23 mg	170 mg	240 mg
RSP	530 mg	13 mg	22 mg	32 mg
BaP	1100 ng	54 ng	13,000 ng	18,000 ng
HCHO	1.2 mg	0.66 mg	3.3 mg	9.7 mg
Assumptions				
TSP and BaP	940 mi/breath	200 m ³ room	Measurements	50% cook
95% respirable	10 puffs/cig.	40 cig./h.	in India,	concentrations
Adult women	2 packs/day	2 ACH	Guatemala, and	14 hours indoors
		perfect mixing	New Guinea	9.7 m ³ total air
		4-hour meeting	1.1 m ³ /h	
		1.1 m ³ /h		

NOTES:

A cigarette smoker in the same 4-hour meeting as the passive smoker would receive a total nominal dose equivalent to approximately the two added together. Similarly, a village cook living in an upland area would receive a nominal dose roughly equal to the two added together.

If the smoker is assumed to exhale half of the respired pollutants, the passive smoker's concentrations and doses could be expected to be larger by CO: 20%; TSP: 30%; BaP: 15%; HCHO: 1%.

Source: 14, 11, 5, 23, 24, 8.

EMISSION FACTORS AND EFFICIENCIES
FOR SMALL-SCALE OPEN BIOMASS COMBUSTION:
TOWARD STANDARD MEASUREMENT TECHNIQUES

S. S. Butcher,* U. Rao,** K. R. Smith, J. F. Osborn,*** P. Azuma, and H. Fields

Resource Systems Institute, East-West Center, Honolulu, Hawaii, 96848

*Department of Chemistry, Bowdoin College, Brunswick, Maine, 04011

**Tata Energy Research Institute, Pondicherry, India 605002

***Civil Engineering, Carnegie-Mellon University, Pittsburgh, PA, 15213

Introduction

A large fraction of the population of the earth is served by the preparation of food and space heating by small fires. In many cases the cooking is done indoors and the combustion products are not vented out of the building, but simply escape through windows, doors, and porous walls and roofing. This report describes a preliminary step in defining a test protocol for the simultaneous measurement of efficiency and emissions of open biomass cooking/heating stoves as they are used in many developing countries. This study is part of a larger study of the health impacts of these combustion sources [Smith and others (1)].

Previous studies of total suspended particulates by Smith *et al.* (2), and carbon monoxide concentrations in village houses by Dary *et al.* (3) show that exposures are significant and may approach or even exceed those experienced by cigarette smokers (4). Another aspect of biomass fuel use which is of considerable importance in some areas is the availability of fuel and ways in which the efficiency of fuel use might be increased [de Montelembert and Clement (5)].

There have been many studies of efficiencies and emissions for metal wood-fired spaceheaters [Cooper & Malek, (6)] and there have also been several studies of the efficiencies of fuel use for undeveloped countries [Prasad (7)]. The test protocol described here attempts to combine two important objectives:

- 1) The burn conditions in the tests should simulate as closely as possible those expected in the field;
- 2) The testing should combine efficiency and emission measurements.

The combustion region in a village house is defined by the stove, which confines the fire and supports the cooking utensil, and also by the cooking utensil itself. An important benefit of combining efficiency and emissions tests is that future work on the design of improved stoves can evaluate changes and potential compromises between emissions and efficiency goals.

Another objective of this study is the design of a measurement system that could be replicated at a reasonably low cost and operated by individuals with limited experience with emissions and efficiency testing. Such easily assembled systems might then be made available at field locations in the relevant countries, where local institutions familiar with local customs and fuel types could examine ways of improving the performance of the combustion systems. While perhaps not satisfying the requirements for accuracy necessary for showing compliance to regulatory requirements, such a system could be very useful for designing and testing improved stove/fuel combinations.

Apparatus and Materials

The tests were conducted in a small (17m³) utility building of the type often

used for equipment storage. The building had a concrete floor, a sliding entrance door, and sliding windows on two sides. This building was also used to stimulate a village hut (8). The cookfire was built in a stove in the corner of the building and the emissions were collected by a hood that is a quarter section of a cone and could be raised and lowered over the fire. The hood fitted into a corner of the building. Air in the hood was exhausted from the building at a rate of about 10 m³/min through a 0.2 m diameter duct with a 1/3 hp blower located just outside.

Such an arrangement is quite different from those typically used to measure emissions from the types of woodfired stoves in common use in industrial countries (6). Such stoves have flues and emissions measurements can be made by insertion of probes into the flue-gas stream. The stoves of interest here, which are the most common stoves in the world, have no flues. The emissions testing equipment must capture all the emissions without significantly altering the combustion characteristics of the stove.

The movable hood met these specifications in our tests. The hood was raised to about 0.6 m in order to change stoves and clean up after tests. Most types of simple biomass-fueled cookstoves (8,9) without flues could be placed or constructed on the floor under this hood. The hood was then lowered to about 0.3 m. This allowed all the emissions from the fire to be captured by the hood exhaust, but is not so close to the stove that it creates a greatly increased air flow through the combustion region.

TSP and CO were sampled just upstream of the blower. The air flowrate through the exhaust duct was inferred from the pressure drop across an orifice plate in a section of 0.15 m diameter duct downstream of the blower. The flowrate was calibrated to the pressure drop by making an absolute measurement of the flowrate with a pitot transverse in a straight section of the duct downstream from the orifice plate. The calibration was performed on two occasions. Although the blower capacity was degraded somewhat by the buildup of particles on the blower vanes, the orifice calibration was not significantly affected. The air was exhausted at a location about three meters from the building. The entrainment of the exhaust gases was not a problem during these experiments.

Stainless steel and copper probes (1/4" I.D.) facing into the air flow removed aliquots of the total emissions. These were passed through filter cassettes (for TSP) or through a damping volume and then taken through an Ecolyzer CO monitor (Model 2100; modified to a detection range of 0-500 ppm). The CO stream was drawn by the pump in the Ecolyzer which operated at about 1.2 liter/min. The Ecolyzer was calibrated with a 203 ppm CO standard (span gas). The sensitivity of the instrument was such that the measurement error of the CO concentration ranged from 4 to 8 ppm.

The particulate matter sample stream was drawn by a battery powered personal sampler (Gilian model HFS113) at rates ranging from 1.5 to 4 liter/min. The personal sampler was operated in the constant flowrate mode and this rate was monitored by the rotameter on the sampler. The rotameters were calibrated by volume displacement. Several types of 37mm filters were used depending on the desired end-point (glass fiber for TSP, Teflon for TSP and trace metals, quartz for elemental carbon determination).

The temperature in the duct at the sampling probes was generally 30-40° C. The collection method is more similar to that used by Butcher and Ellenbecker (10) in a study of residential heaters than it is to EPA Method 5, which has been used to study emissions from a wide range of combustion sources, including residential heaters (11).

Biomass fuels for these tests should be chosen to represent those in common use in developing countries, which are mainly in tropical areas. Anecdotal accounts by villagers (2) and measurements of emissions from wood species from temperate climates indicate that emissions vary by tree species (6,12). Emissions from various kinds of crop residues vary even more significantly because of greatly varying ash contents and physical characteristics (1). Emissions from animal dung also vary somewhat according to the content of dirt incorporated during the collection process. The emissions from all biomass fuels can be expected to vary by moisture content.

In these preliminary tests, six tropical tree species, cow dung, coconut husks, and charcoal were used. Collection, drying, and storage procedures were designed to result in a range of moisture contents typical of what would be expected in the field.

Test Procedure

The heat utilization measurements were based on the provisional international standards developed by Volunteers for International Technical Assistance (13). The temperature of two liters of tap water was determined and then placed in a covered cooking pot. The fire was started under the pot with the aid of a small measured amount of kerosene to help insure that each test began in a consistent manner. The particulate samplers were started as the fire was lit. The fire was actively tended by adding fuel, rearranging fuel, and blowing on the fire through a blowpipe, as needed. Fires in real field situations usually receive similar attention. A fairly vigorous fire was maintained to raise the water to the boiling point and to boil it for 15 minutes. When the water boiled, the time was noted. After boiling for 15 minutes the fire was reduced to keep the water at a simmer (>95°) for 30 minutes. At the end of this period the fire was extinguished and the samplers were turned off.

The amount of fuel added and the fuel residue were determined by a pan balance to an accuracy of 1g. Charcoal and unpyrolyzed wood residues were weighed separately. The amount of kerosene added was recorded and the amount of water remaining in the pot was determined.

Two types of "efficiency" of the cooking process were determined. The first was the "overall heat utilization," which is the ratio of the heat output (sensible + latent heat of the water) to the heat input in terms of the heats of combustion of fuels used (the "low heat value," corrected for moisture content and charcoal residues). The kerosene used for lighting accounted for only a small fraction of energy used. The second was the "net heat utilization" and is the ratio of sensible heat output to heat input. Both measures of heat utilization are useful, depending on the type of cooking being considered. A third "power" measure is sometimes important as well: it is the average stove power during the heat-to-boil phase of the test cycle. This was not determined in these tests because the power test required stopping the fire to weigh the fuel. Starting and stopping the fire, unfortunately, greatly affects emissions. Joint power and emissions tests would require some other technique, perhaps placement of the entire stove on a large scale.

During the burn, the air sampling equipment was monitored more or less continuously and critical values were recorded at 5-minute intervals. These values included orifice-plate pressure drop, sampler flow rates, duct temperature at the sample probes, ambient temperature, and Ecolyzer reading.

The filters were placed in a dessicator for 24 hours before the tare and

sampled weights were taken. Weights were then measured to within 0.01 mg. In most cases, each filter represented an integrated sample over the entire burn. The total particle emissions were determined as the product of the filtered weight and the ratio of the total duct flow to the particle sampler flow. The emission factor for particulate matter was then calculated as the ratio of total particle emissions to net fuel consumed. These particulates could be expected to have mass median aerodynamic diameters of about 0.6 μm or less based on wood and dung smoke measurements in open and closed stoves (8,14). This means that essentially all TSP is within the respirable range (<2.5 μm).

The carbon monoxide concentration in the duct was obtained from the Ecolyzer reading (corrected for temperature). The duct concentration was then integrated over the time of the burn and multiplied by the flow rate through the duct to obtain the total carbon monoxide emissions. The emission factor was obtained by dividing by the fuel consumed, as described above.

Results and Discussion

The results of seventeen test burns are summarized in Table 1. These results are sorted by stove type. The chulas were constructed of firebrick or of large stones. The conventional chula is U-shaped and open at the top to support the cooking utensil. It is constructed of clay or similar indigenous materials. The C.P.R.I. stove is a cylindrical metal stove designed for increased heating efficiency. The fuel use rate ranged from 0.2-1.6 kg/hr. A number of different fuels were tested, but these results are aggregated for present purposes. The large variations in emissions factors very likely resulted from variations in the burning conditions from one burn to the next and also from errors of measurement. Variations in the burning conditions occur naturally and have also been observed in other stove tests (8,10). These variations can only be minimized by conducting many tests. Key among the measurement errors are those which arise from weighing the 37 mm filters. For some cases the particulate weight was less than 0.10 mg and near the limit of sensitivity of the available balance. There may also be problems associated with the adsorption of gases such as SO_2 on glass fiber filters.

Other problems may arise from the configuration of the duct near the sampling probes. The sampling probes were located fairly close to a right angle bend in the ductwork and just upstream of the blower inlet. Substantial inhomogeneity of the flow field was observed in this region and the particle collection efficiency may have depended on the sample probe location and orientation. Particle losses in the duct upstream of the sampler were estimated by measuring the deposition on weighed aluminum foil. For a series of burns in which the total emissions were 62 grams, about 5 grams were estimated to have been deposited in the duct.

The emissions factors in Table 1 may be compared with factors obtained by others for fireplaces. Fireplaces, although usually not tended continuously like chulas, are more similar to chulas than are closed metal stoves. Dasch (14), in a fireplace study using EPA Method 5, obtained an average of 5.4 g/kg for filterable particulates with a range of 2.4-12 g/kg. The condensible organic fraction averaged 6.9 g/kg with a range of 2.3-22 g/kg. DeAngelis, et al. (11), obtained averages of 2.4 g/kg particulates and 6.7 g/kg condensible organics for fireplaces. The results obtained here tend to fall between values for particulates only, and those for particulates plus condensibles from these other studies. Further work is needed to define the sampling method most appropriate for assessing the health effects of these low temperature combustion sources.

Dasch (15,16), Lips (17), and DeAngelis, et al. (11,18) obtained average carbon

monoxide emission factors which ranged from 16 to 110 g/kg in fireplace studies. This range includes several burns carried out at much higher combustion rates than we have used. Smith, *et al.* (8), in a study of concentrations in a simulated village hut which allowed the determination of emission factors by indirect means obtained the results at the low end of the range. Additional research is being conducted to explain this discrepancy.

Table 1
Summary of Results
Mean Values (range)

Stove	Overall Efficiency	Particle Emission Factor	Carbon Monoxide Emission Factor
Small Chula 9 burns	13.3% (9.0-16.6)	9.1 g/kg (4.2-21.3)	84 g/kg (72-92)
Large Chula 2 burns	14.2	12.3 (9.1-15.5)	88 (76->101)
Three Rock Chula 3 burns	11.6 (6.7-14.3)	7.7 (4.2-10.2)	63 (39-81)
C.P.R.I. Stove 3 burns	15.5 (11.8-18.0)	5.2 (0.3-8.3)	182 (86-360)

The current system using personal samplers offers the advantage of simple and stable pumps usable in other applications such as personal sampling. A disadvantage is that the small sample volumes result in particle masses that can only be determined with a sub-milligram level analytical balance. In many cases the filtered masses of 1-5 mg were easily measured, but for some fuels these masses were less than 0.1 mg. The advantages of using the present system will be compared with those using a large volume of air and less demanding weighing procedure in future work.

Some aspects of the sampling method are bound to affect the operation of the fire somewhat and one can only try to minimize these effects. As mentioned, the 0.3 m distance from the hood to the floor means that the hood opening is about 0.54 m² for these studies. At an average flowrate of 10 m³/min, this gives an average face velocity of about 19 m/min. It is difficult to say how much of an effect this airflow has on the fire. We do know that fugitive emissions to the interior of the hut was a minor factor for these tests. Generally speaking, very little smoke was apparent in the hut. The CO concentration was measured at the edge of the hood on three occasions. Two of these measurements were less than the detection limit of the system as set up (less than 2 ppm), and one measurement was about 4 ppm.

Although there are several remaining problems to be solved in this system, it seems that it can be useful as an inexpensive approach to measuring thermal efficiency and air emissions from simple open biomass-fired stoves.

References

- (1) Smith, K.R., and others. Rural biomass fuels and air pollution: a global review. World Health Organization, Geneva (forthcoming), 1984.
- (2) Smith, K.R., Aggarwal, A.L., and Dave, R.M. Atmos. Environ. 1983, 17(11):2343-2362.
- (3) Dary, O., Pineda, O., and Belizan, J.M. Bull. Environ. Contam. Toxicol. 1982, 26:24-30.
- (4) Smith, K.R. Air pollutant emissions, concentrations, and exposures from biomass combustion: the cigarette analogy. To be presented at the Annual Meeting of the Fuel Chemistry Division, American Chemical Society, August 26-31, 1984, Philadelphia, PA.
- (5) deMontalembert, M.R., and Clement, J. Fuelwood Supplies in the Developing Countries. FAO Forestry Paper 42, Food and Agriculture Organization of the United Nations, Rome, 1983.
- (6) Cooper, J.A. and Malek D., eds. Proceedings of the 1981 International Conference on Residential Solid Fuels: Environmental Impacts and Solutions. Beaverton, Oregon, Oregon Graduate Center, 1982.
- (7) Prasad, K.K., ed. Some Studies on Open Fires, Shielded Fires and Heavy Stoves. Woodburning Stove Group, Eindhoven University of Technology, and Division of Technology for Society, TNO, Apeldoorn, Netherlands, 1981.
- (8) Volunteers in Technical Assistance. Wood Conserving Cook Stoves Bibliography. VITA, Arlington, VA, 1983.
- (9) Smith, K.R., Apte, M., Menon P., and Shrestha, M. Carbon monoxide and particulates from cooking stoves: results from a simulated village kitchen. To be presented at the Third International Conference on Indoor Air Quality and Climate, August 20-24, 1984, Stockholm, Sweden, 1984.
- (10) Butcher, S.S. and Ellenbecker, M.J. J. Air. Pollut. Contr. Assoc. 1982, 32:380-384.
- (11) DeAngelis, D.G., Ruffin, D.S., and Reznik, R.B. Preliminary characterization of emissions from wood-fired residential combustion equipment (Monsanto report), EPA-600/7-80-040, USEPA, Research Triangle Park, NC, 1980.
- (12) Ayer, F.A., ed. Proceedings of Conference on Wood Combustion Environmental Assessment. NTIS, New Orleans, LA, 1981.
- (13) Volunteers in Technical Assistance. Testing the Efficiency of Wood-burning Cookstoves; Provisional International Standards. VITA, Arlington, VA, 1982.

- (14) Rau, J.A., and Huntzicker, J.J. Carbonaceous aerosol from residential wood combustion. To be presented at the Annual Meeting of the Fuel Chemistry division, American Chemical Society, August 26-31, 1984, Philadelphia, PA.
- (15) Dasch, J.M. Environ. Sci. Technol. 1982, 16:635-645.
- (16) Dasch, J.M. Particulate and gaseous emissions from residential fireplaces. GMR-3588 ENV #101, General Motors Research Laboratories, Warren, MICH, 1981.
- (17) Lips, H.I., and Lim, K.J. Assessment of emissions from residential and industrial wood combustion, Acurex Draft Report Fr-81-85/EE, EPA Contract 68-02-3188, 1981.
- (18) DeAngelis, D.G., Ruffin, D.S., and Reznik, R.B. Source assessment: residential combustion of wood, EPA-600/2-80-042b, USEPA, Research Triangle Park, NC, 1980.

PARTICULATE EMISSIONS FROM LOW GRADE FUEL HANDLING. Joseph M. Sorge and
J. Spencer Huston. Earth Tech. Inc., 500 Elizabeth Ave., Somerset, NJ, 08873

The harvesting storage and handling of low grade carbonaceous fuel may result in significant particulate emissions if proper mitigation measures are not observed. The paper provides a summary of particulate size distribution data available for peat and biomass fuel processes. Using the size distribution data and EPA transportation emission rates an estimate of dust emissions from a moderate facilities is developed. Several alternative dust control strategies are assessed to determine respective cost and feasibility information. Results are developed for selective climatic regions to project the severity of the dust emission problems in typical areas of the U.S. The results obtained indicated that the use of practical mitigation methods can substantially reduce the impact of dust emissions due to low-grade fuel harvesting, storage and handling processes.

COMPARISON OF ATMOSPHERIC ENVIRONMENTAL INTRUSIONS OF VARIOUS POWER PLANTS

Wm. H. Fischer
Gilbert/Commonwealth
Reading, PA 19603

INTRODUCTION

The conversion of coal into useful products by combustion or gasification results in the emission of waste materials that are undesirable additions to the environment. These emissions must be controlled in order to prevent damage to the environment, its inhabitants, and their possessions, and to comply with regulations. The objective of this environmental analysis is to assess and compare the environmental intrusions into the atmosphere of conventional coal-fired electric utility plants burning pulverized coal (PC), pressurized fluidized bed combustion power plants (PFBC), coal gasification combined cycle power plants (CGCC), magnetohydrodynamic power plants (MHD), and molten carbonate fuel cell power plants (MCFC). The plants are ranked according to their rates and amounts of emissions.

EMISSIONS

The combustion of coal or of coal-derived fuel gases results in the production and emission into the atmosphere of particulates, sulfur oxides (SO_x) nitrogen oxides (NO_x) and carbon oxides (CO_x). These are derived from the mineral matter in the coal, mineral and organic sulfur in the coal, and organic nitrogen in the coal, producing fuel NO_x . Additionally, the high combustion temperatures result in thermal NO_x being formed from nitrogen in the combustion air.

The particulate matter emitted when coal is converted consists primarily of ash derived from the mineral matter of the coal, mixed with some unburned coal, plus elutriated bed material, if any. In the event that the temperature of the flue gas drops below about $300^{\circ}F$, depending on sulfur content of the fuel, droplets of sulfuric acid may condense, giving rise to an acid aerosol or mist.

Coal sulfur is converted to oxides, SO_x , during combustion, or to H_2S during gasification. From combustion, over 95% is in the form of SO_2 , with less than 5% as SO_3 , as emitted. Although SO_2 is considered harmful to health and welfare, SO_3 is even more so. After emission, the SO_2 is slowly converted to SO_3 . The SO_3 combines with water vapor to form sulfuric acid mist or rain and with basic compounds to form sulfates. Emitted H_2S will also be oxidized to SO_3 . Gasification also results in the formation of small amounts of COS and even smaller amounts of CS_2 .

The nitrogen oxides NO and NO_2 are collectively called NO_x . NO_x is formed from nitrogen both in the fuel and in the combustion air. The percentage of fuel N_2 converted to NO_x

decreases as the percentage of fuel-bound nitrogen increases but the absolute amount converted increases, since the percentage conversion decreases less rapidly than the percentage contained increases. Sunlight converts the emitted NO_x , which is about 90 to 95% NO , into NO_2 , which is unhealthy and contributes to acid rain by forming nitric acid. In addition to the NO_x from fuel discussed above, NO_x is also produced from the nitrogen in the combustion air. This is called thermal NO_x . The amount of thermal NO_x produced is a function of combustion temperature, combustion air ratio and dwell time.

The nitrogen-containing emissions from gasifiers arise only from the fuel nitrogen, since no thermal NO_x arises under the reducing conditions prevailing. The nitrogen-containing emissions are not NO_x but rather, ammonia, NH_3 , and a trace of hydrogen cyanide, HCN . When the raw fuel gas is burned, the nitrogen compounds will convert nearly quantitatively to NO_x and thermal NO_x will also be formed. This can easily result in excessive final NO_x emissions. If the raw fuel gas is cleaned of ammonia, then final NO_x emissions will be reduced but not eliminated, since thermal NO_x will still be formed.

As an indication of the amounts of these emissions, a typical uncontrolled 1000 MW boiler burning coal containing 3.5% sulfur and 12% ash will emit around 900 tpd of ash, 600 tpd of SO_x , 100 tpd of NO_x , and 28,000 tpd of CO_2 .

POWER PLANT EMISSIONS

The power plants considered in this task are so different in detail that any discussion must either be very general and thus superficial or very detailed and thus bewildering. An attempt will be made to steer between these obstacles. In general, an effort will be made to pick up the raw gases downstream of the primary energy converter in each power plant and to briefly describe how the gases will be brought into compliance with the emission limits given below.

The various power plants were nominally designed for 500 MWe output. Illinois No. 6 coal was used, of 3.5% sulfur and 12% ash, with a higher heating value of 11,500 Btu/lb. However, each design used a particular coal analysis which varied somewhat from these figures. The various outputs and efficiencies are shown in Table 1, where columns 3 and 4 show the usual net figures. Pollutant emissions, though, come from the gross input, so gross figures are also shown in columns 2 and 5.

The pollutants in the raw gases emerging from the coal converters in the various power plants are summarized in Table 2. These data have been collected and derived from various sources¹⁻⁶ as well as internal studies and computer simulations. They thus are indicative rather than representative and should be used for comparison only, not for design purposes. As the raw gases proceed through other portions of the power plants, their compositions can be expected to change. In general, the changes

TABLE 1
COAL CONVERSION PLANTS

PLANT	MWE		EFFICIENCY (%)	
	GROSS	NET	NET	GROSS
PC	546	503	34.96	38.04
PFBC	513	497	39.75	41.01
CGCC	531	502	37.34	39.53
MCFC	533	460	49.94	57.74
MHD	624	504	40.49	51.79

TABLE 2
EMISSION RATES FROM COAL CONVERTORS
(LB/10⁶ BTU)

PLANT	PARTICULATE		SO _x		NO _x		CO ₂
	U ^A	C	U	C	U	C	U
PC	8.6	0.03	4.9	0.6	0.6	0.6	203
PFBC	14.7	0.03	0.6	0.6	0.3	0.2	206
CGCC	5.1	0.03	4.9 _B	0.6	-0 _C	0.2 _D	203
MCFC	1.5	-0	4.9 _B	-0	0.6 _C	-0	203
MHD	20.2	0.03	-0	-0	0.6	0.6	214
EMISSION LIMIT	0.03		0.6		0.6		

A U = UNCONTROLLED, C = CONTROLLED

B SO_x EQUIVALENT IF ALL H₂S AND COS ARE CONVERTED TO SO_x

C NO_x EQUIVALENT IF ALL NH₃ IS CONVERTED TO NO_x

D THERMAL NO_x

are minor in heat removal or recovery sections but are major in gas cleanup sections. Combustion of fuel gases will increase the NO_x content due to thermal fixation of nitrogen in the combustion air.

Also shown in Table 2 are the emissions to the atmosphere after control measures have been applied to the raw gases. In general, the controls have been designed to comply with the EPA New Source Performance Standard (NSPS) for electric utility steam generating units. Strictly speaking, this NSPS applies only to the pulverized coal (PC) and pressurized fluidized bed (PFBC) plants, but has also been used for the other plants in the absence of regulations for them. The exception is the molten carbonate fuel cell plant in which the requirements are set by the fuel cell. There is currently no emission limit for CO_2 from any plant, so no CO_2 control equipment is required.

PULVERIZED COAL POWER PLANT

A conventional pulverized coal-burning boiler raising steam for a turbine to generate electricity is considered, as shown in Figure 1. Figure 2 is a block diagram of the air pollution control equipment selected for this plant.

Particulates

The uncontrolled fly ash emission of $8.6 \text{ lb}/10^6 \text{ Btu}$ will be reduced to the compliance limit of $0.03 \text{ lb}/10^6 \text{ Btu}$ by a combination of an electrostatic precipitator (ESP) and a wet scrubber. The ESP has a specific collection area (SCA) of $200 \text{ sq. ft. per } 10^3 \text{ acfm}$. Its pressure drop is negligible.

Sulfur Oxides

The main task of the scrubber is not particulate removal but rather sulfur oxides removal. The theoretical SO_x emission is $5.2 \text{ lb}/10^6 \text{ Btu}$ but since five percent is assumed to be retained by the ash, $4.9 \text{ lb}/10^6 \text{ Btu}$ emerges. This must be reduced to 0.6 by means of a limestone flue gas desulfurization system employing a spray tower at a liquid-to-gas ratio (L/G) of $200 \text{ gpm per } 10^3 \text{ acfm}$ at a ΔP of 0.5 psi .

Nitrogen Oxides

A typical PC furnace will just about meet the NO_x emission limit. Use of retrofit low- NO_x burners in an existing installation or use of two stage combustion or low- NO_x burners in a new installation will insure compliance.

PRESSURIZED FLUIDIZED BED COMBUSTION POWER PLANT

A pressurized fluidized bed combustion power plant (Figure 3) has a steam cooled PFBC raising steam for electricity generation and providing hot gas for driving a gas turbine which compresses the

PFBC air and also generates electricity. A block diagram of the air pollution control equipment is shown in Figure 4.

Particulates

The particulate load from a PFBC is high due to carry over of ash in the feed coal, plus unburned coal, plus elutriated bed material. A series of high efficiency, high temperature cyclones reduces the loading to a low enough level to protect the gas turbine. However, this level, approximately $0.4 \text{ lb}/10^6 \text{ Btu}$ is still above the emission limit, so that a bag house is used to clean the cooled gas to compliance level. The total ΔP is 7 psi. Advanced design cyclones may be able to meet the emission limit, eliminating the bag house, but probably at an increased pressure drop.

Sulfur Oxides

The dolomite fed to the PFBC at a Ca/S mole ratio of 2.3 is calcined to the oxides. The calcium oxide reacts with the sulfur dioxide formed from the sulfur in the coal to produce calcium sulfate. The magnesium oxide does not react but improves the porosity and hence the reactivity and utilization of the calcine. Thus, the raw gas has a low enough SO_x content to be in compliance, but at the cost of having an increased particulate loading.

Nitrogen Oxides

The low combustion temperature in a PFBC retards the formation of thermal NO_x . Pressurized operation results in lower NO_x formation than does atmospheric operation. There is evidence that any NO_x formed is partially decomposed by reactions with sulfur dioxide and/or calcium sulfate. The net result is that NO_x emissions from a PFBC are below the emission limit, so that no additional control method is needed.

GASIFICATION COMBINED CYCLE POWER PLANTS

Another different system is shown in Figure 5, with the air pollution control equipment shown in Figure 6. Here, an air blown coal gasifier supplies the fuel gas for a gas turbine whose exhaust raises steam.

Particulates

A venturi scrubber at an L/G of 20 and a ΔP of 15 psi is used to remove the bulk of the particles from the fuel gas. Final removal occurs in the Stretford plant.

Sulfur Oxides

The sulfur in the coal appears principally as hydrogen sulfide in the fuel gas. This is removed as elemental sulfur by the Stretford unit for disposal or sale. Residual sulfur content,

nearly all as carbonyl sulfide, is converted to sulfur dioxide in the gas turbine combustor but its emission is low enough to be in compliance with the regulations.

Nitrogen Oxides

The low pressure Combustion Engineering gasifier selected produces no ammonia from the coal nitrogen, so that the only NO_x released is that formed thermally in the gas turbine combustor. Conventional gas turbine control methods will assure compliance.

FUEL CELL POWER PLANT

This power plant, shown in Figures 7 and 8, is the most complicated one considered. It has three sources of electricity: fuel cells, a gas turbine, and steam turbines. The sensible heat in the gasifier fuel gas is used to raise steam, as is that in the gas turbine exhaust gas and the fuel cell effluent gas. The fuel cell effluent gas also drives the gas turbine. Finally, the chemical energy in the fuel gas drives the fuel cells.

Fuel cell gas cleanliness requirements are set by the fuel cells, not by emission standards, particularly for sulfur compounds, which must be reduced to 1 ppm. Particulate and ammonia are much less troublesome.

Particulates

A venturi scrubber with an L/G of 40 and a ΔP of 15 psi is used to remove particulate matter to a level sufficient to meet fuel cell requirements and thus emission standards.

Sulfur Oxides

The Texaco gasifier selected emits principally hydrogen sulfide, which is easily removed to the desired ppm level, but the carbonyl sulfide is not. Therefore, a hydrolyzer unit is used to convert the carbonyl sulfide to hydrogen sulfide. A Selexol unit is used to separate the hydrogen sulfide from the fuel gas. Claus-Beavon units are used to recover elemental sulfur and prevent sulfur emissions to the atmosphere in violation of applicable regulations. Final hydrogen sulfide removal is accomplished with a throw away bed of zinc oxide which adds another ΔP of 10 psi for a total ΔP of 25 psi.

It is obvious that the resulting low sulfur level in the fuel gas, after conversion to sulfur dioxide in the catalytic burner, is far below the permissible emission limit.

Nitrogen Oxides

The venturi particulate scrubber will remove most of the ammonia in the fuel gas so that little fuel NO_x will be formed. The temperature in the catalytic burner is low, about 1200°F , so that

little if any thermal NO_x is formed⁸. The result is that final NO_x emissions are well in compliance.

MAGNETOHYDRODYNAMIC POWER PLANT

This power plant, shown in Figures 9 and 10 is completely different from those discussed heretofore. Coal is burned in a three stage combustor. The first stage operates with about 50% of stoichiometric oxygen and rejects molten slag. The second stage operates at about 95% of stoichiometry with additional slag rejection and is followed by a third stage where seed material (a mixture of potassium sulfate and carbonate) is added. After generating direct current electricity in a channel, the plasma is finally combusted at about 105% stoichiometry with added air with additional slag and seed rejection. Steam is raised by the hot gas to generate alternating current electricity. Particulate matter is removed for recovery of the seed material and the gas is discharged to the atmosphere.

Particulates

Despite the rejection of slag, the addition of seed material results in a very high particulate loading in the raw gas. An ESP with an SCA of 500 is used to remove the solids down to the compliance limit. An unusually large SCA is required because of the high electrical resistivity of the seed compounds.

Sulfur Oxides

The seed material serves a dual purpose. The potassium contributes conductivity to the plasma followed by the potassium from the carbonate reacting with sulfur dioxide to form additional potassium sulfate. This reaction is essentially quantitative, so that provision of sufficient potassium carbonate can result in the emission of essentially no sulfur oxides.

Nitrogen Oxides

An MHD combustor operates so much hotter than a usual furnace, 4500°F versus 2500°F, that copious amounts of NO_x are formed, up to ten times as much as from a PC furnace, despite the initial substoichiometric combustion. Controlled slow cooling of the gas and recirculation of flue gas to hold down the temperature of final combustion results in a reduced final NO_x emission, one which meets the standard.

DISCUSSION

All of the power plants considered have been designed to meet or better the emission rate performance standards for air emissions as shown in Table 2. The fossil fueled power plant will just meet the standards. The low temperature of combustion and NO_x decomposition reactions inherent in PFBC account for its low NO_x emissions. The baghouse used for final particulate cleanup accounts for the low particulate emissions. The combined cycle

power plant will satisfy SO_x regulations but should be below those for NO_x and particulate matter. The magnetohydrodynamic power plant will emit essentially no SO_x while the particulate and NO_x emissions will meet standards. The fuel cell power plant will have the lowest emissions of all due to the rigid requirements of the fuel cells and the use of a low temperature catalytic burner.

The above paragraph was based on emission rates. Considering the absolute amounts of regulated pollutants emitted, shown in Table 3, the fossil fueled plant will emit the most, followed by the combined cycle and the pressurized fluidized bed combustion power plants having similar emissions, than by the magnetohydrodynamic plant, with the fuel cell power plant having by far the smallest total amount of pollutant emissions. All these emissions should have added to them the fugitive emissions from the coal pile and coal handling and preparation steps, and the ash handling steps. Considering all the emissions in Table 3, including CO_2 , hardly alters the situations.

CONCLUSION

All the subject power plants will have atmospheric environmental intrusions that are currently tolerable. The plants can be ranked, as in Table 4. This ranking is somewhat subjective. It does not take into account any weighting by the effects of one pollutant over another, which perhaps should be done. Under any ranking system, the molten carbonate fuel cell and the magnetohydrodynamic plants can hardly be dislodged from their placings and the pulverized coal plant will probably always be lowest ranked.

TABLE 3
 EMISSION AMOUNTS FROM COAL CONVERTORS
 (LB/HR)

<u>PLANT</u>	<u>PARTICULATE</u>	<u>SO_x</u>	<u>NO_x</u>	<u>CO₂</u>
PC	147	2940	2940	995,000
PFBC	128	2560	850	958,000
CGCC	138	2750	920	931,000
MCFC	~0	~0	~0	640,000
MHD	123	~0	2470	880,000

TABLE 4
 COAL CONVERTORS EMISSION RANKING
 (BEST TO WORST)

- MOLTEN CARBONATE FUEL CELL
- MAGNETOHYDRODYNAMIC
- PRESSURIZED FLUIDIZED BED COMBUSTOR
- COAL GASIFICATION COMBINED CYCLE
- PULVERIZED COAL

REFERENCES

1. Population of Air Pollutant Emission Factors, Office of Air Programs, U.S. Environmental Protection Agency, PUB. No. AP-42, February 1976.
2. Jahmig, C. E. and H. Shaw, Environmental Assessment of an 800 MWe Conventional Steam Power Plant, prepared by EXXON Research and Engineering Company, for U. S. Environmental Protection Agency, EXXON/GRU. IDJAO. 76, September 1976.
3. Shaw, H. and S. E. Tung, Environmental Assessment of Advanced Energy Conversion Technologies - State-of-the-Art, prepared by EXXON Research and Engineering Company, for U.S. Environmental Protection Agency, EXXON/GRU 4DJAO. 77, October 1977.
4. Christian, J.E., Gas-Steam Turbine Combined Cycle Power Plants, prepared by Oak Ridge National Laboratory for U.S. Department of Energy, ANL/CES/TE 78-4, October 1978.
5. Environmental Development Plan, U.S. Department of Energy, DOE/EDP-0045, May 1979.
6. Calculations by T. E. Dowdy, Gilbert/Commonwealth, Reading, PA, based on personal communication from I. W. Henry, Combustion Engineering, Windsor, CT, 5 August 1981.
7. "Development of Molten Carbonate Fuel Cell Power Plant Technology," prepared by United Technologies Corporation, for U. S. Department of Energy, DOE/ET/15440-2, August 1980.
8. King, J. M., Jr., Energy Conversion Alternatives Study-ECAS-United Technologies Phase II Final Report, prepared for National Aeronautics and Space Administration, NASA-CR 134955, October 1976.

FIGURE 1
PULVERIZED COAL PLANT HEAT AND MASS BALANCE

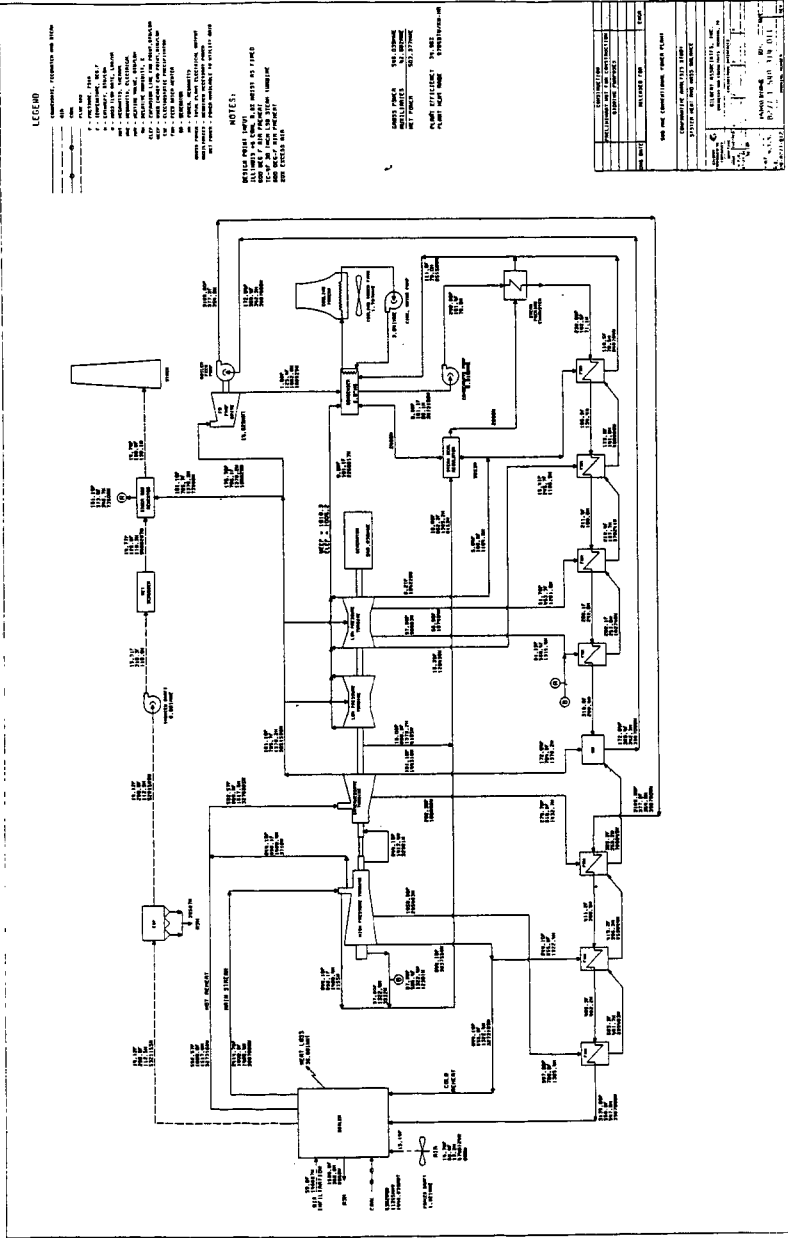


FIGURE 2

PULVERIZED COAL PLANT

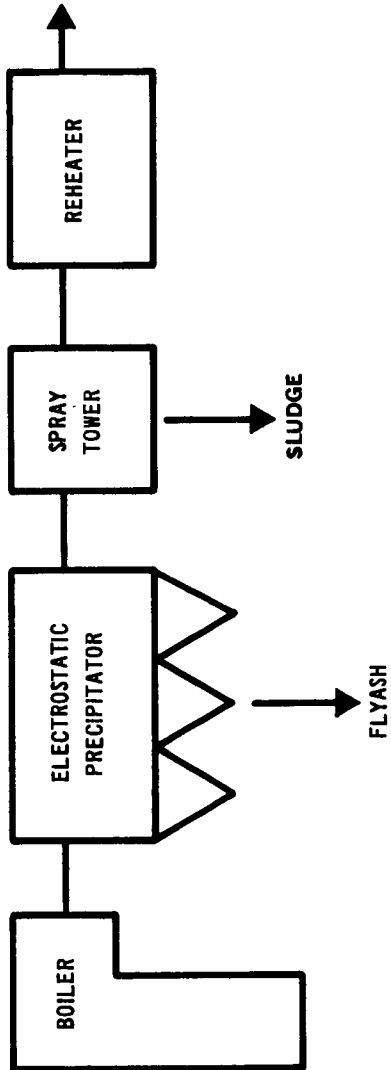


FIGURE 3
PRESSURIZED FLUIDIZED BED PLANT HEAT AND MASS BALANCE

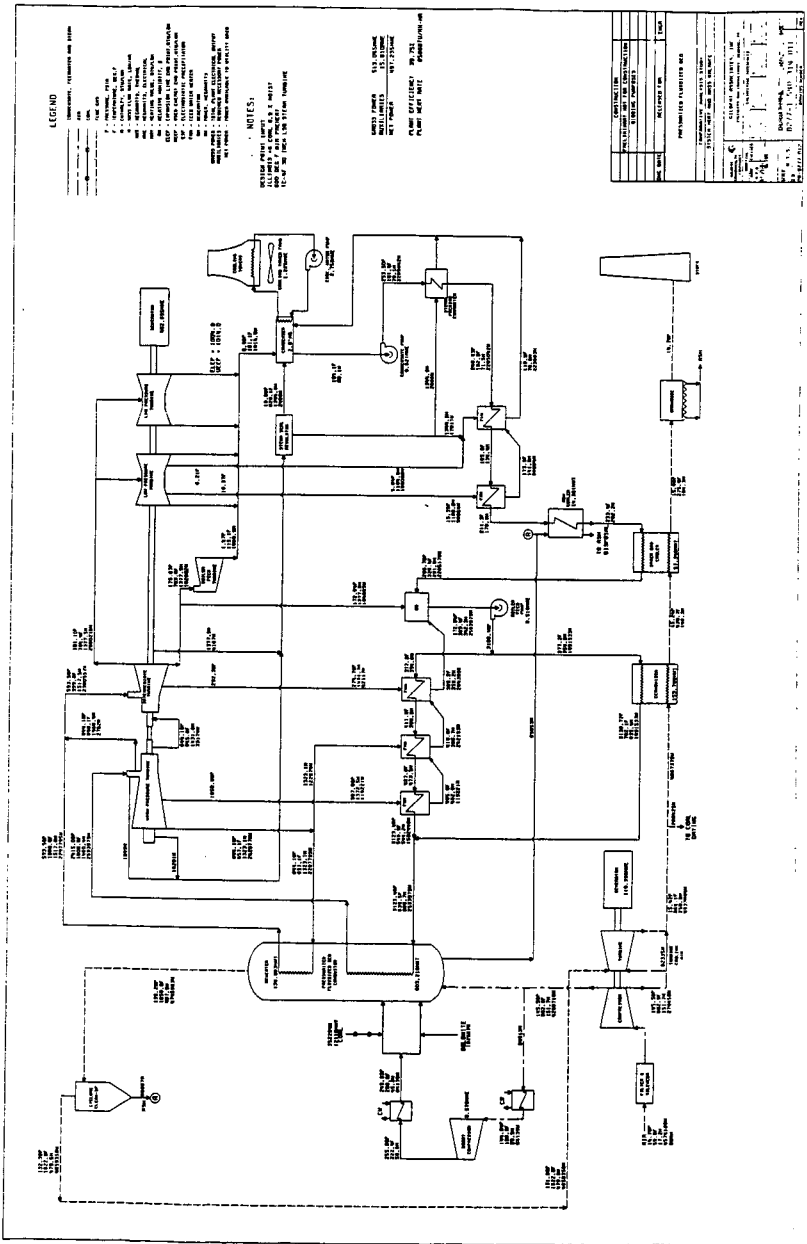


FIGURE 4

PRESSURIZED FLUIDIZED BED PLANT

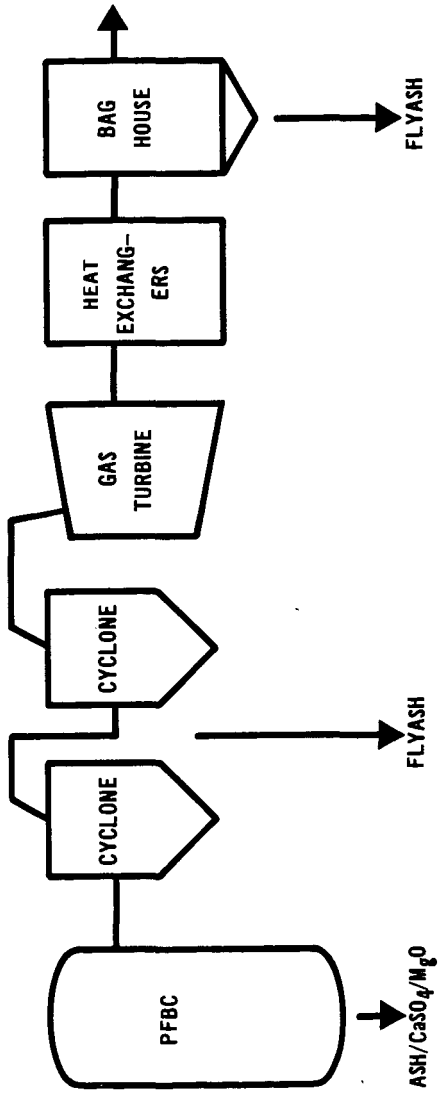


FIGURE 6

COAL GASIFICATION COMBINED CYCLE PLANT

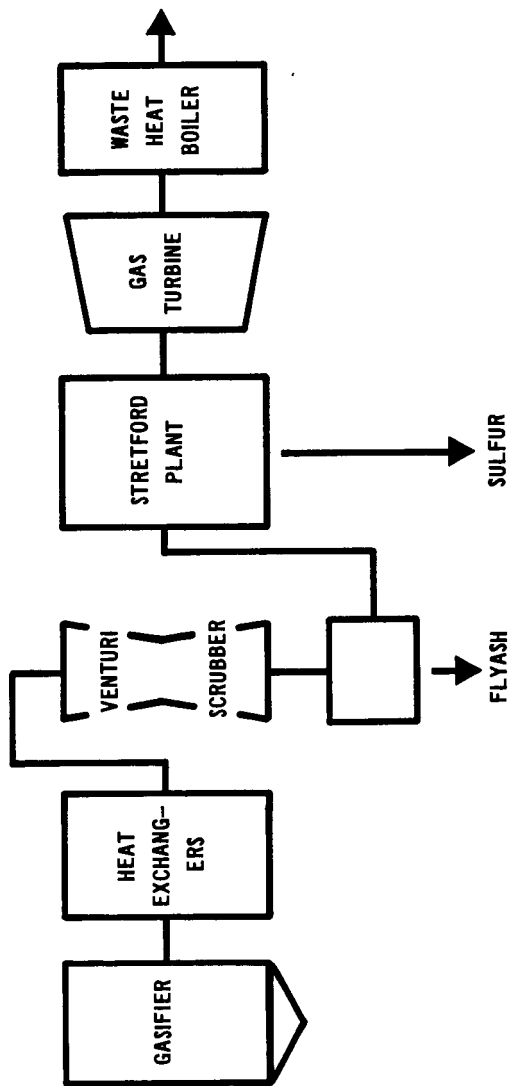


FIGURE 8

MOLTEN CARBONATE FUEL CELL PLANT

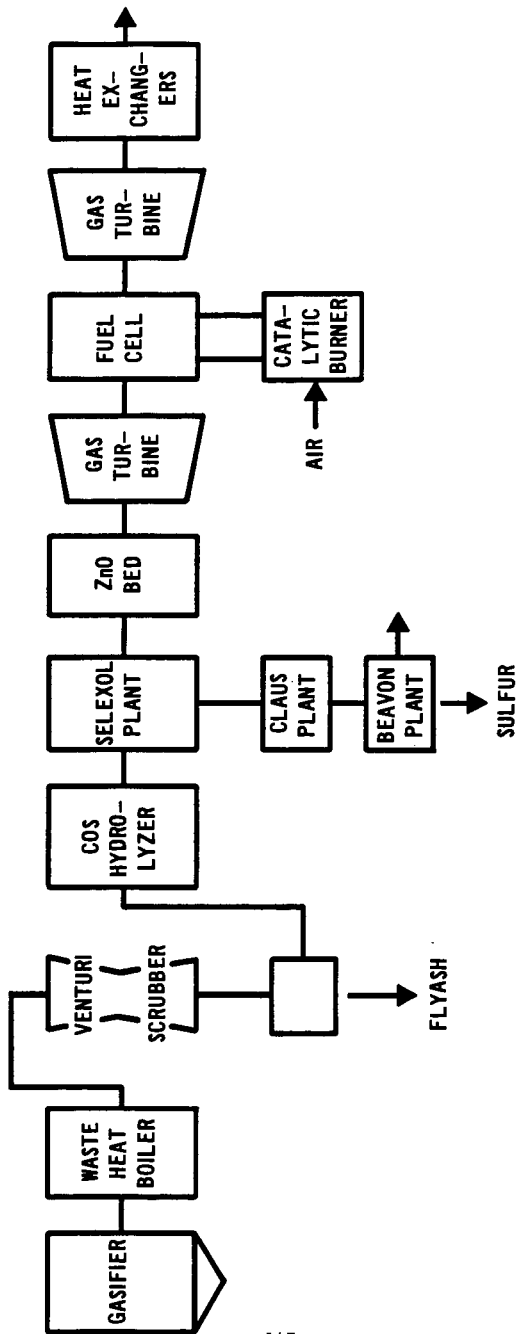


FIGURE 9
MAGNETOHYDRODYNAMIC PLANT HEAT AND MASS BALANCE

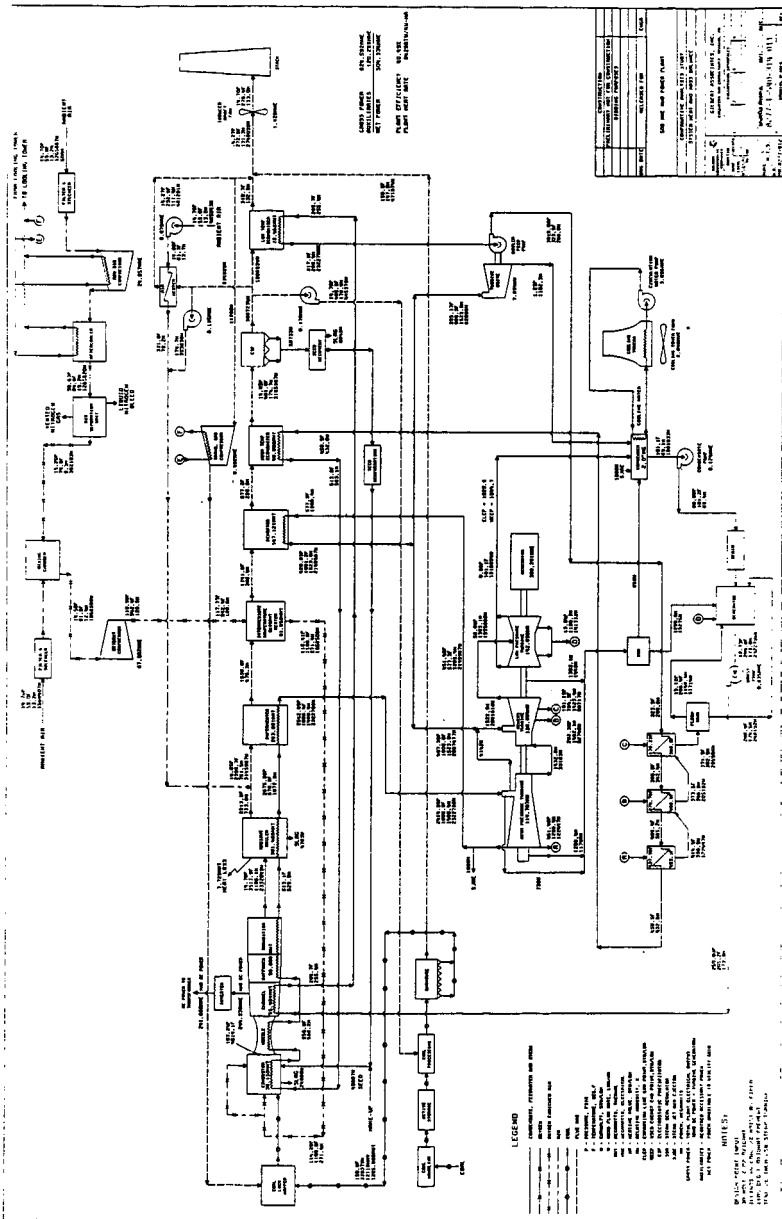
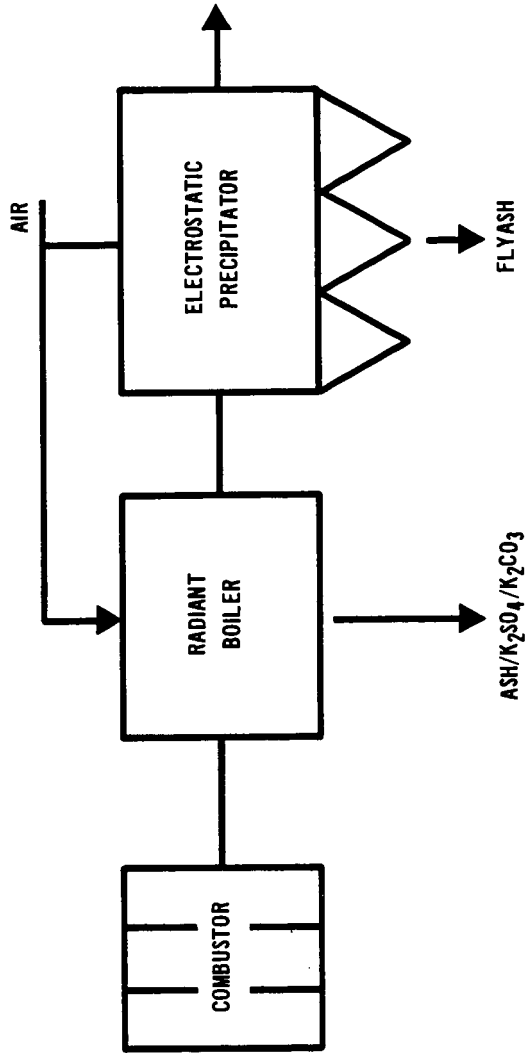


FIGURE 10

MAGNETOHYDRODYNAMIC PLANT



LARGE-SCALE PEAT FEED PREPARATION

Richard Biljetina, Rene M. Laurens, T. Robert Sheng, and Wilford G. Bair

Institute of Gas Technology
3424 S. State Street
Chicago, Illinois 60616

Introduction

In 1980 the Institute of Gas Technology (IGT) installed large-scale drying, grinding, screening and transport equipment for processing of Minnesota peat in an existing pilot plant designed to produce substitute natural gas (1). The facility, located at IGT's Energy Development Center in Chicago, is capable of drying 16 tons per hour of as-received-peat (60-75 wt % moisture content) to a controlled product-moisture-content ranging between 5 and 50 wt %. Subsequent screening and grinding operations produce a -20+80 USS mesh size product for injection into the fluidized bed gasifier. See Figure 1.

Since this was the first large-scale attempt in this country to prepare and transport peat at moisture levels as low as 5 wt %, two major questions were asked: 1) What procedures and what type of equipment would be required to process, transport and store peat, and 2) what affect would these operations have on the physical and chemical characteristics of the peat?

The successful operation of the peat feed preparation system (2000 tons of wet peat processed) provided these answers. The results of these efforts are summarized in this paper.

Design Conditions

Since the selection of appropriate equipment and the definition of handling precautions were prerequisites of the design phase, IGT's process development group concentrated its initial efforts in this area. The selection of drying equipment, capable of providing a wide range of product moisture contents, received the highest priority. One of the most important selection criteria was the ability to moderate temperatures sufficiently such that the chemical composition of the peat would not be affected even when dried to 5 wt % moisture. Both foreign and U.S. companies were contacted and all commercially available equipment evaluated. The types of dryers considered included: rotary drum dryers, flash dryers, and fluidized-bed dryers. Grinding and screening equipment was also evaluated. Design considerations included the ability to handle a range of moisture contents, ability to handle fibrous and woody material, and minimization of fines production.

In order to identify proper handling precautions, IGT commissioned the Technical Research Center of Finland to survey available data in the Scandinavian, Russian, and German literature and to provide summary reports of their findings(2,3). These reports did indicate that additional precautions must be taken as peat moisture contents are lowered. Existing data indicated that:

- o When the moisture content is 35-40%, peat dust is only slightly susceptible to explosion and when the moisture content is 40-50%, the dust is not explosible under ordinary conditions.
- o As the moisture content decreases, the minimum explosible concentration of peat dust decreases.
- o As the moisture content decreases, the maximum pressure and the maximum rate of pressure rise of the peat dust explosion increase.

- o As the moisture content decreases, the minimum ignition energy of the peat dust cloud also decreases.

Commercial experience also provided the following recommendations:

- o Operate continuous rather than batch processes.
- o Isolate high risk equipment.
- o Design mass flow systems for small quantities.
- o Locate equipment outdoors.

As a result of these investigations and recommendations, a final process configuration was selected for the peat preparation facility.

Process Description

Figure 2 presents the equipment selected for the peat feed preparation facility. Peat is received untreated from the bog and stored at the site in an outdoor storage area. In order to facilitate handling, the peat is first dried and then screened and ground to the proper size consistency. A triple-pass rotary drum dryer was chosen to provide the necessary flexibility in drying capacity. See Figure 3. Peat is, for the most part, conveyed by the hot flue gases through the multiple-pass system. Large particles, which require longer residence times to achieve the same moisture reduction, are hindered sufficiently to obtain the necessary drying time. A 50 million Btu/h natural gas burner provides a hot, co-current air stream with a maximum initial contact temperature of 1200°F. Moisture content of the peat is controlled by the exit air temperature, which typically ranged between 110° and 260°F for moisture contents between 40 and 5 wt %.

Since the dryer system presents the highest risk for dust ignition, isolation was provided by rotary valve seals. In addition, a steam quenching system and relief doors were provided as additional safeguards. Sealed screw conveyors and a bucket elevator were used to transport the dried peat to the screening and drying system. Conventional screeners and a hammer mill were chosen to size the product. An overall view of the peat preparation facility is shown in Figure 4.

Product peat was then delivered to either a high-pressure, lockhopper feed injector (4), slurry preparation or 400-ton storage silos. All storage bins were purged with nitrogen to provide an inert atmosphere and were monitored for oxygen content. These design considerations have resulted in the controlled production of peat containing moisture contents as low as 5 wt % in a reliable and safe manner.

Test Results

Once operation of the facility was begun, data were collected to determine the effects on the physical and chemical properties of the peat during the various processing steps. Minnesota peat, obtained from the Northern Peat Company, Grand Rapids, Minnesota, exhibited a remarkable uniformity in chemical composition and moisture content. Average values for size distribution and chemical composition and the standard deviation for a sample size of seven are given in Tables 1 and 2. Of greatest concern was the occasional lacing of the 'raw' peat with semi-decomposed tree roots and stumps, as well as gravel picked up during harvesting operations in the field. These materials were removed by a 2x2 stationary screen.

One of the main design considerations for the selection of the drying system was to minimize overheating and chemical degradation of the peat particle during drying. Samples of peat exiting the dryer were routinely taken and analyzed for chemical composition. Table 3 compares values at moisture levels of 5.3, 10.1, 16.0, and 22.0 wt % against those of raw peat containing 68.9 wt % moisture. It can

be seen that no significant change in chemical composition occurs during the drying operation.

Size distribution changes do occur as peat is dried. Table 4 and Figure 5 provide a comparison of sieve analyses for various moisture levels exiting the dryer. Sufficient size reduction occurs to warrant screening prior to grinding to a -20+80 USS product size.

Another issue of interest is the homogeneity of the moisture level for the peat exiting the drying system. Figure 6 indicates the variation in moisture content as a function of particle size for various peat samples exhibiting average moisture levels of 30, 36, and 42 wt %. This is particularly important in cases where downstream processing would tend to encourage segregation. For instance, screening area requirements can be affected by both the feed rate, particle shape and moisture content of the peat.

Similar concerns were raised about the chemical composition variation as a function of particle size. Data taken of the product, fines and oversize streams from the screening operation (Table 5) do not indicate any significant difference in chemical composition.

Summary

Data collected during an operating period which processed over 2000 tons of as-received Minnesota peat have shown that peat can be dried, screened and finely ground in a reliable and safe manner. Moisture reduction to as low as 5 wt % can be obtained in properly designed systems without chemical degradation of the product. Some reduction in the size distribution of the Minnesota peat did occur during the drying operation. In addition, the moisture content of the product is not completely homogeneous. Moisture content does vary with particle size, however, chemical composition does not vary significantly with particle size. These findings were subsequently used in evaluating process and equipment requirements for downstream operations in the gasification pilot plant. Segregation, for instance, of the product peat was discouraged in order to ensure uniform levels of moisture in the feed to the gasifier.

Acknowledgement

The work presented in this paper was jointly funded by the U.S. Department of Energy and the Gas Research Institute.

REFERENCES

1. "Peat Gasification Pilot Plant Program", Project 70105 Final Report, prepared by Institute of Gas Technology, Chicago, March 1983.
2. Weckman, W., Hyvarinen, P., Olin, J., Rautalin, A., and Vuorio, M., "Reduction of Fire and Explosion Hazards at Peat Handling Plants", Technical Research Centre of Finland, Research Reports, 2/1981, ESPOO.
3. Weckman, H., "Effect of the Moisture Content of Peat on Certain Explosion Properties of Peat Dust", Report 23, Technical Research Centre of Finland, ESPOO, August 1980.
4. Wohadlo, S.J., Biljetina, R., Laurens, R.M., and Bachtta, R., "Solids Flow Control and Measurement in the Peatgas Pilot Plant Program", paper presented at the Sixth Annual 1982 Symposium on Instrumentation and Control for Fossil Energy Processes, Houston, Texas, June 7-9, 1982.

Table 1. AVERAGE SIZE DISTRIBUTION FOR AS-RECEIVED MINNESOTA PEAT

<u>Screen Analysis, U.S.S., wt %</u>		<u>Standard Deviation</u>
+ 10	42.3	4.6
+ 20	25.6	2.1
+ 30	9.2	1.1
+ 60	12.9	3.9
+ 80	3.7	1.0
+100	2.1	0.8
+200	1.2	0.4
+230	2.1	0.5
PAN	<u>0.9</u>	0.6
TOTAL	100.0	

Table 2. AVERAGE CHEMICAL COMPOSITION FOR AS-RECEIVED MINNESOTA PEAT

<u>Chemical Analysis, wt %</u>		<u>Standard Deviation</u>
Proximate (Dry)		
Volatile Matter	59.4	1.1
Fixed Carbon	23.2	1.3
Ash	<u>17.4</u>	1.2
TOTAL	100.0	
Moisture	68.9	1.0
Ultimate (Dry)		
Carbon	48.3	1.3
Hydrogen	5.0	0.2
Sulfur	0.3	0.05
Nitrogen	2.1	0.1
Oxygen	26.9	0.7
Ash	<u>17.4</u>	2.2
TOTAL	100.0	

Table 3. COMPARISON OF PEAT CHEMICAL COMPOSITION AT VARIOUS MOISTURE LEVELS

Description	RAW*	SDEV**		DRIED	SDEV		DRIED	SDEV		DRIED	SDEV	
	PEAT	PEAT	PEAT	PEAT	PEAT	PEAT	PEAT	PEAT	PEAT	PEAT	PEAT	PEAT
Moisture, wt %	68.9	1.0	5.3	0.2	10.1	1.4	16.0	1.1	22.0	2.4		
Proximate Analysis (Dry), wt %												
Volatile Matter	59.4	1.1	59.1	1.1	59.1	1.4	59.6	1.1	59.6	0.8		
Fixed Carbon	23.2	1.3	23.6	0.7	23.5	1.2	23.5	1.1	23.6	1.0		
Ash	17.4	1.2	17.3	1.1	17.4	1.8	16.9	0.7	16.8	0.6		
TOTAL	100.0		100.0		100.0		100.0		100.0			
Ultimate Analysis (Dry), wt %												
Carbon	48.3	1.3	48.2	0.6	48.4	0.8	48.7	0.5	48.2	0.4		
Hydrogen	5.0	0.2	5.0	0.1	5.0	0.1	5.0	0.1	5.1	0.1		
Sulfur	0.3	0.05	0.3	0.08	0.3	0.07	0.3	0.08	0.2	0.05		
Nitrogen	2.1	0.1	2.2	0.1	2.2	0.1	2.3	0.2	2.2	0.1		
Oxygen	26.9	0.7	27.0	0.5	26.7	0.9	26.8	0.5	27.5	0.3		
Ash	17.4	2.2	17.3	1.1	17.4	1.8	16.9	0.7	16.8	0.6		
TOTAL	100.0		100.0		100.0		100.0		100.0			

* As-received from bog.

** SDEV = Standard Deviation

Table 4. COMPARISON OF PEAT SIZE DISTRIBUTION AT VARIOUS MOISTURE LEVELS

Description	RAW	* DRIED		DRIED		DRIED		DRIED	
	PEAT	SDEV	PEAT	SDEV	PEAT	SDEV	PEAT	SDEV	PEAT
Moisture, wt %	68.9	1.0	5.3	0.2	10.1	1.4	16.0	1.1	22.0
Screen Analysis, U.S., wt %									
+ 10	42.3	4.6	9.2	1.8	13.7	5.4	12.7	1.4	11.9
+ 20	25.6	2.1	27.4	5.3	27.2	2.9	33.8	5.0	29.9
+ 30	9.2	1.1	15.4	2.9	13.6	1.3	16.7	0.8	14.0
+ 40	--	--	13.2	3.8	12.1	2.9	8.8	4.4	11.7
+ 60	12.9	3.9	18.5	3.8	16.6	3.3	16.3	3.8	16.0
+ 80	3.7	1.0	4.7	1.3	5.4	1.9	3.9	1.1	5.7
+100	2.1	0.8	3.1	0.7	3.8	1.9	2.6	1.0	2.8
+200	1.2	0.4	4.6	1.7	4.0	0.9	1.9	1.2	3.7
+230	2.1	0.5	1.3	0.9	1.3	1.7	1.5	0.9	1.5
PAN	0.9	0.6	2.6	0.6	2.3	0.3	1.8	0.5	2.8
TOTAL	100.0		100.0		100.0		100.0		100.0

* SDEV = Standard Deviation

Table 5. COMPARISON OF CHEMICAL COMPOSITION FOR PEAT OF DIFFERENT SIZE FRACTIONS

Description	<u>DRYER DISCH.</u>	<u>FINES</u>	<u>OVER SIZE</u>	<u>SIZED PRODUCT</u>
Mass Fraction, wt % (U.S. Sieve)				
+20	30.1	0.1	93.5	3.5
-20 to +80	53.0	7.6	6.1	94.0
-80	16.9	92.3	0.4	2.5
Proximate Analysis, wt %				
Volatile Matter	59.4	57.0	60.2	58.7
Fixed Carbon	25.0	23.0	24.3	24.6
Ash	<u>15.6</u>	<u>20.0</u>	<u>15.5</u>	<u>15.7</u>
TOTAL	100.0	100.0	100.0	100.0
Ultimate Analysis, wt %				
Carbon	49.3	46.7	49.3	49.2
Hydrogen	5.1	4.9	5.1	5.2
Sulfur	0.4	0.3	0.3	0.3
Nitrogen	2.2	2.2	2.1	2.2
Oxygen	27.4	25.9	27.7	27.4
Ash	<u>15.6</u>	<u>20.0</u>	<u>15.5</u>	<u>15.7</u>
TOTAL	100.0	100.0	100.0	100.0
Moisture, wt %	7.1	7.9	11.4	7.7
Bulk Density, lb/ft ³	27.8	30.1	26.6	26.8

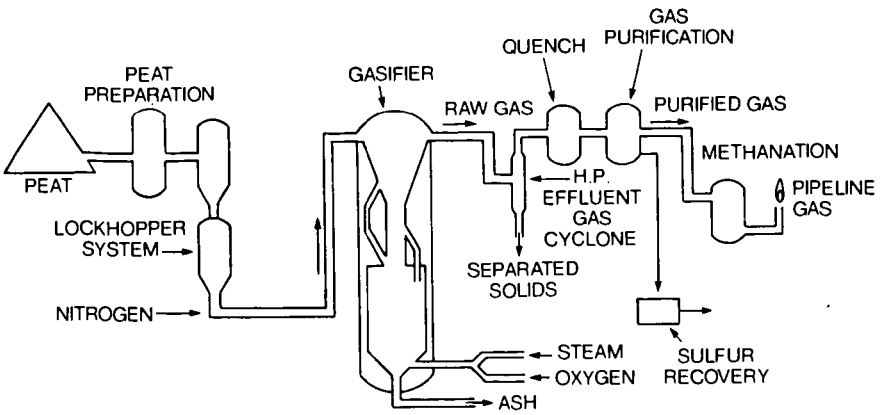


Figure 1. PEATGAS PILOT PLANT FACILITY

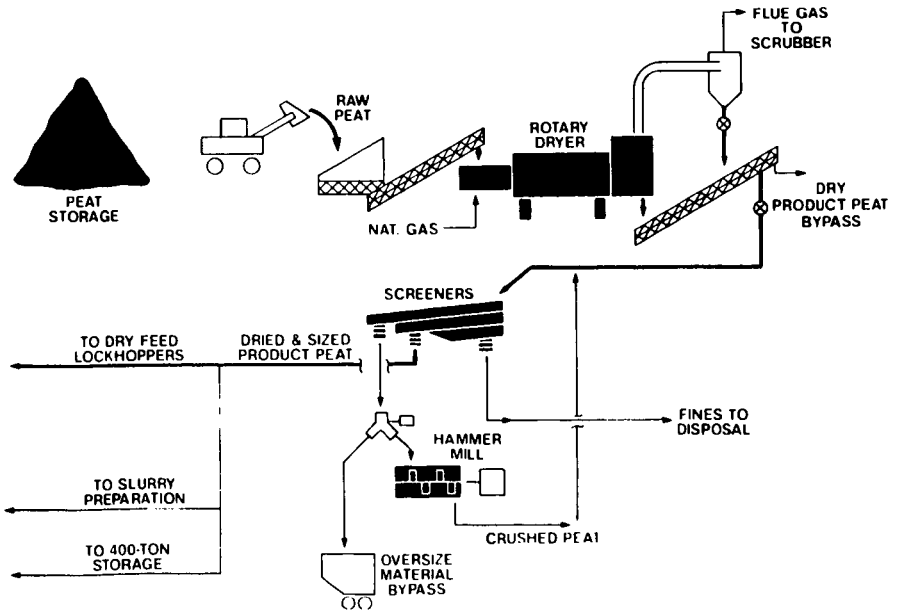


Figure 2. PEAT PREPARATION

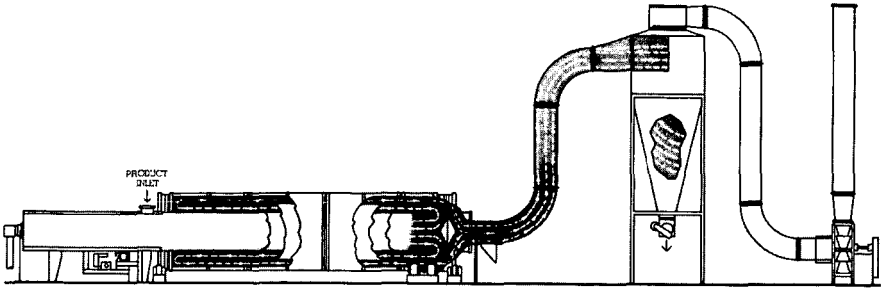


Figure 3. TRIPLE-PASS DRYER SELECTED FOR THE PEAT DRYING SYSTEM

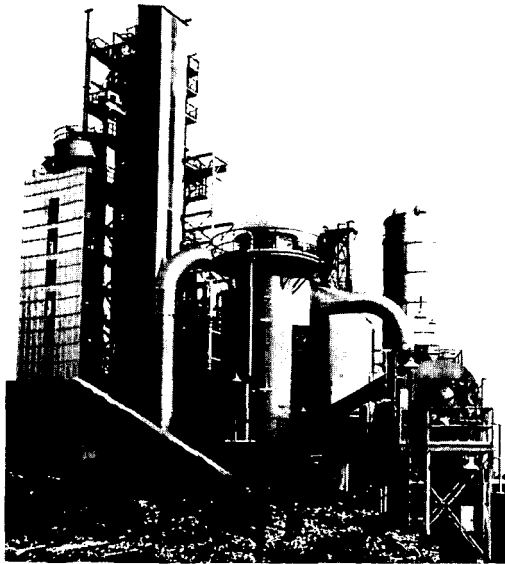


Figure 4. DRYING SYSTEM IN OPERATION

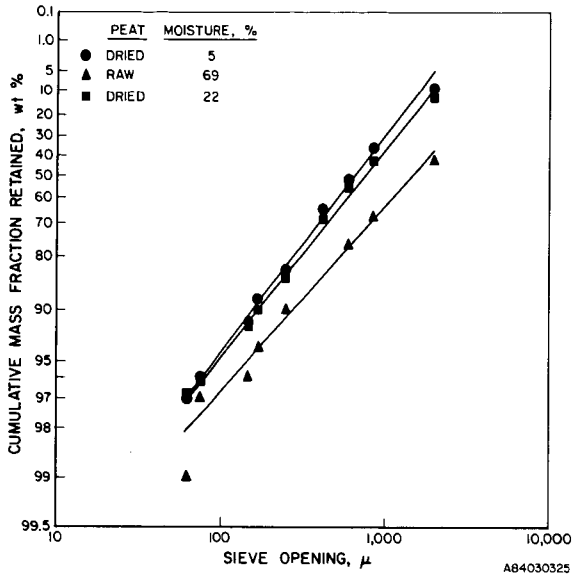


Figure 5. GRAPHICAL REPRESENTATION OF THE SHIFT IN SIZE DISTRIBUTION OF DRIED PEAT

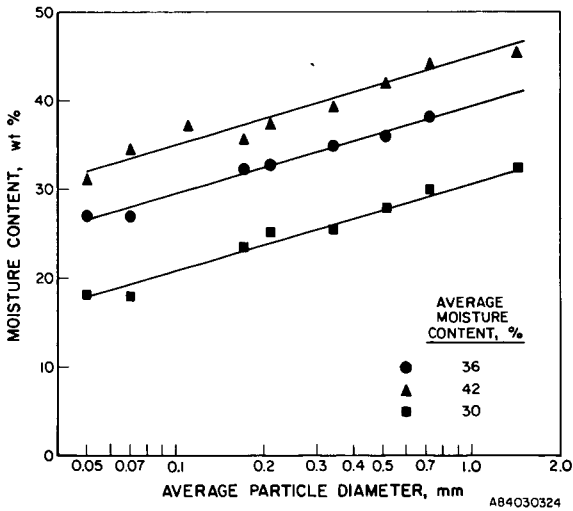


Figure 6. PEAT MOISTURE CONTENT AS A FUNCTION OF PARTICLE SIZE FOR SAMPLES EXHIBITING AN AVERAGE MOISTURE CONTENT OF 42, 36 AND 30 wt %

MULTIPLE MECHANISMS FOR LOSS OF COAL COKING
PROPERTIES CAUSED BY MILD AIR OXIDATION

John W. Larsen, Doyoung Lee, and Thomas E. Schmidt
Department of Chemistry
Lehigh University
Bethlehem, Pennsylvania 18015

There are at least three different mechanisms responsible for the loss of coal coking properties caused by mild air oxidation, weathering. We present here data demonstrating their existence. The chemical changes responsible for the coking loss are only partly characterized. In no case is it understood how they destroy or diminish a coals ability to coke.

We worked with Bruceton coal, a high quality, unoxidized sample provided by the kind folks at PETC. Weathering for more than 250 days at 25 °C and 50% relative humidity produced no change in the free swelling index, and only small changes in the coal. When weathered at 80 °C and a water pressure of 12 mm, the FSI declined as shown in Fig. 1. The swelling of the weathered coal in pyridine is also shown in Fig. 1, and remains constant while the FSI is decreasing. The subsequent decrease in swelling is interesting, but not relevant to the issue under consideration here, that of the causes of the observed decrease in FSI.

A sample of coal weathered for 28 days was treated with lithium aluminum hydride (LAH) following the lead of Orchin et. al.(1). As reported(1), the original FSI of the coal was restored. In this case the FSI went from 3 to 8. There exists a weathering pathway which is rapid and readily reversible by LAH reduction. As we will show in subsequent papers, it involves formation of carbonyl and carboxyl groups. This is the first mechanism.

A sample of the same coal weathered for 220 days was subjected to the same procedure. The FSI before reduction was 0.5 and after reduction was 2. Clearly a second mechanism is operative, one which cannot be reversed by LAH reduction.

These mechanisms do not involve any changes in the coal's cross-link density, as shown by the constant swelling in pyridine during the changes in FSI. The third mechanism does involve changes in the cross-link density. It was reported first by Liotta who worked with Ill. No. 6 coal(2). As the coal weathered, the cross link-density increased. Liotta ascribed this to ether linkages, but this has been questioned(3). Unfortunately, a detailed description of the weathering conditions was not provided. At 25 °C, we see no

change in the cross-link density of Ill. No. 6 coal due to weathering, but do see an increase in cross-link density as reported by Liotta when the coal is weathered at 150 °C. Thus there exists a third weathering mechanism, the one originally reported by Liotta and one which involves changes in the macromolecular structure of the coal.

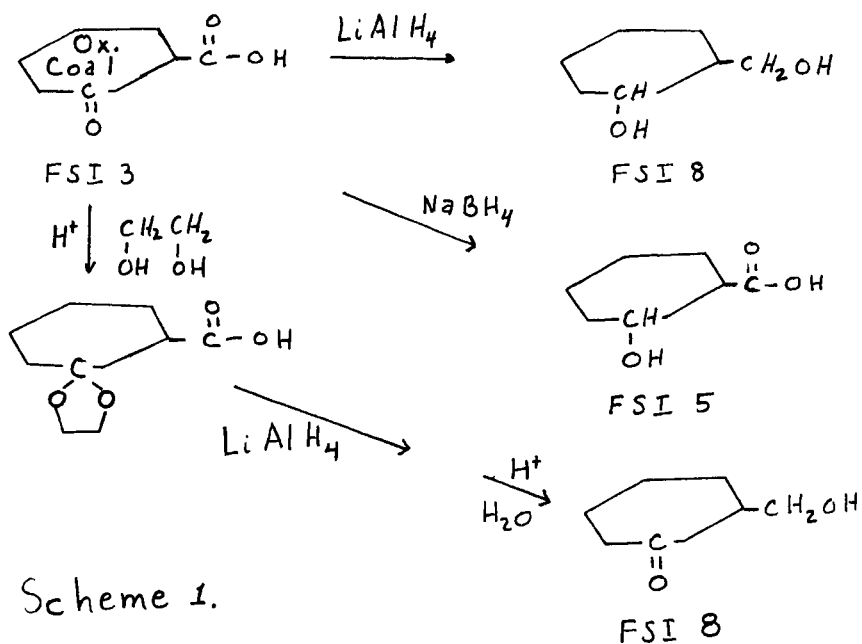
The first two mechanisms have been partly characterized. Using the chemistry shown in Scheme 1, 28 day oxidized Bruceton coal was prepared and the carbonyl groups and the carboxyl groups independently and selectively were reduced. It is clear from the data shown in the scheme that carboxyl groups are more important than carbonyls in the destruction of coking properties.

We thought that changes in the coal's bitumen might be contributing to mechanism two, since the pyridine extractables decreased, roughly paralleling the slow loss of coking ability. Accordingly, the pyridine extract from unoxidized Bruceton coal was added to the 220 day oxidized coal. Adding the extract by soaking the coal in a pyridine solution of the extract and then evaporating the pyridine had a smaller effect on the FSI than grinding the solid coal and extract together. This is consistent with the large amount of surface chemistry involved in these oxidations, a point we will take up in later papers. After grinding with 22% (wt) of extract, the FSI of 220 day oxidized coal was 4. It was 2 before grinding and the increase is due to the addition of a good swelling component, the extract which has an FSI of 5. Removal of the pyridine extractables from the unoxidized coal causes a sharp decline in the FSI, but grinding with the extract causes the FSI to return to its initial value. Clearly changes in the bitumen are not responsible for the loss of coking ability. We hope to know more about this pathway when we present our paper, but are not optimistic.

Acknowledgement. We thank the Gas Research Institute for support and its employees for encouragement, good advice, and cooperation.

REFERENCES

1. Orchin, M., Golumbic, C., Anderson, J. E., and Storch, H. H., U. S. Bureau of Mines Bull., 1951, 505, 13.
2. Liotta, R., Brons, G., and Isaacs, J., Fuel, 1983, 62, 781.
3. Rhoads, C. A., Senftle, J. T., Coleman, M. M., Davis, A., and Painter, P. C., Fuel, 1983, 62, 1387.



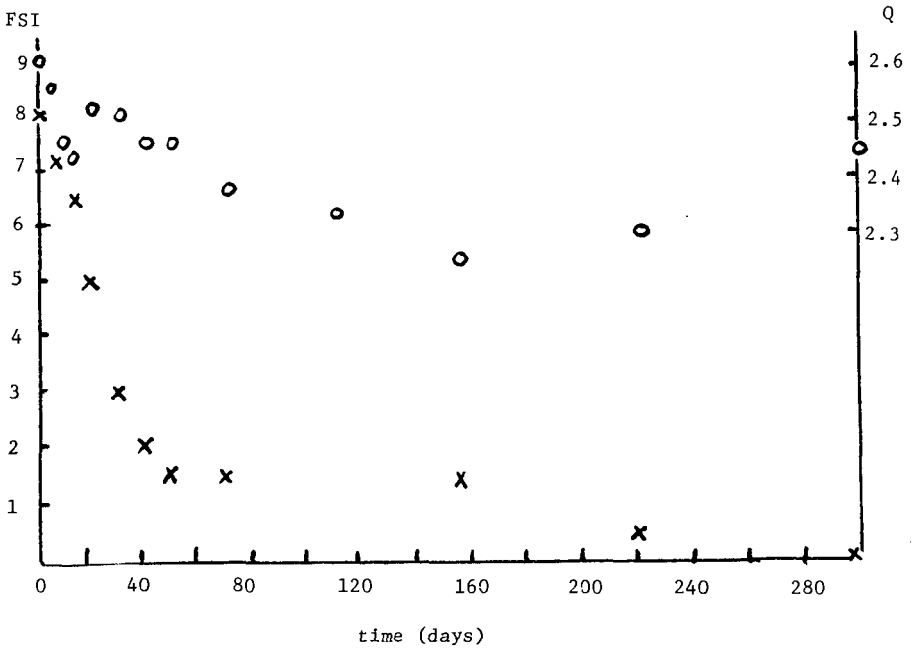


Fig. 1. Change in Free Swelling Index (x) and Volumetric Swelling in Pyridine (o) During Air Oxidation of Bruceton Coal at 80°C.

CHEMICAL COMMINUTION OF COAL

By P. Shu and T. Y. Yan

Mobil Research & Development Corporation
Central Research Division
P.O. Box 1025
Princeton NJ 08540

ABSTRACT

Chemical comminution is an effective means for size reduction and beneficiation of coal. Sodium hydroxide and i-propanol show synergism in chemical comminution of Illinois No. 6 bituminous coal.

The system was effective at low alkali concentrations with low consumption of NaOH. Much of the NaOH consumed was for neutralization of acidity of the coal. Isopropanol serves only as a reaction medium and could be recovered nearly quantitatively for recycle. The system lends itself to application in preparation of coal-water mixture and coal-alcohol slurry fuels.

* * *

INTRODUCTION

The use of coal as a source of energy and hydrocarbons will become more important in the future. In the upgrading and utilization of coal, size reduction is an important preparative step. The beneficiation of coal needs extensive crushing and the preparation of coal-water fuel mixtures, requires even finer particle size. Size reduction by mechanical means is not only energy intensive but also causes heavy wear on the processing equipment.

An alternative method of coal comminution is to weaken the coal structure by chemical action. This concept has been applied to remove mineral matter from coal (1), to desulfurize coal (2,4,5) and to facilitate in-situ coal extraction from underground deposits (6).

Various reagents which have been studied for chemical comminution include pure and aqueous ammonia, alkals such as NaOH, KOH, Na_2CO_3 , $\text{Ca}(\text{OH})_2$, etc. and organic solvents (3,7). The common limitations of the above-mentioned approaches are high reagent consumption and a low degree of effectiveness.

Among the systems studied, NaOH in high concentration (>0.1 N) is one of the most promising. However, the NaOH consumption is >5 wt% of treated coal and this makes it unattractive for practical applications.

We discovered that NaOH and i-propanol show synergism in coal comminution and that coal can be effectively comminuted by NaOH at concentrations less than 0.1 N in 90% i-propanol/water, with a low alkali consumption. The alcohol is not consumed chemically in the process and can be recovered quantitatively for reuse. The mechanism and kinetics of coal-alkali reactions were also investigated.

EXPERIMENTAL

Coal Sample: Illinois No. 6 Bituminous Coal, with the size in the range of 1-1.2 cm³ were hand-picked for the experiments.

Comminution Solution: Reagent grade NaOH and i-propanol were used as received. The comminution solution was prepared as a 9 to 1 volume ratio of i-propanol to aqueous NaOH stock solution. The different NaOH concentrations of the comminution solution were obtained by varying the concentration of NaOH stock solutions. The normality of the NaOH solution is calculated based on the total volume of the caustic and iso-PROH.

Coal Comminution Procedure: Seventy-five ml of comminution solution and 10 g of coal were reacted in a sealed stainless steel vessel at 100°C for 48-86 hours. The treated coal was recovered by filtration and dried in a 100°C oven overnight.

The effect of chemical comminution was judged by the following standards:

- o Very extensive: Coal sample is disintegrated into 10 or more smaller pieces.
- o Extensive: Coal sample is disintegrated into less than 10 pieces of smaller coal.
- o Good: Little coal is degraded. Coal has well developed cracks all over the surface and samples can be crumbled with hand pressure.
- o Fair: Little or no smaller coal pieces are found. Cracks on coal surface are formed mainly along the seam.

The pH values of the initial and spent solution were analyzed with a pH meter. The NaOH concentration of the corresponding solutions were determined by titration.

Determination of i-propanol Consumption: A thick-walled Pyrex tube divided into two compartments with a medium porous glass frit in the middle was employed. Comminution solution (50 ml) was first introduced into the tube and allowed to drain through the frit and fill the lower compartment. Coal (60-100 mesh, 10 g) was then charged into the upper compartment. After the tube was sealed, the tube was inverted to allow the comminution solution to contact the coal. The sealed tube was heated at 100°C at this position for 48 hrs.

After the heating period, the sealed tube was inverted back to its original position to disengage liquid and solid. The coal was dried by freezing the liquid compartment in liquid N_2 and heating the coal compartment with wrapped heating tape. The coal and the solution were recovered by opening the sealed tube and their weights were determined. The i-propanol content in the solution was determined by gas chromatography. A series of experiments consisting of three repeats averaged 99% material balance and i-propanol consumption was 0.1-0.7%.

Determination of NaOH Consumption Rate: A Brinkmann autotitrator E526 was used. Coal (0.5 g, 200+ mesh) was suspended in 50 ml of 90% i-propanol aqueous solution under an argon atmosphere and titrated against 0.01 N NaOH at a pH of 7.

Determination of the Neutralization Equivalent of Coal: Aliquots of 1 ml, 0.5 N NaOH were added to 5 g of coal (200 mesh) suspended in 50 ml of 90% i-PROH. The pH change was followed by a pH meter. Additional NaOH was added when the pH dropped below 7. This procedure was repeated until a steady pH of 7 was reached.

RESULTS AND DISCUSSION

Synergism of NaOH and Alcohols: Alcohol by itself is a very weak comminution agent. Storing coal under alcohols such as methanol, ethanol and i-PrOH for an extended period of time does not weaken the coal structure. Similarly, sodium hydroxide at concentrations lower than 0.1 N is not an effective comminution agent.

It is found in this study that by combining those two ineffective agents, an efficient comminution solution was obtained. Thus, dilute NaOH at levels of 0.025-0.1 N in 90% i-propanol is very effective for comminuting coal with low alkali consumption. Without i-propanol, the concentration of NaOH at these levels is too low to comminute the coal. In the presence of i-propanol, extensive comminution is achieved with low alkali consumption. To achieve these levels of comminution without i-propanol, the NaOH consumption would have been 6.2 wt% of treated coal for 0.1 N NaOH solution. In the presence of isopropanol the typical levels of alkali consumption are in the range of 0.7-2.0 wt% of treated coal (Table 1). For example, the NaOH consumption for an extensive comminution is 2.6% for 0.1 N NaOH in 90% i-PrOH.

The much enhanced comminution effect of NaOH-i-PrOH relative to aqueous NaOH is due to several possible causes:

1. As polar organic compounds, alcohols wet coal better than water and facilitate the contact between alkali and coal. The observed trend in terms of effective comminution medium is:



Apparently higher alcohols are better comminution solvents due to their higher affinity to and more effective wetting of the coal surfaces.

2. The reactivity of the OH^- anion may be enhanced by the solvation of Na^+ cations by alcohol molecules relative to aqueous solution so that the OH^- becomes more exposed and free to attack acidic substrates. It is well known that crown ethers, THF, polyalkylene polyamines are capable of "trapping" alkali and alkali earth cations (13). Therefore n-butyl lithium is a much stronger nucleophile in THF, crown ethers and tetramethylenediamine than in hexane.

Effect of Alkali Concentration: The initial alkali concentration was varied between 0.01 and 0.1 N. Notwithstanding the 10-fold increase in NaOH concentration, the initial pH of the comminution solution remained constant at about 12.5 (Table 1). It is suspected that the 90% i-propanol solution is saturated with NaOH at a concentration greater than 0.01 N. At NaOH concentrations greater than 0.01 N, the solutions appeared turbid.

A linear relationship exists between the initial NaOH concentration and consumption of alkali (Figure 1). The alkali consumption can be lowered by using a more dilute alkali solution but its effectiveness for comminution is reduced. The lowest NaOH concentration in 90% i-PrOH sufficient to comminute coal is about 0.028 N. The NaOH consumption in this case is 0.7 wt% of the coal. This alkali concentration probably is the most cost effective for coal comminution.

At higher NaOH concentrations, the consumption of NaOH increases as the comminution becomes more extensive. At 0.1 N NaOH concentration the degradation of coal structure was extensive and the alkali consumption reached 2.6%. This condition probably is the upper limit for economical coal comminution. (The criteria of comminution effect are defined in the experimental section.)

To obtain effective coal comminution, a minimum pH of 10 should be maintained. It is clear that run A4 and B4 (Table 1) had inadequate alkali strength to result in poor comminution. The alkali concentrations used in A3 and B3 are optimum for good comminution effects.

Alkali Consumption: The alkali consumed in the chemical comminution in the presence of i-PrOH is mainly for neutralization of acidity (8) in the coal. Phenols (9) and carboxylic acids constitute the bulk of the acids in coal. Other materials which consume alkali are metal oxides and minerals. A pH value of 3.4 was detected for a coal/water suspension (0.5 g

of 200 mesh + coal in 50 ml H₂O) indicating the acidic nature of coal.

Alkali consumption due to the acidity in the coal was obtained by neutralizing it exhaustively using dilute NaOH at pH 7. It took 1.4 wt% of NaOH based on coal to neutralize the coal. Since this value is very close to those runs in which extensive comminution was obtained (A2 and B2), we are tempted to conclude that much of the NaOH consumption is for neutralization of acidity in the coal.

Iso-propanol Consumption: The role of alcohol in the comminution of coal using a NaOH - i-PrOH - H₂O system is probably as a solvent which enhances NaOH reactivity rather than as a chemical reagent. By employing a sealed tube technique described in the experimental section, 99.2-99.9% of i-PrOH was recovered from the spent solution. This extremely high i-PrOH recovery rate supports that it does not react with coal functionalities. The very high recovery of alcohol could make the comminution method described in this paper viable for industrial applications.

Kinetics of NaOH Uptake: As mentioned above, much of the alkali taken up by coal is for neutralization of the acid sites of the coal. Therefore, a fast reaction between alkali and coal is expected. The uptake of alkali by coal in an iso-propanol - H₂O system at a constant pH of 7 and 25°C was studied using an automatic titrator. To simplify the analysis of kinetic data the OH⁻ concentration was kept constant.

Plotting the log of NaOH uptake rate against the log of the reaction time, a straight line with a slope of -0.5 was obtained (Figure 3). Thus, the rate of caustic uptake can be represented with the following equation.

$$r = 2.33 \times 10^7 t_{-0.5}$$

where r is the rate of caustic uptake, mole/sec. Kg of coal,
 t is time, sec.

The form of this equation suggests that the reaction is rapid and the reaction rate is mass transfer limited. The initial rate at reaction time of 0.01 sec is in the range of 10^8 mole/sec. Kg which is too fast for organic reactions likely to occur in this system at room temperature. A rate of 10^{-4} to 10^{-6} mole/sec. Kg is expected for typical organic reactions. On the other hand, the reaction rate of H^+ and OH^- is mass transfer limited at a rate of 10^{10} mole/sec. Kg (11). For the neutralization of weak acids in coal it is expected to be somewhat slower than that for the strong acids. A rate of 10^8 mole/sec. Kg is reasonable. This supports the assumption that neutralization of acids in coal is the major reaction in the comminution of coal.

The mechanism of the above reaction can be modeled with the reaction controlled by diffusion through the "ash" layer of a shrinking core. According to this model, and following the notation used by Levenspiel (10), the rate of reaction $-\frac{dN}{dt}$

at any time can be expressed by

$$\frac{-dN}{dt} \left(\frac{1}{r_c} - \frac{1}{R} \right) = 4 \pi D_e C \quad (1)$$

$$t = \frac{\rho R^2}{6D_e C} \left[1 - 3 \left(\frac{r_c}{R} \right)^2 + 2 \left(\frac{r_c}{R} \right)^3 \right] \quad (2)$$

where N is conc. of reacting OH⁻ ion, mole

r_c, R are the radii of the reacting core at t and the original particle, respectively, cm

D_e is the effective diffusivity, cm²/sec

C is the concentration of OH⁻ ions in the bulk phase mole/cc

ρ is density of coal, g/cc

For complete conversion of a particle, the time required is

$$T = \frac{\rho R^2}{6D_e C} \quad (3)$$

The dimensionless time $\left(\frac{t}{T} \right)$ is

$$\frac{t}{T} = 1 - \left(\frac{r_c}{R} \right)^2 + 2 \left(\frac{r_c}{R} \right)^3 \quad (4)$$

$$\frac{t}{T} = 1 - 3(1-X)^{2/3} + 2(1-X) \quad (5)$$

where X is conversion, fraction.

According to Equation 5, conversion, and in turn NaOH consumption rate was calculated as a function of time using a computer. By plotting the log of NaOH consumption rate, log dN/dt against log t, a straight line with a slope of -0.53 was obtained (Figure 2). A similar plot using experimental data also yielded a straight line with a slope of -0.5 (Figure 3). The excellent agreement between the experimental and calculated values demonstrate the validity of this model. Examination of the model indicates that this linear relationship is valid up to a conversion level of about 80%.

The D_e can be estimated from the experimental data. Since the real time for $x = 0.5$ and $t/T = 0.11$ was 5400 sec., the time for complete conversion T was calculated to be 49,090 sec. according to Equation (5). The effective diffusivity D_e calculated from Equation (3) is 1×10^{-6} cm²/sec. This magnitude of diffusivity compares reasonably with literature values, e.g., the self-diffusion rates of Br⁻ in 1 and 6% cross-linked divinyl benzene (Dowex 2 anion resin) at 25°C are 9 and 4×10^{-7} cm²/sec, respectively (12). The consistent value of D_e obtained further substantiates the validity of the model.

SUMMARY

Chemical comminution is an effective method for size reduction and beneficiation of coal. Although NaOH is effective at a concentration >0.1 N, the alkali consumption can be as high as 5-10 wt % of coal treated which makes it unattractive for practical applications.

We find that there is a synergistic comminution effect when NaOH is used in combination with alcohols. Such a system is more effective than NaOH or alcohols when used separately.

This synergistic effect of NaOH/alcohol may be due to its higher affinity for coal and better penetrating ability than that of NaOH/H₂O. A higher alcohol (i-propanol) was found to be more effective than methanol probably due to its larger organic groups. Another contributing factor to the synergism might be the solvation of Na⁺ by alcohol which renders the OH⁻ more

exposed and therefore, a more reactive species. Alcohol appears not to be involved in coal-NaOH reactions, since it can be recovered almost quantitatively. Its role in comminution is a reaction medium to facilitate the OH^- /coal contact.

There is a linear relationship between initial NaOH concentration and its consumption. A higher degree of comminution was affected at higher NaOH consumption. A 0.028 N of NaOH in 90% i-PrOH was effective in coal comminution with an NaOH consumption of only 0.73% of coal. The NaOH consumption is mainly for neutralizing the acidity of the coal. The NaOH consumption for neutralization and exhaustive coal comminution were essentially the same. Studies of NaOH uptake by coal at a fixed pH of 7 using an autotitrator showed that the diffusion of alkali into coal is the rate controlling step in NaOH-coal reaction.

Coal comminution with NaOH-alcohols is effective and could find applications in coal-water slurry and coal-alcohol slurry preparations.

REFERENCES

1. P. H. Howard and R. S. Datta, "Chemical Comminution: A Process for Liberating the Mineral Matter from Coal," Symposium on Desulfurization of Coal and Coal Char," Amer. Chem. Soc. National Meeting, New Orleans, March 20-25, 1977.
2. R. G. Aldrich, "Chemical Comminution of Coal and Removal of Ash Including Sulfur in Inorganic Form Therefrom," U.S. Patents 3,870,237 (1975), 3,918,761(1975).
3. J. N. Chew and J. G. Savins, private communication.
4. P. H. Howard, A. Hanchett and R. G. Aldrich, "Chemical Comminution for Cleaning Bituminous Coal," Clean Fuels from Coal Symposium II, Institute of Gas Technology, June 23-27, 1975, Chicago, Illinois.
5. C. Y. Tai, G. V. Graves and T. D. Wheelock, "Desulfurization of Coal by Oxidation in Alkaline Solutions," Third Symposium on Coal Preparation, NCA/BCR Coal Conference and Expo IV, Oct. 1977, Louisville, KY.
6. R. G. Aldrich, D. V. Keller, Jr. and R. G. Sawyer, "Chemical Comminution and Mining of Coal," U.S. Patent 3,815,826, (1974).
7. I. G. C. Dryden, "Solvent Power for Coals at Room Temperature," Chem. Indust., 502, June 1952.
8. P. K. Dutta and R. J. Holland, Fuel 62 732 (1983).
9. M. Farcasiu, Fuel 56 9 (1977).
10. O. Levenspiel, "Chemical Reaction Engineering," p. 364-367, 2nd Ed., John Wiley and Sons, Inc., New York, 1972.
11. R. P. Bell, "Acids and Bases," p. 65, Chapter 6, 2nd Ed., Methnen and Co. Ltd., London, 1969.
12. B. A. Soldano and G. E. Boyd, "Self-diffusion of Anions in Strong Base Anion Exchangers," J. Amer. Chem. Soc., 75, 6099 (1953).
13. C. J. Pedersen, Aldrichimica. Acta, 4, 1 (1971).

Figure 1. NaOH Consumption - Initial NaOH Concentration

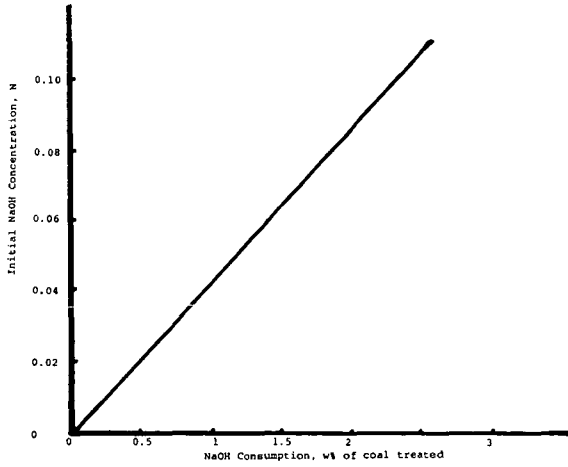
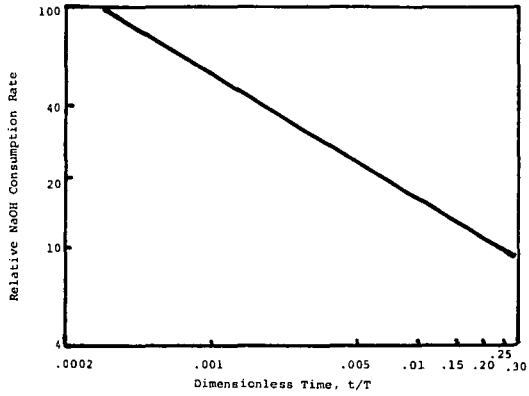


Figure 2. Predicted NaOH Consumption Rate



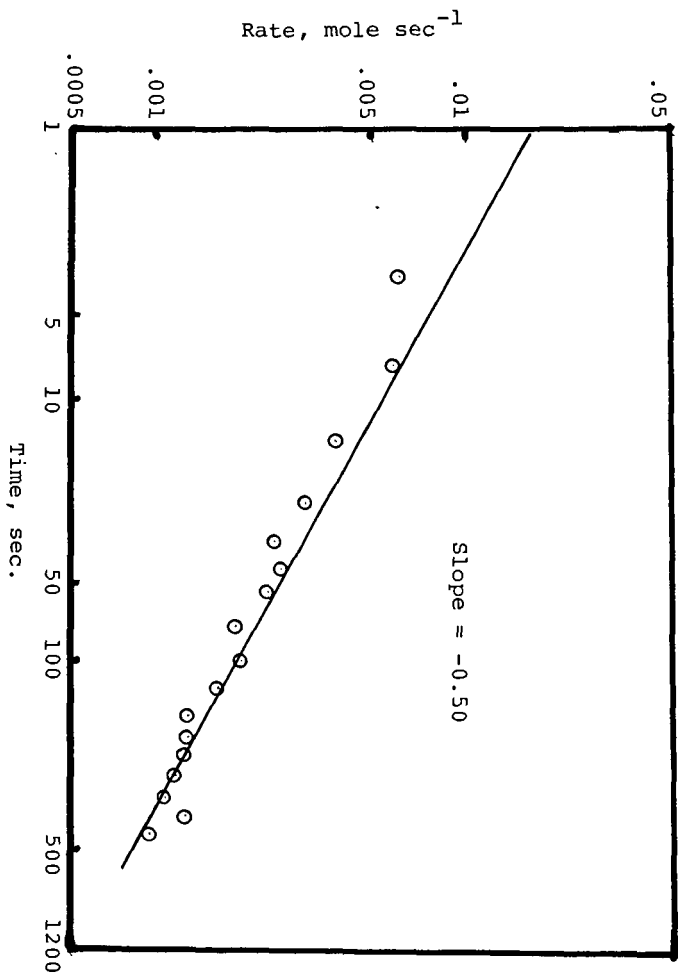


Figure 3. NaOH Consumption Rate vs. Reaction Time

Table 1

Comminution of Illinois No. 6 Bituminous Coal
with NaOH in 90% i-Propanol

Experiment	NaOH Conc. N	Solution pH		NaOH Consumption wt% of coal	Results**	
		Initial	Final			
A*	1	0.111	12.49	11.94	2.59	Very extensive
	2	0.0456	12.49	11.94	1.2	Extensive
	3	0.028	12.48	10.62	0.73	Good
	4	0.011	12.50	8.85	0.28	Fair
B**	1	0.099	12.58	11.93	2.62	Very extensive
	2	0.0452	12.49	11.09	1.20	Extensive
	3	0.0282	12.47	10.72	0.75	Good
	4	0.0104	12.52	8.8	0.25	Fair

* 48 hr @ 100°C, 1/4-1/2 in³ coal used

** 96 hr @ 100°C, 1 in³ coal used.

Technique For Measuring Swelling Tendency and Coke Density
For Catalytic Coal Gasification

Claude C. Culross, LeRoy R. Clavenna and Richard D. Williams

Exxon Research and Engineering Company
P. O. Box 4255
Baytown, Texas 77522

Introduction

Since 1979, Exxon Research and Engineering Company has operated a one ton-per-day Process Development Unit (PDU) at Baytown, Texas in support of the development of the Catalytic Coal Gasification Process (CCG). Details of this process development effort are available elsewhere^{1a-c}. This paper summarizes responses of coal, particularly swelling and coke density, to gasification conditions; some characteristics of the five coals which have been processed in the PDU are given in Table 1. The PDU utilizes a high pressure fluidized bed gasifier that operates at 3.4 MPa (500 psia) and 978°K (1300°F). Coal is typically catalyzed by wet mixing with potassium salts (KOH, K₂CO₃) prior to introduction into the gasifier. The alkali catalyst promotes gasification, shift, and methanation in a single thermo-neutral reactor. Another important catalyst benefit is that it reduces the thermoplasticity of bituminous coals at the same time; however, enough thermoplasticity persists that its impact must be considered when operating a fluid bed gasifier (Figure 1). The thermoplasticity manifests itself as agglomeration which occurs during the transient plastic state and as swollen, structurally weak particles.

Because CCG conditions, viz., high heat-up rate and high pressure, are quite different from the conditions at which conventional tests for thermoplasticity are carried out, it seemed important to develop a technique which best reproduced the CCG conditions. This view is well supported in the literature. In the pyrolysis of coal, both an increase of heating rate^{2a-d} and pressure^{2b,c,e,f} have been associated with decreased viscosity or increased fluidity during the plastic transition of coal. The reduced viscosity associated with increased heating rate is normally attributed to the rapidly increasing temperature which occurs during pyrolysis. This rapid temperature increase results in an enrichment of the liquid products in the plastic mass at a higher temperature. The effect of increased pressure is to repress evolution of the low viscosity, volatile components from the plastic coal.

Typically, swelling is increased by factors that decrease viscosity during the plastic transition. There is general agreement in the literature that an increased heating rate increases the potential for greater swelling^{2a,b}. However, the influence of pressure on swelling is not as clear. Increased pressure reduces viscosity but also, because of compression, reduces the total volume of gases that are released and available to swell the plastic coal. Increasing the pressure has been reported to increase^{2b,f}, decrease^{2g}, or have little effect^{2c,h} on swelling. The differences are likely due to the different procedures and physical arrangement of the techniques used to measure swelling. Therefore, it was important for

us to choose a technique for measuring swelling that was applicable to our high pressure fluid bed in that it would be capable of differentiating good performance potential in a feed coal from marginal or unacceptable potential. In addition, the technique had to be simple and relatively fast for use as a quality control test.

This paper outlines the technique developed and illustrates the use of the test in the study of the impact of process variables of interest (catalyst, catalyst distribution, coal pretreatment, pressure, gas atmosphere) on coal thermoplasticity.

Free Fall Swelling Test

A simple, easy to use laboratory test unit was devised to study coal thermoplasticity within the context of CCG conditions. The test, known as the Free Fall Swelling Test, simulates major CCG process variables such as high pressure and high heat-up rate. A schematic of the Free Fall Unit is shown in Figure 2.

Pressure is controlled by a back pressure regulator 8 (typically between 0.1 and 3.5 MPa). Coal aliquots (150 μ m x 600 μ m, 0.25 g \pm 0.01g) are fed through a set of two valves to the hot drop tube via the feedline 3. The coal particles fall freely through the heated zone (typically operated in the temperature range of 978-1033°K) where they are rapidly heated, pyrolyzed, and form coke or char. A particle heat-up model was applied to estimate heat-up rates and free fall residence times. Time average heat-up rates range from 2,800 to 11,000°K/sec for the range of particle sizes used. The solid residue is removed from the drop tube by withdrawing the quartz liner. The use of a quartz liner allows easy and complete removal of the residue and gives visible evidence that tar evolution has ceased before the residue reaches the bottom of the liner.

On cooling, a measure is made of residue loose bulk density (equation 1) and swelling (equation 2). Generally speaking, residue densities are less than coal densities because of the combined effect of mass loss and swelling due to the transient thermoplastic state, and the densities usually vary between 0.05 and 0.55 g/cc. The Free Fall Swelling Index (FFSI, equation 2) is a measure of swelling, and it usually varies between 1.0 (no swelling) and 12.0 (a twelve-fold increase in loose bulk volume relative to the starting coal).

$$\text{Residue Loose Bulk Density} = \frac{\text{Residue Mass (g)}}{\text{Loose Bulk Volume (cc)}} \quad (1)$$

$$\text{Free Fall Swelling Index} = \text{FFSI} = \frac{\text{Residue Loose Bulk Volume (cc)}}{\text{Coal Loose Bulk Volume (cc)}} \quad (2)$$

The need to develop an alternative to conventional tests for thermoplastic tendency is made more clear by the data in Table 2, a comparison of ASTM Free Swelling Index (FSI) and the FFSI of selected coals determined under CCG conditions. The ASTM FSI's are all low, that is, there is no swelling and little or no agglomeration, but the FFSI's range from 1.0 to 5.6. There are also clear morphological differences in the residues from both tests. The FSI

residues are granular solids which retain the sharp edges and dull surfaces found in the original coal. But the free fall residues "B" and "C" are composed of bloated, reflective spheres which appear to have gone through a fluid stage (as in Figure 1). The thermoplasticity implied by the morphological differences between coal and pyrolyzed residue was later directly observed by capturing on film the behavior of rapidly heated single particles of catalyzed Illinois No. 6 coal in a fast photography cell (FILM SEGMENT #1: Illinois + 12.2 wt % KOH, 0.1 MPa helium, filament heat-up rate = 1000°K/sec). Melting, bubbling, swelling, and thermosetting were clearly evident.

The possibility that a coal could exhibit no swelling at low heat-up rate but exhibit distinct swelling at a higher heat-up rate is implied by the work of Van Krevelen^{2a}. Therefore, the contrasting FSI and FFSI results obtained here come as no surprise because of the large difference in heat-up rates (FSI = 5°K/sec, FFSI >1000°K/sec). Since the conditions of the Free Fall Swelling Test more nearly resemble CCG conditions, and because swelling behavior in the test is at least qualitatively more in line with behavior in a fluid bed gasifier, the Free Fall Swelling Test seemed to be the better choice to study thermoplasticity at CCG conditions.

Effect of Pressure

Thermoplastic behavior of potassium-catalyzed Illinois No. 6 coal was first observed in CCG work during large scale char preparation in a 0.78 MPa/3 kg-ks⁻¹ Fluid Bed Gasifier (FBG). Fluid bed densities which were lower than previously measured were noted in the FBG³. During start-up of the PDU with the same coal, feedline plugging caused by agglomeration was frequently a problem⁴. Fixed bed laboratory tests then identified pressure as one important variable in catalyzed coal agglomeration⁵. PDU runs also suggested the importance of pressure, and of oxidation, to fluid bed density^{1b}. However, since other variables such as superficial velocity changed along with pressure, it was difficult to uniquely determine the effect of pressure on thermoplasticity and gasifier properties.

The variation of the loose bulk density of pyrolyzed coal from the Free Fall Swelling Test with pressure (Figure 3) is in agreement with this earlier data which indicate that higher pressures increase coal thermoplasticity. The densities of uncatalyzed and catalyzed-oxidized Illinois No. 6 coals decrease as the Free Fall Unit pressure is raised above atmospheric pressure. Char densities at 3.5 MPa fall into the expected order: catalyzed-oxidized > catalyzed > uncatalyzed. The reproducibility of the measurement is indicated by good agreement between the two sets of data on catalyzed-oxidized coal (Figure 3, □ and Δ). The effect of pressure on thermoplasticity, as manifested by swelling, was later directly observed by fast photography of single particles of potassium catalyzed Illinois No. 6 coal (FILM SEGMENT #2: Illinois + 12.2 wt % KOH at 3.5 MPa). These films show more swelling at 3.5 MPa than at 0.1 MPa.

This trend is attributed to the effect of pressure on the volatile components during the extremely rapid pyrolysis. It is thought that higher pressure retards the escape of volatile pyrolyzates from coal particles by shifting the boiling points of the volatile components to a higher temperature range. Because of the short time involved with the rapid heating, most of the volatile components will remain in the particle until they begin to boil (i.e., their vapor pressure equals the total pressure of the system). With the more volatile and, hence, likely less viscous and solvent-like components retained to a higher temperature, the coal attains a lower viscosity during the plastic transition. Because of this lower viscosity, the evolving gas has a greater swelling effect on the unconstrained, free falling, plastic coal particle. At a pressure of approximately 1.5 MPa (200

psig), the majority of the components that will affect the viscosity of the particle appear to have been retained, for further increase of pressure has little effect on swelling (loose bulk density). Increased pressure is expected to reduce the total volume of pyrolysis gases released, but because the gas volume is still many times greater than the volume of the resulting char, increasing pressure from 1.5 to 5.5 MPa (200 to 800 psig, or decreasing the volume of the pyrolysis gases by a factor of four) should not have a large effect on swelling. If this line of thinking is extended, it would predict that swelling will begin to decrease at much higher pressures where the volume of the evolving gases is contracted severely (loose bulk density will increase).

Effect of Catalyst, Oxidation and Longer Particle Penetration Time

The effects of catalyst, oxidation, and longer penetration time on thermoplasticity, as measured by FFSI, are summarized for several coals of interest to CCG in Figures 4-7. These include Illinois No. 6, Valley Camp, and Hawk's Nest coals which are bituminous in rank, and Wyodak coal which is sub-bituminous in rank.

The effect of potassium catalyst is to reduce thermoplasticity whether the coal is purposely oxidized prior to catalyst addition or not (Figure 4). The exception is Wyodak coal which is very close to being non-swelling even without potassium catalyst. Decreased swelling upon catalyst addition is thought to be due to the factors of salt formation between the catalyst and the coal, and reduced pyrolysis.

Oxidation after catalyst addition reduces swelling for the more porous Illinois No. 6 (13 wt % equilibrium moisture, uncatalyzed) but does little for the much less porous Hawk's Nest coal (5 wt % equilibrium moisture, uncatalyzed; Figure 5). This suggests that oxygen has difficulty penetrating less porous particles.

Mild oxidation alone can reduce swelling without catalyst addition, and more extensive oxidation reduces swelling still further. However, the application of potassium catalyst after oxidation results in a large additional reduction of swelling, presumably because the aqueous application allows the catalyst to migrate to new surface acids formed during oxidation. This is demonstrated by lower FFSI's after additional penetration time is allowed the catalyst. The effect of poor catalyst dispersion is also discussed in the next section.

The sequence of increasing coal swelling after catalyst application and oxidation in preparation for PDU operation is, as shown in Figure 7, Wyodak (FFSI=1.0) < Illinois (FFSI=2.5-2.85) < Valley camp (FFSI=3.1) < Hawk's Nest (FFSI=3.6-4.5).

Effect of Catalyst Dispersion

Even when mixed with potassium catalyst in an aqueous slurry and given an extended soak at mild conditions, some coals such as Hawk's Nest coal do not take up the catalyst effectively. The catalyst lays down as a rim on the exterior of particles which can clearly be seen in Scanning Electron Microscope (SEM) photomicrographs of particle cross-sections. When heated in the fast photography cell, these particles exhibit two distinct thermal behaviors. The well-catalyzed outer rim does not melt on heating, but merely cracks. The poorly catalyzed particle interior does melt and flows out through the cracks in the unmelted outer rim (FILM SEGMENT #3: Hawk's Nest + 12.2 wt % KOH).

Effect of Atmosphere

The effect of selected inert and reactive gases on residue loose bulk density was examined because there are a variety of gases in a CCG atmosphere which may have different effects on thermoplasticity. Other work has shown that the nature of the gas atmosphere does affect thermoplasticity at pressure as measured by maximum fluidity in a plastometer⁶. In the Free Fall Swelling Test, it was found that H₂, He, CO₂, Ar, and N₂ gave residues with densities which spanned a range of only 0.02 g/cc (Figure 8). The cause of this small difference is thought to be the speed with which pyrolysis takes place in the Free Fall Swelling Test. Under conditions of rapid pyrolysis, it may be possible for particles to become blanketed in an atmosphere of their own pyrolyzates which isolates the particles from the bulk atmosphere. If some additional conversion does occur in reactive gases (H₂, CO₂), then densification must occur at the same time in order for the coke densities to be so similar.

Summary

We have found the Free Fall Swelling Test to be helpful in the guidance of pilot plant work and in determining the effect of several CCG variables on thermoplasticity. Under the test conditions of high pressure and high heat-up rate, the coal thermoplastic property is more pronounced than at conditions of low heat-up rate and low pressure under which more conventional tests for thermoplasticity are run. Thus, the test is a more sensitive probe of the thermoplastic tendency, especially for coals having a limited thermoplastic tendency.

References

1. (a) T. Kalina and N. C. Nahas, "Exxon Catalytic Coal Gasification Process Predevelopment Program", Final Project Report for the U. S. Department of Energy under Contract No. E(49-18)-2369, December, 1978.
- (b) C. A. Euker and R. A. Reitz, "Exxon Catalytic Coal Gasification Process Development Program", Final Project Report for the U. S. Department of Energy under Contract No. ET-78-C-01-2777, November, 1981.
- (c) R. A. Cardello, R. A. Reitz and F. C. R. M. Smits, "Catalytic Coal Gasification Development", presented in Round Table Discussion No. 5, 11th World Petroleum Congress, London, England, August, 1983.
2. (a) D. W. Van Krevelen, "Coal: Typology - Chemistry - Physics - Constitution", Elsevier, New York, 1961.
- (b) D. Habermehl, F. Drywal and H. Beyer, "Chemistry of Coal Utilization", ed. M. A. Elliot, Wiley, New York, 1981, 317-368.
- (c) M. S. Lancet, F. A. Sim and G.P. Curran, Prepr., Am. Chem. Soc., Div. Fuel Chem., 27 (1), 1-24 (1982); EPRI Final Report, AP-2335 (April, 1982).

References (continued)

- (d) R. J. Tyler, FUEL, 58(9), 680-686 (1979).
 - (e) M. S. Lancet and F. A. Sim, Prepr., Am. Chem. Soc., Div. Fuel Chem., 26(3), 167-171 (1981).
 - (f) R. Loison, A. Peytavy, A. F. Boyer and R. Grillot, "Chemistry of Coal Utilization," ed. H. H. Lowry, Wiley, New York, 1963, 150-201.
 - (g) M. R. Khan and R. G. Jenkins, FUEL, 63(1), 109-115 (1984); EPRI, Final Report, AP-2337 (April, 1982).
 - (h) P. Arendt, M. Kaiser, W. Wanzl and K. H. van Heek, in "Proceedings, International Conference on Coal Science", Verlag Glückauf GmbH, Essen, 1981, 618-623.
3. C. A. Euker, "Exxon Catalytic Coal Gasification Process Development Program", Monthly Technical Progress Report for the U. S. Department of Energy under Contract No. ET-78-C-01-2777, November, 1978.
 4. C. A. Euker, "Exxon Catalytic Coal Gasification Process Development Program", Monthly Technical Progress Report for the U.S. Department of Energy under Contract No. ET-78-C-01-2777, July, 1979.
 5. C. A. Euker, "Exxon Catalytic Coal Gasification Process Development Program", Monthly Technical Progress Report for the U.S. Department of Energy under Contract No. ET-78-C-01-2777, January, 1980.
 6. M. Kaiho and Y. Toda, FUEL, 55, 397-398 (1979).

TABLE 1
CHARACTERISTICS OF PDU FEED COALS (UNCATALYZED)

	<u>Illinois No. 6</u> <u>(Monterey No. 1)</u>	<u>Hawk's Nest</u>	<u>Valley Camp</u>	<u>Walden</u>	<u>Wyodak</u>
Coal Rank	Bituminous	Bituminous	Bituminous	Bituminous	Sub-bituminous
Equilibrium Moisture (Wt %)	13.4	5.1	7.4	9.5	28.7
Free Swelling Index	4	3	2	0.5	0
Ultimate Analysis (Wt % Dry Coal)					
Carbon	69.4	75.6	73.3	69.6	67.0
Hydrogen	4.8	5.4	5.6	4.8	5.2
Oxygen (Difference)	8.9	10.2	11.7	12.6	15.3
Nitrogen	1.4	1.7	1.4	1.3	1.0
Sulfur, Total	4.6	0.5	0.7	0.6	1.0
Pyritic	0.8	0.1	0.2	0.3	0.2
Sulfate	0.1	0.0	0.0	0.0	0.2
Organic	3.8	0.4	0.5	0.3	0.7
Chlorine	0.2	0.1	0.0	0.0	0.0
Ash Elements (SO ₃ -Free, % Ash, Dry)					
SiO ₂	51.0	51.1	60.0	54.5	40.6
Al ₂ O ₃	18.4	23.9	11.3	29.0	22.7
P ₂ O ₅	0.4	0.9	0.3	1.0	1.2
TiO ₂	1.1	1.1	1.0	0.7	1.7
Fe ₂ O ₃	19.8	10.7	7.4	5.0	6.0
CaO	4.9	7.8	16.2	8.0	21.2
MgO	1.0	2.0	2.4	0.8	5.2
K ₂ O	2.1	1.4	1.2	0.3	0.5
Na ₂ O	1.4	1.1	0.3	0.8	0.9

Table 2
ASTM Free Swelling Index (FSI) and Free Fall Swelling Index (FFSI)
of Selected CCG Coals

<u>Coal</u>	<u>ASTM FSI</u>	<u>FFSI (a)</u>	<u>Free Fall Residue</u> <u>Density, g/cc</u>
A Wyodak + K	0.0 (no swelling)	1.0	0.37
B Illinois No. 6 + K (oxid.)	0.0 (no swelling)	2.6	0.15
C Illinois No. 6 + K (unox.)	0.5 (no swelling)	5.6	0.09

(a) FFSI conditions were 978°K and 3.5 MPa.

FIGURE 1
SOME CATALYZED BITUMINOUS COALS EXHIBIT UNDESIRABLE THERMOPLASTIC BEHAVIOR WHEN FED TO A FLUID BED GASIFIER

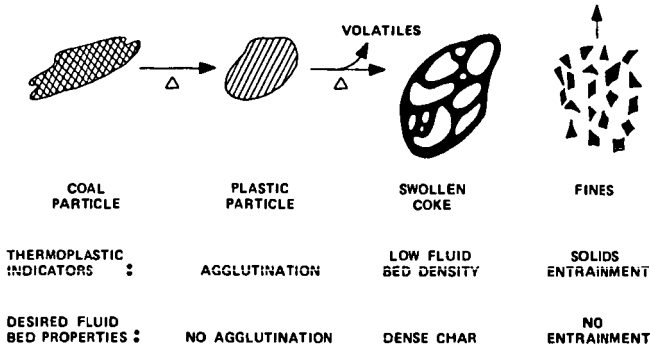


FIGURE 2
FREE FALL UNIT SCHEMATIC

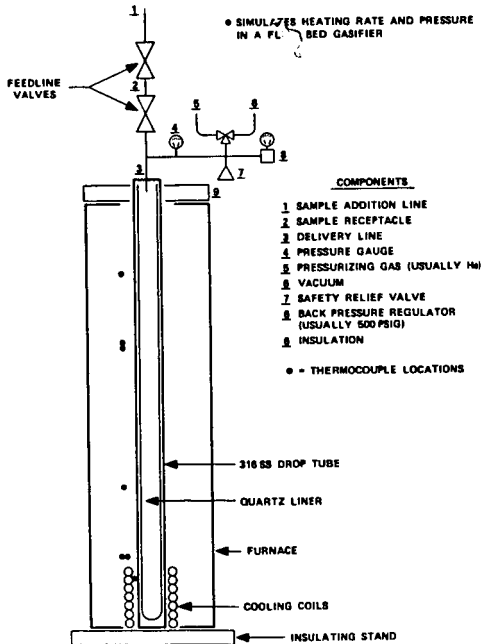
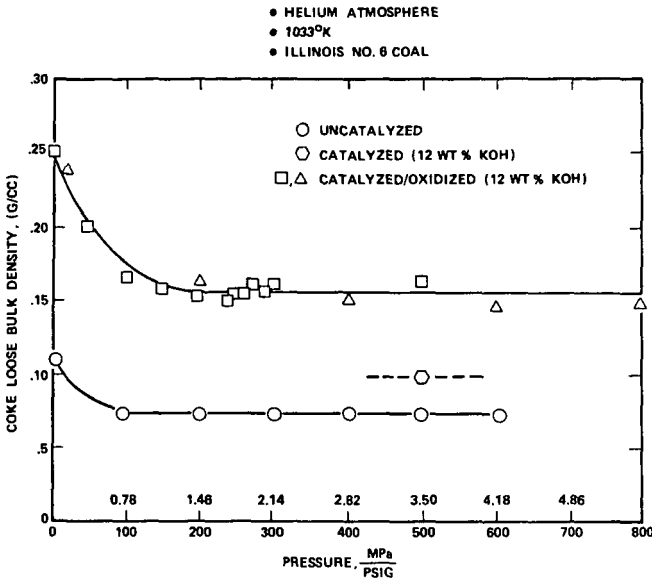


FIGURE 3
INCREASED PRESSURE DECREASES ILLINOIS CHAR DENSITY



84B-3-176

FIGURE 4
CATALYST REDUCES THERMOPLASTIC SWELLING

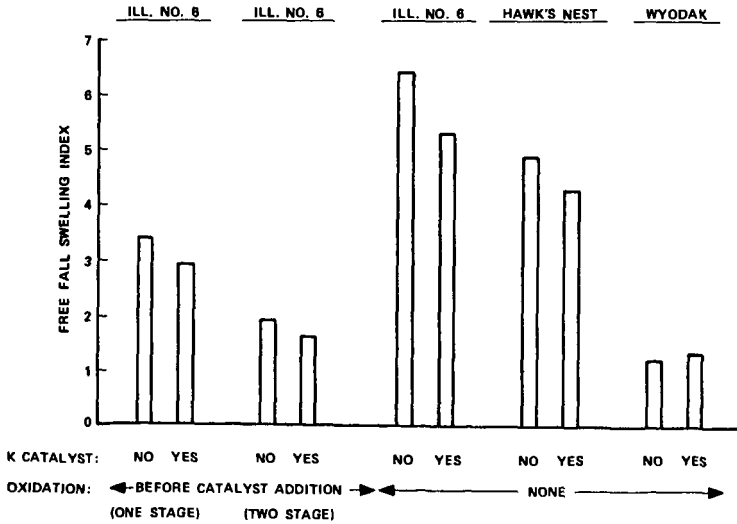
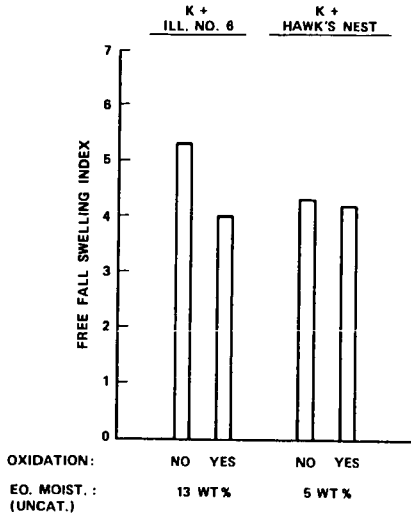


FIGURE 5

OXIDATION REDUCES SWELLING OF THE MORE POROUS COAL



84B-3-178

FIGURE 6

WHILE OXIDATION ALONE HAS AN EFFECT, CATALYST APPLICATION AND INCREASED PARTICLE PENETRATION TIME RESULT IN AN ADDITIONAL REDUCTION OF SWELLING

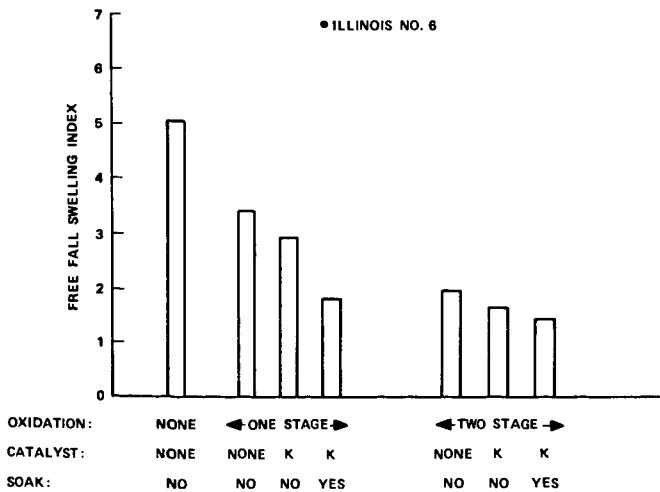
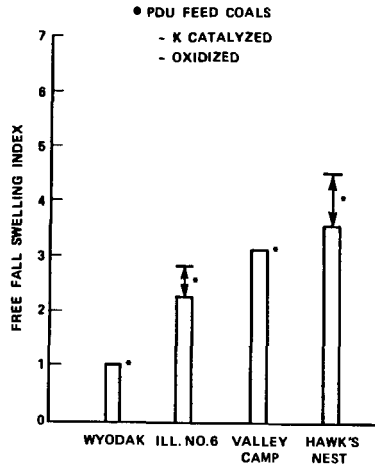


FIGURE 7

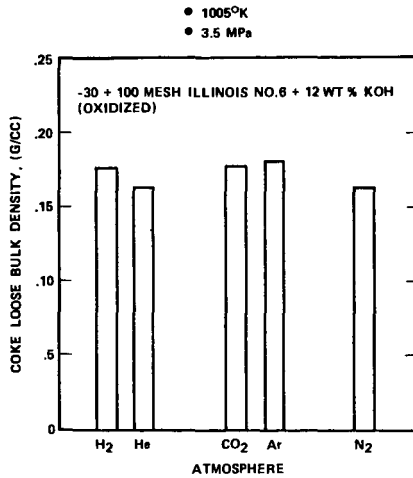
THERMOPLASTIC SWELLING OF CCG COALS VARIES



84B-3-157

FIGURE 8

ATMOSPHERIC EFFECTS ON RESIDUE LOOSE BULK DENSITY ARE SMALL AT HIGH PRESSURE



PRODUCTION AND GASIFICATION TESTS OF COAL FINES/COAL TAR EXTRUDATE

A. Furman
D. Smith
D. Waslo

Corporate Research and Development
General Electric Company
P.O. Box 8
Schenectady, New York 12301

D. Leppin

Gas Research Institute
8600 West Bryn Mawr Avenue
Chicago, Illinois 60631

ABSTRACT

Fixed bed gasifiers, such as those planned to be used to manufacture SNG commercially, require a sized feedstock, e.g., -2 in., +1/4 in. As an alternative to disposing the fines (-1/4 in.) which cannot be used in the boiler of such an SNG plant, they can be compacted and then fed to the gasifiers. General Electric R&D Center in Schenectady is developing an extrusion process which will enable the fines, mixed with an appropriate binder, to be fed directly into a fixed bed gasifier, bypassing the lockhoppers required for lump coal feed. Work is described on a recently completed extrudate manufacture and gasification program sponsored by GRI. GE's 6-inch diameter, single screw extruder was employed to produce the extrudate from Illinois No. 6 coal and coal tar, and the extrudate was subsequently gasified in GE's pressurized air-blown, stirred fixed-bed reactor. The test results indicate that the extrudate makes a satisfactory gasifier feedstock in terms of both thermal and mechanical performance.

INTRODUCTION

Gasification is a fuels conversion technology which permits the production of clean substitute gas from coal and other carbonaceous fuels. The first commercial application of this technology in the U.S. will be the Great Plains substitute natural gas (SNG) plant, which is due to begin production in late 1984. This plant will produce 125M SCF per day of pipeline quality gas using Lurgi, oxygen blown, fixed-bed gasifiers.

While the fixed bed gasifier offers proven performance in terms of both thermal efficiency and reliability, it requires a sized feedstock for optimum performance. Typically, coal below 1/4 inch is removed by screening prior to gasification in order to minimize fines carryover from the bed and to minimize instabilities in gasifier performance caused by excessive fines content in the feed. Run-of-mine (ROM) coal, however, typically contains 25-35% of <1/4-inch material, which means that up to 35% of the coal mined could not be utilized directly in the gasifier. Direct extrusion of the coal fines fraction with a tar binder offers a potentially attractive solution to this problem by consolidating the fines into a feedstock suitable for the fixed-bed gasifier and, at the same time, providing an advanced feed mechanism to the pressurized reactor.

The present paper describes the results of a recently completed extrudate evaluation program conducted at the General Electric Research and Development Center in Schenectady New York, under the joint sponsorship of the Gas Research Institute (GRI) and the New York State Energy Research and Development Authority (NYSERDA). A six-inch single screw extruder previously developed by General Electric was used to produce 88 tons of Illinois No. 6 coal extrudate using a 15% coal-tar pitch binder (Ref. 1). The extrudate was then successfully gasified in General Electric's 1 ton/hr, Process Evaluation Facility (PEF) scale, pressurized fixed-bed gasification system. Data is presented on gasifier performance, fines carryover rate, and tar yields from the extrudate. Performance data on the extrusion process is also included.

EXTRUSION TRIALS

General Process Description

General Electric began development of the coal extruder system in response to industry's need for an improved coal feed system and as a means of utilizing fines in a pressurized fixed-bed reactor. The work was initiated on a 1-inch extruder and progressed to the development of a 6-inch diameter single screw extruder capable of processing in excess of one ton per hour of coal against backpressures up to 350 psig. The later work was done under the sponsorship of EPRI (Project No. 357-1).

The extruder process is shown schematically in Figure 1. Coal under 1/4- inch is mixed with a binder, typically coal tar, in a heated mixer and then conveyed to a screw extruder where it is simultaneously compacted and forced into the pressurized reactor. Proper design and control of the die at the delivery end of the extruder maintains a gas seal and adjusts the frictional resistance of the compacted coal to forward motion. The extrudate exits the die as a solid log of coal which is subsequently broken up by a chopper inside the reactor.

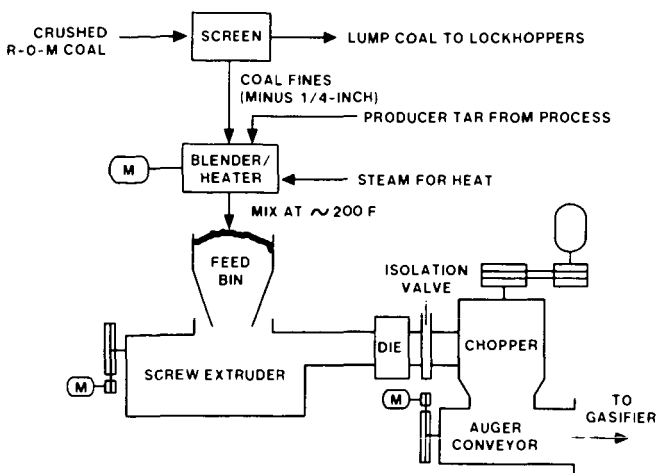


Figure 1. Coal Extrusion Process

The General Electric extruder is driven by a 60 hp variable speed drive which permits screw speed to be varied from 0-45 rpm. Screw construction is segmented with individual auger sections stacked along a central drive shaft to give a continuous worm. The auger sections are cast from high chrome steel having a Rc 60-67 hardness to minimize wear. The length-to-diameter ratio of the machine is 4:1. The barrel is made up of two steam-jacketed sections, each equipped with a hardened and ribbed steel liner. Two counter-rotating packer wheels are used in the feed hopper to help promote flow of the preheated extrudate mix into the screw cavity. Extrudate formation is controlled by a patented variable area, variable length die which permits on-line control of extrudate density. This feature has been found essential for permitting stable operation of the extruder over a range of operating conditions and on a variety of feedstocks. Power consumption and machine wear are also minimized.

Steam-jacketed, 15 ft³ scale-mounted paddle mixers were used to prepare the hot (150-175F) coal-tar extrudate blends. Milled coal was supplied to the mixer via a fines elevator. The coal was prepared for testing by hammermilling stoker grade Illinois No. 6 coal through a nominal 4-mesh screen. A screen analysis of the coal taken after crushing indicated a size distribution nearly identical to that of coal fines obtained from underscreened ROM coal. The coal was not dried prior to size reduction. Typical mix times for a 400 lb test batch were 12-15 minutes.

Mix Evaluation

Several different tar binder-coal combinations were evaluated prior to the start of production to arrive at a mix which extruded well and which possessed sufficient mechanical strength to withstand the handling and bed forces encountered during a gasification test. A total of 17,000 pounds of material was processed using seven different tars at varying weight percentages with Illinois No. 6 coal.

A list of the binders tested is shown in Table 1. All are coke oven derivatives with the exception of the asphalt pitch, and represent a commercially available range of softening points from slightly above room temperature to almost 200°F. Producer tars from actual gasification plants were not included in the study due to the lack of availability of these tars in sufficient quantities.

Table 1
TAR BINDERS TESTED

Tar Supplier	Designation	Softening Point ^a
General Electric	V-1 PEF gasifier tar	<40°C ^b
Koppers	Medium-soft coke oven	50-55°C
Koppers	Medium coke oven pitch	56-64°C
Reilly	No. 12 coke oven tar ^c	<50°C)
Reilly	Medium coke oven pitch	54-62°C
Reilly	Hard coke oven pitch	82-95°C
—	Canadian Asphalt pitch	

^aring and ball

^bestimated

^cselected for production run

Reilly No. 12 coal tar pitch was chosen as the test binder, based on its satisfactory performance in the extruder, its commercial availability, and the satisfactory mechanical properties of the extrudate obtained. The relatively low softening point of this tar also more closely approximated that of the raw tar which would be obtained from an actual gasification plant. A blend of 15% tar, 85% coal by weight was selected for the final production run. The use of this low softening point binder required modifications to be made to the mix preparation system to allow consistent production of extrudate with adequate green strength. This entailed lowering the mixer jacket temperature from 350°F to 190°F, and installation of a tempering water spray just upstream of the extruder inlet to further cool the extrudate mix. With this configuration, mixes of <120°F could be consistently produced, which was sufficiently low to allow production of good quality extrudate.

Extrudate Production

Approximately 88 tons of extrudate were produced offline in the 6-inch extruder over a 9-day operational period. The continuous 6 1/2-inch diameter logs were cut manually into 2-ft lengths, allowed to cool for approximately 2 to 4 hours, then crushed to <1 1/2-inches in a rotary crusher. The resultant extrudate was screened to remove any fines generated during size reduction and stored for testing.

Excellent performance was obtained from the extrusion system throughout the test period. On-line availability of both the mix preparation and extruder exceeded 98% and wear on machine parts including the auger was negligible. Specific power consumption of the extruder was exceptionally low and control over extrudate formation was good once stable operation had been achieved. A summary of the extruder operating conditions is shown in Table 2.

Table 2
PRODUCTION RUN SUMMARY —
EXTRUDER OPERATING CONDITIONS

Machine	6 in. single screw
Die	6.5 in. i.d., adjustable
Auger	3 in. pitch, segmented
Mixture	85% Ill. No. 6, 15% Reilly tar
Total production	175, 500 lbs.
Throughput	1305 lb/hr.
Specific power	1.5 hp-hr/ton
Shaft speed	12 RPM
Die length	4 in.
Flap pressure	150-200 psig
Auger wear	Negligible
Barrel temp	Cooling water on
Control	Excellent

Extrudate Properties

Laboratory evaluations were performed to determine the mechanical properties of the extrudate. Tests run included a crush test to measure the mechanical strength of the extrudate before and after carbonization, a 1000°F oven test to determine the high temperature behavior of the samples, a softening point test to determine at what temperature the extrudate begins to soften, and a standard test to determine extrudate density. The results of the mechanical tests, which are summarized in Table 3, indicated that the extrudate should possess sufficient mechanical strength to withstand the gasification environment. These observations were later verified during the fired gasification trials.

Table 3
EXTRUDATE PROPERTIES

Mixture, wt%	85% Illinois No. 6, 15% Reilly No. 12 tar
Compressive strength, psi	810
Carbonized strength, psi	834
Density, lb/ft ³	72
Softening point, ^a T°F	130
Oven test results	Some swelling and distortion

^aPoint at which extrudate can be deformed by hand

GASIFICATION TRIALS

Gasification Facility

The General Electric Process Evaluation Facility (PEF), located in Schenectady, New York, consists of an advanced fixed-bed reactor, full-flow, low-temperature gas cleanup system, coal extrusion feed system, and an advanced computerized data acquisition, analysis and control system. The facility operates at a nominal pressure of 20 atm. and can gasify approximately 1 ton of feedstock per hour using air and steam as reactants. Deep bed stirring provides the capability for the gasifier to operate on caking coals and at thermodynamically attractive low steam-air ratios. The raw fuel gas is conditioned in a two stage cleanup system which removes solid particulates, hydrocarbon mist, and sulfur compounds from the gas stream. A schematic of the PEF is shown in Figure 2, and the gasifier is shown in cutaway side-section in Figure 3.

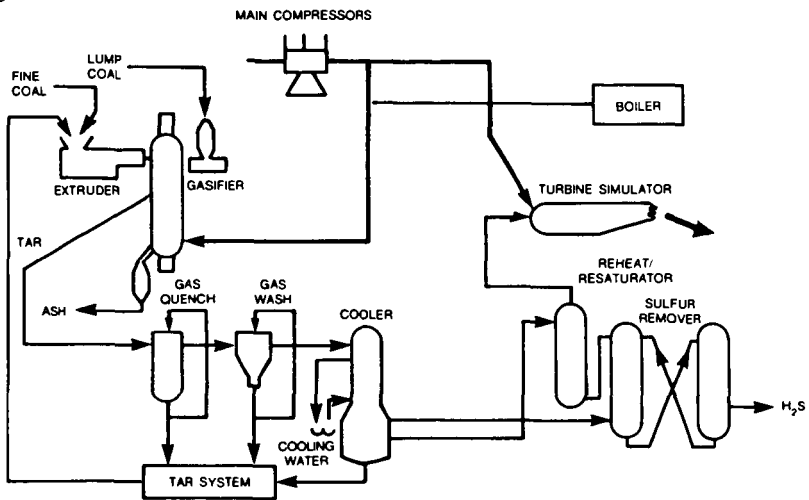


Figure 2. Process Evaluation Facility

Gasifier Performance

Approximately 50 tons of Illinois No. 6-Reilly No. 12 extrudate were successfully gasified in the PEF during a 50 hour operational test period in July, 1983. The gasifier was operated at steady-state, full pressure, full flow design conditions for the duration of the test run. The average gasifier operating conditions for a representative 20-hour time period are presented in Table 4. Ultimate and proximate analyses of the extrudate feedstock appear in Table 5.

Performance parameters characterizing the operation and efficiency of the gasifier were determined for the representative test period. These parameters are presented in Table 6 along with average results from previous baseline testing on Illinois No. 6 lump coal (Ref. 2).

The efficiency of gasification is quantified by the carbon, cold gas, and steam utilization efficiencies. The carbon efficiency provides an indication of the amount of input carbon which is converted to gaseous form in the tar and oil-free product gas. The cold gas efficiency

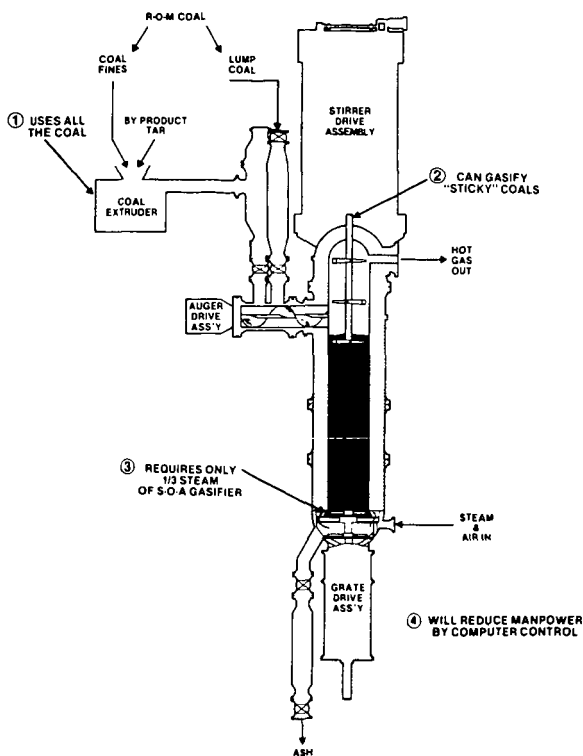


Figure 3. Advanced Fixed Bed Gasifier

Table 4
AVERAGE GASIFIER OPERATING CONDITIONS

Extrudate flow, lb/hr	1925
Air flow rate, lb/s	1.20
Steam flow rate, lb/s	0.48
Steam-to-air, lb/lb	0.40
Blast temperature, °F	363
Hot gas temperature, °F	1040
Vessel pressure, psig	300
Bed level, ft	10.7
Stirrer cycle	
raise, ft/min	1.0
lower, ft/min	0.5
Dry ash removal, lb/hr	176
Sludge removal, lb/hr	90

Table 5
EXTRUDATE ANALYSIS

	As Received	Dry Basis
Proximate Analysis (wt%)		
Moisture	7.60	—
Ash	9.12	9.90
Volatile	34.92	37.80
Fixed Carbon	48.37	52.30
Sulfur	1.34	1.45
Ultimate Analysis (wt%)		
Moisture	7.60	—
Carbon	69.11	74.78
Hydrogen	4.68	5.06
Nitrogen	1.55	1.68
Chlorine	0.11	0.12
Sulfur	1.34	1.46
Ash	9.12	9.90
Oxygen (difference)	6.48	7.01
Metals (wt% in dry ash)		
Sodium		0.35
Potassium		1.71
Iron		10.50
Calcium		2.75
Heating Value (Btu/lbm)	12342	13354
Moisture and Ash Free	—	14822
Free Swelling Index	3.9	

is defined as the higher heating value of the tar and oil-free raw gas at 60°F divided by the extrudate heating value. The steam utilization represents the percentage of the blast steam that takes part in the gasification reactions.

The carbon utilization of 83.5% for the extrudate run indicates good conversion of carbon to fuel gas heating value. The value is slightly lower than that obtained on Illinois No. 6 lump coal, primarily due to the higher condensible hydrocarbon content in the extrudate-produced gas. The higher tars and oils content also resulted in a slightly lower cold gas efficiency than determined for the lump coal. If the heating value of these tars is included, the calculated cold gas and carbon efficiencies would result in slightly higher values for the extrudate feedstock. The steam utilization value is excellent and nearly identical for both feedstocks, indicating good fuel reactivity and good gas-solids contact in the fuel bed.

The gas composition was similar for both fuels, the only detectable difference being a slightly lower methane content and slightly higher CO₂ level for the extrudate case. The overall dry gas heating value of 162 Btu/scf for the extrudate-produced fuel is satisfactory and compares favorably with results obtained from stoker grade lump coal.

Table 6
PERFORMANCE PARAMETERS COMPARISON

Performance Parameter	Extrudate Feedstock	Illinois No. 6 Lump Coal
Carbon utilization, %	83.5	86.0
Steam utilization,	55.7	56.0
Cold gas efficiency, %	71.2	74.7
Gas composition, vol%	64.7	68.0
H ₂	21.0	21.0
CO	17.1	17.1
CO ₂	13.2	12.8
N ₂	43.8	43.9
CH ₄	4.0	4.4
H ₂ S	0.3	0.3
Dry gas heating value, Btu/scf	162	166
Tar yield, wt% dry coal	7.8	4.0
Dry fines carryover, wt% dry coal	2.1	3.6

The dry fines carryover represents the percentage of feedstock carried over from the fuel bed to the quench vessel. The relatively low dry fines carryover value for the extrudate testing indicates that the extrudate maintained its integrity in the fuel bed during gasification. This result is particularly significant considering that the extrudate is produced from essentially 100% fines.

The gasifier exhibited excellent mechanical performance through the extrudate run. No major problems with extrudate feeding, bed conditioning, or ash discharging were experienced during the test. The peak rotational torque loadings on the stirrer and grate paddle were 3,400 and 14,000 ft-lbs, respectively, and were safely below the design limit values. In general, the mechanical performance of the gasifier on the extrudate feedstock was very similar to that experienced during operation on lump coals.

Gas Cleanup System Performance

The gas cleanup system was operated at steady design conditions for the duration of the extrudate test run. All of the cleanup components functioned smoothly, indicating no specific problems associated with the extrudate-produced fuel gas. Results from the particulate sampling indicate that the overall cleanup system particulate removal efficiency was nearly 99%, typical of that seen on lump coal.

Comparative tar collection data is presented in Table 7 for both the extrudate and lump coal runs. The total tar collection rate obtained from the cleanup system components on extrudate was approximately double that obtained during Illinois No. 6 lump coal runs. This higher tar yield can be attributed primarily to carryover of vaporized extrudate binder, which,

when added to the normal tar carryover from the volatile matter in the base coal, yields the rates shown. However, although the total rate is nearly double, it is only approximately 25% of that which would be obtained if all the binder appeared in the raw gas. This translates to an apparent cracking rate of 75% of the extrudate binder during a single pass through the gasifier.

Table 7
TAR CARRYOVER COMPARISON

	Extrudate Feedstock	Illinois No. 6 Lump Coal
Tar Collection Rate, lb/hr	117.7	57.0
Tar Yield, Wt. % Dry Coal	7.8	4.0

SUMMARY

The results of the test program indicate that Illinois No. 6-Reilly No. 12 extrudate makes an attractive feedstock for fixed-bed gasifiers in terms of both fines and tar utilization, as well as overall gasifier performance. Fines carryover was reduced from a typical value of 3 - 4% on lump coal to 2% on extrudate, a result which is particularly significant considering the extrudate is produced from essentially 100% fines. Approximately 75% of the tar binder cracked during the first pass through the gasification process. The cold gas efficiency of 71% and fuel heating value of 162 Btu/scf were comparable to results obtained on Illinois No. 6 lump coal. The mechanical performance of the reactor was also satisfactory.

The 6-inch coal extruder performed well throughout the program. Power consumption was low (1.6 kwh/ton), machine wear was negligible, and reliability excellent. Power consumption and wear would be expected to be somewhat higher under on-line extrusion conditions due to the need to maintain a gas seal in the die area. Accurate temperature control of the mix was found to be a critical variable in producing extrudate with adequate green strength when using a low softening point binder such as Reilly No. 12 tar.

REFERENCES

1. "Development of an Extruder Feed System for Fixed Bed Coal Gasifiers," EPRI AF-954 Project 357-1, January 1979, prepared by General Electric Company.
2. "Experimental Evaluation of the Steady State and Dynamic Performance Characteristics of the Interactive Units of a Coal Gasification Process," Quarterly Report, 28 September 1981-27 December 1981, DOE report ET-14928-4, January 1982.
3. "Production and Gasification Tests of Coal Fines/Coal Tar Extrudate," GRI Contract No. 5082-221-0660, Final Report, January 1984; prepared by General Electric Company.

PYROLYSIS AND HYDROPYROLYSIS OF COAL ASPHALTENES.

M.A. Thomson, W. Kemp and W. Steedman.

Department of Chemistry, Heriot-Watt University,
Edinburgh EH14 4AS, Scotland.

Coal asphaltenes and their behaviour under typical coal liquefaction conditions have attracted considerable attention in recent years (1, and references therein), because of both their proposed role as intermediates in liquefaction processes and the potential problems presented by incomplete conversion of asphaltenes. The present work extends our previous studies on asphaltene fractions from coal extracts (1,2) to permit comparisons to be drawn between two asphaltenes, each derived from a hydrogenated-anthracene-oil extract of bituminous coal, but having significantly different carbon and oxygen contents.

Experimental.

The coal extract used was kindly supplied by the Coal Research Establishment, National Coal Board, Cheltenham, England. It was derived from Point of Ayr coal, extracted by a hydrogenated anthracene oil (Veba Oil).

Cylinder gases were obtained from the British Oxygen Company, and CoO-MoO₃ on AlO₃ from Strem Chemicals Inc. Details of the isolation of asphaltenes, by extraction into benzene followed by precipitation using n-pentane, are given elsewhere (1).

Pyrolysis and Hydropyrolysis Procedure.

Reactions were carried out in the stainless steel autoclave of 250 ml volume described previously (1), which was charged with asphaltene (1.5g) finely ground with catalyst (CoO-MoO₃ on AlO₃, 0.15g). After closure, the bomb was pressured to 87 bar (1300 p.s.i.) cold pressure with the appropriate gas (oxygen-free nitrogen for pyrolysis experiments, hydrogen for hydropyrolysis experiments). The temperature profiles of the reactions were complicated due to the considerable thermal mass of the bomb, and heat-up times varied between 40 mins. (to 200°C) and 60 mins. (to 425°C). Nominal reaction times are given as the number of minutes at the designated temperature, ignoring heat-up and cooling.

Fractionation of Products.

After cooling overnight, the bomb pressure was released by using a specially adapted two-stage needle-valve to leak the gases slowly into a train of three pre-weighed stainless-steel U-tubes loosely packed with dry molecular sieve (1/16in. pellets, type 3A), maintained at liquid nitrogen temperature. After reweighing, the traps were warmed to room temperature and the evaporating gases were transferred to an evacuated glass bulb fitted with a rubber septum to allow withdrawal of samples, using a gas-tight syringe, for injection onto a g.c. column. Following this out-gassing, the bomb was opened, benzene (20 ml) was added and the resulting slurry was coated onto cleaned glass beads (100-200 mesh, 100g) which were successively extracted, according to the method of Awadalla et al.(3), with n-pentane, benzene and pyridine. The bulked n-pentane solution was reduced in volume on a rotary evaporator to ca 20 mls weighed, then a 8µl

sample was withdrawn and injected onto the capillary g.c. column. The percentage of solvent (n-pentane and benzene) present was estimated from the g.c. trace and in this manner an approximate weight was arrived at for the n-pentane soluble product. The method was devised to minimise the under-estimation of light constituents such as methylated benzenes, which is inherent in any total drying of this fraction. The benzene and pyridine were removed from the asphaltene and preasphaltene solutions respectively, using a rotary evaporator and these products were dried in a vacuum oven (60°C, 3 hr) before weighing.

Analytical Procedures.

Elemental analyses were carried out by the University of Strathclyde Microanalytical Service. ¹H-n.m.r. spectra were recorded in deuteriochloroform at 100 MHz on a Jeol MH100 spectrometer and (¹H)-¹³C-n.m.r. spectra in deuteriochloroform at 50MHz using inverse-gated decoupling with a 10 sec. delay, and 100mg chromium acetylacetonate added to the sample.

Characterisation of gaseous products was carried out using a Hewlett-Packard model 5880A gas chromatograph fitted with a 2m, 3.2mm OD stainless-steel column packed with Porapak Q, and an oven temperature of 160°C. Nitrogen carrier gas and a flame ionisation detector were used, permitting identification of hydrocarbon gases only. No attempt was made to detect fixed gases. For the pentane-soluble products, a 50 m open tubular capillary column (fused silica with SE54 silicone gum as stationary phase) was used, with the oven temperature programmed from 50-265°C at 5°C min⁻¹ holding for 48 min. at 265°C. Further identification of the pentane-soluble material was carried out at the Institute of Offshore Engineering, Heriot-Watt University, using computerised g.c. - mass spectrometry with an INCOS data system. Samples were injected onto a 25m QV-101 fused silica column with the oven programmed from 50-260°C at 5°C min⁻¹, holding at 260°C for 48 min.

Pyrolysis Experiments.

Following our earlier work (1) on an asphaltene (A) with carbon content of over 91% and carbon aromaticity of 80%, we have carried out a series of experiments using a second asphaltene (B), with 87.1% carbon and 74% carbon aromaticity. Pyrolysis and hydroxyrolysis reactions were carried out, to allow comparisons with the previous study on asphaltene A.

Pyrolysis at 425°C of asphaltene B in a mini-bomb reaction vessel (1) gave a product (see Table 2) consisting largely of asphaltene and pre-asphaltene (total 78%) with 9% n-pentane soluble material and 8% pyridine-insoluble material ("coke"). This compares with a rather higher coke content (23%) and a low percentage of n-pentane soluble material (3-4%) in the product from asphaltene A, confirming the expectation that the asphaltene of lower carbon content and aromaticity would give rise to more tractable products. However, the results of this kind of pyrolysis experiment are extremely sensitive to changes in the conditions of the reaction. Thus, when asphaltene B was pyrolysed at 425°C in the Parr bomb under nitrogen pressure, in conditions of geometry and pressure

mimicking those used in the hydrogenation studies, a quite different product was obtained, consisting largely of gases (defined as C_1-C_4 hydrocarbons plus H_2S and other minor constituents) and coke. Only 6% was recovered as asphaltene or preasphaltene. Clearly, the changes in geometry, pressure and true reaction time combined to produce a result quite different from that obtained in the mini-bomb. Bearing this in mind, the data from the Parr bomb pyrolyses are used below as the basis for comparisons with hydropyrolysis experiments.

Hydropyrolysis Experiments.

Pyrolysis at $425^\circ C$ of asphaltene B under hydrogen pressure in the presence of a hydrogenation catalyst gave product distributions shown in Fig. 1. Even at the shortest reaction time (10 min) conversion to over 40% pentane-soluble material was achieved, with less than 20% recovery of asphaltene. After 1 hour at $425^\circ C$, only 12% asphaltene was recovered while the pentane-soluble yield was maintained at $> 40\%$. However, the conversion to gas in the latter case was higher than at the shorter reaction time, the level of preasphaltenes and heavier products remaining low. This compares with much lower conversion of asphaltene A under identical conditions (see Fig. 2), accompanied by larger amounts of preasphaltene and coke. In general, for both asphaltenes, pyrolysis under nitrogen led to gas and heavy preasphaltenes and cokes as the major products - a result that can be regarded as a disproportionation of the starting asphaltene. Similar reactions under hydrogen pressure led to increased recovery of liquids and asphaltene, suggesting stabilisation of reactive fragments by hydrogen, but significant amounts of gas were still generated, particularly from asphaltene A, at longer reaction times.

Product Analysis.

Elemental analysis and ^{13}C -n.m.r. spectroscopy (see Table 1) revealed no significant differences in carbon content or carbon aromaticity between starting asphaltene and recovered asphaltene in any of the reactions using asphaltene A. There was, however, an increase in aromaticity, as measured from 1H n.m.r. spectra, of 5% in hydropyrolysis and 9% in pyrolysis. A smaller increase (2% and 4% respectively) in hydrogen aromaticity was observed in the product asphaltene from the more reactive asphaltene B. This presumably reflects the pyrolytic loss, under all the conditions studied, of aliphatic structures present in the parent asphaltene and is reflected in the aliphatic content of the n-pentane soluble liquid products. The overall hydrogen/carbon ratio is also reduced in both asphaltenes recovered from pyrolysis, confirming the pyrolytic loss of hydrogen-rich material.

Differential Pulse Voltammetry [D.P.V.] (4) and Size Exclusion Chromatography [S.E.C.] on asphaltene B and its hydropyrolysis products indicate a slight shift to lower values for the molecular-weight distribution of the asphaltene recovered after reaction compared with asphaltene B itself. This is accompanied by a marked decrease in the D.P.V. peaks assigned to pyrene, anthracene and other polyaromatic structures, which can be characterised by D.P.V. even when substituted and linked together in larger molecules. Diaromatics such as naphthalene remain very much in evidence, however (5). Taken together with the n.m.r. spectroscopic evidence, this suggests that hydrogenation leads to a loss of purely aliphatic side-chains and partial hydrogenation of large polyaromatic structures to leave an asphaltene consisting largely

of diaromatic and monoaromatic centres (the latter not observable by D.P.V.) linked by methylenic bridges that constitute most of the remaining aliphatic character.

A detailed analysis of the composition of the n-pentane soluble products was carried out using gas chromatography-mass spectrometry. We have discussed previously (1,2) the identification in the asphaltene A products of a series of n-alkanes ranging up to C_{29} in the pyrolysis case, and to C_{14} in the hydropyrolysis case. A similar series of n-alkanes was found in the asphaltene B liquid products, together with a range of branched alkanes including traces of isoprenoids such as pristane (C_{17}) and phytane (C_{18}). Altogether the aliphatics (separated by column chromatography, see ref. 6) made up approximately 10% by weight of the B hydrophrolysate. A similar spectrum of aliphatic material was identified in the pyrolysate produced under nitrogen, supporting the suggestion that the majority of the alkanes originate as primary pyrolysis products. The remaining 90% of the liquid product is made up of aromatic hydrocarbons together with a trace (>2%) of polar materials, predominantly alkyl phenols and indoles. No sulphur-containing species has been identified in the liquid product, and most of the sulphur appears to be converted to H_2S .

The composition of the aromatic hydrocarbons that form the bulk of the liquid product - and hence some 40% of the total products - is of interest and has been analysed in some detail. Phenanthrene, pyrene and anthracene peaks are prominent in the D.P.V. trace of the pentane-soluble hydropyrolysate (5) and gas chromatography confirms that the single largest component in the mixture is phenanthrene which, together with other polyaromatics such as pyrene and fluoranthene, dominates the liquid product. This is qualitatively in accord with thermodynamic predictions (7). Both the pyrolysate and hydropyrolysate also contain a wide range of alkyl-benzenes, which may therefore be primary pyrolysis products, and a significant amount of dibenzofuran, possibly formed by condensation of neighbouring phenolic functions. The low level of phenolic material in the pentane-soluble fraction even of the pyrolysate was surprising in the light of earlier results (1) and the fate of the oxygen, phenolic and non-phenolic, requires further study. The hydropyrolysate also contains a range of partially hydrogenated polyaromatics arising from the fully condensed forms produced by pyrolysis. Phenanthrene and pyrene, in particular, are present in association with several hydrogenated forms in sufficient amounts to allow quantitation from capillary g.c. traces (see Figs. 3,4). Comparison of these results with "model-compound" studies of phenanthrene and pyrene hydrogenation (5,6) shows that, in the complex matrix present during asphaltene hydrogenation, the formation of perhydro-species is completely suppressed. Indeed, dihydrophenanthrene and dihydropyrene are the dominant hydrogenated species even at long reaction times. It is hard to envisage complete hydrogenation of these polyaromatic species under any realistic time-temperature-pressure regime. This is partly attributable to the tendency of some of the hydrogenated species to act as hydrogen donors, so that the asphaltene matrix becomes, as it were, a "hydrogen sink", inhibiting stepwise progress along a hydrogenation pathway. We have also found, and confirmed in separate pyrene studies (10) under similar conditions, that at the temperatures we have used a significant amount of pyrene breaks down, presumably via the 1,2-dihydro-form, to 4,5-dimethylphenanthrene which resists further hydrogenation. The character of the pentane-soluble pyrolysate and hydropyrolysate derived from asphaltene A does not differ greatly from that discussed here.

Further hydrogenation studies currently in progress will allow us to build up a more complete picture of the factors at work in asphaltene hydrogenation. However, we can summarise our conclusions to date as follows:

1. The general pattern of asphaltene conversion, viz., to gas and heavy, intractable materials on pyrolysis and to gas and liquids under hydrolypyrolysis conditions, remains the same for both average and high-carbon asphaltenes, but the extent of conversion to liquids upon hydrolypyrolysis is limited when the carbon content is high.
2. The aliphatic content of the liquids formed is low, not exceeding 10%, and arises from aliphatic groups present in the reactant asphaltene. The aliphatic content in the asphaltenes recovered after reaction is probably largely in the form of bridging methylenic functions.
3. The distribution of hydrogenated species in the highly aromatic liquid products indicates that complete hydrogenation of the polyaromatics produced in pyrolysis is difficult in the presence of a complex, hydrogen-hungry matrix. Conclusions drawn from model compound studies, while useful, must be used with caution in interpreting or predicting the behaviour of coal-derived materials.

References.

1. Kemp, W., Steedman, W., Thomson, M.A., Grigson, S.J.W. and Ludgate, P.R. Proc. 1983 International Conference on Coal Science, I.E.A., 1983, 529.
2. Grigson, S.J.W., Kemp, W., Ludgate, P.R. and Steedman, W., Fuel, 1983, 62, 695.
3. Awadalla, A.A., Rix, C.J., Shaw, I.M. and Smith, B.E., Fuel, 1982, 61, 1168.
4. Bartle, K.D., Gibson, C., Mills, D., Mulligan, M.J., Taylor, N., Martin, T.G. and Snape, C.E., Anal. Chem., 1982, 54, 1730.
5. Bartle, K.D., Taylor, N. and Tykko, A., University of Leeds, private communication.
6. A.S.T.M. D2549, as adapted for use at N.C.B. Coal Research Establishment, England.
7. Linton, M. and Turnbull, A.G., Fuel, 1984, 63, 408.
8. Shabtai, J., Veluswamy, L. and Oblad, A.G., A.C.S. Fuel Div. Preprints, 1978, 23(i), 107.
9. Stephens, H.P. and Chapman, R.N., A.C.S. Fuel Div. Preprints, 1983, 161.
10. Craig, L.S., Kemp, W., Steedman, W. and Thomson, M.A., unpublished work.

Table 1 : Analytical and Spectroscopic Data for
Various Coal-Derived Asphaltenes.

	Starting Material		Recovered from Pyrolysis		Recovered from Hydropyrolysis	
	A	B	A	B	A	B
% C	91.9	87.1	92.1	88.2	92.7	88.2
% H	5.8	6.1	5.3	5.9	5.4	6.1
% N	1.0	1.4	trace	1.5	trace	1.5
(direct) % O	0.8	4.1	-	-	-	-
% S	not detected	0.6	-	-	-	-
% Carom	80	74	-	74	79	75
% Harom	44	42	53	46	49	45
H/C	.75	.81	.70	0.80	.70	.83

Table 2 : Yield Structure for Asphaltene Pyrolysis.

	Asphaltene A		Asphaltene B	
	mini-bomb	Parr bomb	mini-bomb	Parr bomb
% gas)	28	< 5	35
% pentane sol.) 5 total	15	9	17
% asphaltene	53	3	44	4
% preasphaltene	19	3	34	2
% coke	23	47	8	36

Figure 1

425°C Hydrogenation of Asphaltene B:

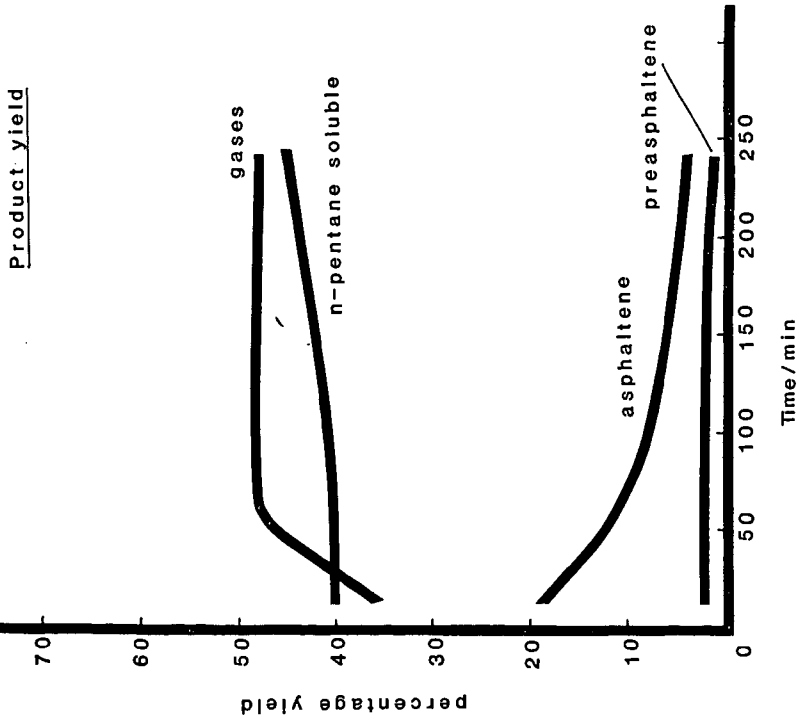
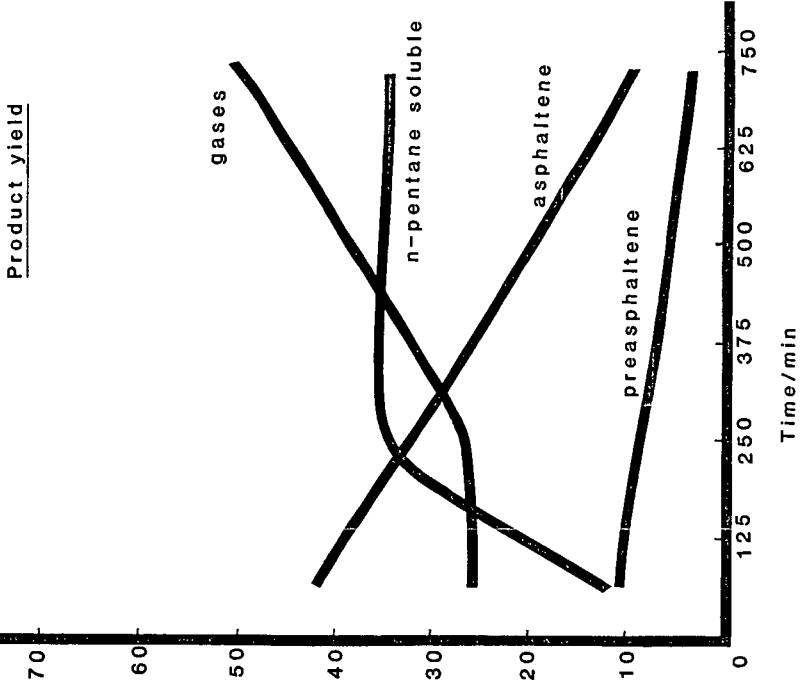
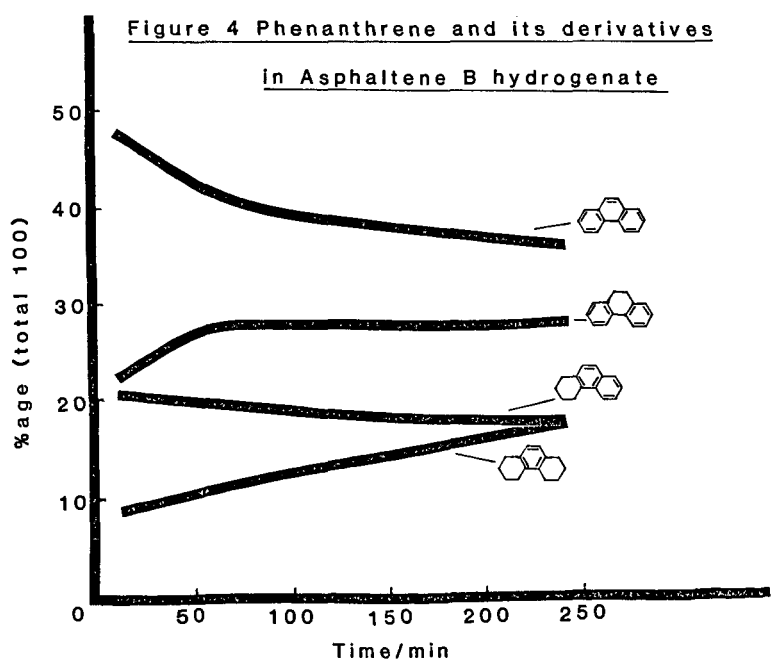
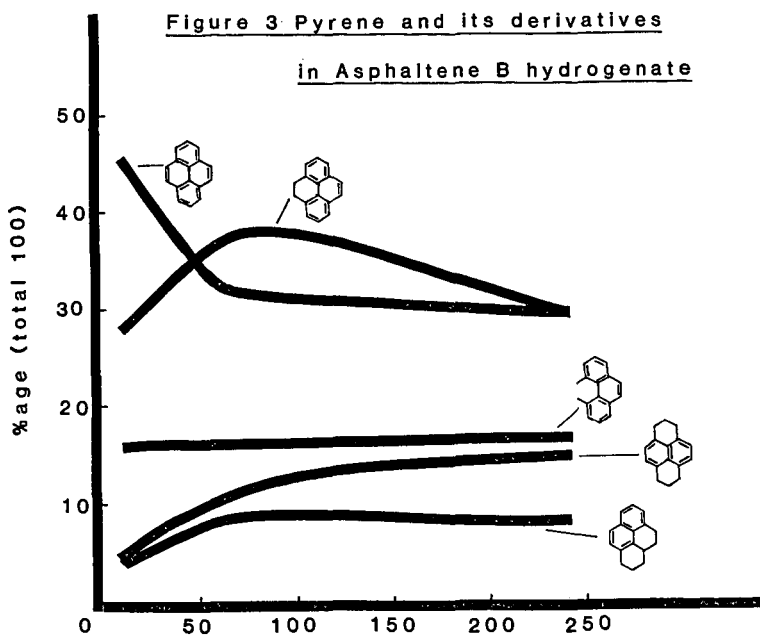


Figure 2

425°C Hydrogenation of Asphaltene A:





COMPARATIVE ELEMENTAL ASSOCIATIONS IN LIGNITES
HAVING SIGNIFICANT WITHIN-MINE VARIABILITY OF SODIUM CONTENT

J.P. Hurley and S.A. Benson

University of North Dakota
Energy Research Center
Box 8213, University Station
Grand Forks, North Dakota 58202

Introduction

The inorganic constituents of lignites from the Fort Union Region are distributed within the coal matrix as cations, coordinated species and minerals (1). The quantities of inorganics present in these lignites have significant within-mine, or intramine, variability (2). Studies have indicated that high-sodium coals from this region cause severe ash fouling of heat exchange surfaces in utility boilers (3). The coals investigated were collected from pits within the Gascoyne Mine, Bowman County, North Dakota and Beulah Mine, Mercer County, North Dakota. From each mine, two samples were selected having significant differences in sodium content and different fouling characteristics in utility boilers.

The distribution of inorganics constituents within the Gascoyne and Beulah coals was determined by non-quantitative identification of mineral matter and by chemical fractionation to ascertain any significant differences in the association of elements within the coals. In addition, the amounts of ion exchangeable cations were related to the carboxylate content of the coals.

Experimental

Samples were collected according to a procedure used by Benson (4). Proximate and ultimate analyses were performed on the air-dried coals using standard ASTM methods (5). Bulk coal mineralogy was determined by x-ray diffraction (XRD) of the coal's low-temperature ash (LTA) (6) and by scanning electron microprobe (SEM) in conjunction with energy dispersive x-ray analysis (EDX) (7) of the coal. Carboxylate contents were determined by exchanging the demineralized coals (8) with 1M barium acetate, followed by potentiometric titration with 0.2N barium hydroxide to pH 8.25 to determine the acid produced (9). The determination of inorganic constituents of the starting coals and subsequent residues was performed by x-ray fluorescence (XRF) (10) and neutron activation analysis (NAA) (11). The chemical fractionation was done with a method modified from that of Miller and Given (1). Two samples of each coal were ground to less than approximately 325 mesh in an alumina grinder and freeze dried for two days. The dried coal was mixed with 100 ml of 1N ammonium acetate and stirred for 24 hours at 70°C in a plastic beaker. The mixture was filtered, the residue washed, and the extract made up to 250 ml. The dried residue was extracted two more times with ammonium acetate, then twice with 1N hydrochloric acid in the same manner. All of the extracts were analyzed with inductively coupled argon plasma spectrometry (ICAP). A portion of the residue left after the ammonium acetate extractions and a portion left after the hydrochloric acid extractions were analyzed by XRF and NAA.

Results and Discussion

Coal Compositions. Table I shows the initial elemental, proximate, ultimate, and carboxylate content analysis of the coals on a moisture free basis.

Table I. Dry Bulk Coal Elemental, Ultimate, Proximate, and Carboxylate Analyses

	Gascoyne Low Sodium	Gascoyne High Sodium	Beulah Low Sodium	Beulah High Sodium
Na ($\mu\text{g/g}$)	1317	2694	1379	4625
Mg ($\mu\text{g/g}$)	2991	2588	1476	979
Al ($\mu\text{g/g}$)	8740	7300	5420	2890
Si ($\mu\text{g/g}$)	28640	10920	8950	3530
K ($\mu\text{g/g}$)	1260	1430	916	ND*
Ca ($\mu\text{g/g}$)	17370	22790	15610	18110
Ti ($\mu\text{g/g}$)	1180	546	503	583
Mn ($\mu\text{g/g}$)	123	163	52	24
Fe ($\mu\text{g/g}$)	3890	2540	10240	5160
Ba ($\mu\text{g/g}$)	593	1268	179	397
C (wt %)	58.3	54.5	61.4	66.4
H (wt %)	4.0	5.2	4.1	3.6
N (wt %)	0.88	0.84	0.42	0.87
S (wt %)	1.7	1.4	3.2	1.2
O (diff.)	19.6	29.3	18.2	19.5
Ash (wt %)	15.5	8.8	12.6	8.4
Carboxylate groups (meq/g)	2.46	2.54	2.47	2.76

*ND - Not determined.

Similarities can be seen between the high-sodium coals versus their intramine low-sodium counterparts. In the high-sodium coals, the carboxylate, calcium, and barium contents are greater. Magnesium, aluminum, silicon, iron, and ash contents are lower in the high-sodium coals than in their intramine low-sodium counterparts.

Coal Mineralogy. The mineralogies of the coals, determined by x-ray diffraction of their low-temperature ashes, are similar. The diffractogram shown in Figure 1 is of the LTA of the Gascoyne high sodium coal. The mineral phases which were in sufficient amounts (2-5% depending on crystal structure) to be clearly delineated include quartz (SiO_2), micaceous clay minerals, and pyrite (FeS_2). Some bassanite ($\text{CaSO}_4 \cdot 1/2 \text{H}_2\text{O}$) was identified in the LTA of the Beulah coals although it is not clear if this forms from sulfur fixation during ashing (12) or from the dehydration of gypsum. The quartz peaks are more prominent in the diffractograms of the ash from the low-sodium (high-ash) coals.

In addition to the minerals mentioned above, the SEM-EDX work showed minor amounts of dolomite ($\text{CaMg}(\text{CO}_3)_2$), calcite (CaCO_3), gypsum

(CaSO₄·2H₂O), rutile (TiO₂), hematite (Fe₂O₃) (7), and barite (BaSO₄) (7). Also, the micaceous clay minerals identified by XRD were seen to include kaolinite, illites, and micas. Most of the SEM-EDX work was not systematic so quantitative comparisons between the coals will not be made here.

Ammonium Acetate Treatments. The percentages of the elements removed from the coals by the ammonium acetate treatments are shown in Table II. The figures for the carboxylate ions are percentages of the carboxyl groups that are in a salt form, under the assumption that all of the cations removed by the ammonium acetate treatments were exchanged from these sites. Minor amounts of these elements may have been exchanged from other organic acids or micaceous clays, or may have come from the dissolution of minerals soluble in ammonium acetate such as gypsum, calcite, and dolomite.

Table II. Elements Removed by Ammonium Acetate (%)

	Gascoyne Low Sodium	Gascoyne High Sodium	Beulah Low Sodium	Beulah High Sodium
Na	100	100	100	100
Mg	74	75	76	84
Al	0	0	0	0
Si	0	1	0	0
K	22	19	7	*31
Ca	78	85	82	77
Ti	0	0	0	0
Mn	34	39	25	21
Fe	0	0	0	0
Ba	39	61	72	88
Carboxyl groups (% in salt form)	38	51	32	35

*ppm removed

The results indicate aluminum, silicon, titanium, and iron are not removed from any of the coals by this treatment. Among those elements that are extracted, a higher percentage of barium is removed from the high-sodium coals than from their intramine low-sodium counterparts. However, more barium is removed by each of the second and third treatments than by the first so we feel that the barium extraction was incomplete. A large percentage of the sodium, calcium, and magnesium was removed from all of the coals.

Hydrochloric Acid Treatments. Table III lists the percentage of elements removed by the hydrochloric acid treatments. The elements removed by this treatment were associated with the coal as oxides, carbonates, coordinated complexes within the coal organic structure and certain elements (Mg, Al, Si, K, Ca, Fe) which can be extracted from the micaceous clay minerals.

A higher percentage of aluminum was removed from the high-sodium (low-ash) coals than from the corresponding intramine low-sodium

Table III. Elements Removed by Hydrochloric Acid (%)

	Gascoyne Low Sodium	Gascoyne High Sodium	Beulah Low Sodium	Beulah High Sodium
Na	0	0	0	0
Mg	12	16	17	16
Al	42	51	60	80
Si	3	12	14	12
K	30	41	19	*206
Ca	20	14	17	22
Ti	4	7	5	2
Mn	64	60	69	76
Fe	73	68	37	42
Ba	43	39	16	12

*ppm removed

(high-ash) coals. Although more aluminum was actually removed from the low-sodium coals, we feel that the solutions were not saturated because much lower levels of aluminum were found in the second extracts than in the first. Instead, we believe that the higher relative removal from the high-sodium coals is due to differences in the types of micaceous clay minerals present. In all the coals the ratio of aluminum to silicon removed (4:1 - 14:1) does not match the ratios found in common micaceous clay minerals. This indicates that the micaceous clays have not dissolved but that a selective attack has occurred on the gibbsite (aluminum containing) layer in the micaceous clays.

Insolubles. Table IV shows the elemental percentages left in the residue after the chemical fractionation process.

Little or no sodium, magnesium, calcium, and manganese remain in the coals. X-ray diffraction of the low temperature ash of the residue from the Gascoyne high-sodium coal shows that the major remaining minerals are the same as those seen in the LTA of the bulk coal; i.e., quartz (SiO_2), micaceous clays, and pyrite (FeS_2). Work done with the SEM-EDX suggests that the potassium remaining in the residue is found in the micaceous clays, titanium in a rutile form (TiO_2), and the barium present as barite (BaSO_4)(7). It is interesting that no barium is left in the high-sodium coals even though they originally contained more barium than the low-sodium coals.

Conclusions

The amount and mode of occurrence of inorganics in lignites can have a pronounced effect on the efficiency of the coal's utilization. This study used a number of the techniques developed by others to investigate variations in the inorganic makeup of coals found in two areas within each of two mines. By better understanding these

Table IV. Elements Remaining After All Treatments (%)

	Gascoyne Low <u>Sodium</u>	Gascoyne High <u>Sodium</u>	Beulah Low <u>Sodium</u>	Beulah High <u>Sodium</u>
Na	0	0	0	0
Mg	14	9	7	0
Al	58	49	40	20
Si	97	87	86	88
K	48	40	74	*ND
Ca	2	1	1	1
Ti	96	93	95	98
Mn	2	1	6	3
Fe	27	32	63	58
Ba	18	0	12	0

*Not determined.

variations, insights into the various depositional and post depositional processes may be gained. Also, understanding the modes of occurrence of the inorganic constituents of a coal may help in determining its appropriate utilization.

A comparison of the elemental associations between the high-sodium coals and their intramine low-sodium counterparts shows:

1. No significant differences in the modes of occurrence of the inorganic constituents exist, only differences in the amounts of inorganic species.
2. A higher percentage of aluminum is extracted from the high-sodium coals indicating different types of predominant micaceous clay minerals.
3. A higher percentage of barium is associated with ion exchange sites in the high-sodium coals.

Further work needs to be done in determining the exact mineralogic makeup and types of organic acids found in the coals, as well as accumulating more data from which to draw further conclusions.

Literature Cited

1. Miller, R.N.; and Given, P.H. A Geochemical Study of the Inorganic Constituents in Some Low-Rank Coals. U.S. DOE Report, FE-2494-TR-1, February 1978.
2. Cooley, S.A.; and Ellman, R.C., Analysis of the Northern Great Plains Province Lignites and Subbituminous Coals and Their Ash, DOE/GFETC/RI-81/2, DE81028366, July 1981.
3. Sondreal, E.A.; Tufte, P.H.; Beckering, W. Ash Fouling in Combustion of Low-Rank Western U.S. Coals, Combustion Science and Technology, Vo. 16, pp. 95-110, 1977.
4. Benson, S.A.; Kleesattel, D.R.; and Schobert, H.H. ACS Division of Fuel Chemistry Preprints 1984, 29, (1), 108.
5. "Annual Book of ASTM Standards" 1983, 05.05, D3172-73; D3176-74.
6. Miller, R.N.; Yarzab, R.F.; and Given, P.H. Fuel, 1979, 58, 4.

7. Zygarlicke, C.J. 'The Occurrence and Distribution of Inorganic Constituents in a North Dakota Lignite: an SEM and Statistical Analysis Approach'. Internal Report, University of North Dakota Energy Research Center, UNDERC-IR-6, 1983.
8. Tarpley, E.C.; and Ode, W.H. 'Evaluation of an Acid-Extraction Method for Determining Mineral Matter in American Coals'. Report of Investigations 5470, U.S. Department of the Interior, Bureau of Mines, 1959.
9. Schafer, H.N.S. Fuel, 1970, 49, 197.
10. Benson, S.A.; Severson, A.L.; and Beckering, W. Amer. Lab. 1980, 12(10), 35.
11. Weaver, J.N. in 'Analytical Methods for Coal and Coal Products, Vol. I' (Ed. C. Karr), Academic Press, New York, 1978, p. 377.
12. Painter, P.C.; Coleman, M.M.; Jenkins, R.G.; and Walker, P.L. Jr., Fuel 1978, 57, 125.

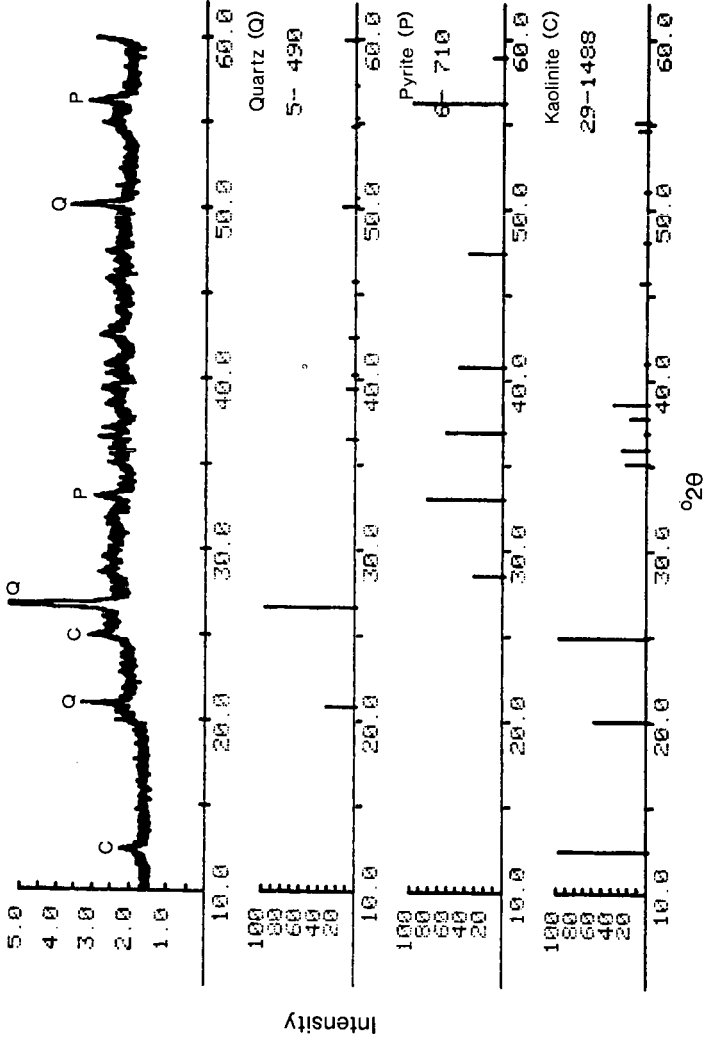


FIGURE 1. Diffractogram of the Gascoyne High-Sodium LTA along with reference graphs for quartz, pyrite, and kaolinite.

RUTHENIUM TETROXIDE OXIDATION OF LIGNITE

E.S. Olson and J.W. Diehl

University of North Dakota Energy Research Center
Box 8213, University Station
Grand Forks, North Dakota 58202

The objective of these studies was to develop new methods for the elucidation of the organic structure of low-rank coals, especially with regard to the nature of the hydroaromatic groups, the substituent groups on aromatic moieties and bridging groups between aromatic moieties. Isolation of the nonaromatic groups in coal could be achieved if the aromatic rings in the structure could be oxidized without degrading the alkyl substituents on the aromatic rings. Selective oxidation of the benzene ring has been observed in reactions with trifluoroperacetic acid (1); however the severe conditions required with this reagent result in extensive degradation of the alkyl groups (2). Thus tetralin gave succinic, glutaric, and adipic acids in the ratio 1:4:4(3). Confusion also resulted from the isolation of different products when different acid concentrations were used in the oxidation, e.g. cyclohexene-1,2-dicarboxylic anhydride was reported as the product from tetralin (1).

Ruthenium tetroxide is a useful reagent for the oxidation of alcohols, ethers, aldehydes, amides, alkenes and aromatic compounds (4). In the case of alkylbenzenes, the benzene ring is preferentially attacked, preserving any alkyl substituents as aliphatic carboxylic acids. Stock has reported the oxidation of Illinois No. 6 coal (5) using ruthenium tetroxide in a coordinating cosolvent, acetonitrile, which enabled the oxidation to proceed with much higher conversions (6).

We have reported the use of the ruthenium tetroxide with a phase transfer catalyst, a quaternary ammonium salt, in a carbon tetrachloride-aqueous system for the analysis of alkylnaphthalenes and a North Dakota lignite sample (3). The phase transfer catalyst transports the primary oxidant (periodate) into the organic phase as well as removes the carboxylate products from the organic phase. Improvement of the yield is believed to result from the avoidance of an inactive complex formed by the acid products with the ruthenium tetroxide. This method was used previously for the synthesis of fatty acids from 1-alkenes (7).

A number of model compounds were oxidized with ruthenium tetroxide in the two-phase system so that the method could be evaluated and compared with ruthenium tetroxide oxidation in acetonitrile. Reactions were carried out as reported earlier (3). Methods which did not require derivatization were devised for the analysis of the reaction products. The aqueous layer was analyzed on an ion moderated reverse phase HPLC column (Aminex HPX-87H) using 0.008 N H_2SO_4 as the eluent (1 ml/min) (refractive index detection). 3-Methyladipic acid was added as an internal standard and the system was calibrated for malonic, succinic, glutaric, adipic, and phthalic acids (single level calibration). The aqueous layer was also analyzed by GC with an AT-1000 phase fused silica capillary column. This column was calibrated for benzoic, phenylacetic and hydrocinnamic acids using 2-methylbutyric acid as the internal standard (multilevel calibration). The carbon tetrachloride layer was analyzed on an SE54 fused silica column calibrated for the aromatics, hydroaromatics and ketones and on the AT1000 column for the same acids as above. Diphenic acid was extracted from the carbon tetrachloride layer with NaOH and analyzed by weighing the crystals obtained after acidification of the extract.

High conversions were observed for the model compounds oxidized with RuO_4 in the two-phase system with a phase transfer catalyst (Table I). The conversions for diphenylmethane and bibenzyl were a little higher than when acetonitrile was used as the solvent. Another indication of higher reactivity for ruthenium tetroxide in the

Table I. Oxidation of Model Compounds With Ruthenium Tetroxide and Phase Transfer Catalyst (PT cat.)

Compound	Conversion	Product	Product Distribution	
			PT Cat.	Acetonitrile ^a
Indan	100%	1-Indanone	31	16
		Glutaric Acid	64	77
		Succinic Acid	5	7
Tetralin	100%	1-Tetralone	26	8
		Adipic Acid	50	75
		Glutaric Acid	24	17
Diphenylmethane	80%	Benzophenone	18	32
		Phenylacetic Acid	70	41
		Benzoic Acid	12	4
Bibenzyl	90%	Benzil	1	Trace
		Succinic Acid	43	35
		Hydrocinnamic Acid	45	63
		Phenylacetic Acid	2	--
		Benzoic Acid	10	--
Phenanthrene	100%	Phenanthrenequinone	2	4
		Diphenic Acid	92	91
		Phthalic Acid	6	5

^a = Data from reference 5.

two-phase system over the acetonitrile system is the greater yield of succinic acid as compared with hydrocinnamic acid in the oxidation of bibenzyl.

Oxidation of the alkyl substituent groups at the α -carbon to give the aryl ketone occurred in all model compounds. This was observed to a greater extent with indan and tetralin and to a lesser extent with diphenylmethane, as compared to the oxidation carried out with acetonitrile cosolvent. The ratio of glutaric to succinic acids resulting from the oxidation of indan was greater than 10 to 1 for both oxidation conditions. The ratio of adipic to glutaric acids from the oxidation of tetralin was higher when acetonitrile was used. The selectivity of the ruthenium tetroxide reagent for aryl versus alkyl attack thus varies in the two methods with the type of substrate being oxidized. Oxidation of the PAH, phenanthrene, showed no difference in product distribution between the two systems.

The oxidation of lignite (Beulah mine) with ruthenium tetroxide proceeded rapidly at room temperature. The products from the oxidation in the aqueous layer could not be analyzed directly by the HPLC method because the solution was too dilute. Diazomethane in ether was stirred with the aqueous layer for two hours to convert the acids to ether soluble esters, which were analyzed by GC (DB1701 capillary column) (see Figure 1). Table II lists major components and the relative GC peak area percentages.

The major components were aliphatic dicarboxylic acids and benzene polycarboxylic acids. Very low concentrations of aliphatic monocarboxylic acids were formed. Since succinic acid is present in the largest concentrations of the diacids, we may infer that a major structural feature of the lignite is a

TABLE II
 CARBOXYLIC ACIDS FROM RuO₄ OXIDATION OF BEULAH LIGNITE (See Figure 1)

Peak No.	Compound (as methyl ester)	Area, %
1	siccinic	10.7
2	methylsuccinic	1.1
3	glutaric	7.6
4	methyl glutaric	1.0
5	adipic	2.7
6	unknown	7.7
7	phthalic	0.7
8	terephthalic	0.4
9	isophthalic	0.2
10	unknown	3.2
11	benzene-1,2,4-tricarboxylic	3.4
12	benzene-1,2,3-tricarboxylic	4.2
13	benzene-1,3,5-tricarboxylic	0.7
14	benzene-1,2,4,5-tetracarboxylic	5.7
15	benzene-1,2,3,4-tetracarboxylic	4.5
16	benzene-1,2,3,5-tetracarboxylic	5.7
17	benzene pentacarboxylic	7.3

dimethylene bridge occurring between aromatic moieties or present in a hydroaromatic such as 4,5-dihdropyrene. The model compound studies with diphenylmethane show that this method is limited in its applicability to the determination of single methylene bridges. Since malonic acid was produced in only trace amounts from oxidation of diphenylmethane, the absence of malonic acid in the lignite oxidation products does not rule out methylene bridges between aromatics in the coal.

The greater amounts of benzenepolycarboxylic acids relative to the benzenedicarboxylic acids which would be expected from naphthalene oxidation may seem surprising, however some of the acid groups were undoubtedly present in the coal before the oxidation. This aspect is being studied by labeling the original acid groups.

In order to fully interpret the results of the lignite oxidation with this reagent, the oxidation of several more model compounds will be studied. Quantitation of the methyl esters of the products from the lignite oxidation is also in progress.

Literature Cited

1. Deno, N.C.; Greigger, B.A.; and Stroud, S.G., Fuel (1978) 57, 455.
2. Liotta, R.; and Hoff, W.S., J. Org. Chem. (1980) 45, 2887; Hessley, R.K.; Benjamin, B.M.; and Larsen, J.W., Fuel (1982) 61, 1085.
3. Olson, E.S.; and Farnum, B.W. Amer. Chem. Soc., Div. Fuel Chem. Preprints (1981) 26, no. 1, 60.
4. Lee, D.G.; and van den Engh, M. in Oxidation in Organic Chemistry, Part B, W.S. Trahanovsky, ed., Academic, 177 (1973).
5. Stock, L.M.; and Tse, K.-t., Fuel (1983) 62, 974.

6. Carlsen, P.H.J.; Katsuki, T.; Martin, V.S.; and Sharpless, K.B., J. Org. Chem. (1981) 46, 3936.
7. Foglia, T.A.; Barr, P.A.; and Malloy, A.J., J. Amer. Oil Chemists' Soc. (1977) 54 858A.

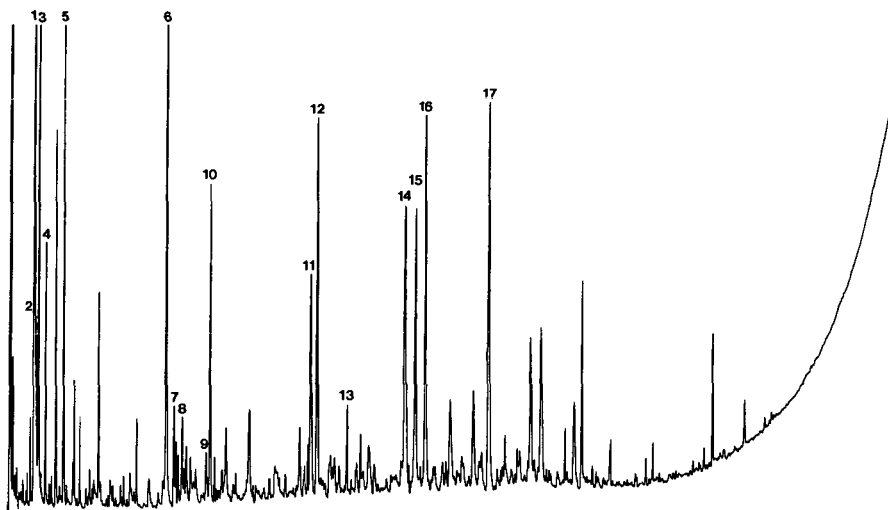


Figure 1. Methyl esters of products of ruthenium tetroxide oxidation of Beulah 3 lignite. DB1701 (0.25 μ) FSOT 15m x 0.32 mm. On-column injection. FID. H₂ carrier (41 cm/sec at 240°C).

FUEL NITROGEN EVOLUTION: COUPLING BETWEEN RANK AND HEATING CONDITIONS. J.F.Freihaut,
United Technologies Research Center, East Hartford, CT 06108.

A range of coals from a variety of geologic provinces have been devolatilized using both heated grid and flash lamp apparatus. Lignite, sub-bituminous, high, medium and low volatile bituminous and anthracite samples have been investigated. Final particle temperatures of 400 to 1500 C were obtained with the heated grid and heating rates approaching 10^6 C/sec in the flash lamp apparatus. In inert conditions and moderate heating rates (10^3 °C/sec or less) the evolution of fuel nitrogen mirrors, on a mass fraction basis, the evolution of parent coal as char, tar or light gas. The evolution of fuel nitrogen as a light gas is observed to be coupled to the fate of primary tars as they evolve. Thus the evolution of fuel nitrogen as a light gas during pyrolysis is observed to be rank dependent via the thermal stability characteristics of the primary tars.

Flash Pyrolysis of Cellulose in a Micro Fluidized Bed

T. Funazukuri, R.R. Hudgins and P.L. Silveston

Department of Chemical Engineering
University of Waterloo
Waterloo, Ontario, Canada N2L 3G1

INTRODUCTION

Short contact time or flash pyrolysis is one of the alternatives under consideration for the conversion of biomass into liquid or gaseous fuel, or perhaps into chemicals feedstock. A variety of compounds are formed in flash pyrolysis so that it would be desirable to be able to predict yields of at least the major products as a function of the pyrolysis device and operating conditions such as heating rate of the biomass, final temperature, particle size, gas phase composition. As a contribution to this goal, this paper considers the flash pyrolysis of micro crystalline cellulose powder and particles in a fluidized bed. By flash pyrolysis, we refer to heating rates (at the particle surface) greater than 100°C/s, final temperatures generally greater than 500°C and contact times of the order of 1-2 seconds or less. Compared with the vast literature on slow pyrolysis of cellulose the literature on flash pyrolysis is very small. A few studies have been made using a Pyroprobe or a Curie point pyrolyzer (Iglauer et al. (1974); Ohnishi et al., (1975) Hileman et al., (1979) and a fluidized bed (Barooah and Long, 1976); Maa and Bailie, (1978); Scott and Piskorz, (1981.) Irradiation was used by Martin (1965) and Shivadev and Emmons (1974) as a heat source. Lewellen et al. (1977) and Hajaligol et al. (1982) pyrolyzed filter paper suspended between two massive electrodes. The latter team succeeded in producing quite a wide range of temperatures and heating rates. Unfortunately, in most past studies, weight loss measurement and analysis of volatile products were not carried out simultaneously. Indeed, identification of volatile products usually came from investigations where the pyrolysis reactions went nearly to completion. In such cases, the product distribution might result from not only cellulose pyrolysis but also from secondary cracking and perhaps even char gasification.

EXPERIMENTAL SYSTEM, ANALYTICAL TECHNIQUES AND STUDY MATERIALS

Figure 1 shows the fluidized bed system used in this study. Details of the bed itself are given in Figure 2. The assembly shown in Figure 2 was built by Scott and Piskorz (1981) and used by them to study the flash pyrolysis of coal and wood.

Pyrolysis occurs in a bed of fluidized sand supported by a porous stainless steel distribution plate. The net reactor volume is 23 mL. Fluidizing gas is introduced from the bottom through a preheating tube 1 meter in length. As Figure 1 shows, the reactor sits in a three-zone Lindberg electric tube furnace, 91 cm in length. The reactor was located in the upper zone and the preheating tube of the reactor was situated in the bottom two zones and was sufficient to heat up the fluidizing gas to bed temperature before it entered the reactor.

The low rate of cellulose feed needed for the system was achieved using an entrainment feeder described by Scott and Piskorz (1981). Feed rate

could be adjusted from 5 to 100 g/h with this unit. Cellulose entrained in carrier gas entered the bed through the central, downwardly directed tube in Figure 2. The tip of this tube was immersed in the fluidized sand. The concentric tube, terminating in a 6.3 mm o.d. outlet was originally supposed to introduce a cold quench gas into the reactor. In this study, it served as sampling line to a Carle G.C. with a heated sampling loop. This G.C. periodically sampled the off gas and was used to insure the assembly operated at steady state.

Most of the volatile products and gas introduced to fluidize the sand bed and to entrain the cellulose feed left the reactor through the 12.7 mm o.d. outlet seen in Figure 2. This outlet was connected to the first of three, water-cooled glass condensers by about 40 cm of Teflon tubing. Almost all the tar formed and the char eluted from the bed was trapped in the condensers or in the connecting tubing. The remaining tar was caught in a glass-wool-filled column. After passing through two further columns to strip out water, the gas was collected in an inflatable bag.

A run using this equipment lasted about 30 minutes once steady state was established. Weighing provided the amount of cellulose fed to the fluidized bed and the char caught in the bed. Washing of the glass wool, tubing and condensers with ethanol provided a measure of the char eluted (by weighing the residue on filtering the solvent) and of the tar formed by weighing the residue after filtering and evaporating the solvent. GC analysis of the gas bag content and measurement of the gas volume gave the non-condensable, volatile products produced.

Analyses were performed using a dual channel GC equipped with a 1.83-m 100/120 mesh Porapak T column on one channel and a 1.83-m 80/100 mesh Porapak Q column in the other. Both channels used FID's and temperature programming was employed. A second chromatograph equipped with a 1.83-m mesh 5A molecular sieve column was also used on the gas bag to measure CO, CO₂ and water.

Tar samples were treated with N-trimethyl silylimidazole in pyridine. This reagent creates a volatilizable compound from levoglucosan; other tar compounds are also converted to volatilizable substances by silylation. Silylated tar solution was injected onto either a 1.83-m 6% OV-101 on 80/100 mesh Chromosorb column or a similar Chromosorb column treated with 6% SE-52. Peak identification was by means of pure levoglucosan dissolved in N-trimethyl silylimidazole.

A microcrystalline cellulose (MCP) furnished as a 200/270 mesh powder was the primary test material. Cellulose particles, as a 20/40 mesh material were made by pelletizing the MCP in a press, crushing the pellets, and then sieving. The particles permitted a test of a particle size on product distribution and pyrolysis rate to be made. Limitations of attainable fluidization velocity limited the size to 20/40 mesh.

Cellulose conversion and product distribution were measured at fluidized bed temperatures between 310 and 770°C. Most experiments were performed in an N₂ atmosphere, but measurements were made as well with CO, CO₂ and a H₂-N₂ mixture as the fluidizing gas. Contact time of cellulose in the bed was not less than 0.5 s (the residence time of the fluidizing gas in the bed), and probably did not exceed 2 to 3 seconds. Based on work with coal,

Tyler (1979) estimates that the heating rate of fine particles in a fluidized bed must be greater than 1°C/ms.

EXPERIMENTAL RESULTS

CO, CO₂ and H₂ pyrolysis yields from cellulose powder are shown in Figure 3. The carbon oxides are the major products. H₂ yields are the same order of magnitude as the hydrocarbon yields. A transition in behaviour occurs around 500°C. Above this temperature the CO yields increase at slower rate but the CO₂ yields level off. Char yields were less than 10 wt% of the sample fed above 500°C so that pyrolysis is essentially complete. The abrupt change in the CO₂ yield reflects, evidently, completion of the cracking reaction.

Yields of light hydrocarbon by carbon number vs temperature appear in Figure 4. A change in slope at about 500°C is evident. With the exception of flattening of the C₃ and C₄ yields above 700°C, the light hydrocarbon behaviour resembles the yield behaviour seen for CO. Probably cracking of C₃⁺ hydrocarbons at 700°C+ accounts for the flattening observation.

The major liquid oxygen-bearing molecules detected were acetaldehyde, acrolein, furan and acetone. While Hajaligol et al. (1982) measured relatively high methanol yields, 1 wt% of the pure cellulose sample, the yields in this study were as low as 0.1 wt% of the sample. Figure 5 shows yields of acetaldehyde while Figure 6 shows those of acetone plotted versus temperature. Data for MCP powder and 20/40 mesh pellets are plotted together. Particle size quite clearly does not affect yield. Measurements taken in different atmospheres are also shown. Once again, the atmosphere surrounding the pyrolyzing material does not change the yield temperature behaviour. Both these observations apply to the CO, CO₂ and H₂ yields and for the light hydrocarbons.

Acetaldehyde yield data (Figure 5) resembles that for CO, while the acetone yields are much more like the data obtained for CO₂ (Figure 3). Indeed, of the other two oxygen containing hydrocarbon which could be accurately measured, acrolein and furan, the former exhibited the CO behaviour with temperature while the latter appeared to show the CO₂ behaviour.

The yields of levoglucosan are shown in Figure 7. Particle size and fluidizing atmosphere do not affect the yields. Replotting the data against weight loss of the original MCP or cellulose particles permits a comparison with the yields data obtained by other workers for slow pyrolysis. Figure 8 provides the comparison. Yields found in this study were smaller by a factor of 2 to 3 than yields measured under slow pyrolysis. It is surprising that the agreement among the data of different investigators is so poor.

The difference between our data and others shown in Figure 8 is that heating and contact times in our study were perhaps an order of magnitude greater than those used by the others. If levoglucosan is a primary product of cellulose pyrolysis, as has been proposed, shorter contact times should increase not decrease yields. Evidently, at high temperatures, some of the cellulose molecules can be directly decomposed into smaller weight fragments and these free radicals can combine to form volatile products. Levoglucosan would not be formed as an intermediate for this route to the lower molecular weight products. This may be the explanation for the deviation of our data from those

obtained by Tsuchiya and Somi (1970) and some of the data of Shafizadeh et al. (1978a, 1979b).

Closure of the material balances to about 2% when MCP was pyrolyzed, permits a reliable picture to be drawn of the product distribution between solid tar, liquid and gas for flash pyrolysis in a fluidized bed. This distribution is shown as a function of temperature in Figure 9. Pyrolysis atmosphere and the particle size of cellulose up to 20 to 40 mesh do not affect the distributions. The levoglucosan product is also shown.

It is clear from the figure that the liquid-tar fraction of the products can be maximized by operating between 450 and 650°C. Higher temperatures increase gas production while lower temperatures result in large char residues.

The remarkably similar yield vs. temperature behavior seen in Figures 3 to 6 suggest cross plotting of the yield data. When this is done it is found that all the pyrolysis products with the exception of levoglucosan and other tar components plot as simple logarithmic functions of the form

$$Y_x = a Y_{CO}^b \quad (1)$$

against CO yield (Y_{CO}) or against CO_2 yield. Examples of such plots appear in figures 10 and 11. The functions are independent of temperature, gas atmosphere, and particle size. Linear relationships on these log-log plots hold very closely from CO yields of from 0.5 to 20 weight percent. Data of other studies, including Tsuchiya and Sumi (1970) who worked with slow pyrolysis, also give linear cross plots and both for furan and the light hydrocarbons these data agree quite well with what was observed in this study even though the pyrolysis technique differed substantially. Probably then, Equation 1 and its parameters are independent of the type of flash pyrolysis unit. Agreement was poorer for other products so probably Equation 1 cannot be generalized to slow pyrolysis. Yield relationships appear to offer a useful means of predicting product distribution in flash pyrolysis operations. The relationships are developed and discussed in more detail in a recent paper by Funazukuri et al. (1984).

REFERENCES

- Barooah, J.N., and Long, V.D., (1976) "Rates of thermal decomposition of some carbonaceous materials in a fluidized bed", *Fuel*, 55, 116-120.
- Funazukuri, T., Hudgins, R.R. and Silveston, P.L., (1984) "Prediction of Volatile Products from Thermal Conversion of Cellulose by Correlation with Carbon Oxides in the Gas", Preprint I.G.T. Conference on Fuels from Biomass and Wastes, Lake Buena Vista, Florida (February).
- Graham, R., Bergougnou, M.A., Mok, L.K. and de Lasa, H.L., (1982) "Flash pyrolysis (ultraprolysis) of biomass using solid heat carriers", research paper presented at Fundamentals of Thermochemical Biomass Conversion: An International Conference, Boulder, Colorado, October.

Hajaligol, M.R., Howard, J.B., Longwell, J.P. and Peters, W.A., (1982), "Product compositions and kinetics for rapid pyrolysis of cellulose", I/EC Process Des. Dev., 21, 457-465.

Halpern, Y. and Patai, S., (1969) "Pyrolytic reactions of carbohydrates. Part V. Isothermal decomposition of cellulose in vacuo", Israel J. of chem., 7, 673-683.

Hileman, F.D., Wojcik, L.H., Futrell, J.H. and Einhorn, I.N., (1976) "Comparison of the thermal degradation products of α -cellulose and douglas fir under inert and oxidative environments" in Thermal Uses and Properties of Carbohydrates and Lignins, Edited by Shafizadeh, F., Sarkanen, K., and Tillman, D.A., 49-71, Academic Press.

Iglauer, N., and Bentley, F.F., (1974) "Pyrolysis GLC for the rapid identification of organic polymers", J. of Chromatog. Sci., 12, 23-33.

Lewellen, P.C., Peter, W.A. and Howard, J.B., (1977) "Cellulose pyrolysis kinetics and char formation mechanism", Sixteenth International Symp. on Combustion, 1471-1480.

Maa, P.S. and Bailie, R.C., (1978) "Experimental pyrolysis of cellulosic material", research paper presented at AIChE 84th National Meeting, Atlanta, February.

Martin, S., (1965) "Diffusion-controlled ignition of cellulosic materials by intense radiant energy", Proc. Tenth International Symposium on Combustion, 877-896.

Scott, D.S. and Piskorz, J., (1981) "Flash pyrolysis of biomass", fuels from biomass and wastes, Edited by Klass, D.L. and Emert, G.H., 421-434, Ann Arbor Science, Michigan.

Shafizadeh, F. and Bradbury, A.G.W., (1979) "Thermal degradation of cellulose in air and nitrogen at low temperatures", J. of Appl. Polym. Sci., 23, 1431-1442.

Shivadev, U.V. and Emmons, H.W., (1974) "Thermal degradation and spontaneous ignition of paper sheets in air by irradiation", Combustion and Flame, 22, 223-236.

Tsuchiya, Y. and Sumi, K., (1970) "Thermal decomposition products of cellulose", J. of Appl. Polym. Sci., 14, 2003-2013.

Tyler, R.J., (1979) "Flash pyrolysis of coals. 1. Devolatilization of a Victorian Brown coal in a small fluidized-bed reactor", Fuel, 58, 680-686.

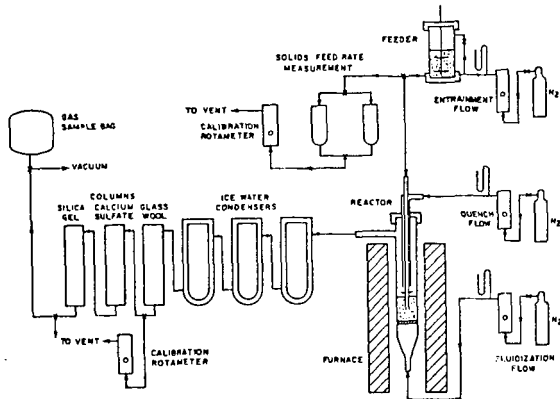


Figure 1 Micro Fluidized bed pyrolysis system (Scott and Piskorz, 1981)

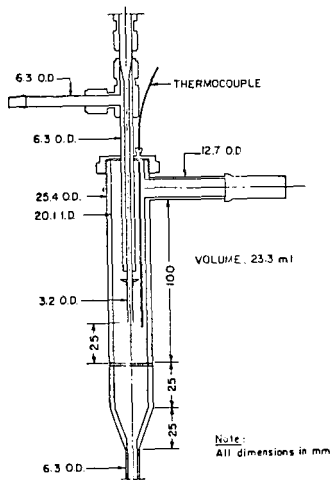


Figure 2 Construction details of fluidized bed (Scott and Piskorz, 1981)

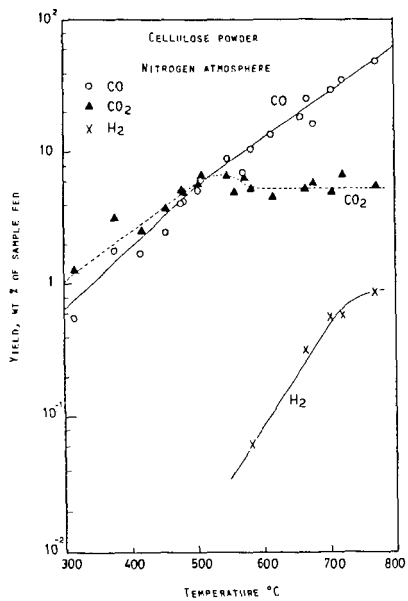


Figure 3 Light gas pyrolysis yield from MCP

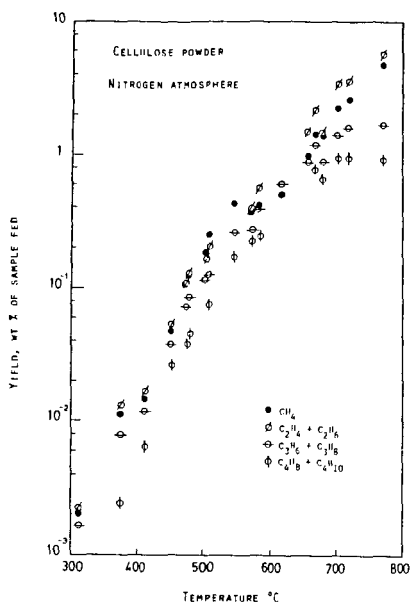


Figure 4 Yield of light hydrocarbon from MCP

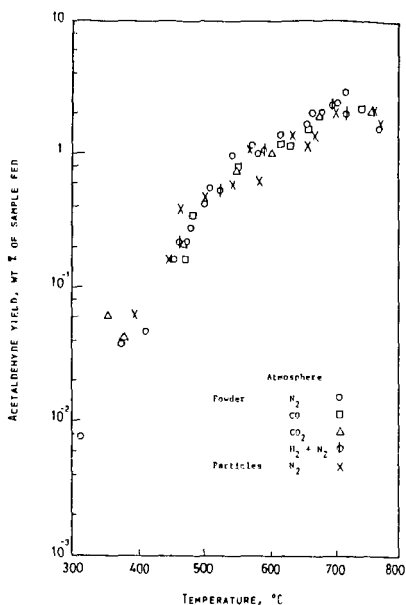


Figure 5 Yield of acetaldehyde from MCP and Cellulose particles

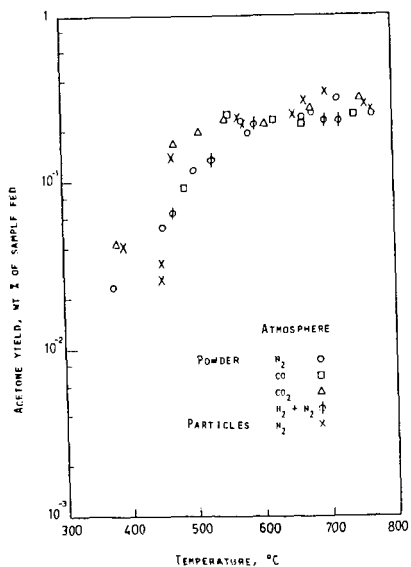


Figure 6 Yield of acetone from MCP and cellulose particles

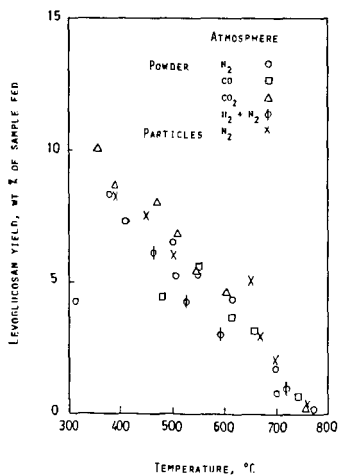


Figure 7 Yield of levoglucosan from MCP and cellulose particles

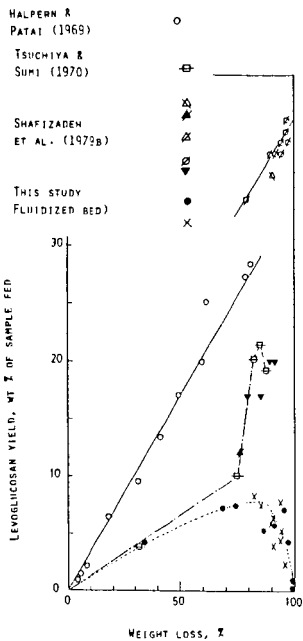


Figure 8 Levoglucosan yield as a function of weight loss with a comparison with slow pyrolysis data

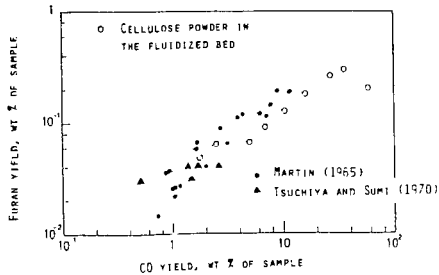


Figure 11 Cross plot of furan yields and CO yields from MCP

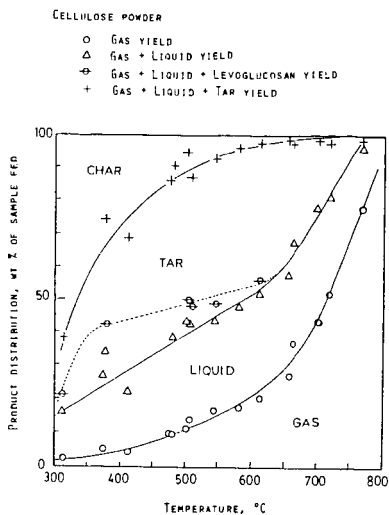


Figure 9 Product distribution in flash pyrolysis of MCP

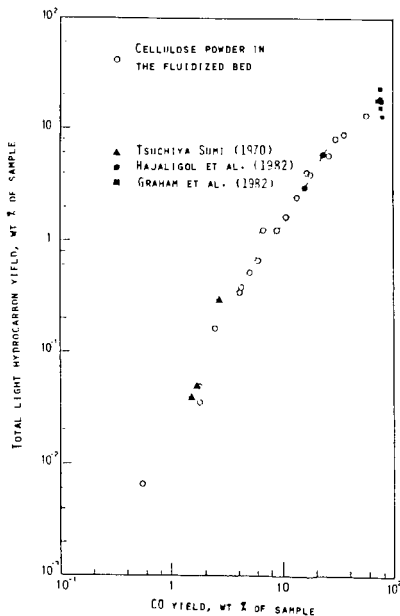


Figure 10 Cross plot of light hydrocarbon yields and CO yield from MCP

THE PREMIUM COAL SAMPLE PROGRAM AT THE ARGONNE NATIONAL LABORATORY

Karl S. Vorres
Chemistry Division, Bldg 211
Argonne National Laboratory
9700 South Cass Avenue
Argonne, Illinois 60439

PURPOSE OF THE PREMIUM COAL SAMPLE PROGRAM

The purpose of the Premium Coal Sample Program is to provide the coal science research community with long term supplies of a small number of premium coal samples that can be used as standards for comparison. The premium coal samples produced from each coal and distributed through this program will be as chemically and physically identical as possible, have well characterized chemical and physical properties, and will be stable over long periods of time. Coals will be mined, transported, processed into the desired particle and sample sizes, and packaged into environments as free of oxygen as possible. Humidity will also be controlled to keep the coals as pristine and in as stable of a condition as possible.

The need for a Premium Coal Sample Program was expressed at the Coal Sample Bank Workshop held March 27 and 28, 1981 in Atlanta, Georgia.

WHAT A PREMIUM SAMPLE IS

A premium coal sample has been specially selected, processed and stored to keep it as close to its original condition as possible. Specifically:

- Contact with oxygen has been minimized at all stages from mining, transport and processing in a nitrogen filled facility to sealing in amber colored glass vials.
- Relative humidity and temperature are controlled in the processing facility to maintain the equilibrium moisture of the original coal.
- Uniformity of samples is achieved by processing about 750 kg of coal in a single batch, mixing thoroughly in a special blender, and finishing with a spinning riffler to assure well-mixed samples. Activation analyses have confirmed the thoroughness of the mixing.
- Stability of the samples is maximized by sealing in amber-colored glass with a fuel-rich hydrogen-oxygen flame.
- Secure, long-term supplies result from an initial production of 10,000 five gram ampoules and 5,000 twenty gram ampoules with 50 five gallon sealed glass carboys in reserve for future ampoule production from each metric ton sample of coal.
- Some special needs can be met from lumps stored in argon in two reserve 55 gallon drums, and one 15 gallon drum as part of the original sample. A separate nitrogen filled glove box will be used for processing these requests.

SELECTION, MINING, AND TRANSPORT

Initially the coals have been selected to cover a wide range of degrees of coalification, mineral content, and sulfur content as well as commercial significance. The first three will be low-, medium- and high-volatile bituminous coals. The next two are planned to be lignite and sub-bituminous coals. These samples will be channel samples, representing a uniform cross section of the seam from top to bottom. Mining, under the supervision of coal geologists, involves removal of large lumps from a freshly exposed face to special plastic containers, transfer to stainless steel drums at the surface, purging with argon, transfer to refrigerated truck and immediate transport to the processing facility. A careful description of the geology of the sample area and location will be prepared and available as a referencable document.

SAMPLE PROCESSING

At the processing facility, a sample of argon from the coal drum will be analyzed to establish the relative humidity for the nitrogen filled processing facility. The stainless steel drums will be loaded into an airlock, which is then purged with nitrogen. The drums will be emptied into a crusher to reduce the size to 1/4", then pulverized in a cooled impact mill to obtain -20 mesh material. Coarse material will be recycled. The pulverized material will be collected in a nitrogen filled mixer-blender selected for gentle but thorough mixing. After thorough mixing the pulverized coal will be conveyed to a spinning riffler and sealed in 20 gram ampoules and 5 gallon glass carboys. The contents of some of the carboys will then be recycled to the pulverizer and crushed to pass a 100 mesh screen. After thorough blending this material will be conveyed to the packaging unit for sealing in 5 gram amber colored ampoules and 5 gallon borosilicate glass carboys. One of the goals of the Program is to complete the processing within seven days of exposing the mine face. Figure 1 indicates the coal storage system for a metric ton sample. Figure 2 is a block diagram of the coal sample preparation.

CHARACTERIZATION

The coals will be characterized by chemical and physical analysis. Results will be available for each coal in the form of a printed sample announcement. Requests to be placed on a mailing list should be sent to the author. The requestor should include mailing address, telephone number and research interests.

The analyses will include proximate, ultimate, calorific values, sulfur forms, equilibrium moisture, oxygen by neutron activation analysis, maceral analysis, Gieseler plasticity for the bituminous coals, and mineral matter major elements among others. Multiple laboratories will be involved in the analyses. Round robin analyses are also being organized.

A variety of stability monitoring tests will be used including evolved gas analysis. In addition the bituminous samples will be monitored by repetitive Gieseler plasticity analyses.

AVAILABILITY

Initial samples are expected to be available in fall, 1984. Samples will be made available to research personnel at a nominal replacement cost. A special glove box filled with nitrogen is available to transfer contents of ampoules to special sample holders on request. Also, a very limited quantity of lump coal, stored under similar inert conditions will be available on special request for special physical property measurements. The processing facility can be made available for occasional processing of special samples.

INFORMATION ON SAMPLES

Each recipient of samples is asked to provide either a literature reference to papers in widely circulated journals, or a copy of less widely circulated reports and papers, to be shared with other users of the samples. Listings of these references will be available on request to the author (phone 312-972-7374) either in printed versions or via computer terminal. The Premium Coal Sample Program expects to work with other coal sample programs in providing samples and sharing information.

Following the reports from the use of a number of samples, workshops are planned to facilitate sharing research results and to foster basic understanding of the chemistry and physical properties of the coal.

USERS ADVISORY COMMITTEE

A Users Advisory Committee provides useful suggestions to the Program Manager. This group includes: Dr. Blaine Cecil, U. S. Geological Survey; Dr. Marvin Poutsma, Oak Ridge National Laboratory; Dr. Ronald Pugmire, University of Utah; Dr. William Spackman, Pennsylvania State University; Dr. Irving Wender, University of Pittsburgh; Dr. Randall Winans, Argonne National Laboratory; Dr. John Young, Argonne National Laboratory.

ACKNOWLEDGEMENTS

The author gratefully acknowledges the support of the U. S. Department of Energy, Office of Basic Energy Sciences, Chemical Sciences Division.

Figure 1. Coal storage system.

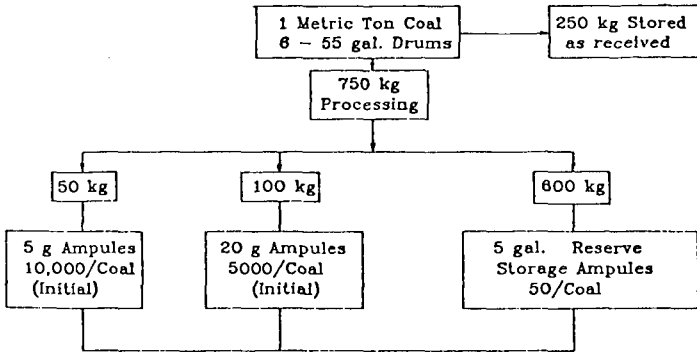
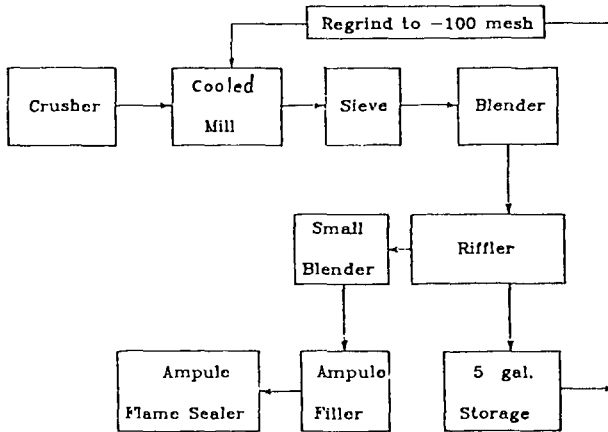


Figure 2. Coal Sample Preparation - Block Diagram



STUDIES OF COAL AND CHAR PROPERTIES

Leslie L. Isaacs
Chemical Engineering Department
The City College of the
City University of New York
New York, New York 10031

INTRODUCTION

A thermodynamic data base is required both for the understanding and the proper design of processes utilizing coal and coal products. Since it is impractical to acquire the necessary data for each process and for each individual coal, it is important to establish predictive correlations between the physical and chemical parameters of the materials and their thermodynamic properties.

Heat capacity data can be used to calculate the variation of the thermodynamic properties, H,S,G, etc. with temperature. Conventional correlations of the heat capacities rely on the additivity approach, namely, that the total heat capacity of a dry coal is a matter, and inorganics (1,2,3). The correlation is successful in the sense that heat load calculations within 20% are possible.

The method has serious shortcomings inasmuch as it does not take into account the thermal history of the chars, the variability of the char structure with the rank of the parent coal and the interactions between the organic and inorganic components of the coal and/or of the char. Factors which affect the heat capacity of coals are:

- o The rank and inorganic matter content of the coal;
- o The moisture content;
- o The aging history of the coal sample.

Factors which affect the heat capacity of chars are:

- o The rank and inorganic matter content of the parent coal;
- o The gaseous atmosphere present during pyrolysis;
- o The thermal history of the char.

The history of a char is determined by:

- o The pyrolysis temperature;
- o The rate at which the coal temperature is increased from ambient to pyrolysis temperature;
- o The residence time of the char at the pyrolysis temperature.

Available data (4,5,6,7,8,9) for chars and coals cover limited temperature ranges and the thermal histories and compositions of the char samples are often ill-defined or unavailable. Thus, it was not possible to derive a universal correlation for the heat capacity, taking the listed factors into account.

In an attempt to establish a thermodynamic data base for coals and chars and to assess the relative importance and effect of the factors listed, on the heat capacity, extensive work was undertaken and is continuing at City College (10,11,12,13). In this presentation we will limit ourselves to the discussion of results on chars.

EXPERIMENTAL DETAILS

A suite of samples was prepared for experimental work in a systematic manner. Three coals of different rank and petrography were used as starting materials. These selected 'parents' were a North Dakota lignite, an Illinois No. 6 HVB sub-bituminous, and a Virginia HVA sub-bituminous coal. The carbon content of these coals range from 63 to 73 weight percent (dry basis). The coals were ground in a ball mill to finer than 250 mesh. Half of the coal grounds were demineralized using the acid wash procedure (14). The other half was used without further treatment.

The pyrolysis was done in an inert atmosphere, by sweeping the furnace with nitrogen gas (1-SCFM flow rate). The samples were heated to the pyrolysis temperature with a relatively slow heating rate of 5°C per minute. Both pyrolysis temperature and residence time at temperature were used as variables for establishing thermal histories for the chars. Pyrolysis temperatures used were 500°C, 700°C, 900°C and 1100°C. Residence times were 0.1, 1, 2, and 24 hours. The char and coal samples were characterized by composition, porosity, pore size distribution and X-ray diffraction.

Heat capacity data were collected between 75K and 300K in a cryostat which was modified in order to use the adiabatic shield technique of calorimetry (15,16). To eliminate the contributions of adsorbed water to the specific heat, the experimental samples were vacuum dried at 110°C prior to loading into the calorimeter. The calorimeter was kept constantly under vacuum during the experimental runs. Each specimen was measured at least twice in separate experimental runs. The accuracy and reproducibility of the calorimetric data, and the validity of the data reduction scheme

were checked by the measurement and the determination of the heat capacity of copper and graphite samples (17,18,19). The data is judged reliable to one percent accuracy in the temperature range of 75K to 220K.

In the 150K to 1000K range heat capacity data was collected using a Differential Scanning Calorimeter (DSC). The heat capacities were measured under an Argon atmosphere. The raw DSC data were converted into heat capacities by calibration of the instrument using a Sapphire heat capacity standard. The accuracy of the DSC data is estimated at 2 percent.

RESULTS; EFFECT OF INORGANIC PHASE

The generality of the additivity hypothesis for the heat capacity of the chars was tested by determining the heat capacities of chars prepared from untreated coals, i.e., including the inorganic matter, and from coals which have been demineralized. The experimental data are shown in Figures 1,2, and 3. It was found that for the chars prepared from Illinois and Virginia coals the total heat capacity could be expressed on a weight basis as:

$$C_s = (1-w)C_o + wC_a \quad 1)$$

Where C_s , C_o and C_a are the heat capacities of the char, ash free organic matter and ash respectively and w is the weight fraction of ash in the char. The temperature dependence of C_a in the 75K to 300K range varies depending on the origin of the ash.

The preparation of lignite based char from untreated coal is complicated by the catalytic effect of the included inorganic matter on the pyrolysis reaction. Both the rate of pyrolysis and the structure of the char formed are affected by the presence of inorganic matter. Therefore, it is not surprising that the total heat capacity of a lignitic char does not follow the additivity hypothesis.

The contribution of the ash to the total heat capacity of the char is not trivial. On a weight basis the ash heat capacity at room temperature is about four times greater than the heat capacity of the corresponding ash free organic matter in the char.

EFFECT OF PYROLYSIS TEMPERATURE AND CHAR PARENTAGE

The dependence of the heat capacities on pyrolysis temperature and origin was examined by determination of the heat capacities of chars prepared at several pyrolysis temperatures from demineralized coals with one hour residence time at the pyrolysis temperatures. In order to compare the data on the different chars quantitatively, the measured heat capacities must be corrected for residual ash contributions and need to be converted from a per unit mass to a per mole (ash free) atom basis.

The heat capacities at a given temperature, of chars of identical thermal history, are not simply related to the rank of the parent coal. As seen in Figure 4 the lignite chars have the highest heat capacities and Virginia chars the lowest at low temperatures. However, this order is reversed at high temperatures.

In Figures 5, 6, and 7 the dependence of the char heat capacities on pyrolysis temperature are shown. The behavior is again complex. On a unit mass basis the heat capacities for a char of a given parentage shows cross-overs with temperature. This phenomenon is especially pronounced for the chars originating from the higher ranked coals.

EFFECT OF RESIDENCE TIME AT PYROLYSIS TEMPERATURE

Demineralized Virginia chars prepared at 1100°C were used to investigate the effect of residence time on the heat capacities. The volatile matter was effectively removed from the coal by the time the pyrolysis reactor reached the pyrolysis temperature. Thus, the only further changes that occur as a function of time are dehydrogenation and graphitization (structural ordering) of the char. The heat capacities of the chars decrease with increasing residence time up to 1 hour, then increase for a 24-hour char. We show this behavior as heat capacity isotherms in Figure 8. This is interpreted as indicating that equilibration to a final H/C ratio at the pyrolysis temperature is a fast process relative to the ordering of the char which must take place by solid phase diffusion.

CORRELATION OF THE CHAR HEAT CAPACITY WITH PHYSICAL PARAMETERS

The primary interest in this research was to find a correlation between the heat capacities and physical parameters that characterize the chars. The parameters should include, at least, the char composition and the thermal history of the chars.

The heat capacity of a solid is reasonably well-described by the Debye theory. One can invert the heat capacity C_V using the well-known relation:

$$C_V = 9R(T/\theta)^3 \int_0^{\theta/T} \frac{u^4 e^{-u} du}{(e^u - 1)^2} \quad 2)$$

To obtain the effective Debye temperature θ as a function of temperature T , the measured specific heat obtained at constant-pressure conditions can be used instead of the constant-volume specific heat C_V , called for by the theory, since for a solid the difference between C_p and C_V is within experimental error at least below 300K. Values of the integral in Equation 2 can be found in standard tables (20). We were able to correlate $\theta(T)$ for the chars with parentage, composition and pyrolysis temperature T_p (in °K).

To apply the Debye model to a char, the ordinary theory must be modified (21). Consider that the carbon and "other kinds" of atoms of the char are distributed randomly in the solid matrix. Since the chars consist of about 90% (or more) carbon atoms, only carbon-carbon and carbon-"other" atom interactions need be considered for calculation of the char vibrational frequency spectrum. If the char consisted of carbon atoms only, the spectrum would depend solely on the arrangement of the carbon atoms in the matrix. The orderliness of this arrangement depends on the pyrolysis temperature (and residence time). This suggests use of the pyrolysis temperature T_p , as a nondimensionalizing parameter to calculate θ as a function of a reduced temperature $T_r = T/T_p$. This allows us to compare the effective Debye temperatures for chars of the same parentage but different thermal histories.

The carbon-other atom interactions will modify the vibrational spectrum by the addition of singular vibrational modes which will add onto the spectrum in the form of Einstein-like terms. These terms should, to the lowest order, be proportional to the product of the carbon atom abundance and the "other" atom abundance.

The correlation which was found (12) to fit the suggested model, using data from 75K to 300K, is given by:

$$\theta(T_r) = \theta_0(T_r) \exp [I(T_r)/x(1-x)] \quad 3)$$

where $1-x$ = the atomic fraction of carbon in the ash-free char,

$\theta_0(T_R)$ = a Debye temperature at a given value of T_R
for a char consisting of carbon atoms alone;

$I(T_R)$ = an interaction parameter connecting the carbon
to the "other" atoms;

θ_0 and I were found by trial and error fitting of Equation 3
to the experimental data.

At the present time we are continuing the interpretive work
to refine the correlation equation and to include into it the
residence time dependence of the heat capacities.

REFERENCES

1. N.Y. Kirov, Br. Coal Util. Res. Assoc. Mon. Bull., 29, 33 (1965).
2. W. Eiserman, P. Johnson and W.L. Conger, Fuel Processing Technology, 3, 39 (1980).
3. D. Merrick, Fuel 62, 540 (1983).
4. E. Melchoir and H. Luther, Fuel 61, 1071 (1983).
5. R.P. Tye, A.O. Desjarlais and J.M. Singer, High Temperature - High Pressures, 13, 57 (1981).
6. V.I. Kasatochkin, K. Usenbaev, V.M. Zhadanov, K. Sabyraliev, M. Rasalbaev, and K. Zhumaliev, Dokl. Akad., Nauk, S.S.S.R., 216, 93 (1974).
7. Internal Report of the Thermodynamics Research Group, Bartlesville Energy Research Center, DOE, "Thermal Data on Gasifier Streams from Synthane Test; (1973).
8. P. Delhaes and Y. Hishiyama, Carbon, 8, 31 (1970).
9. K. Kamiya, S. Mrozowski and A.S. Vagh, Carbon, 10, 267 (1972).
10. W.Y. Wang, Ph.D. Thesis submitted to the Graduate Faculty of Engineering, The City University of New York (Sept. 1981).
11. L.L. Isaacs and W.Y. Wang, "The Specific Heats of Coals and Chars" in the Proceedings of The Governor's Conference on Expanding the Use of Coal in New York State (M.H. Tress, J.C. Dawson, eds.) pp. 379-384 (May 1981).
12. L.L. Isaacs and W.Y. Wang, "Evaluation and Correlation of Coal Char Thermodynamic Functions" in Chemical Engineering Thermodynamics, (S.A. Newman, Ed., Ann Arbor Science) pp. 451-459 (1982).

REFERENCES (cont.)

13. L.L. Isaacs and E. Fisher, Preprint of Paper, A.C.S., Div. of Fuel Chem. 28, #2, pg. 240 (1983).
14. W. Radmacher and P. Mohrhauer, Brennst. Chemie, 236 (1955); M. Bishop and D.L. Ward, Fuel, 37, 191 (1968).
15. L.L. Isaacs and R.L. Panosh, Argonne National Laboratories' Communication Article ANL-MS01270 (1970).
16. L.L. Isaacs, Symposium, Cryogenic Experimental Apparatus, AIChE 71st Annual Meeting (1978).
17. G.T. Furakawa, W.G. Shaba and M.L. Reilly, NSROS-NBS-18, U.S. GPO, Washington, DC (1968).
18. W. Desorbo and W.W. Tyler, J. Chem. Phys. 21, 1660 (1953).
19. L.L. Isaacs and W.Y. Wang, "Thermal Properties of POCO-AMX Graphite", Thermal Conductivity 17 (J.G. Hust, Ed., Plenum Publishing Corp.) pg. 55 (1983).
20. K.S. Pitzer, Quantum Chemistry (Prentice Hall) p. 502 (1959).
21. Review Articles:
 - (a) I.M. Lifshitz, Nuovo Cimento, Suppl., 10, 716 (1956).
 - (b) A.A. Maradudin, P. Mazur, E.W. Montroll and G.H. Weiss, Revs. Mod. Phys., 30, 175 (1968).
 - (c) A.A. Maradudin, E.W. Montroll, G.H. Weiss, Theory of Lattice Dynamics in the Harmonic Approximation, in "Solid Stat Physics," Suppl. 3, Academic Press, New York, 1963.
 - (d) W. Ludwig, "Ergebnisse der exakten Naturwissenschaften," Volume 35, Springer, Berlin, 1964.
 - (e) A.A. Maradudin, in "Phonons and Phonon Interactions," edited by T.A. Bak, W.A. Benjamin, New York, 1964, p. 424.
 - (f) A.A. Maradudin, Theoretical and Experimental Aspects of the Effects of Point Defects and Disorder on the Vibrations of Crystals, in "Solid State Physics," volume 18, Academic Press, New York, 1966, p. 274.
 - (g) G. Leibfried, Lattice Dynamics of Point Defects in "Atomic and Electronic Structure of Metals," (J.J. Gilman and W.A. Tiller, eds., Amer. Soc. for Metals) pg. 207 (1967).

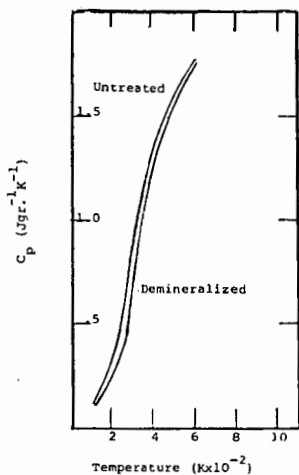


Figure 1. Illinois Char

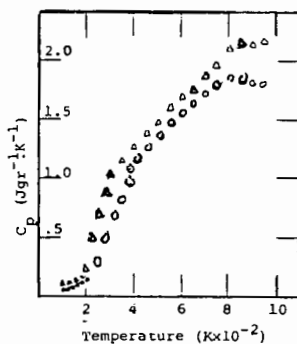
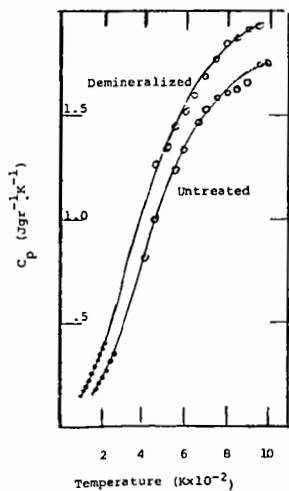
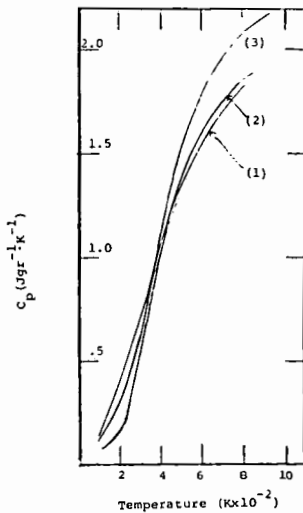
Figure 2. Virginia Chars
○ Demineralized
△ Untreated

Figure 3. North Dakota Char

Figure 4. Demineralized Chars
(1) N. Dakota
(2) Virginia 700°C
(3) Illinois 1 Hour

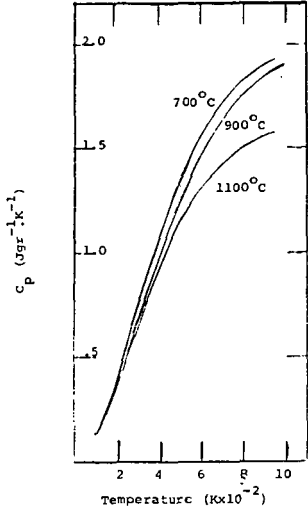


Figure 5. N. Dakota Chars

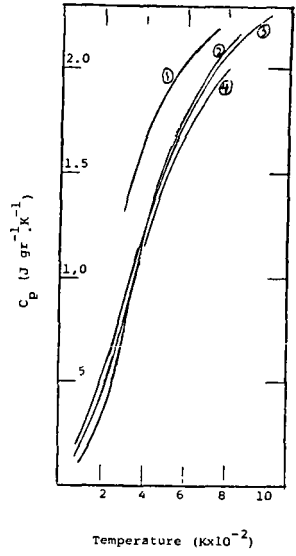


Figure 6. Illinois Chars
 (1) 500°C (3) 900°C
 (2) 700°C (4) 1100°C

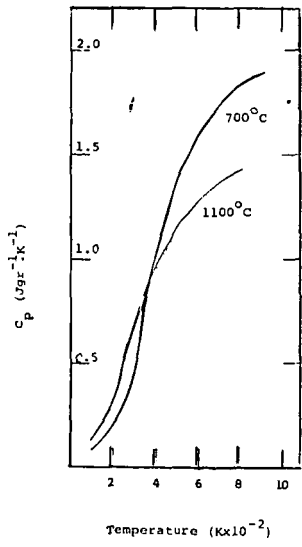


Figure 7. Virginia Chars

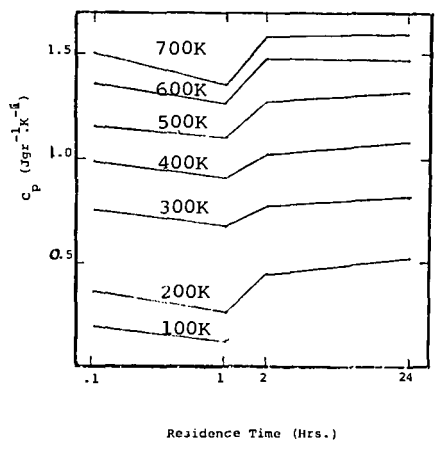


Figure 8. Virginia Chars

9.

REMOVAL OF SYNTHETIC CRUDE NITROGENOUS COMPOUNDS
USING WASTE MINERALS

BY

G. JEAN, M. POIRIER, and H. SAWATZKY

ENERGY RESEARCH LABORATORIES

CANMET, OTTAWA, CANADA, K1A 0G1

INTRODUCTION

Nitrogenous compounds in crude oils and petroleum products have been associated with several problems in processing operations and must be removed in the early stages of upgrading. With conventional technology this is done by severe hydrotreating which has several disadvantages: high capital cost investment, degradation of valuable material, and high operating cost due to energy and hydrogen consumption. A method allowing the separation of nitrogenous compounds from feedstocks would greatly reduce the costs of upgrading.

Several analytical procedures are known for the separation of nitrogenous compounds (1-7). These methods, however, are not feasible for large scale operation.

In this study waste minerals have been tested as low cost adsorbents. Since sulphide minerals are known as good adsorbents a series of sulphides was tested (5). We also tested brominated ilmenite in an attempt to take advantage of the complexing properties of titanium and iron (6,7).

EXPERIMENTAL

SULPHIDE MINERALS

The adsorption studies were conducted by liquid chromatographic methods. The feed was a solution of four or five nitrogenous model compounds dissolved in 50:50 heptane/toluene. Each compound contributed 25 ppm N to the solution. The adsorbents were natural waste minerals: pyrrhotite (FeS), pyrite (FeS₂), sphalerite (ZnS), and chalcopyrite (FeCuS₂).

The adsorbent (200 mesh) was dry-packed in a stainless steel column (60 cm long x 0.4 cm I.D.).

The solution of the nitrogen compounds was pumped into the column at 1 mL/min. Samples of 2 mL were collected and analyzed by gas chromatography using a Varian 6000 gas chromatograph and a Dexsil-300 packed column.

The area of the chromatographic peaks was used to calculate the percentage of each component present in the effluents. The calculations were made as follows:

$$\% \text{ Species } i = \frac{\text{area of peak } i \text{ in sample} \times 100}{\text{area of peak } i \text{ in feed}}$$

$$\% \text{ Total nitrogen} = \frac{\sum \text{area of peak } i \text{ in sample} \times 100}{\sum \text{area of peak } i \text{ in feed}}$$

Brominated Ilmenite

The ilmenite ore was taken from within 0.8 km of a point situated about 2.4 km southwest of St-Urbain and about 11.2 km north of the village of Baie St-Paul, Québec, on the north shore of the St-Lawrence River. It contained 39% TiO_2 , 28% FeO and 19% Fe_2O_3 . The ore was crushed to about 200 mesh and treated as follows:

In a 100-ml round bottom flask equipped with a reflux condenser, and containing 15-g of crushed ilmenite an excess of bromine (about 10 ml) was added. The mixture was heated to 58°C for 2 h, cooled, washed with 50-ml pentane to remove excess bromine. The treated ilmenite was filtered off and then washed again with pentane until the workings became colourless. The treated ilmenite was then dried with a stream of nitrogen, and used as adsorbent.

MODEL COMPOUND STUDY

A standard solution of 18 nitrogenous compounds in toluene was prepared. Its composition is given in Table 1. This solution was pumped continuously at 0.5 ml/min into a 30 cm long x 0.4 cm I.D. column, packed with 20 g of treated ilmenite. Samples of 5-ml were collected and analyzed by gas chromatography using a 12.5 m long SE-30 capillary column.

RESULTS

The fate of the various nitrogenous compounds was monitored by analyzing the effluent by gas chromatography. A comparison of the results clearly shows that certain nitrogenous compounds have a greater affinity for the surface of the sulphides. Figure 1 shows the percentage of each species present in the effluent vs. the volume pumped into the column. These results show that three of the four compounds broke through the column after 5-ml compound was pumped. Tributylamine, however, was the only compound selectively removed. Thus the surface can differentiate between the various nitrogenous compounds. The same type of behaviour was observed for the other sulphide minerals.

Titanium is known to form complexes with various nitrogenous compounds (6,7). Ilmenite was treated with bromide in order to form $TiBr_x$ and $FeBr_x$ on the surface. Treated ilmenite was found to be a much better sorbent than untreated ilmenite. To better characterize the sorption properties of treated ilmenite a feed containing 18 model compounds was used. Figure 2 describes the fate of these 18 compounds during the run.

Compounds such as benzylamine and 2,2¹-dipyridyl are extensively adsorbed and are still completely retained by the ilmenite after 150 ml has been pumped into the column. Other compounds such as carbazole are hardly adsorbed and elution occurs after 15 ml. The amount of benzylamine adsorbed is at least 20 times that of carbazole. Table 1 gives the order of elution of the 18 compounds. It is interesting to note that there seems to be a general correlation between the extent of adsorption and the basicity of the compound.

Another important feature observed in Fig. 2 is that some compounds are irreversibly adsorbed while others are reversibly adsorbed. Compounds such as indole are irreversibly adsorbed; in other words these compounds saturated the sites that were available to them and were not subsequently displaced. Conversely, compounds such as aniline are reversibly adsorbed. Their behaviour is typical of displacement chromatography where a compound is desorbed by another thus giving rise to a concentrated front that eventually elutes in the effluent. Figure 2 shows that these compounds elute in the effluent at a concentration of about three times that of the original feed. A rough mass balance indicates that these compounds are quantitatively desorbed and practically none is left on the column after the concentrated front has eluted.

DISCUSSION

The main conclusion in this study is that sulphide minerals have a very low adsorption capacity for nitrogenous compounds. These adsorbents, however, were found to be selective. For example, pyrrhotite adsorbs about 20 times more tributylamine than carbazole or trimethylpyrrole. The more basic compounds are usually more quantitatively adsorbed which suggests that these compounds are adsorbed on the Lewis and/or Bronsted acid sites. Therefore, increasing the surface acidity should increase the amount of nitrogenous compounds adsorbed.

Ilmenite was treated with bromide to form $TiBr_x$ and $FeBr_x$ on the surface. These salts are known as strong Lewis acids. The capacity of the treated ilmenite is much higher than that of the natural material.

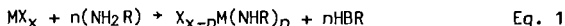
The model compound study gives some insight into the adsorption mechanism. Indeed, the adsorptive properties of the 18 compounds differ depending on their nature. The compounds can be subdivided into four classes according to their adsorption behaviour as follows:

<u>I</u>	<u>II</u>	<u>III</u>	<u>IV</u>
carbazole	aniline	1,2,5-trimethylpyrrole	dibenzylamine
tetrahydrocarbazole	2-phenylpyridine	n-octylamine	1-phenethyl-piperidine
indole	3,4-benzacridine	n-decylamine	2,2'-dipyridyl
3-methylindole	quinoline	2-aminochrysene	benzylamine
phenothiazine	2-methylacridine		

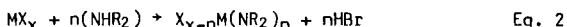
In class I all compounds are pyrrolic with active protons on the nitrogen and are weakly acidic. Carbazole is hardly retained and the rest only slightly. Due to the absence of a concentrated elution front it appears that the adsorption is irreversible. In contrast, class II compounds, being weakly basic, are more quantitatively retained but are also displaced and elute as a concentrated front. Their behaviour is typical of displacement chromatography. Classes III and IV are definitely more basic and more quantitatively adsorbed. In class IV only benzylamine has broken through.

Since classes I and III, with the exception of the trimethylpyrrole, contain an active hydrogen, a possible explanation of these results is given below.

It is well known that titanium halides will react with primary and secondary amines to form a complex (6). Nitrogenous compounds with an active hydrogen can displace halides to give complexes $X_2Ti(NHR)_2$ or $X_3Ti(NR_2)$. Similar reactions are probably occurring at the surface of the treated ilmenite for titanium and iron salts.



or



where M = Ti or Fe
 X = halide
 n = 1 or 2 depending on the nature of the amine
 R = alkyl group

In this case adsorption is really a surface complexation. For purposes of this paper the term adsorption is used.

Contrary to class I, class II compounds were reversibly adsorbed. These compounds with the exception of aniline, do not have an active hydrogen on the nitrogen atom. This implies that the only mechanism of adsorption would be through the donation of the electron pair of the nitrogen to the Lewis centers. (Here, physical forces, interactions of the pi electrons with the surface, and hydrogen bond formation are neglected). The reaction can be illustrated as follows:



Delocalization of the lone pair of electrons over the ring decreases its availability for bonding. Since class II compounds are aromatics it is expected that they will form only weak bonds with the surface. This reaction is found to be reversible. The more basic compounds of classes III and IV probably displace compounds of class II according to the reaction:



Class IV compounds have the highest affinity for the surface. These compounds are basic and will react with a great portion of the sites. 2,2'-dipyridyl is particularly interesting. It does not have an active hydrogen on the nitrogen atom, but is known to be a strong ligand (8). It gives stronger complexes than ligands such as primary and secondary amines. It will react with the surface in a way similar to that described by Eq. 3.

The difference in adsorption capacity between the various classes can be explained in terms of their relative basicity. The surface is made of sites of various activity. The site distribution is expected to resemble a Boltzmann distribution where the highly active sites represent only a small fraction of the sites. The extent of adsorption of the nitrogenous compounds with the surface Lewis acids will depend on the availability of the lone pair of electrons on the nitrogen atom. Compounds of class I are not basic and will react only with the highly active sites. These represent only a small percentage of the sites which explains the low level of adsorption of class I compounds. Compounds of classes III and IV are much more basic and will react with a much broader range of sites than those of class I and have a higher level of adsorption. Steric hindrance could also possibly play a role.

CONCLUSIONS

This study suggests that the adsorption of nitrogenous compounds on sulphide minerals and ilmenite proceeds via an acid-base interaction. These adsorbents would successfully remove basic nitrogenous compounds, but not the acidic nitrogenous compounds. This implies that the effective capacity of the adsorbent will vary with the feed composition. This uncertainty would inhibit the use of such an adsorbent for routine use with feeds of changing composition such as petroleum feedstocks.

Therefore, the waste minerals investigated are not feasible adsorbents for industrial use. However, this study suggests a new approach to design an effective adsorbent. The ideal adsorbent would separate these compounds by a non-acid/base interaction which would allow both acid and basic nitrogenous compounds to be separated indiscriminantly. Such an adsorbent has been identified and the results will be published soon.

REFERENCES

1. Jewel, D.M., and Snyder, R.E., *J. Chromatog.*, 38, 351 (1968)
2. Ford, C.D. et al. *Anal. Chem.*, 53, 831 (1981)
3. Guerin, M.A. et al. *Environ. Res.*, 23, 42 (1980)
4. Audeck, C.A., PREPRINTS, Div. of Petrol. Chem., ACS, 27, 998 (1982)
5. Jean, G.E., Ph.D. Thesis, University of Western Ontario (1983)
6. Cotton, F.A. and Wilkinson, G., *Advanced Inorganic Chemistry*, 3rd ed., Interscience Publishers, New York, (1972), p. 813
7. Ben Kovski, V.G. and Olzseva, M.D., *Chem. Techn. of Fuel and Oil*, 474 (1979)
8. Huhey, J.E., *Inorganic Chemistry: principles of structures and reactivity*, Harper and Row, Publishers, New York (1972)

TABLE 1
ORDER OF BREAKTHROUGH FOR MODEL COMPOUNDS

Curve No. on Fig. 2	Compound	Initial Concentration ppm	Volume at which 10% is reached (mL)	PKa*
1	Carbazole	25.24	1	
2	3-methylindole	26.74	20	
3	Phenothiazine	29.60	25	
4	Indole	29.37	31	
5	Tetrahydrocarbazole	27.70	30	
6	Aniline	30.12	45	4.63
7	2-phenylpyridine	24.26	45	
8	2-aminochrysene	13.90	45	
9	1,2,5-Trimethylpyrole	28.20	48	
10	3,4-benzacridine	7.85	51	
11	n-octylamine	32.62	55	10.65
12	n-decylamine	27.08	60	10.63
13	Quinoline	32.02	65	4.90
14	2-methylacridine	18.40	100	
15	Benzylamine	39.79	100	9.33
-	1-phenethylpiperidine	22.88	-	
-	2,2'-dipyridyl	55.58	-	
-	Dibenzylamine	26.48	-	

*CRC - Handbook of Chemistry and Physics, R.C. Weast Ed., CRC press 1976, 57th edition.

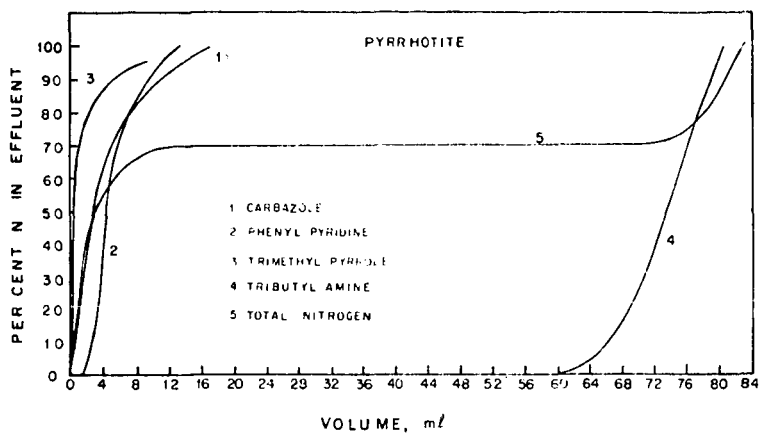


Fig. 1 - Adsorption of nitrogenous compounds on pyrrhotite

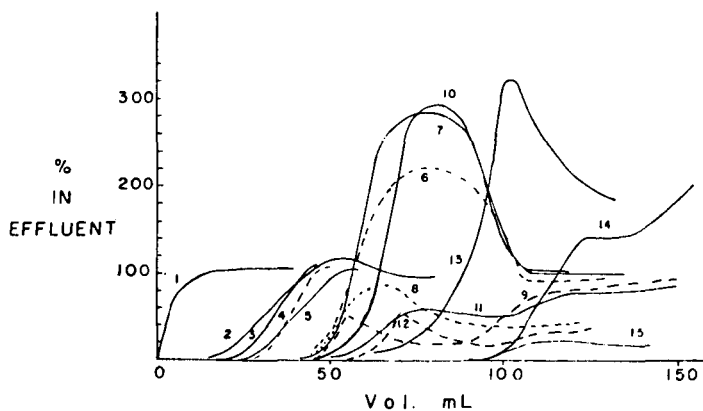


Fig. 2 - Breakthrough curves of individual compounds 1) carbazole; 2) 3-methylindole; 3) penothiazine; 4) indole; 5) tetrahydrocarbazole; 6) aniline; 7) 2-phenylpyridine; 8) 2-aminochrysene; 9) 1,2,5-trimethylpyrrole; 10) 3,4-benzacridine; 11) n-ocylamine; 12) n-decylamine; 13) quinoline; 14) 2-methylacridine; 15) benzylamine; not broken through: dibenzylamine; 1 phenethylpiperidine; 2,2^l dipyridyl.

FT-IR DETERMINATION OF COAL AND SOOT PARTICLE TEMPERATURES DURING PYROLYSIS

Philip E. Best†, Robert M. Carangelo, and Peter R. Solomon, Advanced Fuel Research, Inc., 87 Church Street, East Hartford, CT 06108.

INTRODUCTION

The literature currently reports up to four orders of magnitude variation in the rate for coal pyrolysis at high temperature. The discussion of this problem with references to the literature is presented in (1,2). The wide variations appear to be caused by the inability to separate heat transfer from chemical kinetics. To resolve this issue, it is essential to measure particle temperatures in a pyrolyzing or combusting system. Several (two or more) color pyrometry systems have been developed for this purpose. A system which allows the measurement of single particle temperatures simultaneously with particle size and velocity was recently described by Tichenor et al. (3). The ability to measure temperatures of individual particles is important when there are temperature differences among particles. However, these systems have some disadvantages which limit their application. They employ wavelengths in the visible, which misses most of the emitted radiation. It is difficult to measure low temperatures (Tichenor et al. (3) estimate a 900 K limit for 10 micron particles) and to distinguish particle temperatures in the presence of soot or high temperature regions which can reflect radiation from the particle. Also, particle densities must be low, and it may sometimes be difficult to get a complete picture of a reacting system because low temperature particles will be overlooked.

The application of FT-IR emission and transmission spectroscopy is a good complement to the measurements in the visible, having advantages where the pyrometric techniques have disadvantages. It appears that contributions from soot and particulates can be separated by examining both the emission and transmission spectra and employing a knowledge of the soot's characteristic signature in the IR. Under conditions of uniform temperatures, particulate temperatures and soot densities can be determined. The FT-IR technique has advantages at low temperatures. At the temperatures of interest the emitted radiation has a maximum in the IR, providing good sensitivity. Also, because the measured spectrum covers the whole infrared range, the optical properties of the coal, char and soot (which vary in the infrared) can be measured and used to distinguish the nature of the particulates and the magnitude of reflected radiation. Finally, the technique can determine temperature for clouds of particles by comparing both the amplitude and shape of the emission and transmission spectra.

This paper discusses the application of the technique and preliminary results in a study of coal and acetylene pyrolysis.

EXPERIMENTAL

The emission of infrared light from, and transmission through, dispersed particles involves the processes of emission and absorption in the particle's interior, and reflection, diffraction and refraction at its surfaces. The infrared energy in these measurements can originate in the spectrometer, in the particles or from the hot experimental apparatus. To sort out these effects, as well as the influence of temperature, coal composition and morphology on the spectra, the studies described below have been carried out in a number of geometries.

Measurements In A Hot Cavity

Emission and transmission spectra were recorded in an entrained flow reactor (EFR) in which coal particles are fed into the furnace from a water cooled injector. In this geometry the coal "sees" hot furnace walls with the exception of the injector and the KBr windows that provide entrance and exit for the IR beam.

† permanent address: Department of Physics and Institute of Material Science, University of Connecticut, Storrs, CT 06268

Transmission spectra are recorded in the normal manner, as the ratio of transmission with and without the sample in the beam. In this experiment, the radiation from the spectrometer is amplitude modulated, so radiation originating from within the furnace is not detected. In the sample area, the beam geometry is identical for the emission and transmission experiments. In the emission experiment the detection sensitivity is wavelength dependent. The overall detection efficiency is measured by recording the spectrum from a cavity radiator of known temperature. The cavity serves both to provide a path correction at each wavenumber, and as a reference for the calculation of the shape and amplitude of black-body radiators of other temperatures. The reported emission spectra are also corrected for background.

An example of an emission spectrum for lignite in the furnace is presented in Fig. 1a. For the conditions at which each emission spectrum was recorded a corresponding transmission measurement was made, as shown in Fig. 1b which presents (1-transmission). Except for the gas lines, these spectra show a monotonic variation with wavenumber in a manner which can be accounted for by diffraction theory (2). Since we want to compare emission from particles which fill only a fraction of the viewing area with that from the cavity which fills 100% of the viewing area, we have computed a "normalized emission", Fig. 1c, in which the emission is divided by (1-transmission). The detailed significance of this "normalized emission" will be considered later. For the present we will discuss this function for the case in which the coal particles are of such size and texture that each one effectively blocks 100% of the radiation incident on it. In addition, we work in a dilute particle regime, so that less than 20% of the total beam is blocked. The particles can be considered to act as individual scatterers. In this case (1-transmission) is a measure of the projected area of the coal particles, and represents the fraction of the beam blocked by the sample. It also represents the projected emitting surface area as a fraction of the beam area. If we divide an emission spectrum by the corresponding (1-transmission) we obtain the spectrum that would appear if the sample completely filled the entrance aperture. We call these "normalized emission" spectra. The normalized spectra from a sample of black-body particles at temperature T would agree in shape and amplitude with the black-body spectrum corresponding to temperature T and generated from the information in the reference source spectrum. A similar set of emission, transmission and "normalized emission" spectra is presented for soot (Fig. 2). For sufficiently small soot particles the normalized spectrum can be rigorously equated to a black-body curve at the soot temperature. An appropriate theoretical black-body curve is also presented in Figs. 1c and 2c. Indeed, the "normalized emission" is quite close to the theoretical black-body in both shape and amplitude.

An example of normalized emission data, obtained for a lignite injected at several positions above the optical port in the EFR, is presented in Fig. 3. The data illustrate some of the potential benefits as well as the caution required in the interpretation. The figure shows the normalized emission spectra compared to a theoretical black-body curve at the window height wall temperature. Figure 3a presents data for coal injected just above the port. The coal at this position is cold. But there is obviously radiation emerging from the optical port which was not there in the absence of the coal. This must be scattered radiation. As the coal's residence time increases between injection and observation, the spectrum gets closer to the spectrum for the wall. At 36 cm the coal's absorption spectrum is gone, and the spectrum amplitude and temperature is higher than that of the wall. In this case the coal is cooling after having been heated to a higher temperature in the upper part of the furnace. This measurement without any further information can be used to determine the distance required for the coal to reach the reactor temperature.

For later purposes we have also reported the normalized emission from KCl particles in the EFR (Fig.4).

Measurements In A Room Temperature Cavity

To allow separation of contributions from emission and scattering, a second geometry was used employing a tube furnace. In this experiment, the particles have been

heated in a high temperature tube prior to their coming into view of the IR beam. The turbulent environment of the tube convectively heats the coal particles very quickly ($>10^5$ K/sec). The only hot surface seen by the coal when it is in view is the overhead tube. Since the FT-IR spectrometer transmits only radiation which has its electric vector in the vertical plane, radiation from the tube scattered by one scattering event cannot be detected, in contrast to the case for the EFR experiment in which there is substantial scattering of wall radiations.

Figure 5 presents "normalized emission" spectra taken at the exit of the tube reactor after sufficient residence time to bring the coal up to the tube temperature. Each spectrum is compared with a black-body curve at the measured gas temperature at the position of the optical focus. At temperatures below 650 K, (Fig. 5a and b), only the region below 1700 wavenumbers has sufficient emissivity (absorptivity) to emit much radiation. As discussed later, the emissivity, ϵ_y , of the coal can be calculated from the data of Fig. 5 together with the extinction coefficient. We have calculated ϵ_y from the data of Fig. 5d and used it to compute the fraction of radiation from a 1800 K environment that is absorbed by the coal. The results indicate an equivalent grey-body emissivity of 0.2. **Raw coal of pulverized coal size is, therefore, a poor emitter of radiation and consequently, is a poor absorber of radiation. It absorbs much less radiative energy than is usually computed assuming a grey-body with $\epsilon = 0.7$ to 1.0.** This fact is important in computing the heating rate of the coal.

At temperatures of 750 K and 825 K the hydroxyl and aliphatic regions of the coal begin to emit (Figs. 5c and d). At 925 K, char condensation reactions are starting to produce a broad band emission as the char behaves more "graphitic"; this trend continues until, at 1200 K, the char is a grey-body with an emissivity between .7 and .8, similar to that of graphite.

Transmission And Reflection Measurements

Transmission measurements of coal in KBr pellets of coal films were recorded in a typical sample holder geometry for this experiment. The absorbances of two coal films of the same nominal thickness were measured. Figure 6a shows the spectrum of a uniform film of $1\mu\text{m}$ particles pressed into a KBr flat. The spectrum of Fig. 6b is for a film pressed at moderate pressure from a starting material of nominal $30\mu\text{m}$ diameter particles. Under an optical microscope the surface roughness of this latter film appeared comparable to that of an unpressed sample of the same coal. These spectra display the effect of morphology. The film made of ground ($1\mu\text{m}$) diameter particles has residual surface inhomogeneities of the order of the original particle size and can be expected to strongly scatter wavelengths in this region, with the scattering falling off as $(1/\lambda)$ towards longer wavelengths. In the region of 1800 cm^{-1} this $40\mu\text{m}$ thick film is moderately transparent. Extinction at longer wavelengths is due primarily to absorption, while at shorter wavelengths there is increased extinction due to scattering as well as absorption. For a film of similar thickness, but made of pressed $30\mu\text{m}$ diameter particles, (Fig. 6b) extinction over the long wavelength end of the spectrum is dramatically increased, showing qualitatively the dominance of scattering. The coal particles in our experiments have inhomogeneities more of the scale of the film of Fig. 6b than that of Fig. 6a: **scattering plays a significant part in the interaction of the particles with radiation.**

The specular reflection of coal was measured at an angle of incidence of 45° (Fig. 6c). This spectrum can be accounted for by standard theory using optical constants which lie within the range of published values (5). The reflection is small, (between 6 and 10%) and will be important only for rays which nearly graze the surface.

DISCUSSION

The scattering, absorption, transmission and emission of electromagnetic radiation from particles depend both on material properties in the form of the optical

constants, and on morphology, which can be represented by the scales of inhomogeneity relative to wavelength. The interaction of particles with the radiation field is characterized by efficiency factors, Q , which are the effective cross sections for scattering or absorption divided by the geometric cross section of the particles.

$$Q_{\text{ext}} = Q_s + Q_{\text{abs}} \quad (1)$$

where the subscripts stand for extinction, scattering and absorption, respectively (6). Q_s refers to radiation scattered out of the acceptance angle of the optics. Similarly, the other Q'_s are specific to our optical beam path. We will describe a simple model that semiquantitatively accounts for many features of the observed normalized emission spectra. The first feature of the model is due to the geometry of the experiment in the EFR. In this geometry, radiation from the transmission beam can scatter into almost a 360° solid angle of the furnace, while conversely, radiation from this almost 360° solid angle can scatter into the emission beam. The beam-defining aperture is just smaller than the furnace wall opening. For particles within the focus volume, for each incident beam 1 scattered into direction 2, we can find a beam 1' from the furnace wall that is scattered through the same angle into the original beam direction 2' (Fig. 7). From this discussion the following statement can be made about the relative scattering in emission and transmission experiments. If Q_s is the efficiency for scattering out of the beam path in a transmission experiment in this EFR, then

$$Q_s = Q'_s \quad (2)$$

where Q'_s is the efficiency for scattering wall radiation into the beam in an emission experiment, for particles within the focus volume. All the Q 's and ϵ 's that we subsequently discuss are wavenumber dependent but we have dropped the subscript, ν , for convenience.

If we observe the particle in an isothermal environment, then with the usual Kirchoff analysis, the radiation entering the optical aperture of the spectrometer would be

$$Q'_s \cdot \text{BB}(T) + \epsilon \cdot \text{BB}(T) = \text{BB}(T) \quad (3)$$

when the transmission through the particle is zero and where ϵ is the particle emissivity into the spectrometer acceptance angle, compared to the black-body emissivity of unity and where $\text{BB}(T)$ is the black-body spectrum corresponding to temperature T . As usual,

$$\epsilon = Q_{\text{abs}} \quad (4)$$

where both parameters refer to radiation entering or leaving the particle in the cone defined by the spectrometer aperture.

With these definitions we describe the normalized emission results as

$$\begin{aligned} & \frac{(\text{"observed emission"})}{(1-\text{transmission})} \\ & N_p \cdot A_p \cdot \left[\epsilon \cdot \text{BB}(T_p) + Q'_s \cdot \text{BB}(T_w) \right] \\ & = \frac{N_p \cdot A_p \cdot (Q_{\text{abs}} + Q_s)}{Q_{\text{abs}} \cdot \text{BB}(T_p) + Q_s \cdot \text{BB}(T_w)} \quad (5) \\ & \quad \quad \quad Q_{\text{abs}} + Q_s \end{aligned}$$

where $\text{BB}(T_p)$ and $\text{BB}(T_w)$ are the black-body emission curves appropriate to the particle and EFR wall temperatures, respectively, N_p and A_p are the numbers of

particles in view, and their average geometrical cross-section, respectively. Equation 5 can be applied to explain the results of Figs. 1-5.

Case 1) If $Q_{\text{abs}} = 0$, as for KCl, the normalized emission should be equivalent in shape and amplitude to $BB(T_w)$, as is observed (Fig. 4).

Case 2) For soot particles of sufficiently small dimensions, the scattering is negligible (7). In that case the normalized emission (eq. 5) is given by $Q_{\text{abs}} \cdot BB(T_p) / Q_{\text{abs}} = BB(T_p)$. This predicts that the normalized emission from soot will be equal in amplitude and shape to the black-body curve corresponding to the soot temperature. This is indeed the case (Fig. 2). For KCl and soot, as well as all subsequent cases, there are no adjustable parameters in the comparisons we make.

Case 3) Another occasion in which a particularly simple result comes from this analysis is when the particle and wall temperatures are the same. Equation 5 shows that the normalized emission will be a good black-body curve, this time corresponding to the wall (and particle) temperature (Fig. 1).

The last cases to be considered are when non-black-body shape or amplitude is observed in the normalized emission (Figs. 3 and 5).

Case 4) Taking the case of the tube furnace first, and noting that there is no wall radiation to be scattered into the spectrometer in an emission measurement in that situation, the normalized emission is

$$\epsilon \cdot BB(T_p) / (Q_{\text{abs}} + Q_s) \quad (6)$$

For coal particles, the variation of the demoninator of eq. 5 with wavenumber is similar to that of Fig. 1b: $Q_{\text{ext}} = Q_{\text{abs}} + Q_s$ has a value between 1 and 2, which can be estimated from diffraction theory (2). Multiplying the normalized emission by Q_{ext} , and dividing by the black-body curve corresponding to the measured temperature, gives an experimental estimate of ϵ , the coal emissivity. As expected from eq. 4, maxima in the emission in the tube furnace spectra (Fig. 5) correspond to maxima in the absorbance spectrum of the coal (Fig. 6).

Case 5) The most difficult case is for particles in the EFR where contributions come from both emission and scattering. In this case one can select regions of the spectrum which still permit simplification. For regions where the coal absorbs strongly (eg. 1600 cm^{-1}), Q_{abs} approaches unity for sufficiently large particles. Such regions of the spectrum can be used to determine the particle temperature.

CONCLUSIONS

Normalized FT-IR emission spectra appear to contain a considerable amount of information about the solid phases in pyrolyzing coal and gas systems. In this preliminary work we have deduced solid phase temperatures for a number of circumstances, demonstrated the ability to detect chemical change in high temperature reactions, and deduced a grey-body emissivity for coal. With improved evaluation of how the emissivity changes with pyrolysis, there are good prospects that the temperature determining capability of the method can be extended.

ACKNOWLEDGEMENTS

This work was supported by the U. S. Department of Energy, Morgantown Energy Technology Center under Contract No. DE-AC21-81FE05122, U.S. Department of Energy, Pittsburgh Energy Technology Center under Contract No. DE-AC22-82PC50254 and The National Science Foundation under Contract No. CPE-83-60666.

REFERENCES

1. Solomon, P.R., Hamblen, D.G., Carangelo, R.M., Markham, J.R., and DiTaranto, M.B., ACS Division of Fuel Chemistry Preprints 29, #2, p. 3 (1984).
2. Solomon, P.R. and Hamblen, D.G., Finding Order in Coal Pyrolysis Kinetics, Progress in Energy and Combustion Science, 9, 323 (1983).
3. Tichenor, D.A., Mitchell, R.E., Hencken, K.R. and Niksa, S., Simultaneous In-Situ Measurement of the Size, Temperature and Velocity of Particles in a Combustion Environment, presentation at the 20th Symposium (Int) Conference on Combustion; Aug. 12-17, 1984, University of Michigan, Ann Arbor Michigan.
4. Gumbrecht, R.O. and Sliepcevich, C.M., J. Phys. Chem. 57, 90 (1953).
5. Foster, P.J. and Howarth, C.R., Carbon, 6, 719, (1968).
6. van de Hulst, H.C., Light Scattering by Small Particles, Dover Publications, NY, (1981).
6. D'Alessio, A., Cavaliere, A. and Menna, P., Soot in Combustion Systems, Edited by J. Lahaye and G. Prado, Vol. 7, pg. 327, (Plenum Press, NY), (1983).

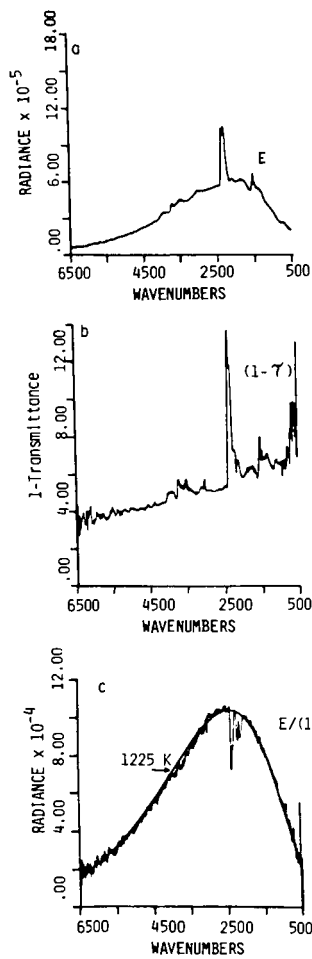


Figure 1. a) Emission, b) (1-transmission), and c) $E/(1-\tau)$. Curves for a Lignite (mesh size -300+425) Injected into the Furnace at 36 cm above the Window. Furnace Wall Temperature at Window Height is 1170 K.

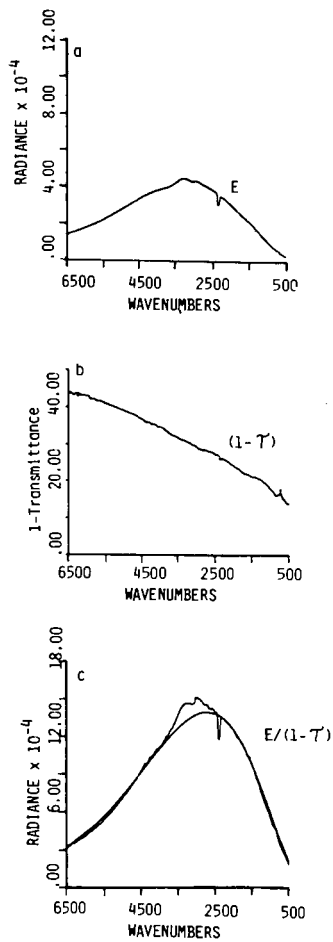


Figure 2. a) Emission, b) (1-transmission), and c) $E/(1-\tau)$. Curves for Soot formed by Acetylene Injected into a Furnace at a Height of 66 cm above the Window. Furnace Wall Temperature is 1250 K. Curve c is a Quantitative Black-body Curve Corresponding to a Temperature of 1350 K.

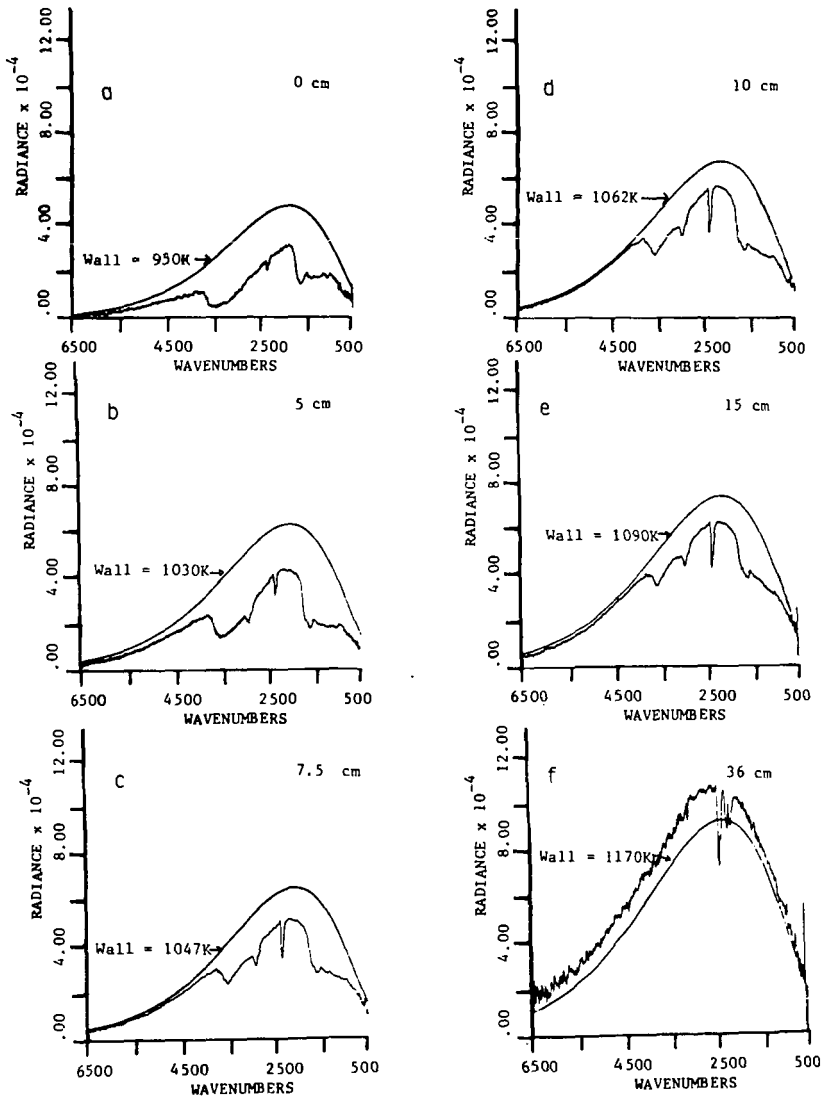


Figure 3. Series of $E/(1-T)$ Curves for Lignite Particles in the Furnace for Increasing Residence Time.

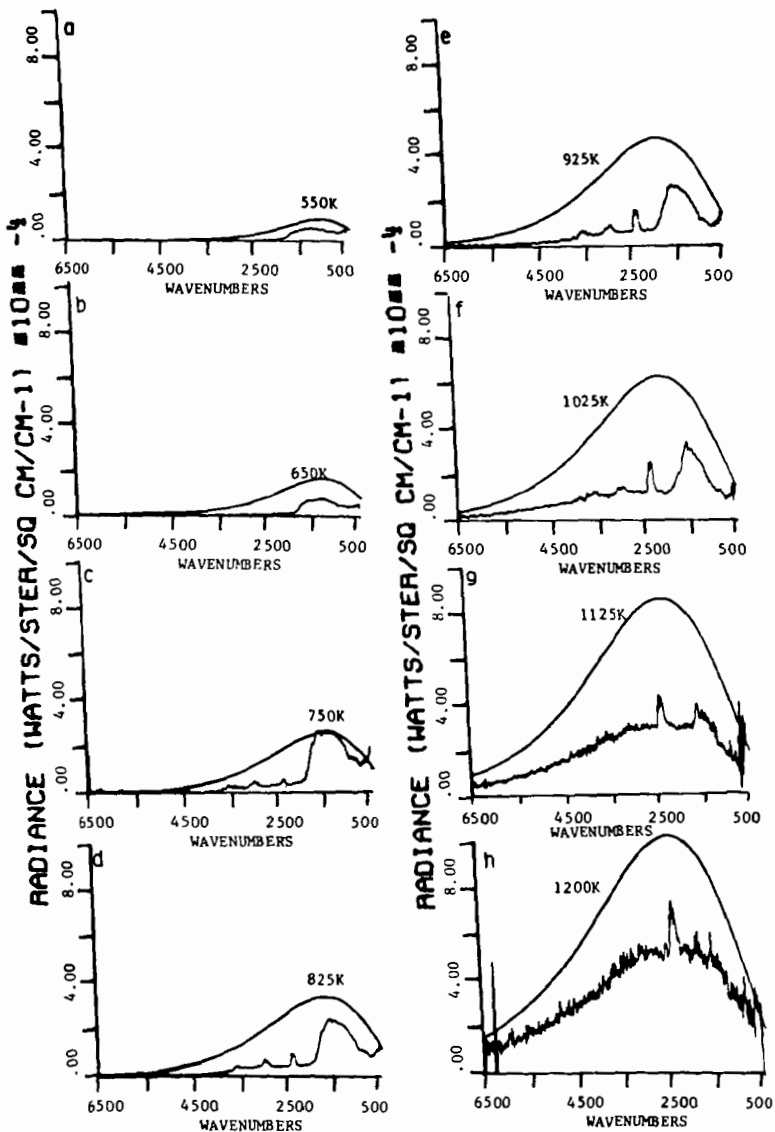


Figure 5. Series of Emission Normalized by (1-transmission) for Lignite Particles in the Tube Reactor for Increasing Temperature.

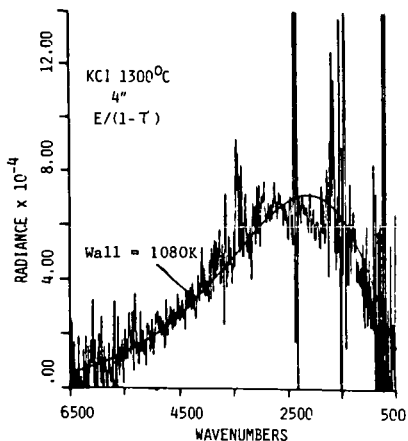


Figure 4. $E/(1-T)$ for Cold KCl Particles in a Hot Furnace. Furnace Wall Temperature is 1080 K. This Curve is a Quantitative Black-body Curve Corresponding to a Temperature of 1080 K.

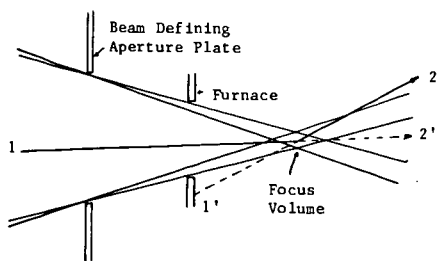


Figure 7. Configuration of Beam Defining Aperture and Furnace Wall in EFR.

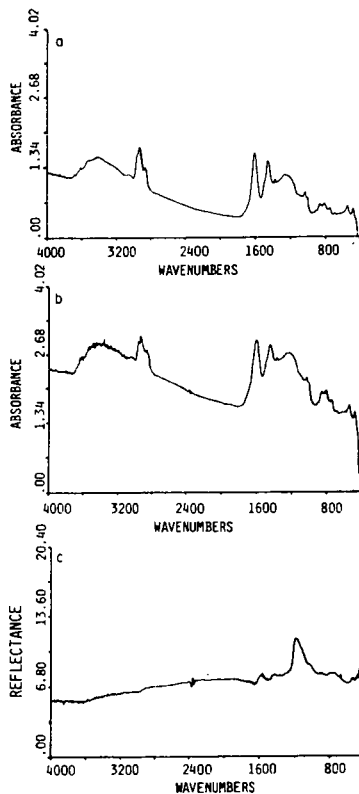


Figure 6. a) Spectrum of $40 \mu\text{m}$ Coal Film Pressed from $1 \mu\text{m}$ Diameter Particles, b) Spectrum of $40 \mu\text{m}$ Coal Film Pressed from $30 \mu\text{m}$ Particles, and c) Specular Reflection of a Coal Pellet Pressed from $1 \mu\text{m}$ Diameter Particles.

THE EFFECT OF OXIDATION OF COAL
ON THE COMPOSITION OF LIQUEFACTION PRODUCTS

Muthu S. Sundaram* and Peter H. Given
Coal Research Section
College of Earth and Mineral Sciences
The Pennsylvania State University
University Park, PA 16802

ABSTRACT

In an effort to understand the effect of oxidation of coal on the composition of liquefaction products, a sample of hvAb coal from the Lower Kittanning Seam in Pennsylvania, labelled PSOC-1336, was oxidized in the presence of air in a convection oven at 140°C for 16 days and liquefied in tubing bomb reactors in the presence of tetralin. The oxidation of coal decreased the liquefaction conversion. The aromatic fraction of the hexane-soluble oil from oxidized coal contained smaller amounts of phenanthrenes and pyrenes and larger amounts of tetralin-related artifacts when compared to that from the fresh coal. Relatively larger amounts of the hydroxy derivatives of indane, naphthalene, fluorene and phenanthrene were present in the polar fraction from the oxidized coal.

INTRODUCTION

It is known that coals deteriorate on oxidation and the extent of deterioration depends on the severity of oxidation conditions. The earliest study on the mechanism of oxidation of coals was reported by Jones and Townend in 1945 (1). After a lack of interest for more than two decades, there has been renewed interest in studying the effect of oxidation on the physical and chemical characteristics of coals (2,3). New analytical techniques to detect oxidation (4,5) and the mechanism and kinetics of oxidation have been reported (6,7). Few studies exist on the effects of partial oxidation on the liquefaction behavior of coals (8-10).

EXPERIMENTAL

The objective of this study is to understand the effects of oxidation on the liquefaction behavior of coals and on the composition of liquefaction products. A sample of hvAb coal from the Lower Kittanning seam in Pennsylvania (PSOC-1336) was oxidized by exposure to air in an oven at 140°C for 16 days and then liquefied in tubing bomb reactors using tetralin as donor vehicle under fairly mild conditions (400°C, one hour, no hydrogen gas). The unoxidized coal was also liquefied under identical conditions for comparison.

Present address: Process Sciences Division, Department of Applied Science,
Brookhaven National Laboratory, Upton, New York 11973

RESULTS AND DISCUSSION

The characteristics of the coal are given in Table 1 and the basic liquefaction data are shown in Table 2. The total conversion into ethyl acetate-soluble products plus gases was slightly higher in the case of the unoxidized coal. The higher conversion was reflected in a higher yield of liquid products whereas yield of gases actually decreased. This shows that oxidation is detrimental to coal liquefaction. Similar results have been reported (9,10).

The hexane-soluble oil was vacuum distilled at 70°C (about 2 mm Hg pressure) to remove naphthalene and excess tetralin as completely as possible. A primary fractionation of the oil into saturate, aromatic and polar fractions was made by HPLC (Waters Associates) using a semi-preparative micro-Bondapak NH₂ column. Table 2 does not show appreciable differences with respect to the yield of individual fractions.

All fractions were analyzed by capillary-GC/MS (Finnigan 4000) using a 30 meter SE-54 column to obtain product composition data. The n-alkane distribution in the saturate fraction of the oil from unoxidized coal is compared with that of the oxidized coal in Figure 1. The differences are minor with respect to the modality of distribution as well as the yield of individual hydrocarbons. However, GC/MS characterization of the aromatic fractions revealed important differences.

Figure 2 shows the gas chromatograms of aromatic fractions and the peaks are identified in Table 3. The aromatic fractions contained various dimeric artefacts (hydrogenated binaphthyls) formed from the tetralin donor vehicle during coal liquefaction. Pyrites and clay minerals were found to independently catalyze these reactions (11). Table 4 shows that the yield of selected artifacts, binaphthyl, tetrahydro-, and octahydro-binaphthyl, were much higher when the coal was oxidized.

It is known that exposure of coals to air at temperatures below 80°C, leads to the formation of peroxides (1). These unstable species may be transient intermediates at somewhat higher temperatures, leading to the formation of various oxygen functions, notably carbonyl. Carbonyl is easily reduced if a supply of hydrogen is available, and so will tend to promote both generation of free radicals from the solvent and increased consumption of it. This, perhaps, is the chief factor responsible for the production of dimers from the solvent. Additionally, the oxidation would have converted the pyrite present in the coal (2.1% dmmf) to sulfates and sulfuric acid, which might have influenced the dimerization. In any case, an enhancement in the production of artefacts could limit the availability of hydrogen from the donor solvent which, in turn, can affect the yield of smaller molecules that are formed via hydrocracking and there are obvious implications for recycle solvent quality and consumption.

Benzylic CH₂ groups in diaryl-methanes and diaryl-ethanes are likely to be particularly susceptible for oxidation. Once oxidized, they can no longer cleave to methyl-substituted aromatic structures. Thus, one might expect methyl substitution to be reduced in the liquefaction products of an oxidized coal. The product yield data in Table 4 for some selected polynuclear aromatic hydrocarbons, lend support to this argument, though they cannot be said to prove it.

The differences in composition of the polar fraction are considerably larger. The oxidized coal afforded a richer, more complex mixture of compounds and structural types than the unoxidized (Figure 3 and Table 5). At the lower end of the molecular weight range, there are large numbers of alkyl-hydroxy-benzenes and alkyl-indanols. The fractions from both oxidized and unoxidized coals showed a number of alkyl-hydroxy-naphthalenes, but in the higher end of the molecular weight range, hydroxy-fluorene and hydroxy-phenanthrenes were more abundant and richer in the polar fractions from the oxidized sample.

A comparison of the FTIR spectra of oxidized and unoxidized coals showed the expected increase due to carbonyl group absorption (1690 cm^{-1}), but also showed an increase of singly-bonded oxygen (ether or phenolic). Reduction of carbonyl and cleavage of ethers, as well as direct insertion of OH, could all contribute to a more complex mixture of phenols in the liquefaction product of an oxidized coal.

CONCLUSIONS

The laboratory low-temperature oxidation of a coking Pennsylvania coal, PSOC-1336, decreases the liquefaction conversion into ethylacetate solubles plus gases. The ratio of dimeric solvent artefacts to coal products was much greater in hexane-soluble oil from the oxidized sample. An enhancement in the yield of solvent artefacts could indirectly affect the yield of smaller molecules that are formed via cracking. The liquefaction products of the oxidized coal contained less methyl substitution but larger amounts of hydroxy derivatives of indane, naphthalene, fluorene and phenanthrene.

ACKNOWLEDGEMENTS

This work was supported by the U.S. Department of Energy, Contract No. EX-76-C-01-2494 and the coal used in this study was drawn from the Penn State/DOE Coal Sample and Data Base.

REFERENCES

1. Jones, R. E., and Townend, D. T. A., Nature, 155, 424 (1945).
2. Rhoads, C. A., Senftle, J. T., Coleman, M. M., Davis, A., and Painter, P. C. Fuel, 62, 1387 (1983).
3. Cronauer, D. C., Ruberto, R. G., Jenkins, R. J., Davis, A., Painter, P. C., Hoover, D. S., Strasinic, M. E., and Schlyer, D., Fuel, 62, 1127 (1983).
4. Gray, R. J., Rhodas, A. H., and King, D. T., Soc. Mining Engineers, Trans., 260(4), 334 (1976).
5. Painter, P. C., Snyder, R. W., and Kwong, J., Fuel, 59, 282 (1980).
6. Marinov, V. N., Fuel, 56, 158 (1977).
7. Cronauer, D. C., Ruberto, R. G., Silver, R. S., Jenkins, R. J., Ismail, I. M. K., Schlyer, D., Fuel, 62, 1117 (1983).
8. Cronauer, D. C., Ruberto, R. G., Silver, R. S., Jenkins, R. J., and Davis, A. EPRI Report No. AP-1625, Project 779-25, EPRI, Palo Alto, CA., 1980.
9. Whitehurst, D. D., Mitchell, T. O., and Farcasiu, M., "Coal Liquefaction: The Chemistry and TEchnology of Thermal Processing", Academic Press, NY., 1980.
10. Neavel, R. C., Fuel, 55, 237 (1976).
11. Sundaram, M. S., and Given, P. H., ACS Div. Fuel Chem., Prepr. 28(5), 26 (1983).

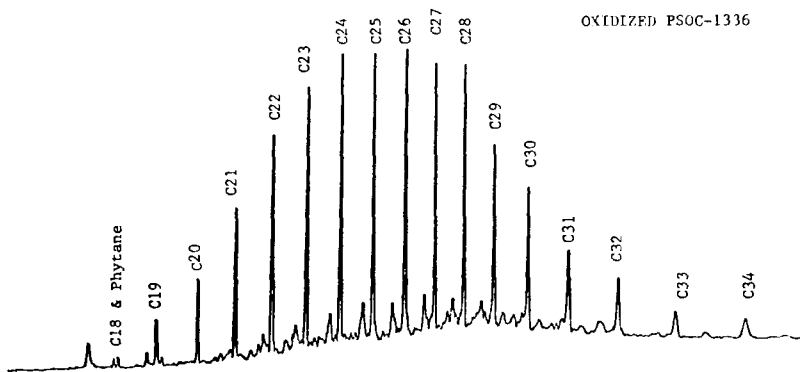
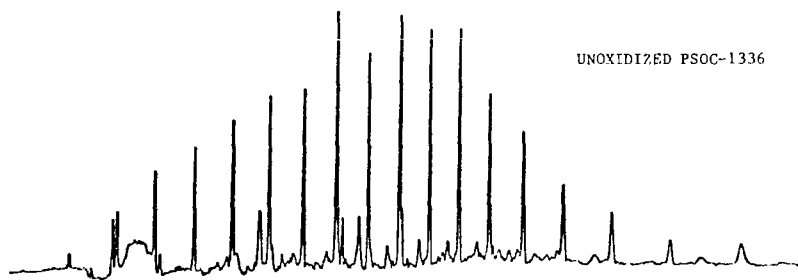


FIGURE 1. TOTAL ION CHROMATOGRAM OF SATURATED FRACTIONS

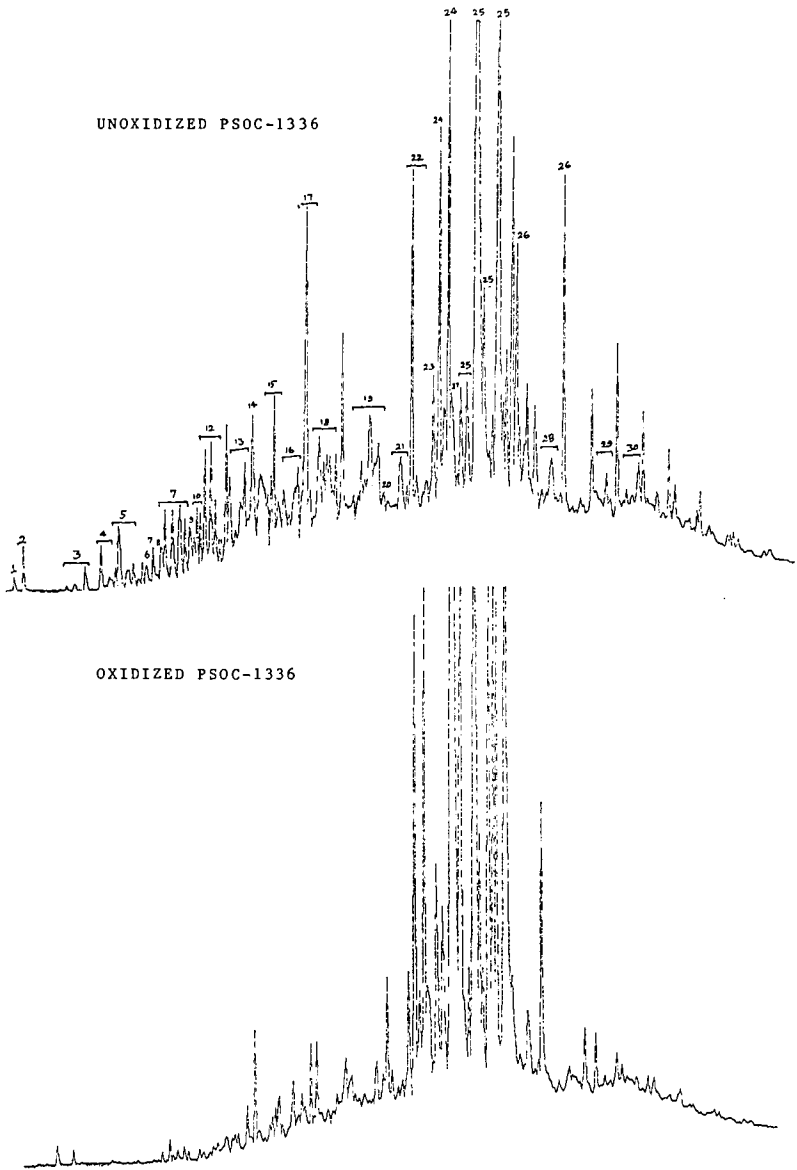
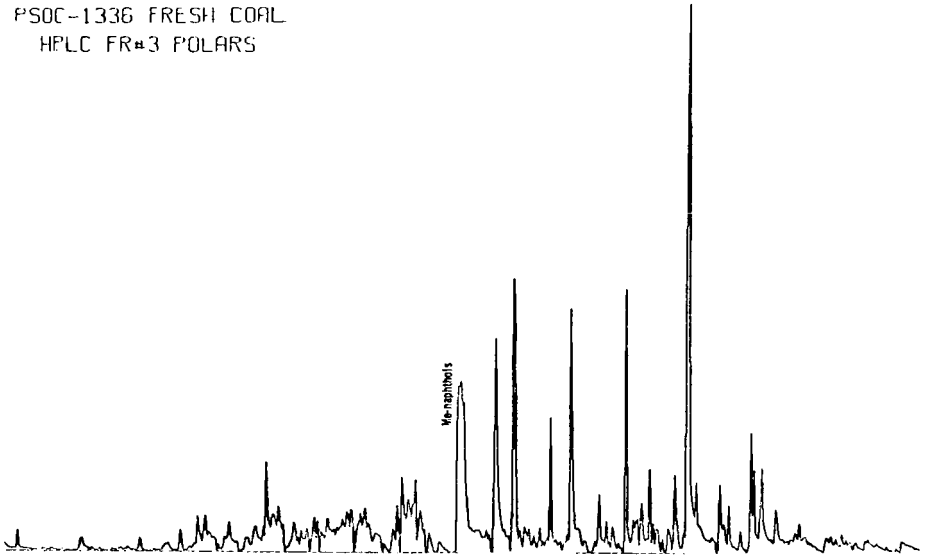


FIGURE 2. TOTAL ION CHROMATOGRAM OF AROMATIC FRACTIONS

PSOC-1336 FRESH COAL
HPLC FR#3 POLARS



PSOC-1336 OXIDISED COAL
HPLC FR#3 POLARS

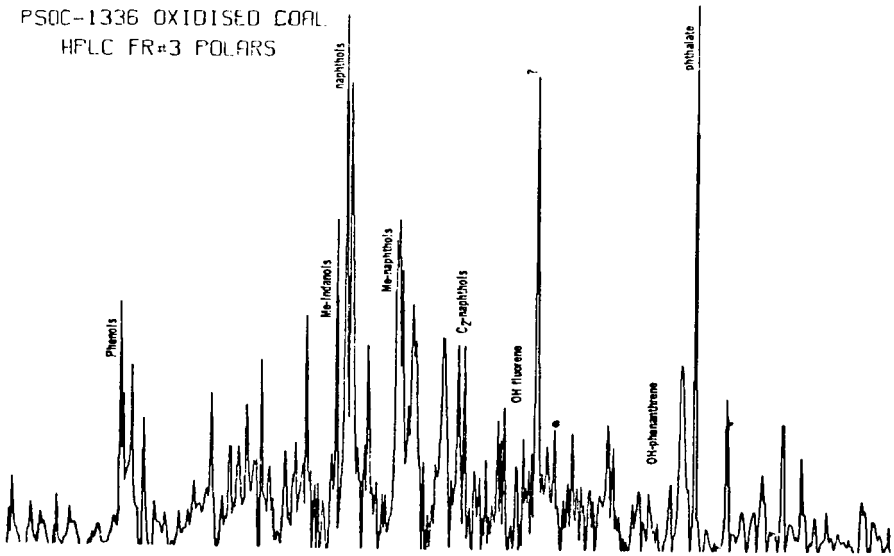


FIGURE 3. TOTAL ION CHROMATOGRAM OF POLAR FRACTIONS

TABLE 1.

Analytical Data for P50C-1336, Lower Kittanning Seam, Pa.

	dry mineral matter free
C	87.2% vitrinite 85%
H	5.4 lipinites 5%
N	1.6 inertinite 10%
S	1.0 dry basis:
Cl	0.1 mineral matter 16.7%
O(diff)	4.6 (including pyrite 2.1%)

ASTM rank class: hvAb

TABLE 2

Product Yields: (%dmmf coal)	Liquefaction Data	
	Unoxidized	Oxidized
Asphaltenes	19.9	14.9
Oil	11.0	7.2
Gases	3.3	7.2
Conversion	34.2	29.3
<u>Oil Composition: (% oil)</u>		
Saturates	2.8	2.6
Aromatics	42.3	40.0
Polars	54.9	57.4

TABLE 3
Identification of Aromatic Hydrocarbons

Peak Number	Identification
1	Tetralin
2	Naphthalene
3	Methylnaphthalene
4	Tetrahydromethylnaphthalene
5	C ₂ -Naphthalene
6	Acenaphthene
7	C ₃ -Naphthalene
8	C ₁ -Acenaphthene
9	Fluorene
10	C ₁ -Biphenyl
11	C ₂ -Acenaphthene
12	C ₁ -Dibenzofuran + C ₄ -Naphthalene
13	C ₂ -Dibenzofuran/C ₂ -Biphenyl
14	Phenanthrene
15	C ₃ -Biphenyl
16	C ₄ -Biphenyl
17	C ₁ -Phenanthrene
18	C ₂ -Phenanthrene
19	Fluoranthene/C ₃ -Phenanthrene
20	Pyrene
21	C ₃ -Phenanthrene
22	C ₁ -Pyrene
23	Benzofluorene
24	Tetrahydrobinaphthyl
25	Octahydrobinaphthyl
26	Binaphthyl
27	Chrysene/Triphenylene/ Benzanthracene, Methyl
28	Benzofluoranthene
29	Benzopyrene/Perylene
30	Benzopyrene/Perylene, Methyl

TABLE 4

Yields of Selected Components in
the Aromatic Fraction of PSOC-1336

	<u>Unoxidized</u>	<u>Oxidized</u>
<u>Artefacts (ug/gm oil)</u>		
Binaphthyl	73	290
Tetrahydrobinaphthyl	103	336
Octahydrobinaphthyl	211	348
Total artefacts	387	973
<u>Coal-derived (in ug/gm dry coal)</u>		
Phenanthrene	3.3	1.8
C ₁ -Phenanthrenes	11.3	5.6
C ₂ -Phenanthrenes	18.1	8.8
Pyrene	3.0	2.5
C ₁ -Pyrenes	23.7	16.5
C ₂ -Pyrenes	25.3	20.4
C ₃ -Pyrenes	8.1	5.0
Benzopyrene and its isomers	28.5	26.8

TABLE 5

Compounds identified in the Polar Fraction *

Phenol	Naphthol
Methylphenol	Methylnaphthol
C ₂ -Phenol	C ₅ -Phenol
C ₃ -Phenol	C ₂ -Naphthol
Indole	Hydroxyfluorene
Indanol	C ₁ -Dibenzofuran
Dihydroxybenzene	Xanthene
C ₄ -Phenol	C ₁ -Hydroxyfluorene
Indenol	C ₂ -Hydroxyfluorene
Methylindanol	Hydroxyphenanthrene
Methylindole	Diisobutylphthalate (impurity)
C ₂ -Indanols	
Phenylfuran	* From Oxidized Coal